NUREG/CR-3577

# The Measurement of Countercurrent Phase Separation and Distribution in a Two-Dimensional Test Section

Prepared by K. M. Bukhari, R. T. Lahey, Jr.

**Rensselaer Polytechnic Institute**
**Department of Nuclear Engineering**



**Prepared for**
**U.S. Nuclear Regulatory Commission**

Availability of Reference Materials Cited in NRC Publications

Most documents cited in NRC publications will be available from one of the following sources:

1. The NRC Public Document Room, 1717 H Street, N.W.
   Washington, DC 20555
2. The NRC/GPO Sales Program, U.S. Nuclear Regulatory Commission,
   Washington, DC 20555
3. The National Technical Information Service, Springfield, VA 22161

Although the listing that follows represents the majority of documents cited in NRC publications, it is not intended to be exhaustive.

Referenced documents available for inspection and copying for a fee from the NRC Public Document Room include NRC correspondence and internal NRC memoranda; NRC Office of Inspection and Enforcement bulletins, circulars, information notices, inspection and investigation notices; Licensee Event Reports; vendor reports and correspondence; Commission papers; and applicant and licensee documents and correspondence.

The following documents in the NUREG series are available for purchase from the NRC/GPO Sales Program: formal NRC staff and contractor reports, NRC-sponsored conference proceedings, and NRC booklets and brochures. Also available are Regulatory Guides, NRC regulations in the *Code of Federal Regulations*, and *Nuclear Regulatory Commission Issuances*.

Documents available from the National Technical Information Service include NUREG series reports and technical reports prepared by other federal agencies and reports prepared by the Atomic Energy Commission, forerunner agency to the Nuclear Regulatory Commission.

Documents available from public and special technical libraries include all open literature items, such as books, journal and periodical articles, and transactions. *Federal Register* notices, federal and state legislation, and congressional reports can usually be obtained from these libraries.

Documents such as theses, dissertations, foreign reports and translations, and non-NRC conference proceedings are available for purchase from the organization sponsoring the publication cited.

Single copies of NRC draft reports are available free upon written request to the Division of Technical Information and Document Control, U.S. Nuclear Regulatory Commission, Washington, DC 20555.

Copies of industry codes and standards used in a substantive manner in the NRC regulatory process are maintained at the NRC Library, 7920 Norfolk Avenue, Bethesda, Maryland, and are available there for reference use by the public. Codes and standards are usually copyrighted and may be purchased from the originating organization or, if they are American National Standards, from the American National Standards Institute, 1430 Broadway, New York, NY 10018.

GPO Printed copy price: $6.50

---

NUREG/CR-3577
R2

# The Measurement of Countercurrent Phase Separation and Distribution in a Two-Dimensional Test Section

NUREG/CR--3577

DE84 900662

Manuscript Completed: September 1983
Date Published: January 1984

Prepared by
K. M. Bukhari, R. T. Lahey, Jr.

Rensselaer Polytechnic Institute
Department of Nuclear Engineering
Troy, NY 12181



**Prepared for**
**Division of Accident Evaluation**
**Office of Nuclear Regulatory Research**
**U.S. Nuclear Regulatory Commission**
**Washington, D.C. 20555**
**NRC FIN B7272**
**Under Contract No. NRC 04-76-301**

Availability of Reference Materials Cited in NRC Publications

Most documents cited in NRC publications will be available from one of the following sources:

1. The NRC Public Document Room, 1717 H Street, N.W.
   Washington, DC 20555
2. The NRC/GPO Sales Program, U.S. Nuclear Regulatory Commission,
   Washington, DC 20555
3. The National Technical Information Service, Springfield, VA 22161

Although the listing that follows represents the majority of documents cited in NRC publications, it is not intended to be exhaustive.

Referenced documents available for inspection and copying for a fee from the NRC Public Document Room include NRC correspondence and internal NRC memoranda; NRC Office of Inspection and Enforcement bulletins, circulars, information notices, inspection and investigation notices; Licensee Event Reports; vendor reports and correspondence; Commission papers; and applicant and licensee documents and correspondence.

The following documents in the NUREG series are available for purchase from the NRC/GPO Sales Program: formal NRC staff and contractor reports, NRC-sponsored conference proceedings, and NRC booklets and brochures. Also available are Regulatory Guides, NRC regulations in the *Code of Federal Regulations,* and *Nuclear Regulatory Commission Issuances.*

Documents available from the National Technical Information Service include NUREG series reports and technical reports prepared by other federal agencies and reports prepared by the Atomic Energy Commission, forerunner agency to the Nuclear Regulatory Commission.

Documents available from public and special technical libraries include all open literature items, such as books, journal and periodical articles, and transactions. *Federal Register* notices, federal and state legislation, and congressional reports can usually be obtained from these libraries.

Documents such as theses, dissertations, foreign reports and translations, and non-NRC conference proceedings are available for purchase from the organization sponsoring the publication cited.

*Single copies of NRC draft reports are available free upon written request to the Division of Technical Information and Document Control, U.S. Nuclear Regulatory Commission, Washington, DC 20555.*

Copies of industry codes and standards used in a substantive manner in the NRC regulatory process are maintained at the NRC Library, 7920 Norfolk Avenue, Bethesda, Maryland, and are available there for reference use by the public. Codes and standards are usually copyrighted and may be purchased from the originating organization or, if they are American National Standards, from the American National Standards Institute, 1430 Broadway, New York, NY 10018.

GPO Printed copy price $6.50

## ABSTRACT

The degree of phase separation that occurs in the core of a pressurized water reactor (PWR) during various postulated accidents is an important consideration for studying the course of events during such accidents. The dependence of countercurrent phase separation and distribution phenomena on flow quality, mass flux and system geometry was studied experimentally in a two-dimensional (2-D) test section. A two-phase (air/water) mixture flowed upwards and single-phase water flowed downward along one side of the test section. This countercurrent flow configuration was intended to simulate the so-called "chimney effect" in the diabatic JAERI 2-D experiments in Japan.

A large air/water loop was used with a 3' X 3' X 0.5" (91.44 cm X 91.44 cm X 1.27 cm) test section to study phase separation and distribution effects. A traversing single beam gamma-densitometer was used to measure the chordal average void fractions at several elevations along the test section. Cross-plots between various flow conditions and geometries were made. An error analysis giving the total error in the void fraction measurements was also performed.

High speed photographs were also made of the flow structure, to provide information on flow regimes. The photographic records and the void fraction and hydraulic inflow/outflow data are presented in a form suitable for the assessment of advanced generation computer codes (eg: TRAC).

CONTENTS

CONTENTS (Continued)

LIST OF FIGURES

LIST OF FIGURES

LIST OF FIGURES

LIST OF FIGURES

LIST OF FIGURES

LIST OF FIGURES

LIST OF TABLES

LIST OF TABLES (Continued)

Page

LIST OF TABLES (Continued)

LIST OF TABLES (Continued)

LIST OF TABLES (Continued)

## NOMENCLATURE

Bg : Background counts (cpm)

C : Count rate (cps)

C' : Normalized count rate (dimensionless)

E : Elastic modulus (psi; kpa)

I : Intensity of gamma-ray beam (for two-phase conditions if without any subscript) (counts/sec-$cm^2$)

I' : Normalized intensity, $I/I_{ref}$ (dimensionless)

I : Moment of inertia

L : Test section channel gap (inch; cm)

l : Length of beam (inch; cm)

n : A number

N : Counts obtained in time interval t (for two-phase conditions if without any subscript)

N' : Normalized counts (dimensionless)

R : Length of long side of plate (inch; cm)

r : Length of short side of plate (inch; cm)

S : Stress (psi; kpa)

T : Thickness of plexiglass wall (inch; cm)

t : Counting interval (seconds)

W : Total load (lb; N)

w : Load per unit area ($lb/in^2$; $N/m^2$)

w : Flow rate (lbm/min; kg/hr)

X : Flow quality

y : Maximum deflection (inch; cm)

z : Distance (inch; cm)

Subscripts

air : For air

b : Brace

c : Corrected counts

g : Gas phase

gref: At reference position with air in test section

i : $i^{th}$ component

$\ell$ : Liquid phase

$\ell$ref: At reference position with water in test section

o : Incident value

p : Plexiglass (plate)

ref : At Reference position with two-phase mixture in test section

s : Statistical

t : Total

w : Wall

$2\phi$ : Two-phase

Greek

$\alpha$ : Void Fraction

$\overline{\alpha}$ : Chordal averaged void fraction

$\Delta\xi$ : Error in $\xi$

$\tau$ : Dead time (seconds)

$\mu$ : Linear macroscopic attenuation coefficient ($cm^{-1}$)

# CHAPTER-1

## INTRODUCTION

Two-phase flows occur in many industrial processes. Our understanding of this type of fluid flow phenomena has improved dramatically in the last two decades. However, there are still a number of problems in two-phase flow that require further research. One such problem is concerned with the phase separation and distribution that may occur when two phases flow through channels of complex geometry. The study of phase separation and distribution has been an area of study at Rensselaer Polytechnic Institute (RPI) for some time. The present work is part of this continuing study.

At RPI, phase separation and distribution phenomena has previously been studied for a number of different flow conditions in a variety of channels. These experiments included circular channels having a side branch at three different angles (ie: a wye or tee); a vertical triangular channel; and a 3' X 1' X 0.5" (91.44 cm X 30.48 cm X 1.27 cm) two dimensional vertical channel with and without simulated fuel rods. The 3' X 1' (91.44 cm X 30.48 cm) 2-D channel had an aspect ratio of 1:24 (ie: ratio of channel depth to channel width). The present work was done in a vertical 3' X 3' (91.44 cm X 91.44 cm) channel having a depth of 0.5" (1.27 cm) (thus an aspect ratio 1:72). This test section simulates the so-called chimney effect in the core of a PWR during the reflood phase of a loss of coolant accident (LOCA). This effect is due to natural circulation. The vertical upflow of the two-phase mixture in the central part of the core is due to boiling and the liquid downflow in the peripheral region of the core is due to heat loss and the lower decay heat in that region.

The test section being relatively thin (only a half inch [1.27 cm]), simulates a 2-D slice through the core. It was used with and without stainless steel rods to simulate the lateral hydraulic resistance of the fuel rods. The two-phase (air/water) inlet was located in the middle of the lower edge of the test section. As shown in Fig. 1.1, this inlet is labelled as port no. 4. Port no. 1 in the top right hand corner is used as a single-phase (water) inlet. The two-phase upflow from the middle port simulates the upflow in the central part of the core, while the liquid downflow at the right hand side simulates the liquid downflow near the core periphery. In addition, there are two outlets, one in the top left corner (no. 2) and one in the bottom right hand corner (no. 3). Port no. 5 was not used in this test series, but can be used to change the location of the inlet port for the two-phase mixture.

A number of different inlet flow conditions were established in the test section. The parameters varied were the air and water flow rates entering the test section, the water flow ratio between ports 1 and 4, and the quality of the two-phase flow entering through port no. 4. All of these flow conditions were repeated with the simulated fuel rods in the test section. The various flow conditions have been labeled different cases, which are described in section 5.3.

For each case, the void fraction profile was determined using a single beam gamma densitometer, using the gamma ray attenuation technique

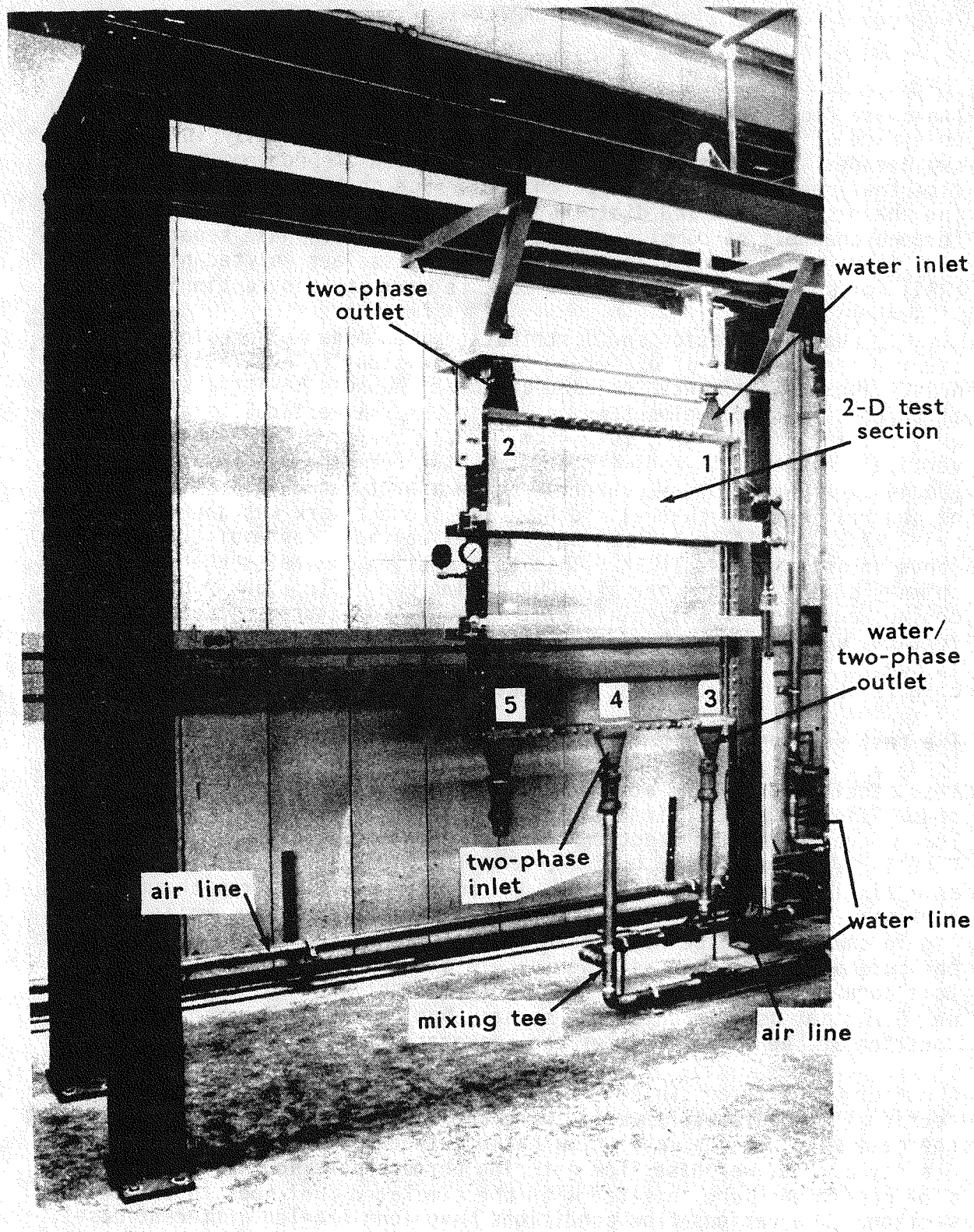


Figure 1.1 The 3' X 3' X 0.5" two-dimensional test section and experimental area

described in Chapter-4. The gamma densitometer scanned the test section from left to right at three (3) different axial positions. The void fraction results for the various cases obtained are presented in Tables 5.4.1 to 5.4.36 and plots of this data are given in Figs. 5.2 to 5.61. In addition, the flows were photographed for all the cases run, and the pictures are included as Figs. 5.62 to 5.97.

The results of this experiment are intended to simulate the diabatic JAERI 2-D experiment in Japan. In addition, the data can be used for the assessment of various advanced generation computer codes, such as TRAC and COBRA-TF.

# CHAPTER-2

# THE AIR/WATER LOOP

## 2.1 About the Loop

The large air/water loop built at RPI under the sponsorship of the United States Nuclear Regulatory Commission (USNRC) for the study of phase separation and distribution phenomena, was used for this experiment. This loop has been described in detail previously(1) and thus, this description will not be repeated here. Some changes in the original system have been made to simultaneously accommodate the 3' X 3' test section and another test section. These changes included an extension of the support structure and some additional piping, with associated valves and flow meters. The loop can now have two experiments set up in it simultaneously.

As can be seen in Fig. 2.1, the water in the system is stored in a water collection tank, from where it flows into the suction of a centrifugal pump. Part of the flow leaving the pump enters a bypass line containing a filtering element, and then returns to the water collection tank. The remainder passes through a globe valve which controls the water flow rate. This flow rate is measured with a calibrated orifice meter. The flow can then enter any one of the two test sections depending on the position of two ball valves. The flow going towards the 3' X 3' (91.44 cm X 91.44 cm) test section then splits into two branches. One goes through a mixing tee, where water mixes with air coming from the air compressor to form a two-phase mixture. This two-phase (air/water) mixture then enters the 2-D test section through inlet no. 4, as seen in Fig. 2.1. The other branch goes through a separate orifice meter and then into the test section through inlet no. 1. Both branches have globe valves on main 1.5" (3.81 cm) diameter copper tubing as well as smaller globe valves on 0.5" (1.27 cm) diameter bypass lines. These valves are used for both coarse and fine flow control. The lowest point in the water line has a drain valve which was used to drain the water at the end of each day's run. The heat absorbed by the water due to the energy input of the centrifugal pump was removed by a copper coil heat exchanger installed in the water collection tank. The heat removal medium was house service water whose flow rate could be adjusted by a globe valve. All water and air lines are made of 1.5" (3.81 cm) diameter copper tubing, except the two outlet lines from the test section which are 2" (5.08 cm) diameter copper tubing and all the bypass lines which are 0.5" (1.27 cm) diameter copper tubing.

The air supply is from an electrically driven air compressor rated for 192 SCFM air at 100 psi. It is located in an annex room to reduce the noise level in the experimental area. The compressed air passes through an oil separator, moisture separator, a pressure reducing valve and a check valve. It then enters the experimental area where the flow rate is measured with a calibrated orifice meter and is controlled by a globe valve on the main 1.5" (3.81 cm) diamter copper tubing, and a globe valve on the 0.5" (1.27 cm) diameter bypass line. Air then enters the mixing tee of either of the two test sections, depending on the positions of two air line ball valves (not shown in Fig. 2.1).

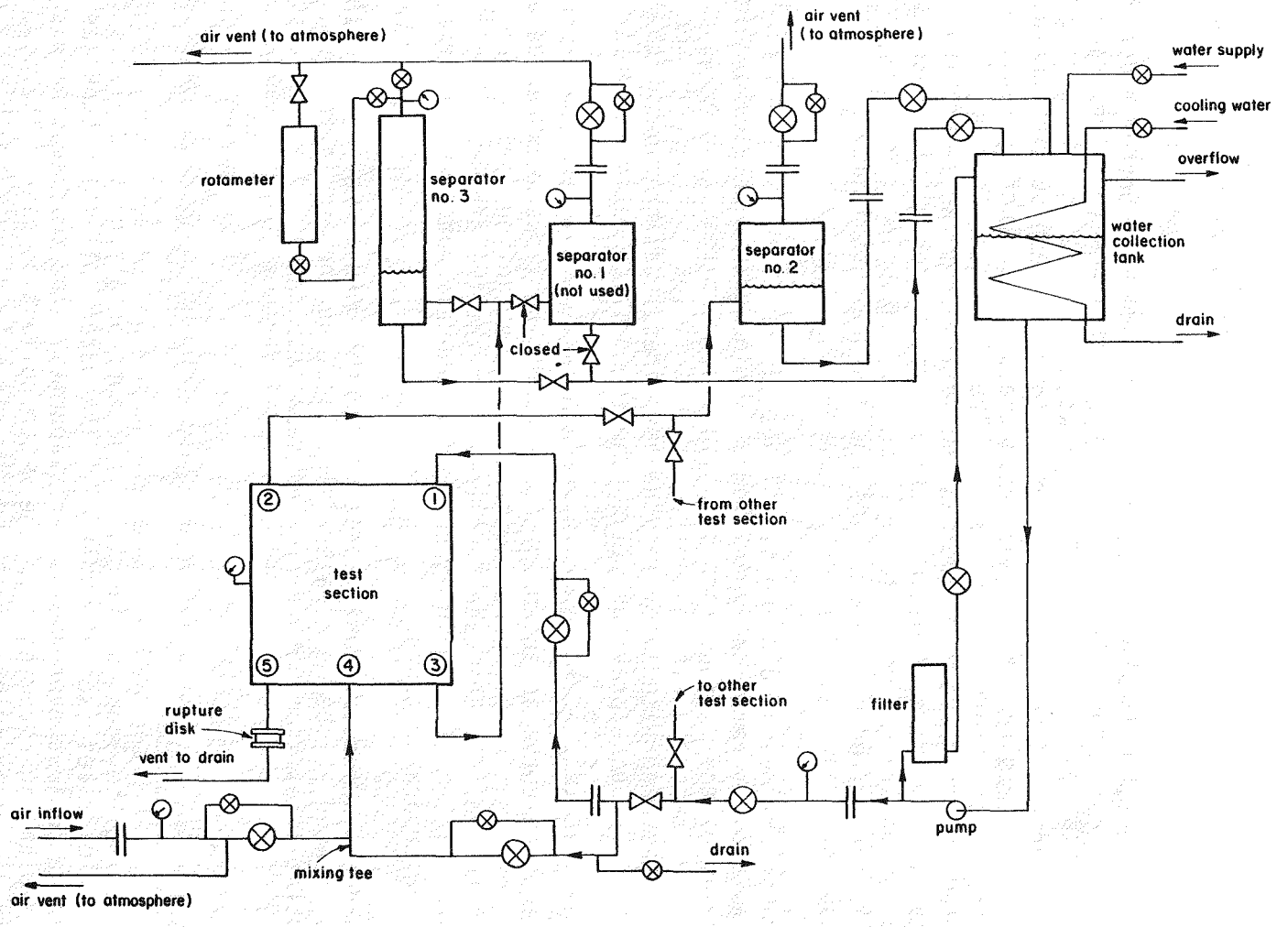


Figure 2.1 Air/water loop

The fluid exits the test section from outlet ports no. 2 and no. 3. The fluid is then piped into air/water separation tanks located above the test section area. Two inch (5.08 cm) diameter copper tubing is used for these discharge lines. Three air/water separation tanks are available. Two of these are for relatively larger air flow rates than the third. We used one of the larger tanks (separator no. 2 in Fig. 2.1) for the fluid exiting through outlet port no. 2 since most of the air comes out of the test section there. The fluid exiting through outlet port no. 3 was taken into the smaller air/water separator (no. 3 in Fig. 2.1), since the air flow from outlet no. 3 was very small.

After phase separation in the tanks, water exits from the bottom and air exits from the top of these tanks. The water exit lines (one from each tank) run parallel under the separation tanks, then up along the side of the water collection tank. Here the water flow was measured with calibrated orifice meters and then dumped into the water collection tank, where it returns to atmospheric pressure. The air passes through a demister to remove excessive moisture and then exits from the separation tank. Here its flow rate is measured using a calibrated orifice meter for the larger tank and a rotameter for the smaller tank. The flow rate from each tank is controlled by globe valves and its pressure is measured using pressure gauges.

The flow rates are measured using six flange tap orifice plates and one rotameter as shown schematically in Fig. 2.1. The orifice plates are located upstream of the various throttling valves. The resulting pressure differences are measured with U-tube manometers filled with mercury for the liquid lines, and with water for the air lines. Calibration of the orifice meters was done previously(1). One new orifice meter was installed for the flow going to inlet port no. 1, which was cross-calibrated with the already calibrated orifice meter on the main line near the pump. The cross-calibration curve is shown in Figure 2.2. The flows measured were the water flow at inlet port no. 1, the total water inflow (ie: inlet ports no. 1 and no. 4), the water outflows from the two air/water separator tanks, air inlet flow at inlet port no. 4 and air outflows from the two air/water separator tanks.

Fluid pressure was measured using pressure gauges. As shown in Fig. 2.1, these were located at the main water inlet line, at the air inlet line, at the air outlet lines from both air/water separator tanks and at the test section.

## 2.2 Operating the Loop

Before operating the loop, we installed the appropriate orifice plates for the desired flow rates (see Appendix-C). The water collection tank was then filled up to just over one-half of capacity. The test section was then filled with water coming from the water collection tank. The test section air and water inlet valves and the air exit valves from both air/water separation tanks were then closed. (The air/water separation tank water exit valves were always kept in an open state.) The water pump and the air compressor were then turned on. Due to the closed state of the inlet valves, there was no air or water flow through the test section at

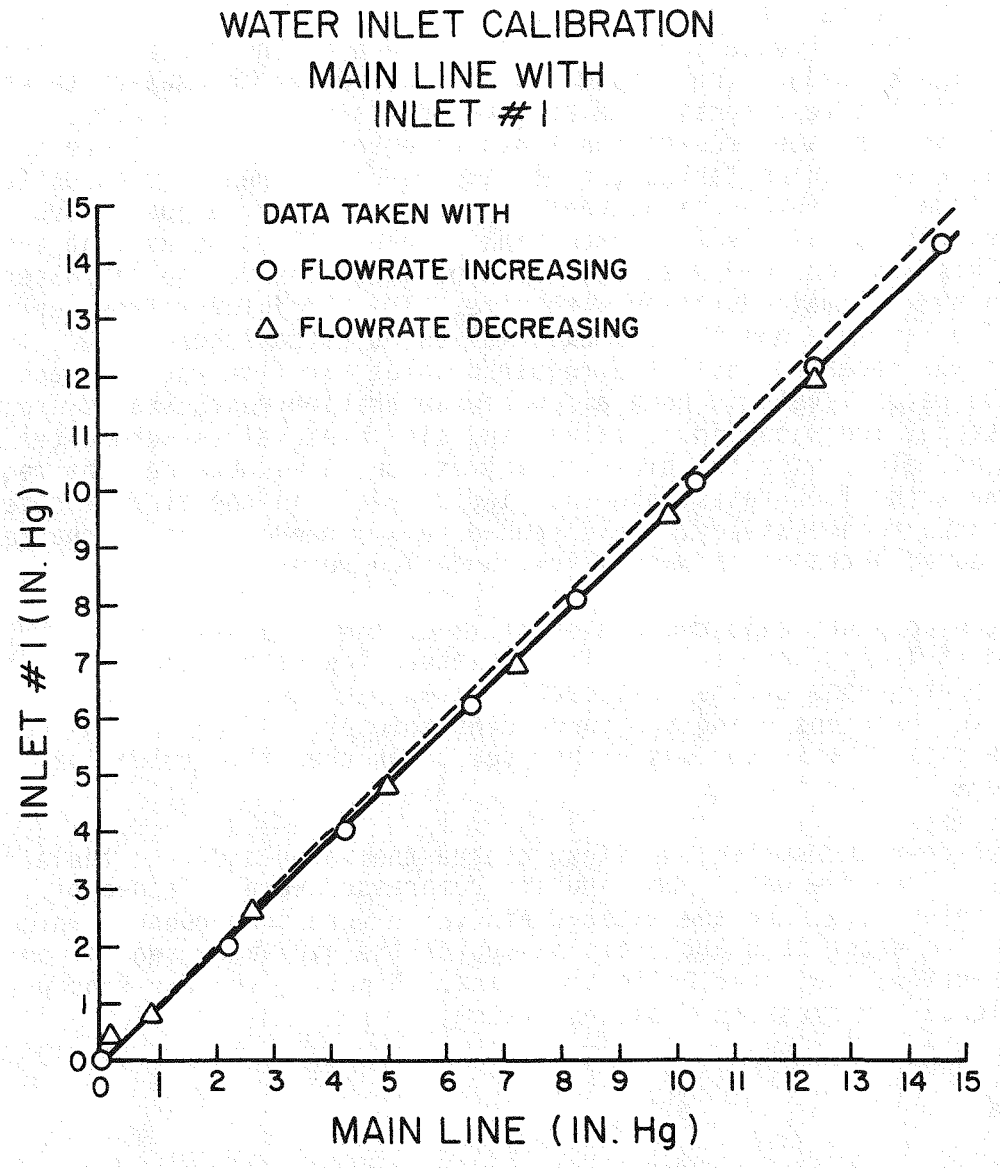


Figure 2.2 Cross calibration of main line with inlet no. 1

this stage. The entire water passing through the pump circulated through the water filter and went back to the water collection tank. The manometers connected to the water inlet lines were bled to remove any air bubbles that might be present in them. The water inlet valves at inlet ports no. 1 and no. 4 were then opened and flow through the test section brought to the required level, taking care that no valve was opened too rapidly to cause a pressure spike (ie: water hammer) in the test section.

The air inlet valves at inlet port no. 4, consisting of the one on the 1.5" (3.81 cm) diameter line, and the one on the 0.5" (1.27 cm) diameter bypass line were then opened a bit. This caused the air to start accumulating in the air/water separation tanks (due to the air exit valves on them being closed). The pressure in the air/water separation tanks, as well as in the test section, also started rising. So the air exit valves beyond the air/water separation tanks were opened. Since there are two air/water separation tanks, and air and water entered them at different rates from the test section, these valves have to be adjusted such that the quantity of air leaving each tank is about the same as that entering it. This was obtained when the level of water inside the air/water separation tanks remained steady with time. The air inlet valves were then opened a bit more and the air exit valves adjusted accordingly. This procedure was repeated until the required inlet air flow rate was achieved and the water levels in both air/water separation tanks stayed steady. At this stage, the water inlet valves and air inlet valves were alternately adjusted, along with the air exit valves, until we obtained the required air and water flow rates, and the liquid levels in the air/water separation tanks became steady. This procedure was needed since a change in air flow caused a change in water flow, and vice versa.

Once the loop was adjusted and stabilized, the data was taken. This consisted of taking the various air and water flow rates, pressures, high speed photographs of the test section flow regimes, and the chordal average void fractions using the gamma densitometer. After taking the appropriate data, the system was either set to another flow condition, or was shut down and drained.

To shut down the system, we first closed the water and then the air inlet valves. Then the water pump and air compressor were switched off. The water inlet valve and the water drain valve were then opened, which caused the water to start draining out of the air/water separation tanks, test section, and water collection tank. Finally, the air vent was opened to release air pressure from the system.

CHAPTER-3

## THE TWO-DIMENSIONAL TEST SECTION

A picture of the 2-D test section used for the experiment reported herein is shown in Fig. 3.1. The test section has inside dimensions of 36" X 36" X 0.5" (91.44 cm X 91.44 cm X 1.27 cm). The two-phase mixture can enter from ports no. 4 or no. 5 and the water enters from port no. 1. Ports no. 2 and no. 3 are exits. When port no. 4 was used as the two-phase inlet, port no. 5 was connected to a large diameter vent pipe through a carbon rupture disk which had a setting of 40 psi. This was a safety measure to prevent damage to the test section in case of accidental over-pressurization. If port no. 5 had been used as the two-phase inlet, the rupture disk and vent pipe would have been connected to port no. 4.

The test section consists essentially of a stainless steel frame with a sheet of one inch thick plexiglass bolted to it on either side. The frame consists of four stainless steel bars 0.5" (1.27 cm) thick and 1" (2.54 cm) wide welded together to form a square. Five slots, 4.5" (11.43 cm) long and 3/8" (0.9525 cm) wide with radius rounded ends (to make a total length of 4 $^{11}/_{16}$" [11.91 cm]) were made in the top and bottom bars to allow the fluid to enter and leave the test section. Stainless steel funnels were fabricated and welded to the frame to connect the rectangular slots to the circular piping. The top and bottom sides of the frame also had 0.25" (0.635 cm) wide and 0.25" (0.625 cm) deep slots made in them to accommodate 0.25" (0.625 cm) diameter rods. There were 71 such slots on each side, spaced one-half inch (1.27 cm) apart. Between the frame and the plexiglass sheets were placed 1/32" (0.0794 cm) thick volumoid gaskets to prevent leakage. Stainless steel straps were placed on the plexiglass sheets and bolts were passed through them. In this way, the plexiglass did not experience high stresses near the bolt holes and the amount of bowing under pessurization of the test section was reduced. To further reduce the bowing, two braces made of steel I-beams, 40" (101.6 cm) long, 2.5" (6.35 cm) wide and 4" (10.16 cm) high, were placed across the test section on either side, and bolted together, the bolts being outside the test section. Calculations made for the amount of bowing are shown in Appendix-A. The actual amount of bowing measured at different pressures is given in Table 5.8.

The 2-D test section was operated both with and without the 71 0.25" (0.625 cm) diameter stainless steel rods. These rods simulated the fuel rods inside a PWR core. As shown in Fig. 3.2, they were placed inside the test section by attaching brass blocks 0.25" X 0.25" X 0.5" (0.635 cm X 0.635 cm X 1.27 cm) to both ends of each rod. Each block had a 3/16" (0.476 cm) diameter hole drilled through it and both ends of the rod were reduced to this diameter and inserted into the block and held there by epoxy. The blocks then fit into the slots in the top and bottom bars of the test section frame.

It had been observed in an earlier test section(1) that the rods often vibrate during operation. In order to prevent flow-induced vibrations (FIV), and to simulate the effect of the grid spacers in the core, a stainless steel strip of width 3/8" (0.9525 cm) and thickness 1/32" (0.0794 cm) was placed across the rods and each rod was welded to it (Fig.

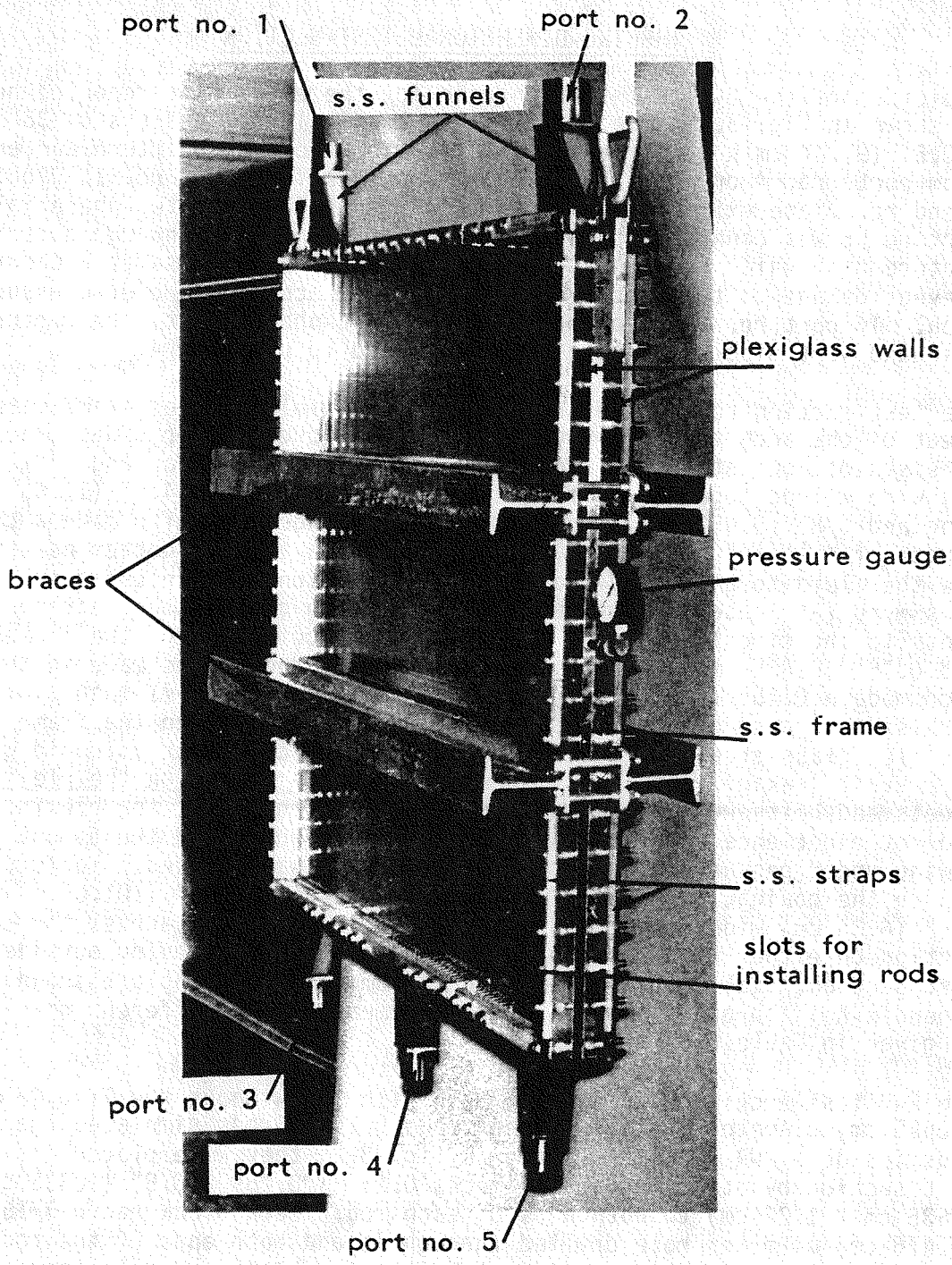


Figure 3.1 The two-dimensional test section

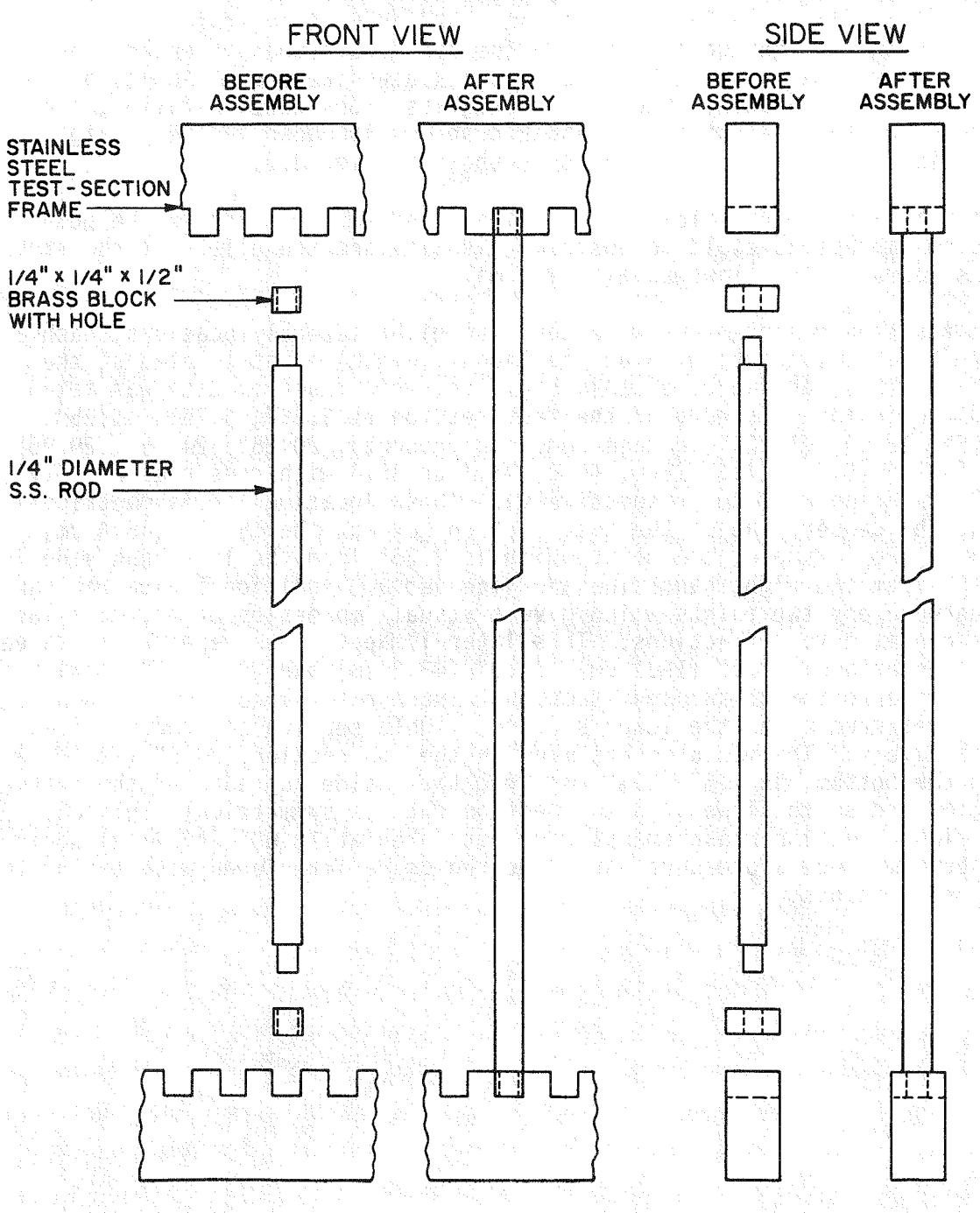


Figure 3.2 Arrangement for mounting the rods in the two-dimensional test section

3.3). The strip was then attached to the insides of the two vertical members of the test section frame by screws. This eliminates vibrations of the rods in the plane of the test section. To prevent vibrations perpendicular to this plane, stainless steel spacers were welded on the strip at four locations. The spacers were pieces of the same stainless steel strip [ie: 3/8" (0.9525 cm) wide and 1/32" (0.0794 cm) thick] and had a notch in them. They were placed on the strip such that it enters the notch and welded to it. The ends of the spacers were bent 90° to give a larger frontal surface. When the plexiglass sides were installed, these spacers pressed against small rubber cushions imbedded in the plexiglass for this purpose. This apparatus is shown in Fig. 3.3.

With this arrangment, flow-induced vibrations were reduced to the point that no vibrations could be observed visually and the effect of the strip and spacers on the flow was also minimal.

Void fraction measurements were taken at eight lateral locations, each 4.5" (11.43 cm) apart, with an additional (ninth) point located at the center. Thus, as can be seen in Fig. 3.4, void fraction data was taken from the inside left edge of the test section at 2.25", 6.75", 11.25", 15.75", 18.00" (18.25" in case rods are present), 20.25", 24.75", 29.25" and 33.75" (5.71, 17.1, 28.6, 40.0, 45.7 or 46.4 with rods present, 51.4, 62.9, 74.3 and 85.7 cm, respectively). These locations are symmetrical about the center line of the test section [except the 18.25" (46.4 cm) point]. For example, the point which is 2.25" from the left hand side is 33.75" from the right hand side and vice versa. Additional data was taken in between any two points which gave a visual impression of having a large difference in void fractions. This lateral mapping was repeated at three axial locations: 7.5" (19.1 cm), 17.0" (43.2 cm) and 28.5" (72.4 cm) from the inside bottom of the test section. These axial locations are henceforth referred to as the lower section, middle section and top section, respectively. The measurements made in the top section, 28.5" (72.4 cm) from the bottom, is 7.5" (19.1 cm) from the inside top edge of the test section and so the lower and top section data is symmetrically placed. The middle section measurements were not taken at 18.00" (45.7 cm) above the bottom since a pressure gauge located there interfered with taking the reference counts.

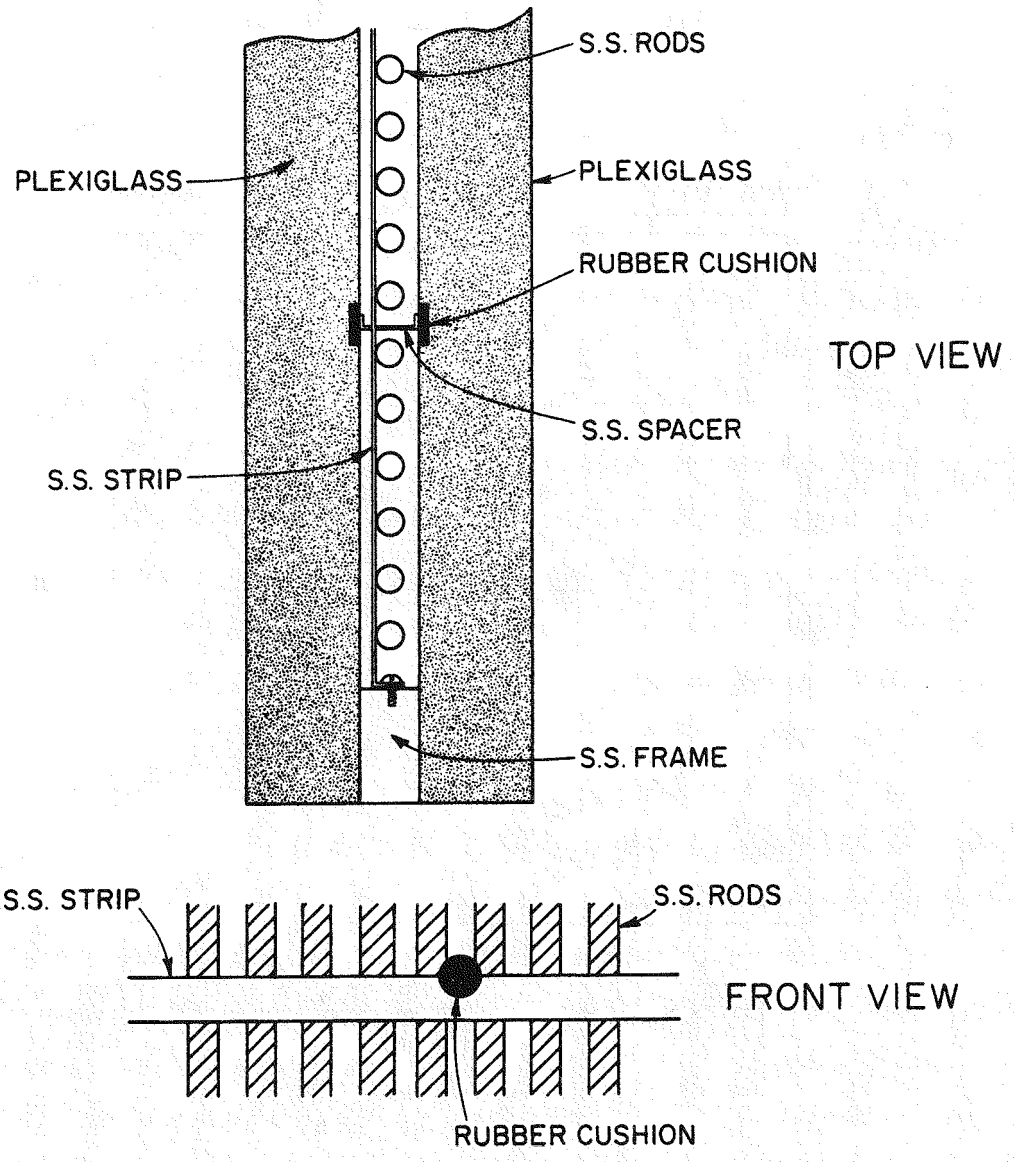


Figure 3.3 Arrangement for preventing flow-induced vibrations (FIV) of the rods

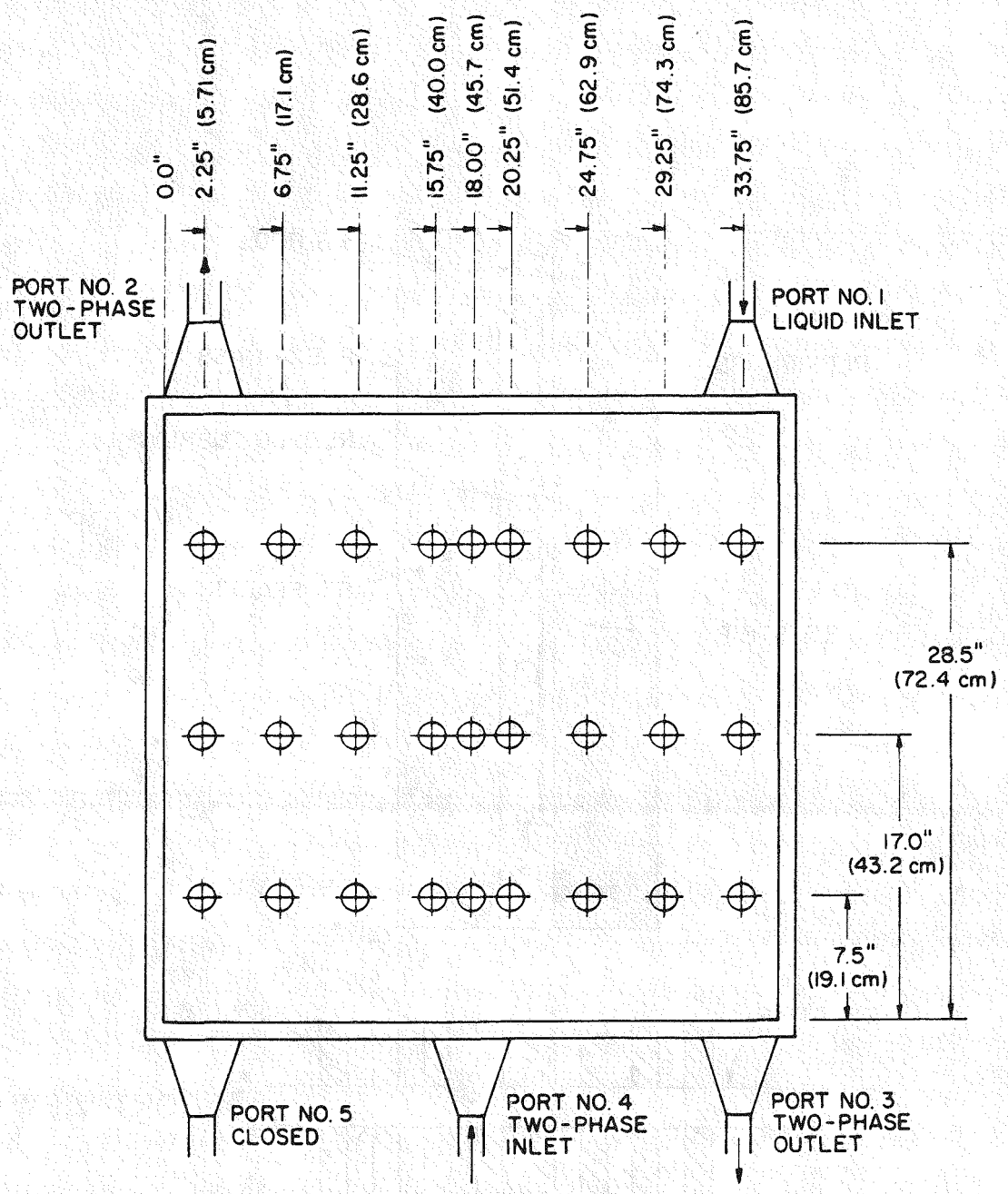


Figure 3.4 Locations in the test section where void-fraction data was taken

# CHAPTER-4

# THE GAMMA DENSITOMETER

## 4.1 Gamma Densitometry

In order to find the void fraction distribution within the 2-D test section, we used a single beam gamma ray attenuation technique. This was preferred since:

(i) it was non-intrusive and therefore did not affect the flow behavior,

(ii) it could be used to find the void fraction at any location in the test section without having to make an entry port available,

(iii) its accuracy can be quantified, and

(iv) a suitable system was already available.

The available system used a 5 Curie Cs-137 source contained in a cylindrical lead shield that had a collimator on one side. Within the cylindrical shield, the source could be moved and placed directly in front of the collimator hole, in which case a gamma ray beam emerges, or it could be moved away from the collimator, in which case it was safely shielded. Details of the shield and collimator design have been given previously(2) and thus will not be repeated herein.

As can be seen in Fig. 4.1, the source and shield are placed in front of the test section to be used such that the beam passes through the test section and the gamma rays are counted with a suitable radiation detector (eg: a photomultipler coupled to a NaI crystal).

The amount of attenuation that the photon beam undergoes between the source and the detector is due to that which takes place in the two plexiglass walls, in the water inside the test section, and to a much smaller degree, in the air inside and outside the test section.

For a monoenergetic, collimated beam of gamma rays, the beam intensity $I(z)$ (photons/sec-cm$^2$) at any depth $z$ (cm) in a given medium is,

$$I(z) = I_0 \exp(-\mu z)$$

where,

$I_0$ = intensity of beam at z=0 (ie: the intensity of beam incident on the medium),

$\mu$ = the macroscopic attentuation coefficient of the medium for gamma rays at the source energy (cm$^{-1}$).

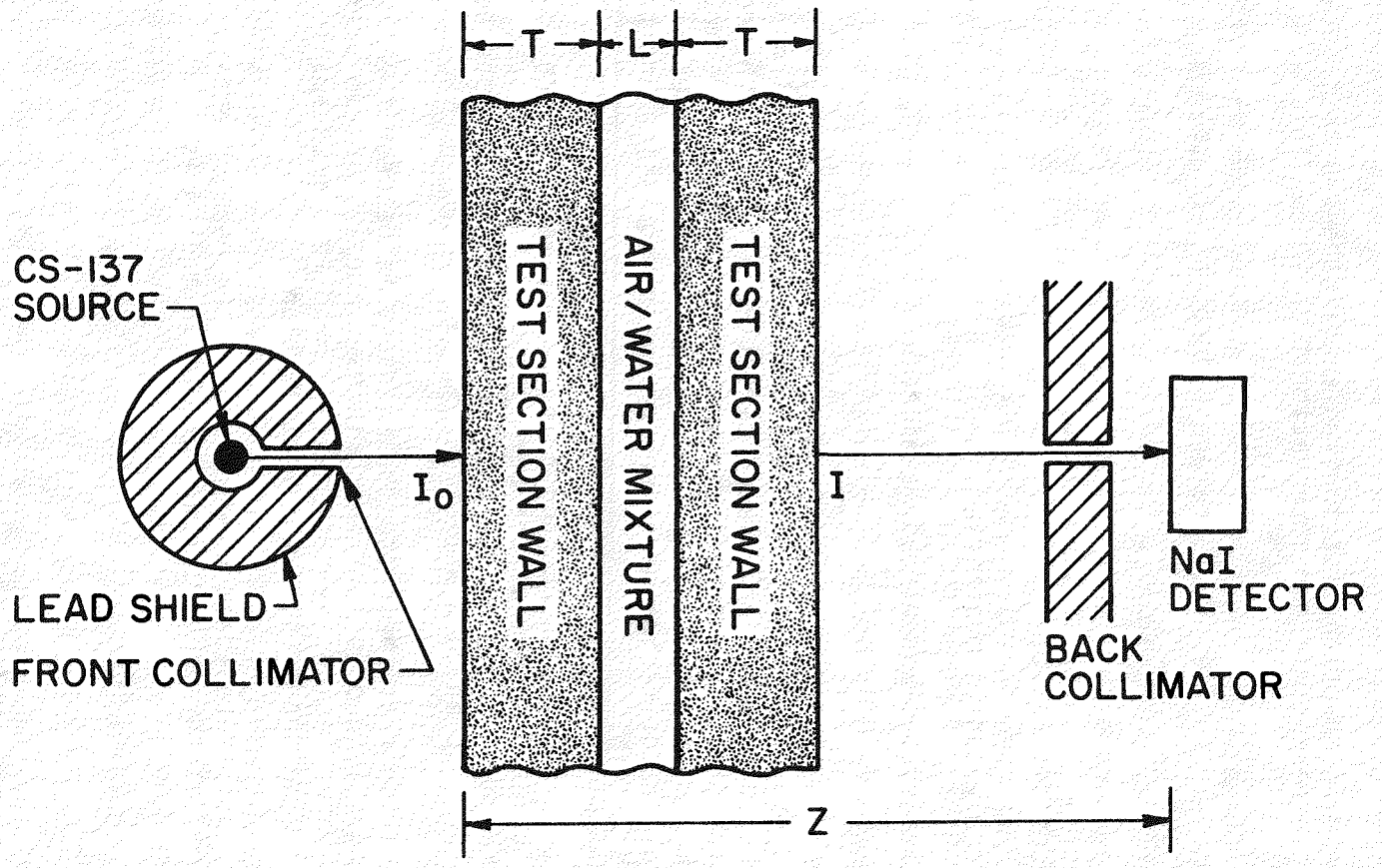


Figure 4.1 Source, test section and detector geometry

For a system consisting of more than one medium (and thus different attenuation coefficients), we have:

$$I(z) = I_o \exp\left(-\sum_{i=1}^{n} \mu_i z_i\right)$$

where,

$$z = \sum_{i=1}^{n} z_i ,$$

$\mu_i = \mu$ for the i-th component of the system,

$z_i$ = thickness of the i-th component of the system.

Since the test section consisted of two plexiglass walls, each of thickness T, and there was a two-phase mixture in between, we have (neglecting the attenuation in the air between the source and the detector):

$$I = I_o \exp -\left(2\mu_w T + \bar{\mu} L\right) \qquad (4.1)$$

where,

I = intensity of beam leaving the test section (photons/sec-cm$^2$),

$I_o$ = intensity of beam entering the test section (photons/sec-cm$^2$),

$\mu_w$ = macroscopic attentuation coefficient of plexiglass (cm$^{-1}$),

$\bar{\mu}$ = macroscopic attentuation coefficient of the two-phase mixture (cm$^{-1}$),

T = thickness of each plexiglass wall (cm),

L = channel thickness (cm).

For a well mixed two-phase flow, we have:

$$\bar{\mu} = \bar{\alpha}\, \mu_g + (1-\bar{\alpha})\, \mu_\ell$$

or,

$$\bar{\mu} = \mu_\ell + \bar{\alpha}(\mu_g - \mu_\ell) \qquad (4.2)$$

where,

$\bar{\alpha}$ = chordal-average void fraction

$\mu_g$ = macroscopic attenuation coefficient for air ($cm^{-1}$),

$\mu_\ell$ = macroscopic attenuation coefficient for water ($cm^{-1}$).

Combining equations (4.1) and (4.2),

$$I = I_o \exp(-2\mu_w T) \exp[-(\mu_\ell + \bar{\alpha}(\mu_g - \mu_\ell))L] \quad (4.3)$$

Since the thickness of the plexiglass walls, T, may vary slightly across the test section, it is best to eliminate the $\mu_w T$ term from Eq. (4.3). In the process, we can also eliminate all the attenuation coefficient and channel thickness terms. To do this, we set $\bar{\alpha} = 0$ and $\bar{\alpha} = 1$ in Eq. (4.3) to get:

$$\bar{\alpha} = 0: \quad I_\ell = I_o \exp(-2\mu_w T) \exp(-\mu_\ell L) \quad (4.4a)$$

$$\bar{\alpha} = 1: \quad I_g = I_o \exp(-2\mu_w T) \exp(-\mu_g L) \quad (4.4b)$$

where,

$I_\ell$ = the intensity for the case of $\bar{\alpha} = 0$ (ie: test section is full of water),

$I_g$ = the intensity for the case of $\bar{\alpha} = 1$ (ie: test section is full of air).

Dividing Eq. (4.4b) by Eq. (4.4a) we get:

$$I_g/I_\ell = \exp[(\mu_\ell - \mu_g)L] \quad (4.5)$$

Combining Eqs. (4.3), (4.4) and (4.5) gives,

$$\bar{\alpha} = \frac{\ln (I/I_\ell)}{\ln (I_g/I_\ell)} \quad (4.6)$$

Thus, in order to determine the void fraction at a given location, we must find the intensity of the beam emerging from the test section in conditions when the test section is full of air ($I_g$), full of water ($I_\ell$), and has a two-phase mixture flowing in it (I). In practice, we must take each of these at each location of interest. Since this takes considerable time (about 2 hours for each of the $I_g$, $I_\ell$ and I readings at an axial location across the test section), and we normally run the system for several different void fractions, data was taken over a period of several months. At the end of each day, the source was re-inserted into the shield and pulled out in front of the collimator the next. Since it is possible that the source does not come back to exactly the same location every time, we could have a different initial intensity ($I_o$) each day. Moreover, during the period of each experiment, there could be drift in the count rate due to changes in temperature, humidity and high voltage drift.

To take such effects into account, we used "normalized intensities" defined as:

$$I' \triangleq I/I_{ref}$$

$$I'_\ell \triangleq I_\ell/I_{\ell ref}$$

$$I'_g \triangleq I_g/I_{gref}$$

Where $I_{ref}$, $I_{\ell ref}$ and $I_{gref}$ are intensities at the reference location (outside the test section) when I, $I_\ell$ and $I_g$ readings were being taken, respectively. Since the reference counts are taken outside the test section, they are almost the same as $I_o$. That is, from Fig. 4.1, we have,

$$I_{ref} = I_o \exp(-\mu_{air}Z)$$

Since $\mu_{air}Z$ is a constant, no matter what the flow inside the test section, and no matter what the $I_o$ is, we have,

$$I_{ref} \propto I_o$$

or, using C as the constant of proportionality,

$$I_o = I_{ref}/C$$

Replacing $I_o$ by $I_{ref}/C$ in Eqs. (4.3) and (4.4) we obtain,

$$I = (I_{ref}/C) \exp(-2\mu_w T) \exp[-(\mu_\ell + \bar{\alpha}(\mu_g - \mu_\ell))L] \quad (4.7a)$$

$$I_\ell = (I_{\ell ref}/C) \exp(-2\mu_w T) \exp(-\mu_\ell L) \quad (4.7b)$$

$$I_g = (I_{gref}/C) \exp(-2\mu_w T) \exp(-\mu_g L) \quad (4.7c)$$

Dividing Eq. (4.7c) by (4.7b),

$$I_g/I_\ell = (I_{gref}/I_{\ell ref}) \exp[-(\mu_g - \mu_\ell)L] \quad (4.8)$$

Equation (4.7a) can be written as,

$$I = (I_{ref}/C) \exp(-2\mu_w T) \exp(-\mu_\ell L) \{\exp[-(\mu_g - \mu_\ell)L]\}^{\bar{\alpha}}$$

Using Eq. (4.7b), we get,

$$I = (I_{ref}/C) (I_\ell C/I_{\ell ref}) \{\exp[-(\mu_g - \mu_\ell)L]\}^{\bar{\alpha}}$$

Now using Eq. (4.8), we have,

$$I = (I_{ref}/C)\ (I_\ell C/I_{\ell ref})\ \{(I_g/I_\ell)\ (I_{\ell ref}/I_{gref})\}^{\bar{\alpha}}$$

or,

$$I/I_{ref} = (I_\ell/I_{\ell ref})\ \{(I_g/I_{gref})\ (I_{\ell ref}/I_\ell)\}^{\bar{\alpha}}$$

or,

$$I'/I'_\ell = \{I'_g/I'_\ell\}^{\bar{\alpha}}$$

Taking the natural logarithm of both sides,

$$\ln(I'/I'_\ell) = \bar{\alpha}\ \ln\ (I'_g/I'_\ell)$$

or,

$$\bar{\alpha} = \frac{\ln(I'/I'_\ell)}{\ln(I'_g/I'_\ell)} \tag{4.9}$$

Since the normalized intensities are independent of $I_0$, we can combine data taken on different days and use Eq. (4.9) to calculate $\bar{\alpha}$. In this way, we can measure $I'_\ell$ and $I'_g$, the normalized intensities with water and air in the test section, respectively, once and use the same values repeatedly for different flows in the test section.

## 4.2 Error Analysis

Let us rewrite Eq. (4.9) as,

$$\bar{\alpha} = \frac{\ln[(I/I_\ell)\ (I_{\ell ref}/I_{ref})]}{\ln[(I_g/I_\ell)\ (I_{\ell ref}/I_{gref})]} \tag{4.10}$$

Applying the formula for propagation of errors,(5)

$$\begin{aligned}(\Delta\bar{\alpha})^2 = {} & (\partial\bar{\alpha}/\partial I)^2\ (\Delta I)^2 + (\partial\bar{\alpha}/\partial I_\ell)^2\ (\Delta I_\ell)^2 + (\partial\bar{\alpha}/\partial I_g)^2\ (\Delta I_g)^2 \\ & + (\partial\bar{\alpha}/\partial I_{ref})^2\ (\Delta I_{ref})^2 + (\partial\bar{\alpha}/\partial I_{\ell ref})^2\ (\Delta I_{\ell ref})^2 \\ & + (\partial\bar{\alpha}/\partial I_{gref})^2\ (\Delta I_{gref})^2.\end{aligned}$$

Dividing through by $\bar{\alpha}^2$, we obtain,

$$(\Delta\bar{\alpha}/\bar{\alpha})^2 = (\partial\alpha/\partial I)^2 (\Delta I/\bar{\alpha})^2 + (\partial\alpha/\partial I_\ell)^2 (\Delta I_\ell/\bar{\alpha})^2$$

$$+ (\partial\bar{\alpha}/\partial I_g)^2 (\Delta I_g/\bar{\alpha})^2 + (\partial\bar{\alpha}/\partial I_{ref})^2 (\Delta I_{ref}/\bar{\alpha})^2$$

$$+ (\partial\bar{\alpha}/\partial I_{\ell ref})^2 (\Delta I_{\ell ref}/\bar{\alpha})^2 + (\partial\bar{\alpha}/\partial I_{gref})^2 (\Delta I_{gref}/\bar{\alpha})^2 \qquad (4.11)$$

From Eq. (4.10),

$$\partial\bar{\alpha}/\partial I = \frac{1}{I} \frac{1}{\ln(I'_g/I'_\ell)} \qquad (4.12a)$$

$$\partial\bar{\alpha}/\partial I_\ell = \frac{\ln(I'/I'_g)}{I_\ell[\ln(I'_g/I_\ell)]^2} \qquad (4.12b)$$

$$\partial\bar{\alpha}/\partial I_g = \frac{-\ln(I'/I'_\ell)}{I_g[\ln(I'_g/I'_\ell)]^2} \qquad (4.12c)$$

$$\partial\bar{\alpha}/\partial I_{ref} = \frac{-1}{I_{ref} \ln(I'_g/I'_\ell)} \qquad (4.12d)$$

$$\partial\bar{\alpha}/\partial I_{\ell ref} = \frac{\ln(I'_g/I')}{I_{\ell ref}[\ln(I'_g/I'_\ell)]^2} \qquad (4.12e)$$

$$\partial\bar{\alpha}/\partial I_{gref} = \frac{\ln(I'/I'_\ell)}{I_{gref}[\ln(I'_g/I'_\ell)]^2} \qquad (4.12f)$$

Combining Eqs. (4.12a)-(4.12f) with Eq. (4.11):

$$\left(\frac{\partial\bar{\alpha}}{\bar{\alpha}}\right)^2 = \frac{1}{I^2\left[\ln\left(I'_g/I'_\ell\right)\right]^2}\left[\frac{\Delta I}{\bar{\alpha}}\right]^2 + \frac{\left[\ln\left(I'/I'_g\right)\right]^2}{I_\ell^2\left[\ln\left(I'_g/I'_\ell\right)\right]^4}\left[\frac{\Delta I_\ell}{\bar{\alpha}}\right]^2$$

$$+ \frac{\left[\ln\left(I'/I'_\ell\right)\right]^2}{I_g^2\left[\ln\left(I'_g/I'_\ell\right)\right]^4}\left[\frac{\Delta I_g}{\bar{\alpha}}\right]^2 + \frac{1}{I_{ref}^2\left[\ln\left(I'_g/I'_\ell\right)\right]^2}\left[\frac{\Delta I_{ref}}{\bar{\alpha}}\right]^2$$

$$+ \frac{\left[\ln\left(I'_g/I'\right)\right]^2}{I_{\ell ref}^2\left[\ln\left(I'_g/I'_\ell\right)\right]^4}\left[\frac{\Delta I_{\ell ref}}{\bar{\alpha}}\right]^2 + \frac{\left[\ln\left(I'/I'_\ell\right)\right]^2}{I_{gref}^2\left[\ln\left(I'_g/I'_\ell\right)\right]^4}\left[\frac{\Delta I_{gref}}{\bar{\alpha}}\right]^2 \qquad (4.13a)$$

Noting Eq. (4.9), and that:

$$\bar{\alpha} - 1 = \frac{\ln\left(I'/I'_g\right)}{\ln\left(I'_g/I'_\ell\right)}$$

or,

$$1 - \bar{\alpha} = \frac{\ln\left(I'_g/I'\right)}{\ln\left(I'_g/I'_\ell\right)}$$

we can simplify Eq. (4.13a) to:

$$\left(\frac{\partial\bar{\alpha}}{\bar{\alpha}}\right)^2 = \left[\frac{\Delta I}{I}\right]^2 \frac{1}{\bar{\alpha}^2\left[\ln\left(I'_g/I'_\ell\right)\right]^2} + \left[\frac{\Delta I_\ell}{I_\ell}\right]^2 \frac{\left(\bar{\alpha} - 1\right)^2}{\bar{\alpha}^2\left[\ln\left(I'_g/I'_\ell\right)\right]^2}$$

$$+ \left[\frac{\Delta I_g}{I_g}\right]^2 \frac{1}{\left[\ln\left(I'_g/I'_\ell\right)\right]^2} + \left[\frac{\Delta I_{ref}}{I_{ref}}\right]^2 \frac{1}{\bar{\alpha}^2\left[\ln\left(I'_g/I'_\ell\right)\right]^2}$$

$$+ \left[\frac{\Delta I_{\ell ref}}{I_{\ell ref}}\right]^2 \frac{\left(1 - \bar{\alpha}\right)^2}{\bar{\alpha}^2\left[\ln\left(I'_g/I'_\ell\right)\right]^2} + \left[\frac{\Delta I_{gref}}{I_{gref}}\right]^2 \frac{1}{\left[\ln\left(I'_g/I'_\ell\right)\right]^2} \qquad (4.13b)$$

Now since the magnitudes of I, $I_\ell$ and $I_g$ are similar, and the magnitudes of $I_{ref}$, $I_{\ell ref}$ and $I_{gref}$ are also similar, and provided that the only source of error in these measurements is due to statistical fluctuations of the gamma ray source* we have,

$$\Delta I/I \simeq \Delta I_\ell/I_\ell \simeq \Delta I_g/I_g \tag{4.14a}$$

and,

$$\Delta I_{ref}/I_{ref} \simeq \Delta I_{\ell ref}/I_{\ell ref} \simeq \Delta I_{gref}/I_{gref} \tag{4.14b}$$

Substituting Eqs. (4.14) into Eq. (4.13b),

$$\left(\frac{\Delta\bar{\alpha}}{\bar{\alpha}}\right)^2 = \left(\frac{\Delta I}{I}\right)^2 \frac{[1 + (\bar{\alpha}-1)^2 + \bar{\alpha}^2]}{\bar{\alpha}^2 [\ln(I_g'/I_\ell')]^2} + \left(\frac{\Delta I_{ref}}{I_{ref}}\right)^2 \frac{[1 + (1-\bar{\alpha})^2 + \bar{\alpha}^2]}{\bar{\alpha}^2 [\ln(I_g'/I_\ell')]^2}$$

or,

$$\Delta\bar{\alpha}/\bar{\alpha} = \frac{[2(1 - \bar{\alpha} + \bar{\alpha}^2)]^{1/2}}{\bar{\alpha} \ln(I_g'/I_\ell')} \left[(\Delta I/I)^2 + (\Delta I_{ref}/I_{ref})^2\right]^{1/2}$$

This equation can be used to find the relative error in the chordal averaged void fraction. This equation differs from a similar result obtained previously(1) in that it contains a

$$(\Delta I_{ref}/I_{ref})^2$$

term.

Since, during the experiment we actually count the number of photons entering the detector over a time interval t, we can replace I, $I_\ell$, $I_g$, $I_{ref}$, $I_{\ell ref}$, and $I_{gref}$ by N, $N_\ell$, $N_g$, $N_{ref}$, $N_{\ell ref}$ and $N_{gref}$, respectively, where $N_i$ are the number of counts obtained over the time interval t. We thus have,

$$\bar{\alpha} = \frac{\ln[(N/N_\ell)\ (N_{\ell ref}/N_{ref})]}{\ln[(N_g/N_\ell)\ (N_{\ell ref}/N_{gref})]} \tag{4.15a}$$

*This is true if counting is done for a time period that is long compared to fluctuations in the flow structure.

and,

$$\Delta\bar{\alpha}/\bar{\alpha} = \frac{[2(1 - \bar{\alpha} + \bar{\alpha}^2)]^{1/2}}{\bar{\alpha}\ \ln[(N_g/N_\ell)\ (N_{\ell ref}/N_{gref})]} \left[\left(\frac{\Delta N}{N}\right)^2 + \left(\frac{\Delta N_{ref}}{N_{ref}}\right)^2\right]^{1/2} \qquad (4.15b)$$

where,

$N$ = counts observed over a time interval t when there is a two-phase mixture in the test section,

$N_\ell$ = counts for the same time interval with liquid in test section,

$N_g$ = counts for the same time interval with air in test section,

$N_{ref}$ = counts for the same time interval at reference location (while taking two-phase data),

$N_{\ell ref}$ = counts for the same time interval at reference location (while taking water data),

$N_{gref}$ = counts for the same time interval at reference location (while taking air data),

$\Delta N$ = error in the counts N,

$\Delta N_{ref}$ = error in the counts at the reference location, $N_{ref}$.

Here it has been assumed that,

$$\Delta N/N \simeq \Delta N_\ell/N_\ell \simeq \Delta N_g/N_g$$

and,

$$\Delta N_{ref}/N_{ref} \simeq \Delta N_{\ell ref}/N_{\ell ref} \simeq \Delta N_{gref}/N_{gref}$$

In the present work, Eq. (4.15a) has been used to find the chordal average void fraction, $\bar{\alpha}$, and Eq. (4.15b) has been used to find the relative error in the void fraction, $\Delta\bar{\alpha}/\bar{\alpha}$. It is seen that the relative error depends on the void fraction itself and on the total counts obtained in the time interval over which counting is done. In order to reduce the relative error, we have to try to increase the denominator and/or decrease the numerator in Eq. (4.15b). The term $(N_g/N_\ell)(N_{\ell ref}/N_{gref})$ in the denominator is fixed by the geometry of the system, specifically by the channel width L, and the attenuation coefficients of water and air. Thus, for a given void fraction, we can only improve the relative error by reducing the values of $\Delta N/N$ and $\Delta N_{ref}/N_{ref}$.

If the only, or dominant, source of the errors $\Delta N$ and $\Delta N_{ref}$ is due to statistical fluctuations in the gamma ray source, then this can be achieved by increasing the values of N and $N_{ref}$. Since the counting rates,

$$C = N/t,\ C_g = N_g/t,\ C_\ell = N_\ell/t$$

and

$$C_{ref} = N_{ref}/t$$

are fixed by the geometry and void fraction, the only way to increase N and $N_{ref}$ for a given void fraction is by increasing the counting time. Using,

$$\Delta N = \sqrt{N}$$

and,

$$\Delta N_{ref} = \sqrt{N_{ref}}$$

we can rewrite Eq. (4.15b) as,

$$\Delta\bar{\alpha}/\bar{\alpha} = \frac{[2(1 - \bar{\alpha} + \bar{\alpha}^2)]^{1/2}}{\bar{\alpha}\ \ln(C'_g/C'_\ell)} \left[1/Ct + 1/C_{ref}t\right]^{1/2} \qquad (4.16)$$

where,

$C$ = count rate for two-phase mixture, = N/t (counts/sec),

$C_{ref}$ = count rate in the reference position, = $N_{ref}/t$ (counts/sec),

$C'_g$ = normalized counts with air in test section = $C_g/C_{gref}$,

$C_\ell$ = normalized counts with water in test section = $C_\ell/C_{\ell ref}$.

Eq. (4.16) relates the relative error in the chordal average void fraction, $\Delta\bar{\alpha}/\bar{\alpha}$, based on the statistical fluctuations of the gamma ray source, to the time interval, t, over which the counting is done. In order to determine the counting interval required to obtain an acceptably low error in the void fraction, the following analysis is performed.

The count rates with air and water in the test section, $C_g$ and $C_\ell$, and the count rate at the reference location outside the test section, $C_{ref}$, were determined several times and typical values are given below:

$C_g \approx 37{,}000$ counts/sec.

$C_\ell \approx 34{,}000$ counts/sec.

$C_{ref} \approx 51{,}000$ counts/sec.

Using the equation,

$$\bar{\alpha} = \frac{\ln(C/C_\ell)}{\ln(C_g/C_\ell)}$$

we get,

$$C = C_\ell \exp[\bar{\alpha} \ln(C_g/C_\ell)]$$

which can be used to get the values of C for various values of $\bar{\alpha}$. These values of $C_g$, $C_\ell$, $C_{ref}$ and C can then be used to calculate the relative error in the void fraction for different values of counting time, t, by using Eq. (4.16). The results obtained are listed in Table 4.1.

A consideration of the relative error as seen from Table 4.1, of the inherent fluctuations in two-phase flow (see section 5.2), and of time limitations, led us to choose a counting interval of six (6) minutes. This was done in the experiment by taking two 3 minute counts (to prevent counter overflow) and ensemble averaging.

In actual practice we also get a certain amount of error due to detector drift caused by voltage fluctuations, and temperature and humidity variations. That is, the electronics introduced errors which were not due to statistical fluctations. We observed that the error due to detector drift could be significant compared to the error due to statistical fluctuations of the source and therefore proceeded both to measure it and to reduce its impact.

The total error (due to statistical fluctuations, detector drift and inherent fluctuations in the two-phase flow) can still be represented by Eq. (4.15b) provided the relative errors in the measurements of N, $N_\ell$ and $N_g$ and of $N_{ref}$, $N_{\ell ref}$ and $N_{gref}$ are similar so that the assumptions in Eq. (4.14) are valid. If each of the counts are taken n times, and denoted by $N_i$ and $N_{refi}$, then the errors in the average values of the counts, $\Delta N$ and $\Delta N_{ref}$ are:

$$\Delta N = \pm \sqrt{\frac{\sum_{i=1}^{n} (N_i - \bar{N})^2}{n(n-1)}} \qquad (4.17a)$$

Table 4.1 Representative values of $\Delta\bar{\alpha}/\bar{\alpha}$ due to statistical fluctuations for selected values of $\bar{\alpha}$ and counting intervals

| Counting interval t | ± Δα/α for void fraction ($\bar{\alpha}$) of: | | | | | |
|---|---|---|---|---|---|---|
| | 0.05 | 0.1 | 0.2 | 0.5 | 0.8 | 0.10 |
| 30 sec | 0.417 | 0.203 | 0.0975 | 0.0366 | 0.0240 | 0.0208 |
| 1 min | 0.295 | 0.144 | 0.0689 | 0.0258 | 0.0170 | 0.0147 |
| 2 min | 0.208 | 0.102 | 0.0487 | 0.0183 | 0.0120 | 0.0104 |
| 3 min | 0.170 | 0.0830 | 0.0398 | 0.0149 | 0.00980 | 0.00851 |
| 4 min | 0.147 | 0.0719 | 0.0345 | 0.0129 | 0.00849 | 0.00737 |
| 5 min | 0.132 | 0.0643 | 0.0308 | 0.0116 | 0.00759 | 0.00659 |
| 6 min | 0.120 | 0.0587 | 0.0281 | 0.0105 | 0.00693 | 0.00602 |
| 7 min | 0.111 | 0.0544 | 0.0260 | 0.00977 | 0.00642 | 0.00557 |
| 8 min | 0.104 | 0.0508 | 0.0244 | 0.00914 | 0.00600 | 0.00521 |
| 9 min | 0.0982 | 0.0479 | 0.0230 | 0.00862 | 0.00566 | 0.00491 |
| 10 min | 0.0932 | 0.0455 | 0.0218 | 0.00818 | 0.00537 | 0.00466 |

and,

$$\Delta N_{ref} = \pm \sqrt{\frac{\sum_{i=1}^{n} (N_{refi} - \overline{N}_{ref})^2}{n(n-1)}} \qquad (4.17b)$$

where,

$\overline{N}$ = average value of $N = (1/n) \sum_{i=1}^{n} N_i$

$\overline{N}_{ref}$ = average value of $N_{ref} = (1/n) \sum_{i=1}^{n} N_{refi}$

We took, for several flow conditions, six (6) values of N at a number of locations in the middle section and $N_{ref}$. Each value of N was recorded for a period of one minute so that the total time was still six minutes. Table 5.5 has some of the results for errors. It gives values of $\overline{\alpha}$, $\Delta\overline{\alpha}/\overline{\alpha}$ for error due to statistical fluctuations alone, and error based on Eqs. (4.15b) and (4.17) (total error). The total error in $\Delta\overline{\alpha}/\overline{\alpha}$ then includes the effects of statistical fluctuations, detector drift, fluctuations in the flow and dynamic error associated with taking measurements in the count mode rather than in the current mode(2).

In order to minimize the effect of detector drift on the results, reference counts were taken before and after each data count. The reference counts were taken at a fixed location outside the test section, at a distance sufficiently far away from it to avoid counting any scattered gamma rays from the test section. If the two reference counts are denoted by $N_{r1}$ and $N_{r2}$, and the two data counts taken through the test section are $N_1$ and $N_2$, then the normalized counts were,

$$N' = (N_1 + N_2) / (N_{r1} + N_{r2})$$

The reference and data counts were taken in the sequence: $N_{r1}$, $N_1$, $N_2$, $N_{r2}$. In this way, if the detector drift is linear over a period of about 15 minutes (time required to take the four 3 minute counts), then the effect of the drift on the normalized counts is minimal.

## 4.3 Detector Characteristics

The detection system consisted of a 2" (5.08 cm) diameter NaI crystal with a photomultiplier, preamplifier, amplifier, discriminator, counter, timer and power supply as shown in Fig. 4.2. A typical plot of the count rate versus energy for photons from the 5 Ci Cs-137 source is shown in Fig. 4.3. In order to count only those photons that reach the detector without having undergone any interaction on the way, we counted only those photons that deposited energy within the photoelectric peak. As can be seen from Fig. 4.3, this was done by setting the window of the scalar between $V_1$ and

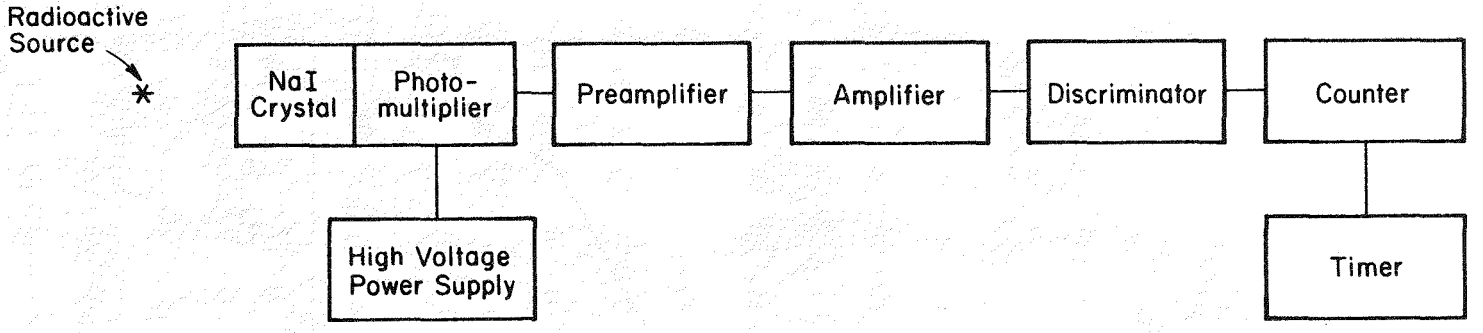


Figure 4.2 The NaI photomultiplier detection system used for counting gamma rays

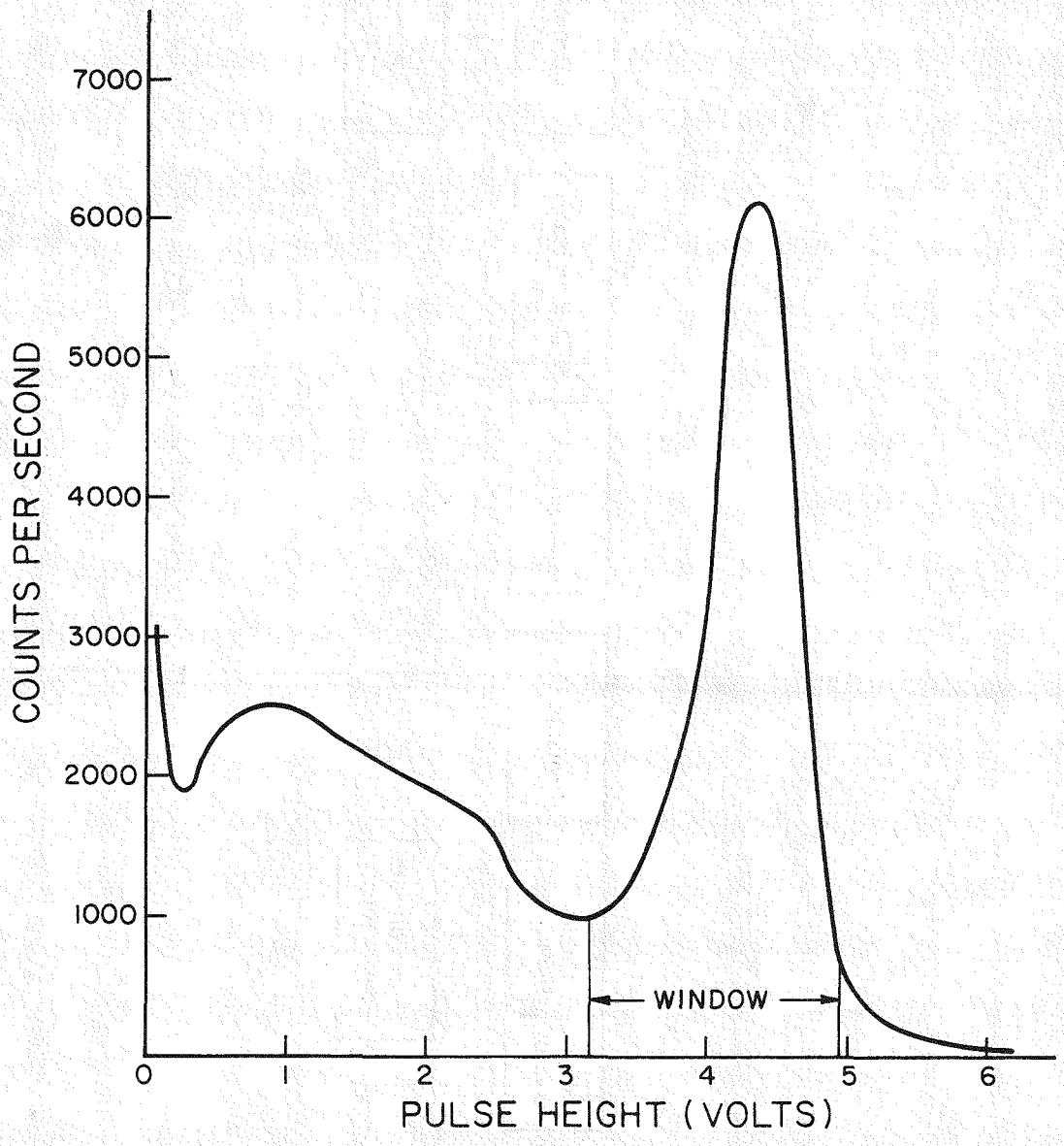


Figure 4.3 A typical pulse height spectrum obtained for the Cs-137 source

$V_2$. An obvious disadvantage of doing this is that the count rate is lower and we have to count for a longer time. However, this avoided the counting of multiple scattered gamma rays and we did not have to apply the buildup factor correction.

## 4.4 Dead Time Correction

Due to the high count rate (~2 million counts per minute), the dead time error must be considered. We determined the dead time by the two source method and found it to be 3 microseconds (see Table 5.1). All measured counts were then corrected by using(3),

$$N_c = N/(1 - \tau N/t)$$

where,

$N_c$ = corrected counts in time interval t,

N = measured counts in time interval t,

$\tau$ = dead time in seconds,

t = counting time interval in seconds.

It was found that although applying the dead time correction increases the measured counts by about 10%, it didn't effect the value of the void fraction $\overline{\alpha}$ by more than a few percent. This is because the effect is almost cancelled out in the numerator and denominator terms of Eq. (4.15a). Its use does, however, reduce the relative error $\Delta\overline{\alpha}/\overline{\alpha}$ since in Eq. (4.15b) the ratio $N_g/N_\ell$ increases and $\Delta N/N$ and $\Delta N_{ref}/N_{ref}$ decrease by the use of the dead time correction.

## 4.5 Aligning the Gamma Densitometer to Edge of the Test Section

Whenever we moved the gamma densitometer vertically (eg: when we went from the middle section to the top section), we had to determine the lateral location of the gamma densitometer with respect to the test section so that we knew exactly where we were taking data. This was done by using the gamma densitometer itself.

Counts were taken while moving the densitometer closer to the edge. As soon as the gamma-ray beam started entering the steel frame of the test section, the count rate dropped dramatically. Counts versus position was plotted and the curve looked as shown in Fig. 4.4. The location where the count rate became midway between the constant value inside the test section and the value in the middle of the steel frame was taken as the inside edge of the test section. The zero of the scale on which the gamma densitometer's position was read off was then adjusted accordingly.

The location where the reference counts were taken was similarly found. The gamma densitometer was moved outside the test section and the count

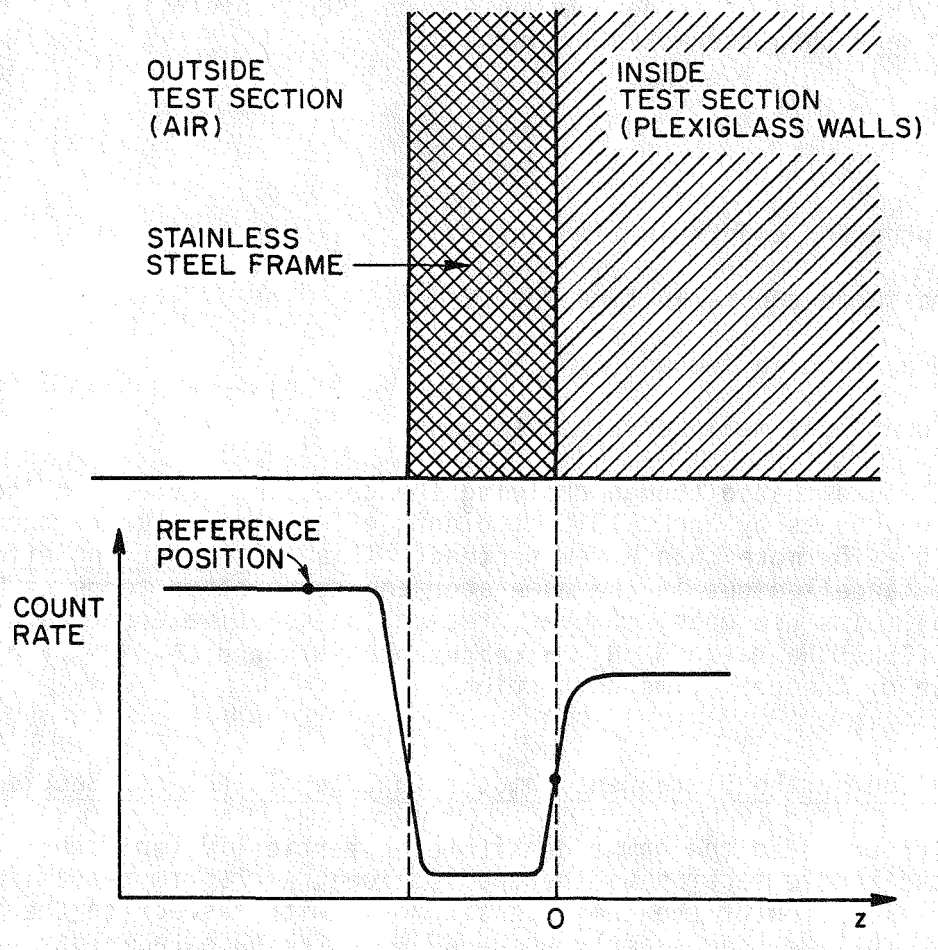


Figure 4.4 Count rate versus position near the edge of the test section

rate was taken. The count rate versus position was plotted (also shown in Fig. 4.4) and the position of the reference was chosen a little distance beyond the location where the count rate levelled off.

# CHAPTER-5

## EXPERIMENTAL RESULTS

The results obtained in the experiments that were performed during this study are presented below. Each section of this chapter contains a description of the methods used to perform the experiment, the formulae used in data reduction, the results of the experiment, and a discussion on the results.

### 5.1 Dead Time Determination

The dead time of the sodium iodide P.M. detection system was found by the two-source method. This requires the use of two gamma ray sources of the same isotope of approximately equal strength. The sources available in the lab were a 1.2 microCurie Cs-137 source and the 5 Curie Cs-137 source. Even though they are not of equal strength, we used the larger source sufficiently shielded so that the number of gamma rays reaching the detector per unit time was about the same as those reaching the detector from the small source when it was placed directly in front of the detector. The procedure taken was as follows. Both sources were kept shielded far away from the detector and background counts were taken for 15 minutes. Then the 5 Curie source was placed in the lead shield having a collimator and located behind the collimator such that we obtained about 2500 counts per second. A measurement was taken for 60 seconds (called $N_1$). The small source was then placed very close to the detector and counts were taken for another 60 seconds. The counts now obtained were due to gamma rays from both sources (denoted $N_{12}$). The 5 Curie source was then taken out of the shield and taken to the well shielded container in another room. A 60 second count was again taken which is due only to gamma rays from the small source (called $N_2$). The dead time, $\tau$, is then found by(3),

$$\tau = 60 \left[\frac{N_1 + N_2 - N_{12} - Bg}{N_{12}^2 - N_1^2 - N_2^2}\right] \text{, seconds} \qquad (5.1)$$

where Bg is number of background counts per 60 seconds. This determination of dead time was repeated four times and the average was found to be 3 microseconds. Table 5.1 gives the data and the results obtained.

### 5.2 Measurement of the Time Interval Required to Reduce the Effect of Flow Fluctuations

Since two-phase flows are inherently fluctuating in character, we have to count the gamma rays over a period of time that is large compared to the period of these fluctuations, and then integrate the results. To find this time interval, void fraction was determined by taking measurements over different lengths of time. When the value of the void fraction did not change appreciably by increasing the measuring time, we knew that the

Table 5.1 Dead time for the sodium iodide, photomultiplier detection system

| Source used | Counts obtained in 60 seconds | | | |
|---|---|---|---|---|
| | 1 | 2 | 3 | 4 |
| Partially shielded 5 Curie ($N_1$) | 127404 | 137811 | 132214 | 135603 |
| 1.2 μCi ($N_2$) | 143617 | 142463 | 141244 | 142982 |
| Both ($N_{12}$) | 269074 | 278076 | 271324 | 276302 |
| Dead time | 2.81 μs | 3.03 μs | 3.08 μs | 3.20 μs |

Average dead time = $\tau$ = 3.03 microseconds

Background = 277 counts in 60 seconds

flow fluctuations had been averaged out. Table 5.2 gives the results for such a measurement for several time periods ranging from 10 seconds to 3 minutes. These results are also plotted in Fig. 5.1. We see that the void fraction fluctuation decreases as the time interval increases.

To determine a period of time that is sufficiently large for the flow fluctuations to be averaged out, we found the error in the individual measurements of void fraction, $\bar{\alpha}$, by using,

$$\Delta\bar{\alpha}_t = \pm \sqrt{\frac{\sum_{i=1}^{n} (\bar{\alpha}_i - \bar{\alpha}_{ave})^2}{(n-1)}} \qquad (5.2)$$

where,

$\bar{\alpha}_i$ = i-th value of chordal average void fraction, $\bar{\alpha}$,

$\bar{\alpha}_{ave}$ = average value of the n measurements of $\bar{\alpha}$, = $(1/n) \sum \bar{\alpha}_i$,

n = number of measurements of $\bar{\alpha}$,

$\Delta\bar{\alpha}_t$ = total standard error in $\bar{\alpha}$.

This value of $\Delta\bar{\alpha}_t$ includes the effects of flow fluctuations and detector drift as well as those of statistical fluctuations of the gamma ray source. In order to find the error due to statistical fluctuations alone, we used Eq. (4.13b). For this part of the experiment, $N_{\ell ref}$, $N_{gref}$, $N_{ref}$, $N_\ell$ and $N_g$ were all measured for long periods of time and their values were large compared to those of N. We thus have:

$$\Delta I/I > \Delta I_\ell/I_\ell \simeq \Delta I_g/I_g$$

and

$$\Delta I/I > \Delta I_{ref}/I_{ref} \simeq \Delta I_{\ell ref}/I_{\ell ref} \simeq \Delta I_{gref}/I_{gref}.$$

So, all errors except $\Delta I/I$ were neglected, and thus Eq. (4.13b) reduced to,

$$(\Delta\alpha/\alpha)^2 \simeq (\Delta I/I)^2 \frac{1}{\bar{\alpha}^2[\ln(I_g'/I_\ell')]^2}$$

Then, replacing I with N,

$$\Delta\alpha = \pm (\Delta N/N) \frac{1}{\ln(N_g'/N_\ell')}$$

which for $\Delta N = \sqrt{N}$ becomes,

Table 5.2 Experimental values of void fractions and errors for different measuring intervals

| No. | Void fraction ($\overline{\alpha}$) from data taken for measuring intervals of (secs.): | | | | | |
|---|---|---|---|---|---|---|
| | 10 | 20 | 30 | 60 | 100 | 180 |
| 1 | 0.4818 | 0.4464 | 0.4718 | 0.4658 | 0.4613 | 0.4438 |
| 2 | 0.4667 | 0.4220 | 0.4555 | 0.4579 | 0.4487 | 0.4528 |
| 3 | 0.4758 | 0.4063 | 0.4418 | 0.4496 | 0.4564 | 0.4557 |
| 4 | 0.4526 | 0.4619 | 0.4544 | 0.4613 | 0.4452 | 0.4563 |
| 5 | 0.3917 | 0.4262 | 0.4372 | 0.4597 | 0.4591 | 0.4492 |
| 6 | 0.3862 | 0.4393 | 0.4369 | 0.4382 | 0.4508 | 0.4615 |
| Average: | 0.4425 | 0.4337 | 0.4496 | 0.4554 | 0.4536 | 0.4532 |
| Actual error $\Delta\overline{\alpha}_t$ | 0.0426 | 0.0196 | 0.0136 | 0.0100 | 0.00632 | 0.00615 |
| Statistical error ($\Delta\overline{\alpha}_s$) | 0.0215 | 0.0152 | 0.0124 | 0.0088 | 0.00656 | 0.00513 |
| Statistical/ actual $\Delta\alpha_s/\Delta\alpha_t$ | 0.505 | 0.775 | 0.912 | 0.880 | 1.038 | 0.834 |

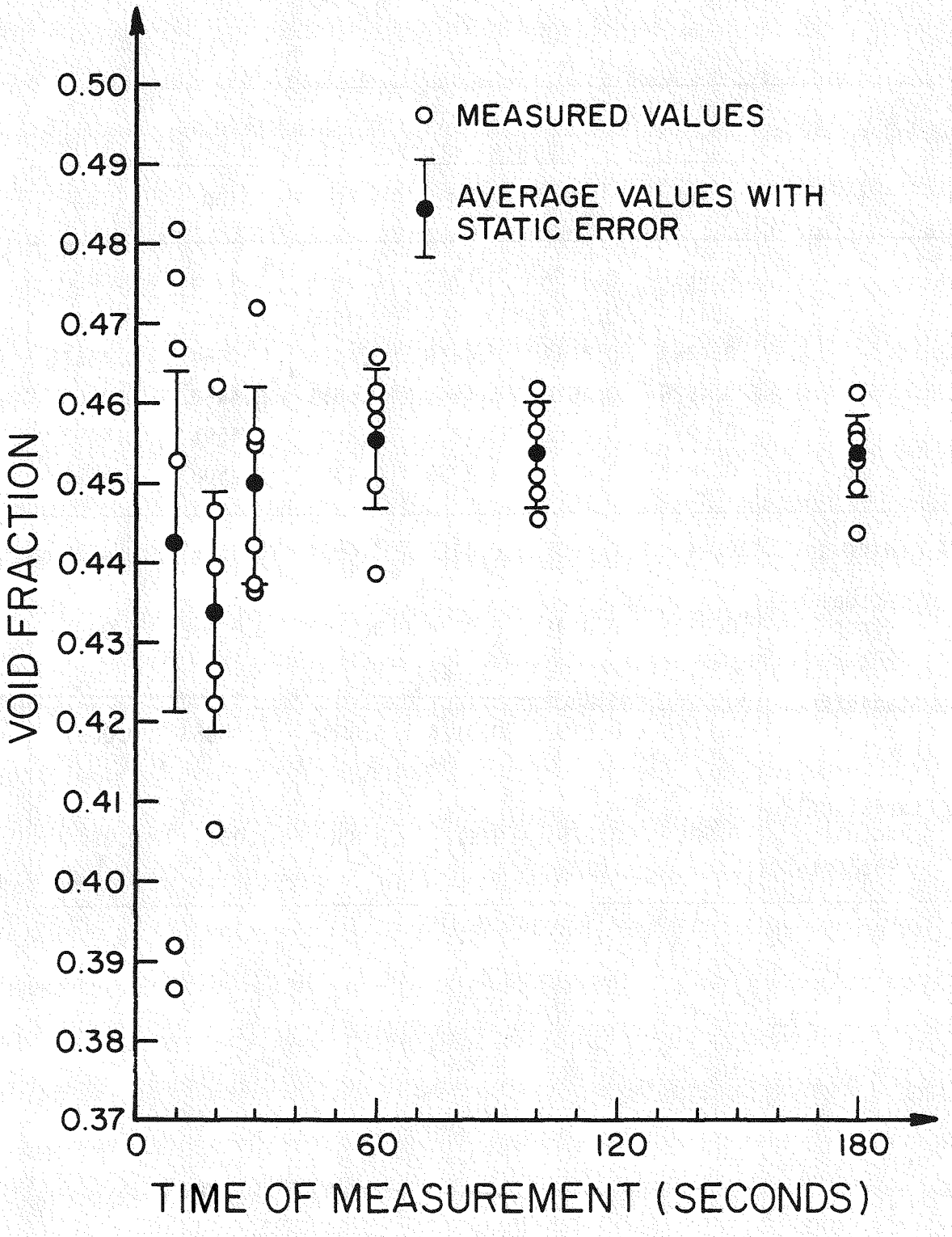


Figure 5.1 Void fractions obtained for different counting intervals

$$\Delta\bar{\alpha}_s = \pm \frac{1}{\sqrt{N}\,\ln(N'_g/N'_\ell)} \qquad (5.3)$$

where,

$\Delta\bar{\alpha}_s$ = standard error in $\bar{\alpha}$ due to statistical fluctuations alone.

Eliminating all the errors ecept those in N while deriving Eq. (5.3) is also justified because in determining $\Delta\bar{\alpha}_t$, the values of $N_\ell$, $N_g$, $N_{\ell ref}$, $N_{gref}$ and $N_{ref}$ were held constant.

The values of $\Delta\bar{\alpha}_t$ and $\Delta\bar{\alpha}_s$ and the ratio $\Delta\bar{\alpha}_s/\Delta\bar{\alpha}_t$, that is, the statistical-error/total-error are listed in Table 5.2. As the flow fluctuations are averaged out, this ratio will approach unity. Since six measurements do not constitute a sufficiently large number for statistical analyses, there will always be some difference between $\Delta\bar{\alpha}_t$ and $\Delta\bar{\alpha}_s$, even when the only source of error is statistical. However, from the way the ratio approaches unity in Table 5.2, it is seen that less than 100 seconds is enough to average out the flow fluctuations. It should be noted that this measurement was done at one location for one flow condition. At other locations and flow conditions, the minimum time needed may be different. On the basis of Tables 4.1 and 5.2 and of visual inspection of all the flow conditions, a counting interval of six (6) minutes was chosen.

## 5.3 Measurement of the Void Fractions

The chordal-average void fraction calculated from the data taken for six (6) minutes at each location are given in this section. Data was taken at three axial positions, 7.5" (19.1 cm), 17.0" (43.2 cm) and 28.5" (72.4 cm) above the inside bottom of the test section. At each axial position, data was taken at no less than nine (9) locations across the test section (as is shown in Fig. 3.4).

In all, 36 different flow conditions were studied. Of these, 18 were with rods and 18 were without rods. Of each 18 runs, half (ie: 9) were at a low liquid flow rate and pressure and the other 9 were at higher pressure and twice the flow rate. For each flow rate, we had three different flow splits between the two inlet ports no. 1 and no. 4. For each flow split, we had three different air flow rates entering through inlet port no. 4 giving us three different flow qualities.

Each flow condition is labelled and has a distinct "case" number, based on a 4-digit code: WXYZ, explained below.

W: The first digit is a number ranging from 1 to 6. It tells us the quality as well as the flow rate. Thus, W=1, 2 or 3 implies that flow quality in inlet port no. 4 is 0.3%, 0.6%, or 0.9%, respectively, at a total liquid flow rate (through ports 1 and 4) of 240 lbm/min (6532 kg/hr) or equivalently, a water

mass flux of 0.115 X $10^6$ lbm/hr-$ft^2$ (0.562 X $10^6$ kg/hr-$m^2$) without rods and 0.143 X $10^6$ lbm/hr-$ft^2$ (0.697 X $10^6$ kg/hr-$m^2$) with rods installed, through the test section (ie: low flow). W=4, 5 or 6 implies quality is 0.3%, 0.6%, or 0.9%, respectively, at a total liquid flow rate of 480 lbm/min (13063 kg/hr) or a water mass flux of 0.230 X $10^6$ lbm/hr-$ft^2$ (1.125 X $10^6$ kg/hr-$m^2$) without rods and 0.286 X $10^6$ lbm/hr-$ft^2$ (1.395 X $10^6$ kg/hr-$m^2$) with rods (ie: high flow).

X: The second digit is the letter A, B or C. It denotes the ratio in which the liquid flow is divided between inlet ports no. 1 and 4. Thus, X=A implies that of the total liquid entering the test section, 50% enters through port no. 1 and 50% enters through port no. 4. X=B implies port no. 1 has 37.5% and port no. 4 has 62.5% of the total liquid inlet flow. X=C implies port no. 1 has 62.5% and port no. 4 has 37.5% of the total liquid inlet flow.

Y: The third digit is the letter N or R. It tells us whether or not the rods are present. Thus, Y=N implies rods are not present; and Y=R implies rods are present.

Z: The fourth digit is the number 4 or 5. It is the number of the inlet port that is used as the inlet for the two-phase mixture. For the present series of experiments, Z=4 always, since data has not been taken with flow entering from port no. 5.

A given flow condition may then be written as, for example, 3BN4, which would be the label for the flow that is of 0.562 X $10^6$ kg/hr-$m^2$ liquid mass flux (ie: low flow), the total liquid inflow is coming in in the ratio 62.5%:37.5% from inlet ports no. 4 and 1, the quality of the fluid entering from port no. 4 is 0.9%, and the rods are not present. Later on, when we plot the void fraction data, each case will have a distinct symbol, determined by the shape of the star representing the data point and by the length of the dashes that make up the line joining the various data points.

Table 5.3 contains the list of all cases that were run, with the values of liquid mass flux, flow ratio between ports no. 4 and 1, flow quality at inlet port no. 4, whether the rods were in or not, and the symbol used in plotting them. Tables 5.4.1 to 5.4.36 contain the values of the chordal averaged void fractions found for each of the cases that were run.

## 5.4 Errors in the Void Fractions

To calculate the actual error in the void fractions determined, we took void fraction data across the middle section for different flow conditions. For each flow condition, we took six (6) one minute counts alternately at the reference and the measurement location. The void fractions were then calculated by using Eq. (4.15a),

Table 5.3 List of all cases run with values of associated parameters

| CASE | SYMBOL FOR FIGURES | LIQUID MASS FLUX KG/HR.M$^2$ | FLOW SPLIT IN#4 : IN#1 | QUALITY | RODS IN |
|---|---|---|---|---|---|
| 1AN4 |  | 0.562 E6 | 50.0% : 50.0% | 0.3% | NO |
| 2AN4 | | 0.562 E6 | 50.0% : 50.0% | 0.6% | NO |
| 3AN4 | | 0.562 E6 | 50.0% : 50.0% | 0.9% | NO |
| 1BN4 |  | 0.562 E6 | 62.5% : 37.5% | 0.3% | NO |
| 2BN4 | | 0.562 E6 | 62.5% : 37.5% | 0.6% | NO |
| 3BN4 | | 0.562 E6 | 62.5% : 37.5% | 0.9% | NO |
| 1CN4 |  | 0.562 E6 | 37.5% : 62.5% | 0.3% | NO |
| 2CN4 | | 0.562 E6 | 37.5% : 62.5% | 0.6% | NO |
| 3CN4 | | 0.562 E6 | 37.5% : 62.5% | 0.9% | NO |
| 4AN4 |  | 1.125 E6 | 50.0% : 50.0% | 0.3% | NO |
| 5AN4 | | 1.125 E6 | 50.0% : 50.0% | 0.6% | NO |
| 6AN4 | | 1.125 E6 | 50.0% : 50.0% | 0.9% | NO |
| 4BN4 |  | 1.125 E6 | 62.5% : 37.5% | 0.3% | NO |
| 5BN4 | | 1.125 E6 | 62.5% : 37.5% | 0.6% | NO |
| 6BN4 | | 1.125 E6 | 62.5% : 37.5% | 0.9% | NO |
| 4CN4 |  | 1.125 E6 | 37.5% : 62.5% | 0.3% | NO |
| 5CN4 | | 1.125 E6 | 37.5% : 62.5% | 0.6% | NO |
| 6CN4 | | 1.125 E6 | 37.5% : 62.5% | 0.9% | NO |
| 1AR4 |  | 0.697 E6 | 50.0% : 50.0% | 0.3% | YES |
| 2AR4 | | 0.697 E6 | 50.0% : 50.0% | 0.6% | YES |
| 3AR4 | | 0.697 E6 | 50.0% : 50.0% | 0.9% | YES |
| 1BR4 |  | 0.697 E6 | 62.5% : 37.5% | 0.3% | YES |
| 2BR4 | | 0.697 E6 | 62.5% : 37.5% | 0.6% | YES |
| 3BR4 | | 0.697 E6 | 62.5% : 37.5% | 0.9% | YES |
| 1CR4 |  | 0.697 E6 | 37.5% : 62.5% | 0.3% | YES |
| 2CR4 | | 0.697 E6 | 37.5% : 62.5% | 0.6% | YES |
| 3CR4 | | 0.697 E6 | 37.5% : 62.5% | 0.9% | YES |
| 4AR4 |  | 1.395 E6 | 50.0% : 50.0% | 0.3% | YES |
| 5AR4 | | 1.395 E6 | 50.0% : 50.0% | 0.6% | YES |
| 6AR4 | | 1.395 E6 | 50.0% : 50.0% | 0.9% | YES |
| 4BR4 |  | 1.395 E6 | 62.5% : 37.5% | 0.3% | YES |
| 5BR4 | | 1.395 E6 | 62.5% : 37.5% | 0.6% | YES |
| 6BR4 | | 1.395 E6 | 62.5% : 37.5% | 0.9% | YES |
| 4CR4 | 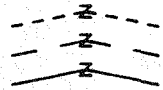 | 1.395 E6 | 37.5% : 62.5% | 0.3% | YES |
| 5CR4 | | 1.395 E6 | 37.5% : 62.5% | 0.6% | YES |
| 6CR4 | | 1.395 E6 | 37.5% : 62.5% | 0.9% | YES |

Table 5.4.1 Void fraction data for case 1AN4 (liquid mass flux = 0.562 X $10^6$ kg/hr-$m^2$; without rods; 50.0/50.0 flow split; and quality at inlet no. 4 = 0.3%)

| Position Inches (cm) | Lower Section (%) | Middle Section (%) | Top Section (%) |
|---|---|---|---|
| 0.0 ( 0.0) | 0.0 | 0.0 | 0.0 |
| 2.25( 5.7) | 10.97 | 24.49 | 19.89 |
| 4.50(11.4) | 10.16 | - | - |
| 6.75(17.1) | 4.22 | 20.07 | 26.60 |
| 11.25(28.6) | 0.0 | 17.68 | 35.20 |
| 13.50(34.3) | 2.44 | - | - |
| 15.75(40.0) | 22.32 | 27.58 | 38.23 |
| 18.00(45.7) | 46.48 | 50.90 | 38.96 |
| 20.25(51.4) | 28.00 | 53.51 | 37.20 |
| 22.50(57.1) | 10.54 | - | - |
| 24.75(62.9) | 8.35 | 36.99 | 36.23 |
| 29.25(74.3) | 17.63 | 36.18 | 39.72 |
| 33.75(85.7) | 17.49 | 33.89 | 27.24 |
| 36.00(91.4) | 0.0 | 0.0 | 0.0 |

Table 5.4.2 Void fraction data for case 2AN4 (liquid mass flux = 0.562 X $10^6$ kg/hr-$m^2$; without rods; 50.0/50.0 flow split; and quality at inlet no. 4 = 0.6%)

| Position Inches (cm) | Lower Section (%) | Middle Section (%) | Top Section (%) |
|---|---|---|---|
| 0.0 ( 0.0) | 0.0 | 0.0 | 0.0 |
| 2.25( 5.7) | 19.43 | 32.94 | 31.29 |
| 4.50(11.4) | 21.62 | - | - |
| 6.75(17.1) | 14.38 | 26.51 | 42.57 |
| 11.25(28.6) | 5.97 | 23.07 | 49.79 |
| 13.50(34.3) | 11.86 | - | - |
| 15.75(40.0) | 28.70 | 38.44 | 52.00 |
| 18.00(45.7) | 59.27 | 56.07 | 49.19 |
| 20.25(51.4) | 53.02 | 63.90 | 46.51 |
| 22.50(57.1) | 30.97 | - | - |
| 24.75(62.9) | 22.74 | 46.27 | 44.48 |
| 29.25(74.3) | 30.47 | 40.36 | 54.80 |
| 33.75(85.7) | 33.52 | 36.34 | 40.56 |
| 36.00(91.4) | 0.0 | 0.0 | 0.0 |

Table 5.4.3 Void fraction data for case 3AN4 (liquid mass flux = 0.562 X $10^6$ kg/hr-$m^2$; without rods; 50.0/50.0 flow split; and quality at inlet no. 4 = 0.9%)

| Position Inches (cm) | Lower Section (%) | Middle Section (%) | Top Section (%) |
|---|---|---|---|
| 0.0 ( 0.0) | 0.0 | 0.0 | 0.0 |
| 2.25( 5.7) | 43.14 | 24.11 | 27.86 |
| 6.75(17.1) | 38.82 | 18.85 | 43.35 |
| 11.25(28.6) | 25.00 | 16.95 | 48.39 |
| 13.50(34.3) | 28.42 | - | - |
| 15.75(40.0) | 44.72 | 26.92 | 50.34 |
| 18.00(45.7) | 69.32 | 54.53 | 45.83 |
| 20.25(51.4) | 68.01 | 64.46 | 43.85 |
| 22.50(57.1) | 43.18 | - | - |
| 24.75(62.9) | 28.05 | 53.56 | 44.74 |
| 29.25(74.3) | 35.23 | 44.24 | 50.37 |
| 33.75(85.7) | 37.49 | 36.35 | 40.64 |
| 36.00(91.4) | 0.0 | 0.0 | 0.0 |

Table 5.4.4 Void fraction data for case 1BN4 (liquid mass flux = 0.562 X $10^6$ kg/hr-$m^2$; without rods; 62.5/37.5 flow split; and quality at inlet no. 4 = 0.3%)

| Position Inches (cm) | Lower Section (%) | Middle Section (%) | Top Section (%) |
|---|---|---|---|
| 0.0 ( 0.0) | 0.0 | 0.0 | 0.0 |
| 2.25( 5.7) | 1.55 | 26.63 | 20.16 |
| 6.75(17.1) | 0.0 | 22.66 | 24.28 |
| 11.25(28.6) | 0.0 | 18.39 | 31.98 |
| 13.50(34.3) | 0.0 | - | - |
| 15.75(40.0) | 5.96 | 23.10 | 40.31 |
| 18.00(45.7) | 31.56 | 43.03 | 45.91 |
| 20.25(51.4) | 44.85 | 52.02 | 47.27 |
| 22.50(57.1) | 27.33 | 58.55 | - |
| 24.75(62.9) | 15.93 | 57.53 | 43.32 |
| 29.25(74.3) | 21.93 | 48.35 | 28.05 |
| 33.75(85.7) | 20.75 | 38.81 | 21.02 |
| 36.00(91.4) | 0.0 | 0.0 | 0.0 |

Table 5.4.5 Void fraction data for case 2BN4 (liquid mass flux = 0.562 X $10^6$ kg/hr-$m^2$; without rods; 62.5/37.5 flow split; and and quality at inlet no. 4 = 0.6%)

| Position Inches (cm) | Lower Section (%) | Middle Section (%) | Top Section (%) |
|---|---|---|---|
| 0.0 ( 0.0) | 0.0 | 0.0 | 0.0 |
| 2.25( 5.7) | 27.35 | 31.76 | 20.02 |
| 6.75(17.1) | 21.38 | 28.10 | 30.93 |
| 11.25(28.6) | 8.42 | 23.79 | 41.52 |
| 13.50(34.3) | 11.16 | - | - |
| 15.75(40.0) | 24.73 | 32.12 | 47.71 |
| 18.00(45.7) | 45.60 | 45.80 | 53.91 |
| 20.25(51.4) | 60.50 | 57.37 | 55.95 |
| 22.50(57.1) | 41.88 | 65.60 | - |
| 24.75(62.9) | 27.28 | 66.00 | 51.58 |
| 29.25(74.3) | 31.05 | 59.01 | 32.13 |
| 33.75(85.7) | 29.10 | 40.69 | 23.33 |
| 36.00(91.4) | 0.0 | 0.0 | 0.0 |

Table 5.4.6 Void fraction data for case 3BN4 (liquid mass flux = 0.562 X $10^6$ kg/hr-$m^2$; without rods; 62.5/37.5 flow split; and quality at inlet no. 4 = 0.9%)

| Position Inches (cm) | Lower Section (%) | Middle Section (%) | Top Section (%) |
|---|---|---|---|
| 0.0 ( 0.0) | 0.0 | 0.0 | 0.0 |
| 2.25( 5.7) | 26.54 | 31.37 | 20.71 |
| 6.75(17.1) | 24.91 | 27.64 | 40.71 |
| 11.25(28.6) | 11.17 | 26.41 | 49.91 |
| 13.50(34.3) | 12.17 | - | - |
| 15.75(40.0) | 27.97 | 36.44 | 53.49 |
| 18.00(45.7) | 46.61 | 32.67 | 64.57 |
| 20.25(51.4) | 66.20 | 45.42 | 65.22 |
| 22.50(57.1) | 46.80 | 59.91 | - |
| 24.75(62.9) | 26.31 | 56.63 | 61.57 |
| 29.25(74.3) | 26.05 | 49.72 | 44.32 |
| 33.75(85.7) | 28.30 | 28.99 | 30.22 |
| 36.00(91.4) | 0.0 | 0.0 | 0.0 |

Table 5.4.7 Void fraction data for case 1CN4 (liquid mass flux = 0.562 X $10^6$ kg/hr-$m^2$; without rods; 37.5/62.5 flow split; and quality at inlet no. 4 = 0.3%)

| Position Inches (cm) | Lower Section (%) | Middle Section (%) | Top Section (%) |
|---|---|---|---|
| 0.0 ( 0.0) | 0.0 | 0.0 | 0.0 |
| 2.25( 5.7) | 30.63 | 27.22 | 7.86 |
| 6.75(17.1) | 23.76 | 23.90 | 16.08 |
| 11.25(28.6) | 12.01 | 33.27 | 22.10 |
| 13.50(34.3) | 18.65 | 44.52 | - |
| 15.75(40.0) | 40.70 | 47.47 | 22.98 |
| 18.00(45.7) | 52.81 | 38.79 | 27.69 |
| 20.25(51.4) | 21.03 | 32.46 | 26.96 |
| 22.50(57.1) | 14.04 | - | - |
| 24.75(62.9) | 12.37 | 27.09 | 29.18 |
| 29.25(74.3) | 18.94 | 30.22 | 29.26 |
| 33.75(85.7) | 22.23 | 26.56 | 16.95 |
| 36.00(91.4) | 0.0 | 0.0 | 0.0 |

Table 5.4.8 Void fraction data for case 2CN4 (liquid mass flux = 0.562 X $10^6$ kg/hr-$m^2$; without rods; 37.5/62.5 flow split; and quality at inlet no. 4 = 0.6%)

| Position Inches (cm) | Lower Section (%) | Middle Section (%) | Top Section (%) |
|---|---|---|---|
| 0.0 ( 0.0) | 0.0 | 0.0 | 0.0 |
| 2.25( 5.7) | 34.12 | 30.50 | 16.19 |
| 6.75(17.1) | 30.96 | 27.82 | 29.68 |
| 11.25(28.6) | 18.48 | 38.42 | 35.90 |
| 13.50(34.3) | 28.29 | 49.17 | - |
| 15.75(40.0) | 52.06 | 55.01 | 36.93 |
| 18.00(45.7) | 57.53 | 42.46 | 33.22 |
| 20.25(51.4) | 32.71 | 32.29 | 32.03 |
| 22.50(57.1) | 19.24 | - | - |
| 24.75(62.9) | 17.51 | 26.81 | 34.08 |
| 29.25(74.3) | 23.87 | 31.12 | 42.53 |
| 33.75(85.7) | 22.35 | 25.71 | 31.40 |
| 36.00(91.4) | 0.0 | 0.0 | 0.0 |

Table 5.4.9 Void fraction data for case 3CN4 (liquid mass flux = 0.562 X $10^6$ kg/hr-$m^2$; without rods; 37.5/62.5 flow split; and quality at inlet no. 4 = 0.9%)

| Position Inches (cm) | Lower Section (%) | Middle Section (%) | Top Section (%) |
|---|---|---|---|
| 0.0 ( 0.0) | 0.0 | 0.0 | 0.0 |
| 2.25( 5.7) | 33.47 | 20.00 | 38.73 |
| 6.75(17.1) | 26.76 | 19.14 | 52.54 |
| 11.25(28.6) | 15.09 | 27.68 | 57.31 |
| 13.50(34.3) | 22.32 | 43.05 | - |
| 15.75(40.0) | 53.10 | 50.36 | 56.78 |
| 18.00(45.7) | 63.28 | 47.33 | 57.34 |
| 20.25(51.4) | 31.68 | 33.59 | 56.22 |
| 22.50(57.1) | 17.59 | - | - |
| 24.75(62.9) | 13.02 | 24.09 | 61.96 |
| 29.25(74.3) | 19.21 | 28.44 | 72.97 |
| 33.75(85.7) | 17.94 | 22.49 | 62.04 |
| 36.00(91.4) | 0.0 | 0.0 | 0.0 |

Table 5.4.10 Void fraction data for case 4AN4 (liquid mass flux = $1.125 \times 10^6$ kg/hr-m$^2$; without rods; 50.0/50.0 flow split; and quality at inlet no. 4 = 0.3%)

| Position Inches (cm) | Lower Section (%) | Middle Section (%) | Top Section (%) |
|---|---|---|---|
| 0.0 ( 0.0) | 0.0 | 0.0 | 0.0 |
| 2.25( 5.7) | 13.68 | 31.08 | 20.69 |
| 6.75(17.1) | 1.73 | 29.02 | 26.26 |
| 11.25(28.6) | 0.0 | 36.15 | 21.19 |
| 13.50(34.3) | - | 38.92 | - |
| 15.75(40.0) | 53.96 | 28.13 | 20.93 |
| 18.00(45.7) | 25.31 | 22.17 | - |
| 20.25(51.4) | 21.01 | 11.62 | 31.08 |
| 24.75(62.9) | 2.51 | 9.75 | 57.19 |
| 29.25(74.3) | 10.66 | 17.22 | 55.40 |
| 33.75(85.7) | 0.0 | 6.97 | 60.60 |
| 36.00(91.4) | 0.0 | 0.0 | 0.0 |

Table 5.4.11 Void fraction data for case 5AN4 (liquid mass flux = $1.125 \times 10^6$ kg/hr-$m^2$; without rods; 50.0/50.0 flow split; and quality at inlet no. 4 = 0.6%)

| Position Inches (cm) | Lower Section (%) | Middle Section (%) | Top Section (%) |
|---|---|---|---|
| 0.0 ( 0.0) | 0.0 | 0.0 | 0.0 |
| 2.25( 5.7) | 25.18 | 39.93 | 35.86 |
| 6.75(17.1) | 7.54 | 29.68 | 41.71 |
| 11.25(28.6) | 5.83 | 39.04 | 35.90 |
| 15.75(40.0) | 62.91 | 54.85 | 34.28 |
| 18.00(45.7) | 47.27 | 48.55 | 45.51 |
| 20.25(51.4) | 26.47 | 41.19 | 52.58 |
| 24.75(62.9) | 0.0 | 33.65 | 76.08 |
| 29.25(74.3) | 4.64 | 37.64 | 86.94 |
| 33.75(85.7) | 0.0 | 22.93 | 71.30 |
| 36.00(91.4) | 0.0 | 0.0 | 0.0 |

Table 5.4.12 Void fraction data for case 6AN4 (liquid mass flux = 1.125 X $10^6$ kg/hr-$m^2$; without rods; 50.0/50.0 flow split; and quality at inlet no. 4 = 0.9%)

| Position Inches (cm) | Lower Section (%) | Middle Section (%) | Top Section (%) |
|---|---|---|---|
| 0.0 ( 0.0) | 0.0 | 0.0 | 0.0 |
| 2.25( 5.7) | 26.78 | 35.48 | 48.63 |
| 6.75(17.1) | 6.40 | 25.47 | 48.99 |
| 11.25(28.6) | 4.28 | 37.73 | 35.25 |
| 15.75(40.0) | 63.74 | 59.39 | 31.01 |
| 18.00(45.7) | 59.32 | 58.59 | 47.09 |
| 20.25(51.4) | 44.70 | 53.74 | 58.72 |
| 24.75(62.9) | 10.78 | 51.26 | 77.47 |
| 29.25(74.3) | 16.68 | 53.67 | 84.45 |
| 31.50(80.0) | - | 46.91 | - |
| 33.75(85.7) | 6.24 | 45.64 | 28.86 |
| 36.00(91.4) | 0.0 | 0.0 | 0.0 |

Table 5.4.13 Void fraction data for case 4BN4 (liquid mass flux = $1.125 \times 10^6$ kg/hr-m$^2$; without rods; 62.5/37.5 flow split; and quality at inlet no. 4 = 0.3%)

| Position Inches (cm) | Lower Section (%) | Middle Section (%) | Top Section (%) |
|---|---|---|---|
| 0.0 ( 0.0) | 0.0 | 0.0 | 0.0 |
| 2.25( 5.7) | 21.61 | 21.10 | 47.94 |
| 6.75(17.1) | 0.0 | 16.33 | 53.21 |
| 11.25(28.6) | 0.0 | 19.50 | 50.47 |
| 15.75(40.0) | 38.69 | 37.85 | 43.02 |
| 18.00(45.7) | 41.68 | 41.75 | 53.04 |
| 20.25(51.4) | 38.31 | 42.67 | 56.90 |
| 22.50(57.1) | - | 41.90 | - |
| 24.75(62.9) | 5.00 | 41.73 | 71.48 |
| 29.25(74.3) | 10.49 | 45.25 | 86.76 |
| 33.75(85.7) | 5.30 | 35.81 | 61.24 |
| 36.00(91.4) | 0.0 | 0.0 | 0.0 |

Table 5.4.14 Void fraction data for case 5BN4 (liquid mass flux = $1.125 \times 10^6$ kg/hr-$m^2$; without rods; 62.5/37.5 flow split; and quality at inlet no. 4 = 0.6%)

| Position Inches (cm) | Lower Section (%) | Middle Section (%) | Top Section (%) |
|---|---|---|---|
| 0.0 ( 0.0) | 0.0 | 0.0 | 0.0 |
| 2.25( 5.7) | 20.72 | 33.93 | 37.47 |
| 6.75(17.1) | 0.0 | 23.49 | 40.58 |
| 11.25(28.6) | 0.0 | 26.02 | 25.20 |
| 15.75(40.0) | 43.11 | 47.40 | 30.47 |
| 18.00(45.7) | 57.20 | 49.61 | 33.62 |
| 20.25(51.4) | 52.40 | 53.68 | 41.96 |
| 22.50(57.1) | - | 58.49 | - |
| 24.75(62.9) | 12.98 | 60.98 | 52.36 |
| 29.25(74.3) | 24.87 | 71.60 | 64.80 |
| 33.75(85.7) | 21.50 | 62.24 | 40.80 |
| 36.00(91.4) | 0.0 | 0.0 | 0.0 |

Table 5.4.15 Void fraction data for case 6BN4 (liquid mass flux = $1.125 \times 10^6$ kg/hr-m$^2$; without rods; 62.5/37.5 flow split; and quality at inlet no. 4 = 0.9%)

| Position Inches (cm) | Lower Section (%) | Middle Section (%) | Top Section (%) |
|---|---|---|---|
| 0.0 ( 0.0) | 0.0 | 0.0 | 0.0 |
| 2.25( 5.7) | 33.21 | 32.82 | 70.98 |
| 6.75(17.1) | 1.97 | 31.76 | 69.41 |
| 9.00(22.9) | 0.10 | - | - |
| 11.25(28.6) | 0.63 | 36.45 | 64.86 |
| 15.75(40.0) | 54.53 | 53.94 | 57.45 |
| 18.00(45.7) | 63.86 | 50.74 | 57.01 |
| 20.25(51.4) | 68.50 | 57.97 | 60.52 |
| 24.75(62.9) | 30.42 | 67.44 | 74.01 |
| 29.25(74.3) | 33.60 | 78.14 | 83.54 |
| 33.75(85.7) | 29.05 | 70.87 | 45.14 |
| 36.00(91.4) | 0.0 | 0.0 | 0.0 |

Table 5.4.16 Void fraction data for case 4CN4 (liquid mass flux = $1.125 \times 10^6$ kg/hr-$m^2$; without rods; 37.5/62.5 flow split; and quality at inlet no. 4 = 0.3%)

| Position Inches (cm) | Lower Section (%) | Middle Section (%) | Top Section (%) |
|---|---|---|---|
| 0.0 ( 0.0) | 0.0 | 0.0 | 0.0 |
| 2.25( 5.7) | 16.90 | 28.13 | 30.63 |
| 4.50(11.4) | - | 39.92 | 46.63 |
| 6.75(17.1) | 5.63 | 43.13 | 39.93 |
| 9.00(22.9) | 4.24 | 47.50 | - |
| 11.25(28.6) | 21.80 | 40.85 | 33.75 |
| 13.50(34.3) | 52.22 | 28.88 | - |
| 15.75(40.0) | 48.12 | 21.46 | 42.29 |
| 18.00(45.7) | 27.31 | 14.91 | 48.34 |
| 20.25(51.4) | 12.83 | 8.58 | 47.54 |
| 24.75(62.9) | 14.32 | 6.97 | 37.14 |
| 29.25(74.3) | 15.10 | 4.01 | 28.29 |
| 33.75(85.7) | 7.32 | 0.0 | 70.33 |
| 36.00(91.4) | 0.0 | 0.0 | 0.0 |

Table 5.4.17 Void fraction data for case 5CN4 (liquid mass flux = 1.125 X $10^6$ kg/hr-$m^2$; without rods; 37.5/62.5 flow split; and quality at inlet no. 4 = 0.6%)

| Position Inches (cm) | Lower Section (%) | Middle Section (%) | Top Section (%) |
|---|---|---|---|
| 0.0 ( 0.0) | 0.0 | 0.0 | 0.0 |
| 2.25( 5.7) | 27.11 | 33.12 | 32.30 |
| 4.50(11.4) | 33.75 | - | - |
| 6.75(17.1) | 6.85 | 42.21 | 48.23 |
| 11.25(28.6) | 16.07 | 45.91 | 39.41 |
| 13.50(34.3) | 47.14 | 35.57 | - |
| 15.75(40.0) | 56.85 | 26.43 | 47.16 |
| 18.00(45.7) | 24.35 | 19.52 | 64.75 |
| 20.25(51.4) | 9.74 | 10.12 | 74.53 |
| 24.75(62.9) | 5.19 | 13.03 | 75.77 |
| 29.25(74.3) | 7.67 | 15.22 | 64.24 |
| 33.75(85.7) | 0.0 | 4.81 | 75.63 |
| 36.00(91.4) | 0.0 | 0.0 | 0.0 |

Table 5.4.18 Void fraction data for case 6CN4 (liquid mass flux = $1.125 \times 10^6$ kg/hr-m$^2$; without rods; 37.5/62.5 flow split; and quality at inlet no. 4 = 0.9%)

| Position Inches (cm) | Lower Section (%) | Middle Section (%) | Top Section (%) |
|---|---|---|---|
| 0.0 ( 0.0) | 0.0 | 0.0 | 0.0 |
| 2.25( 5.7) | 22.87 | 46.23 | 25.02 |
| 4.50(11.4) | - | 49.95 | - |
| 6.75(17.1) | 4.42 | 51.23 | 39.05 |
| 9.00(22.9) | - | 53.69 | - |
| 11.25(28.6) | 8.50 | 59.69 | 34.11 |
| 13.50(34.3) | 38.09 | 54.18 | - |
| 15.75(40.0) | 65.80 | 43.33 | 40.11 |
| 18.00(45.7) | 38.49 | 34.46 | 54.42 |
| 20.25(51.4) | 18.26 | 24.93 | 70.67 |
| 24.75(62.9) | 4.05 | 22.15 | 90.47 |
| 29.25(74.3) | 8.22 | 26.16 | 91.28 |
| 33.75(85.7) | 0.0 | 7.41 | 81.13 |
| 36.00(91.4) | 0.0 | 0.0 | 0.0 |

Table 5.4.19 Void fraction data for case 1AR4 (liquid mass flux = 0.697 X $10^6$ kg/hr-$m^2$; with rods; 50.0/50.0 flow split; and quality at inlet no. 4 = 0.3%)

| Position Inches (cm) | Lower Section (%) | Middle Section (%) | Top Section (%) |
|---|---|---|---|
| 0.0 ( 0.0) | 0.0 | 0.0 | 0.0 |
| 2.25( 5.7) | 0.0 | 0.0 | 33.12 |
| 6.75(17.1) | 0.0 | 0.0 | 55.37 |
| 11.25(28.6) | 4.53 | 7.50 | 49.02 |
| 15.75(40.0) | 52.07 | 32.35 | 44.69 |
| 18.25(46.4) | 61.96 | 58.17 | 50.53 |
| 20.25(51.4) | 48.19 | 35.02 | 40.04 |
| 24.75(62.9) | 20.93 | 19.32 | 41.03 |
| 29.25(74.3) | 20.31 | 23.55 | 36.96 |
| 33.75(85.7) | 23.49 | 18.83 | 69.01 |
| 36.00(91.4) | 0.0 | 0.0 | 0.0 |

Table 5.4.20 Void fraction data for case 2AR4 (liquid mass flux = 0.697 X $10^6$ kg/hr-$m^2$; with rods; 50.0/50.0 flow split; and quality at inlet no. 4 = 0.6%)

| Position Inches (cm) | Lower Section (%) | Middle Section (%) | Top Section (%) |
|---|---|---|---|
| 0.0 ( 0.0) | 0.0 | 0.0 | 0.0 |
| 2.25( 5.7) | 0.0 | 17.44 | 42.47 |
| 6.75(17.1) | 0.0 | 28.61 | 59.00 |
| 11.25(28.6) | 4.19 | 36.46 | 53.47 |
| 15.75(40.0) | 61.59 | 66.11 | 53.49 |
| 18.25(46.4) | 70.73 | 60.30 | 60.10 |
| 20.25(51.4) | 50.96 | 29.54 | 48.91 |
| 24.75(62.9) | 29.06 | 17.91 | 58.53 |
| 29.25(74.3) | 31.46 | 22.05 | 58.10 |
| 33.75(85.7) | 31.25 | 13.52 | 54.10 |
| 36.00(91.4) | 0.0 | 0.0 | 0.0 |

Table 5.4.21 Void fraction data for case 3AR4 (liquid mass flux = 0.697 X $10^6$ kg/hr-$m^2$; with rods; 50.0/50.0 flow split; and quality at inlet no. 4 = 0.9%)

| Position Inches (cm) | Lower Section (%) | Middle Section (%) | Top Section (%) |
|---|---|---|---|
| 0.0 ( 0.0) | 0.0 | 0.0 | 0.0 |
| 2.25( 5.7) | 0.0 | 18.31 | 48.98 |
| 6.75(17.1) | 0.0 | 36.67 | 50.59 |
| 11.25(28.6) | 4.54 | 41.09 | 52.92 |
| 15.75(40.0) | 62.18 | 67.44 | 53.76 |
| 18.25(46.4) | 73.14 | 73.32 | 71.83 |
| 20.25(51.4) | 56.71 | 58.60 | 66.54 |
| 24.75(62.9) | 33.41 | 33.98 | 61.97 |
| 29.25(74.3) | 36.36 | 38.68 | 96.20 |
| 33.75(85.7) | 36.32 | 25.16 | 63.81 |
| 36.00(91.4) | 0.0 | 0.0 | 0.0 |

Table 5.4.22 Void fraction data for case 1BR4 (liquid mass flux = 0.697 X $10^6$ kg/hr-$m^2$; with rods; 62.5/37.5 flow split; and quality at inlet no. 4 = 0.3%)

| Position Inches (cm) | Lower Section (%) | Middle Section (%) | Top Section (%) |
|---|---|---|---|
| 0.0 ( 0.0) | 0.0 | 0.0 | 0.0 |
| 2.25( 5.7) | 0.0 | 3.85 | 33.98 |
| 6.75(17.1) | 0.0 | 15.00 | 65.10 |
| 11.25(28.6) | 3.22 | 21.29 | 60.26 |
| 15.75(40.0) | 35.18 | 55.74 | 59.15 |
| 18.25(46.4) | 56.74 | 62.42 | 30.65 |
| 20.25(51.4) | 63.77 | 54.96 | 35.40 |
| 24.75(62.9) | 34.01 | 27.68 | 53.94 |
| 29.25(74.3) | 38.34 | 34.59 | 30.91 |
| 33.75(85.7) | 37.97 | 25.26 | 70.11 |
| 36.00(91.4) | 0.0 | 0.0 | 0.0 |

Table 5.4.23 Void fraction data for case 2BR4 (liquid mass flux = 0.697 X $10^6$ kg/hr-$m^2$; with rods; 62.5/37.5 flow split; and quality at inlet no. 4 = 0.6%)

| Position Inches (cm) | Lower Section (%) | Middle Section (%) | Top Section (%) |
|---|---|---|---|
| 0.0 ( 0.0) | 0.0 | 0.0 | 0.0 |
| 2.25( 5.7) | 0.0 | 41.43 | 41.30 |
| 6.75(17.1) | 0.0 | 49.85 | 54.82 |
| 11.25(28.6) | 0.0 | 45.48 | 48.21 |
| 15.75(40.0) | 41.43 | 70.31 | 48.32 |
| 18.25(46.4) | 61.81 | 77.14 | 41.80 |
| 20.25(51.4) | 64.71 | 75.86 | 47.28 |
| 24.75(62.9) | 34.98 | 45.83 | 41.29 |
| 29.25(74.3) | 39.76 | 50.21 | 81.10 |
| 33.75(85.7) | 33.56 | 40.09 | 73.01 |
| 36.00(91.4) | 0.0 | 0.0 | 0.0 |

Table 5.4.24 Void fraction data for case 3BR4 (liquid mass flux = 0.697 X $10^6$ kg/hr-$m^2$; with rods; 62.5/37.5 flow split; and quality at inlet no. 4 = 0.9%)

| Position Inches (cm) | Lower Section (%) | Middle Section (%) | Top Section (%) |
|---|---|---|---|
| 0.0 ( 0.0) | 0.0 | 0.0 | 0.0 |
| 2.25( 5.7) | 0.0 | 35.99 | 54.70 |
| 6.75(17.1) | 0.0 | 47.08 | 54.66 |
| 11.25(28.6) | 6.32 | 28.54 | 47.18 |
| 15.75(40.0) | 24.37 | 41.91 | 46.91 |
| 18.25(46.4) | 56.08 | 61.67 | 72.96 |
| 20.25(51.4) | 63.78 | 57.79 | 73.24 |
| 24.75(62.9) | 80.67 | 60.13 | 82.38 |
| 29.25(74.3) | 81.82 | 76.17 | 85.73 |
| 33.75(85.7) | 74.64 | 73.02 | 63.51 |
| 36.00(91.4) | 0.0 | 0.0 | 0.0 |

Table 5.4.25 Void fraction data for case 1CR4 (liquid mass flux = 0.697 X $10^6$ kg/hr-$m^2$; with rods; 37.5/62.5 flow split; and quality at inlet no. 4 = 0.3%)

| Position Inches (cm) | Lower Section (%) | Middle Section (%) | Top Section (%) |
|---|---|---|---|
| 0.0 ( 0.0) | 0.0 | 0.0 | 0.0 |
| 2.25( 5.7) | 0.0 | 11.35 | 46.23 |
| 6.75(17.1) | 0.0 | 22.42 | 64.00 |
| 11.25(28.6) | 0.0 | 39.36 | 51.33 |
| 15.75(40.0) | 51.32 | 59.82 | 43.01 |
| 18.25(46.4) | 41.49 | 28.73 | 50.58 |
| 20.25(51.4) | 14.11 | 17.66 | 40.16 |
| 24.75(62.9) | 0.41 | 11.66 | 40.03 |
| 29.25(74.3) | 6.81 | 17.44 | 31.25 |
| 33.75(85.7) | 2.45 | 6.74 | 53.43 |
| 36.00(91.4) | 0.0 | 0.0 | 0.0 |

Table 5.4.26 Void fraction data for case 2CR4 (liquid mass flux = 0.697 X $10^6$ kg/hr-$m^2$; with rods; 37.5/62.5 flow split; and quality at inlet no. 4 = 0.6%)

| Position Inches (cm) | Lower Section (%) | Middle Section (%) | Top Section (%) |
|---|---|---|---|
| 0.0 ( 0.0) | 0.0 | 0.0 | 0.0 |
| 2.25( 5.7) | 0.0 | 29.46 | 57.99 |
| 6.75(17.1) | 0.0 | 43.38 | 72.87 |
| 11.25(28.6) | 11.61 | 59.22 | 59.42 |
| 15.75(40.0) | 62.68 | 57.91 | 47.94 |
| 18.25(46.4) | 44.80 | 29.55 | 62.47 |
| 20.25(51.4) | 20.00 | 24.21 | 57.95 |
| 24.75(62.9) | 3.57 | 22.79 | 52.22 |
| 29.25(74.3) | 7.38 | 21.25 | 48.27 |
| 33.75(85.7) | 4.91 | 10.88 | 76.58 |
| 36.00(91.4) | 0.0 | 0.0 | 0.0 |

Table 5.4.27 Void fraction data for case 3CR4 (liquid mass flux = 0.697 X $10^6$ kg/hr-$m^2$; with rods; 37.5/62.5 flow split; and quality at inlet no. 4 = 0.9%)

| Position Inches (cm) | Lower Section (%) | Middle Section (%) | Top Section (%) |
|---|---|---|---|
| 0.0 ( 0.0) | 0.0 | 0.0 | 0.0 |
| 2.25( 5.7) | 0.0 | 26.60 | 72.19 |
| 6.75(17.1) | 0.0 | 39.70 | 78.14 |
| 11.25(28.6) | 16.49 | 75.45 | 61.51 |
| 15.75(40.0) | 65.85 | 57.79 | 54.15 |
| 18.25(46.4) | 48.16 | 32.43 | 55.78 |
| 20.25(51.4) | 23.76 | 26.29 | 46.14 |
| 24.75(62.9) | 10.53 | 24.21 | 47.36 |
| 29.25(74.3) | 14.62 | 21.61 | 57.17 |
| 33.75(85.7) | 11.97 | 8.61 | 79.01 |
| 36.00(91.4) | 0.0 | 0.0 | 0.0 |

Table 5.4.28 Void fraction data for case 4AR4 (liquid mass flux = 1.395 X $10^6$ kg/hr-$m^2$; with rods; 50.0/50.0 flow split; and quality at inlet no. 4 = 0.3%)

| Position Inches (cm) | Lower Section (%) | Middle Section (%) | Top Section (%) |
|---|---|---|---|
| 0.0 ( 0.0) | 0.0 | 0.0 | 0.0 |
| 2.25( 5.7) | 46.69 | 44.54 | 82.04 |
| 6.75(17.1) | 53.71 | 72.86 | 57.06 |
| 11.25(28.6) | 46.16 | 62.84 | 46.78 |
| 15.75(40.0) | 59.04 | 41.78 | 48.57 |
| 18.25(46.4) | 51.26 | 49.71 | 58.24 |
| 20.25(51.4) | 31.25 | 45.36 | 52.20 |
| 24.75(62.9) | 35.18 | 42.54 | 48.48 |
| 29.25(74.3) | 34.35 | 34.76 | 47.02 |
| 33.75(85.7) | 17.50 | 24.25 | 72.10 |
| 36.00(91.4) | 0.0 | 0.0 | 0.0 |

Table 5.4.29 Void fraction data for case 5AR4 (liquid mass flux = 1.395 X $10^6$ kg/hr-$m^2$; with rods; 50.0/50.0 flow split; and quality at inlet no. 4 = 0.6%)

| Position Inches (cm) | Lower Section (%) | Middle Section (%) | Top Section (%) |
|---|---|---|---|
| 0.0 ( 0.0) | 0.0 | 0.0 | 0.0 |
| 2.25( 5.7) | 21.13 | 55.95 | 89.80 |
| 6.75(17.1) | 9.28 | 85.94 | 64.62 |
| 11.25(28.6) | 24.36 | 78.93 | 61.10 |
| 15.75(40.0) | 59.75 | 63.53 | 54.93 |
| 18.25(46.4) | 49.81 | 65.60 | 66.90 |
| 20.25(51.4) | 45.33 | 58.33 | 60.33 |
| 24.75(62.9) | 28.11 | 57.60 | 61.59 |
| 29.25(74.3) | 27.94 | 51.27 | 60.52 |
| 33.75(85.7) | 12.14 | 31.07 | 81.24 |
| 36.00(91.4) | 0.0 | 0.0 | 0.0 |

Table 5.4.30 Void fraction data for case 6AR4 (liquid mass flux = $1.395 \times 10^6$ kg/hr-m$^2$; with rods; 50.0/50.0 flow split; and quality at inlet no. 4 = 0.9%)

| Position Inches (cm) | Lower Section (%) | Middle Section (%) | Top Section (%) |
|---|---|---|---|
| 0.0 ( 0.0) | 0.0 | 0.0 | 0.0 |
| 2.25( 5.7) | 32.82 | 49.11 | 92.39 |
| 6.75(17.1) | 8.66 | 81.39 | 67.26 |
| 11.25(28.6) | 21.05 | 73.01 | 64.27 |
| 15.75(40.0) | 71.04 | 62.52 | 60.91 |
| 18.25(46.4) | 58.15 | 64.44 | 77.19 |
| 20.25(51.4) | 61.55 | 55.55 | 68.26 |
| 24.75(62.9) | 35.09 | 51.24 | 68.68 |
| 29.25(74.3) | 31.90 | 47.76 | 86.16 |
| 33.75(85.7) | 12.50 | 19.86 | 85.21 |
| 36.00(91.4) | 0.0 | 0.0 | 0.0 |

Table 5.4.31 Void fraction data for case 4BR4 (liquid mass flux = 1.395 X $10^6$ kg/hr-$m^2$; with rods; 62.5/37.5 flow split; and quality at inlet no. 4 = 0.3%)

| Position Inches (cm) | Lower Section (%) | Middle Section (%) | Top Section (%) |
|---|---|---|---|
| 0.0 ( 0.0) | 0.0 | 0.0 | 0.0 |
| 2.25( 5.7) | 49.16 | 50.37 | 79.92 |
| 6.75(17.1) | 59.11 | 74.12 | 60.30 |
| 11.25(28.6) | 57.92 | 69.00 | 59.41 |
| 15.75(40.0) | 59.02 | 53.69 | 58.20 |
| 18.25(46.4) | 59.68 | 58.80 | 62.59 |
| 20.25(51.4) | 64.52 | 62.22 | 57.16 |
| 24.75(62.9) | 53.25 | 73.09 | 48.90 |
| 29.25(74.3) | 48.95 | 65.38 | 88.64 |
| 33.75(85.7) | 31.08 | 39.74 | 89.16 |
| 36.00(91.4) | 0.0 | 0.0 | 0.0 |

Table 5.4.32 Void fraction data for case 5BR4 (liquid mass flux = 1.395 X $10^6$ kg/hr-$m^2$; with rods; 62.5/37.5 flow split; and quality at inlet no. 4 = 0.6%)

| Position Inches (cm) | Lower Section (%) | Middle Section (%) | Top Section (%) |
|---|---|---|---|
| 0.0 ( 0.0) | 0.0 | 0.0 | 0.0 |
| 2.25( 5.7) | 55.78 | 55.18 | 81.80 |
| 6.75(17.1) | 63.64 | 79.95 | 66.76 |
| 11.25(28.6) | 65.38 | 77.36 | 63.98 |
| 15.75(40.0) | 72.15 | 62.66 | 59.37 |
| 18.25(46.4) | 67.90 | 62.86 | 63.22 |
| 20.25(51.4) | 82.57 | 69.82 | 68.38 |
| 24.75(62.9) | 88.75 | 75.94 | 48.90 |
| 29.25(74.3) | 76.46 | 72.88 | 100.00 |
| 33.75(85.7) | 48.17 | 42.11 | 86.13 |
| 36.00(91.4) | 0.0 | 0.0 | 0.0 |

Table 5.4.33 Void fraction data for case 6BR4 (liquid mass flux = 1.395 X $10^6$ kg/hr-$m^2$; with rods; 62.5/37.5 flow split; and quality at inlet no. 4 = 0.9%)

| Position Inches (cm) | Lower Section (%) | Middle Section (%) | Top Section (%) |
|---|---|---|---|
| 0.0 ( 0.0) | 0.0 | 0.0 | 0.0 |
| 2.25( 5.7) | 68.22 | 57.05 | 84.12 |
| 6.75(17.1) | 75.89 | 71.79 | 68.28 |
| 11.25(28.6) | 88.61 | 75.53 | 66.38 |
| 15.75(40.0) | 87.56 | 65.97 | 60.61 |
| 18.25(46.4) | 74.44 | 64.89 | 68.16 |
| 20.25(51.4) | 95.20 | 79.32 | 78.53 |
| 24.75(62.9) | 98.91 | 85.16 | 66.80 |
| 29.25(74.3) | 91.77 | 70.72 | 100.00 |
| 33.75(85.7) | 76.91 | 69.71 | 87.25 |
| 36.00(91.4) | 0.0 | 0.0 | 0.0 |

Table 5.4.34 Void fraction data for case 4CR4 (liquid mass flux = 1.395 X $10^6$ kg/hr-$m^2$; with rods; 37.5/62.5 flow split; and quality at inlet no. 4 = 0.3%)

| Position Inches (cm) | Lower Section (%) | Middle Section (%) | Top Section (%) |
|---|---|---|---|
| 0.0 ( 0.0) | 0.0 | 0.0 | 0.0 |
| 2.25( 5.7) | 0.0 | 44.49 | 69.06 |
| 6.75(17.1) | 0.0 | 71.48 | 49.14 |
| 11.25(28.6) | 44.11 | 56.64 | 28.29 |
| 15.75(40.0) | 57.15 | 38.44 | 22.46 |
| 18.25(46.4) | 31.82 | 21.92 | 21.28 |
| 20.25(51.4) | 6.47 | 13.76 | 14.54 |
| 24.75(62.9) | 6.78 | 19.11 | 19.91 |
| 29.25(74.3) | 3.19 | 21.37 | 16.23 |
| 33.75(85.7) | 0.0 | 8.71 | 7.16 |
| 36.00(91.4) | 0.0 | 0.0 | 0.0 |

Table 5.4.35 Void fraction data for case 5CR4 (liquid mass flux = 1.395 X $10^6$ kg/hr-$m^2$; with rods; 37.5/62.5 flow split; and quality at inlet no. 4 = 0.6%)

| Position Inches (cm) | Lower Section (%) | Middle Section (%) | Top Section (%) |
|---|---|---|---|
| 0.0 ( 0.0) | 0.0 | 0.0 | 0.0 |
| 2.25( 5.7) | 1.74 | 42.78 | 78.31 |
| 6.75(17.1) | 0.0 | 69.59 | 56.20 |
| 11.25(28.6) | 27.13 | 60.01 | 42.52 |
| 15.75(40.0) | 57.21 | 47.99 | 33.60 |
| 18.25(46.4) | 48.29 | 31.08 | 33.88 |
| 20.25(51.4) | 25.16 | .17.79 | 31.09 |
| 24.75(62.9) | 18.01 | 20.51 | 24.40 |
| 29.25(74.3) | 13.62 | 20.16 | 20.52 |
| 33.75(85.7) | 0.60 | 7.98 | 11.83 |
| 36.00(91.4) | 0.0 | 0.0 | 0.0 |

Table 5.4.36 Void fraction data for case 6CR4 (liquid mass flux = 1.395 X $10^6$ kg/hr-$m^2$; with rods; 37.5/62.5 flow split; and quality at inlet no. 4 = 0.9%)

| Position Inches (cm) | Lower Section (%) | Middle Section (%) | Top Section (%) |
|---|---|---|---|
| 0.0 ( 0.0) | 0.0 | 0.0 | 0.0 |
| 2.25( 5.7) | 1.35 | 51.38 | 82.35 |
| 6.75(17.1) | 0.0 | 81.56 | 65.18 |
| 11.25(28.6) | 31.35 | 72.11 | 51.36 |
| 15.75(40.0) | 65.63 | 49.26 | 43.18 |
| 18.25(46.4) | 57.54 | 35.13 | 40.13 |
| 20.25(51.4) | 37.55 | 22.41 | 43.25 |
| 24.75(62.9) | 29.05 | 22.14 | 32.95 |
| 29.25(74.3) | 27.16 | 23.67 | 22.35 |
| 33.75(85.7) | 16.01 | 9.22 | 15.79 |
| 36.00(91.4) | 0.0 | 0.0 | 0.0 |

$$\bar{\alpha} = \frac{\ln(N'/N'_\ell)}{\ln(N'_g/N'_\ell)} \tag{5.4}$$

and the relative errors were calculated by using Eq. (4.15b),

$$\Delta\bar{\alpha}/\bar{\alpha} = \frac{[2(1 - \bar{\alpha} + \bar{\alpha}^2)]^{1/2}}{\bar{\alpha}\ln(N'_g/N'_\ell)} \left[(\Delta N/N)^2 + (\Delta N_{ref}/N_{ref})^2\right]^{1/2} \tag{5.5}$$

where, to find the error due to statistical fluctuations alone, we took,

$$\Delta N = \pm \sqrt{N} \tag{5.6a}$$

and,

$$\Delta N_{ref} = \pm \sqrt{N_{ref}} \tag{5.6b}$$

and for the error due to all sources, we took (with n=6),

$$\Delta N = \pm \left[\frac{\sum_{i=1}^{n} (N_i - \bar{N})^2}{n(n-1)}\right]^{1/2} \tag{5.7a}$$

and,

$$\Delta N_{ref} = \pm \left[\frac{\sum_{i=1}^{n} (N_{refi} - \bar{N}_{ref})^2}{n(n-1)}\right]^{1/2} \tag{5.7b}$$

The values of $\bar{\alpha}$, $\Delta\bar{\alpha}/\bar{\alpha}$ based on statistical fluctuations of the source alone and $\Delta\bar{\alpha}/\bar{\alpha}$ based on Eqs. (5.7) at one location [2.25" (5.71 cm) in the middle section] are shown in Table 5.5. From the given values of $\Delta\bar{\alpha}/\bar{\alpha}$, we get the ratio (total error)/(statistical error) which is also listed in Table 5.5. The average value of this ratio is 2.27, thus, on the average, the actual error in our measurements was about 2.3 times the statistical error. The ratio at other locations where such data was taken was also similar. It is this error (ie: the total error) that we should expect for a counting time of six (6) minutes. It includes effects of statistical fluctuations in the source, fluctuations in the flow and detector drift. Table 5.6 lists the expected total error $\Delta\bar{\alpha}$, as well as the relative error $\Delta\bar{\alpha}/\bar{\alpha}$ for different values of $\bar{\alpha}$, which are obtained by multiplying the statistical error by 2.3.

We see from Table 5.6 that the error, $\Delta\bar{\alpha}$, in $\bar{\alpha}$ is between ±1.2% and ±1.4%. Thus, the values of $\bar{\alpha}$ listed in Tables 5.4.1 to 5.4.36 should be read as $\bar{\alpha} \pm \Delta\bar{\alpha}$, where $\Delta\bar{\alpha}$ is at most 1.4%. The reason why $\Delta\bar{\alpha}$ is almost the same for different values of $\bar{\alpha}$ can be seen from the error equation Eq. (4.15b) which may written as:

Table 5.5 Errors in void fraction for several cases at location 2.25 inches (5.71 cm) in the middle section

| Case | $\bar{\alpha}$ (%) | Fractional error $\Delta\bar{\alpha}/\bar{\alpha}$ using Eq. (5.5) with Eq.: (5.6) (Statistical) | (5.7) (Total) | Ratio, Total/ Statistical |
|---|---|---|---|---|
| 1AN4 | 24.49 | 0.0249 | 0.0400 | 1.61 |
| 2AN4 | 32.94 | 0.0182 | 0.0452 | 2.48 |
| 3AN4 | 24.11 | 0.0253 | 0.0867 | 3.43 |
| 1BN4 | 26.63 | 0.0228 | 0.106 | 4.65 |
| 2BN4 | 31.76 | 0.0188 | 0.0257 | 1.37 |
| 3BN4 | 31.37 | 0.0191 | 0.0338 | 1.77 |
| 1CN4 | 27.22 | 0.0224 | 0.0301 | 1.34 |
| 2CN4 | 30.50 | 0.0200 | 0.0302 | 1.51 |
| 3CN4 | 20.00 | 0.0315 | 0.0705 | 2.24 |

Average error ratio, total/statistical = 2.27

Table 5.6 Expected error and fractional error in the measured values of the void fraction

| Void fraction $\bar{\alpha}$ | Representative value of $\Delta\bar{\alpha}/\bar{\alpha}$ by statistical error from Table 4.1 | Expected fractional error = statistical error X 2.3 | Expected error in chordal average void fraction $\Delta\bar{\alpha}$ |
|---|---|---|---|
| 0.05 | ±0.119 | ±0.274 | ±0.0137 |
| 0.10 | ±0.0581 | ±0.134 | ±0.0134 |
| 0.20 | ±0.0279 | ±0.0642 | ±0.0128 |
| 0.50 | ±0.0106 | ±0.0244 | ±0.0122 |
| 0.80 | ±0.00698 | ±0.0160 | ±0.0128 |
| 1.00 | ±0.00609 | ±0.0140 | ±0.0140 |

$$\Delta\bar{\alpha} = \pm \frac{[2(1 - \bar{\alpha} + \bar{\alpha}^2)]^{1/2}}{\ln(N_g'/N_\ell')} [(\Delta N/N)^2 + (\Delta N_{ref}/N_{ref})^2]^{1/2} \qquad (5.8)$$

Notice, as $\bar{\alpha}$ goes from 0 to 1.0, the term

$$(1 - \bar{\alpha} + \bar{\alpha}^2)^{1/2}$$

goes from 1.0 (at $\bar{\alpha}$=0.0) to 0.866 (at $\bar{\alpha}$=0.5) and back to 1.0 (at $\bar{\alpha}$=1.0). So this term does not change much with changes in $\bar{\alpha}$. The term $\ln(N_g'/N_\ell')$ comes from measurements with air and water in the test section and is independent of $\bar{\alpha}$. The value of N changes by at most about 10% when $\bar{\alpha}$ goes from 0.0 to 1.0. Thus, the term $(\Delta N/N)$ doesn't change very much either. The value of $N_{ref}$ is found outside the test section and so the term $\Delta N_{ref}/N_{ref}$ is not $\alpha$-dependent at all. Thus, each of the components of the equation that determines $\Delta\bar{\alpha}$ is either mildly $\bar{\alpha}$-dependent or is not $\bar{\alpha}$-dependent at all, and therefore $\Delta\bar{\alpha}$ is only mildly dependent on $\bar{\alpha}$.

## 5.5 Repeatability of Void Fraction Measurements

It is important that data taken at a given location be repeatable (ie: if we take the counts again, we should, within experimental errors, get the same void fraction). The void fraction was determined at one location five (5) times on different days and the resulting void fractions are shown in Table 5.7. The error in the individual measurement was calculated by:

$$\Delta\bar{\alpha} = \pm \left[\frac{\sum_{i=1}^{5} (\bar{\alpha}_i - \bar{\alpha}_{ave})^2}{(5 - 1)}\right]^{1/2}$$

and is also listed in Table 5.7. It is seen that the values of $\bar{\alpha}$ are within the experimental errors tabulated in Table 5.6.

## 5.6 Discussion of Void Fraction Plots

The data tabulated in Tables 5.4.1 to 5.4.36 has been plotted using an IBM 3033 computer and a Calcomp plotter. The following cross plots have been made to compare the void fractions under various flow conditions:

(1) for the same flow split but different inlet quality (Figs. 5.2 to 5.13),

(2) for the same inlet quality, but different flow split (Figs. 5.14 to 5.25),

(3) for low flows and high flows (Figs. 5.26 to 5.43),

(4) with rods present and not present (Figs. 5.44 to 5.61).

Table 5.7 Values of void fraction determined five times at a fixed location

| Case 3BN4, Location 33.75" (85.7 cm), in Lower Section | |
|---|---|
| Number | Void Fraction, $\overline{\alpha}$ |
| 1 | 0.2830 |
| 2 | 0.3031 |
| 3 | 0.2748 |
| 4 | 0.3063 |
| 5 | 0.2954 |
| Average $\overline{\alpha}$ | 0.2925 |
| $\Delta\overline{\alpha}$ | ±0.0134 |

| CASE | SYMBOL | LIQUID MASS FLUX KG/HR.M$^2$ | FLOW SPLIT IN#4 : IN#1 | QUALITY | RODS IN | PRESSURE KPA |
|---|---|---|---|---|---|---|
| 1AN4 | | 0.562 E6 | 50.0% : 50.0% | 0.3% | NO | 31.3 |
| 2AN4 | | 0.562 E6 | 50.0% : 50.0% | 0.6% | NO | 31.6 |
| 3AN4 | | 0.562 E6 | 50.0% : 50.0% | 0.9% | NO | 31.4 |

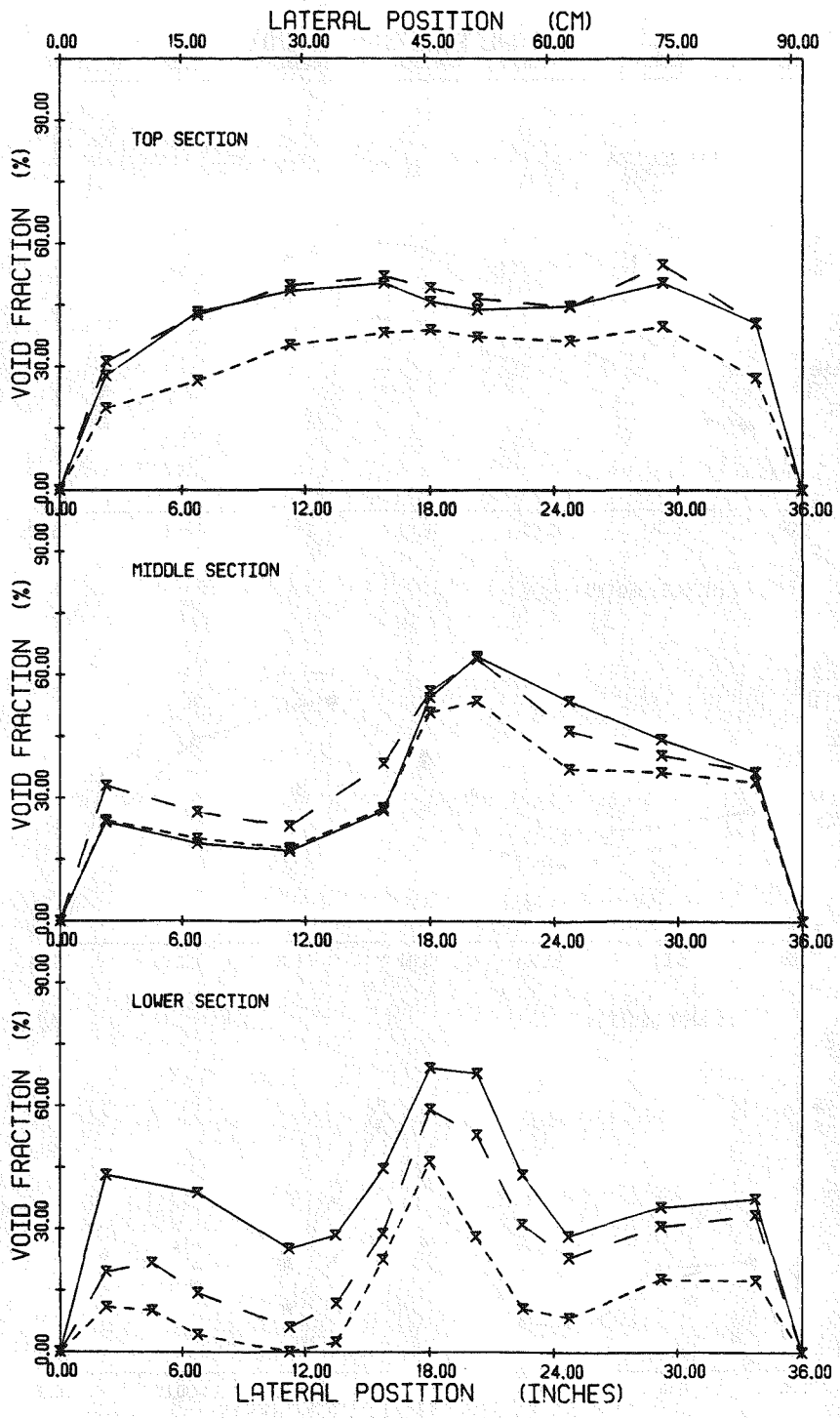


Figure 5.2 Void fraction for cases 1AN4, 2AN4 and 3AN4

| CASE | SYMBOL | LIQUID MASS FLUX KG/HR.M$^2$ | FLOW SPLIT IN#4 : IN#1 | QUALITY | RODS IN | PRESSURE KPA |
|---|---|---|---|---|---|---|
| 1BN4 | | 0.562 E6 | 62.5% : 37.5% | 0.3% | NO | 31.4 |
| 2BN4 | | 0.562 E6 | 62.5% : 37.5% | 0.6% | NO | 32.4 |
| 3BN4 | | 0.562 E6 | 62.5% : 37.5% | 0.9% | NO | 32.4 |

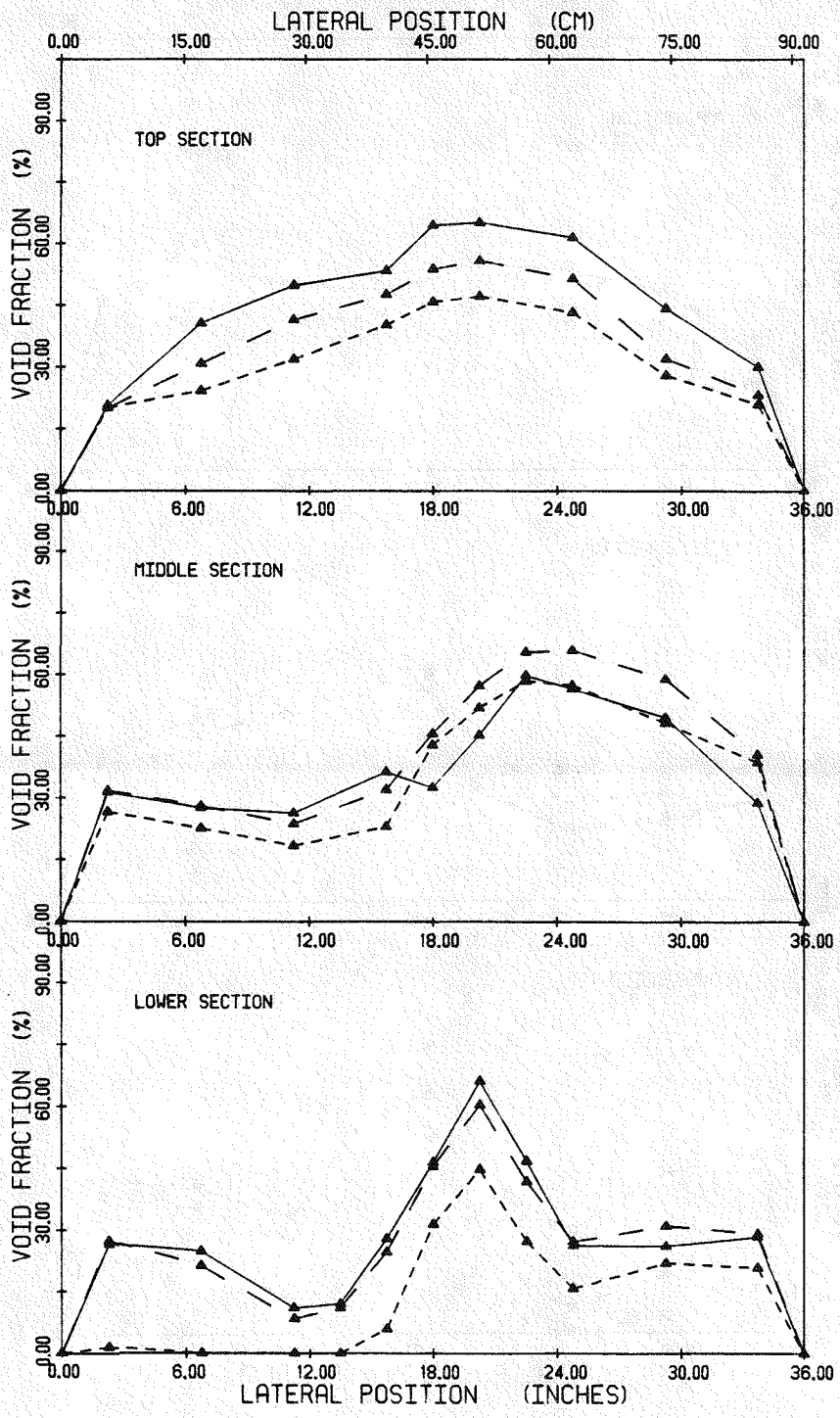


Figure 5.3 Void fraction for cases 1BN4, 2BN4 and 3BN4

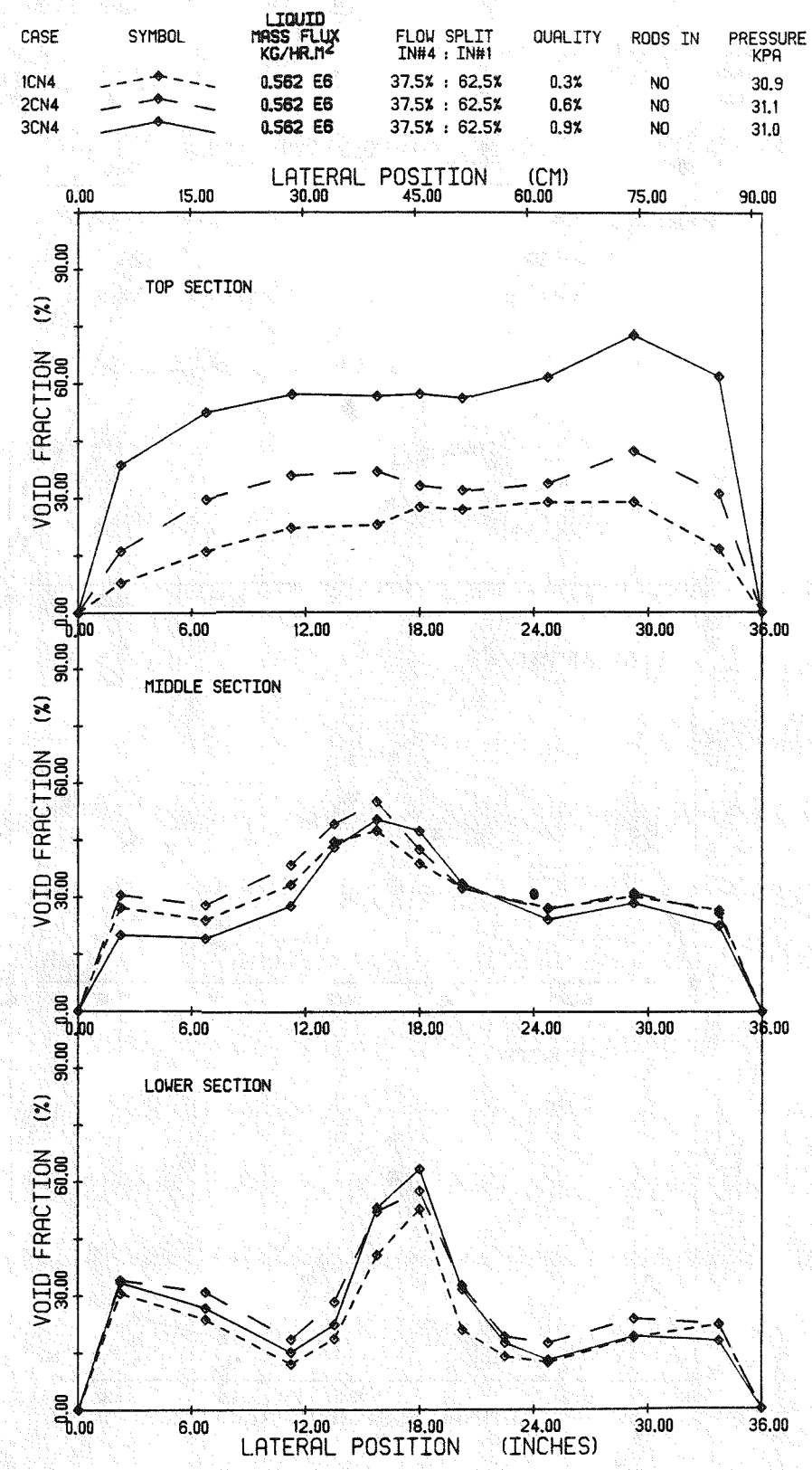


Figure 5.4 Void fraction for cases 1CN4, 2CN4 and 3CN4

| CASE | SYMBOL | LIQUID MASS FLUX KG/HR.M$^2$ | FLOW SPLIT IN#4 : IN#1 | QUALITY % | RODS IN | PRESSURE KPA |
|---|---|---|---|---|---|---|
| 4AN4 | | 1.125 E6 | 3 : 3 | 0.3 | NO | 60.2 |
| 5AN4 | | 1.125 E6 | 3 : 3 | 0.6 | NO | 63.7 |
| 6AN4 | | 1.125 E6 | 3 : 3 | 0.9 | NO | 68.1 |

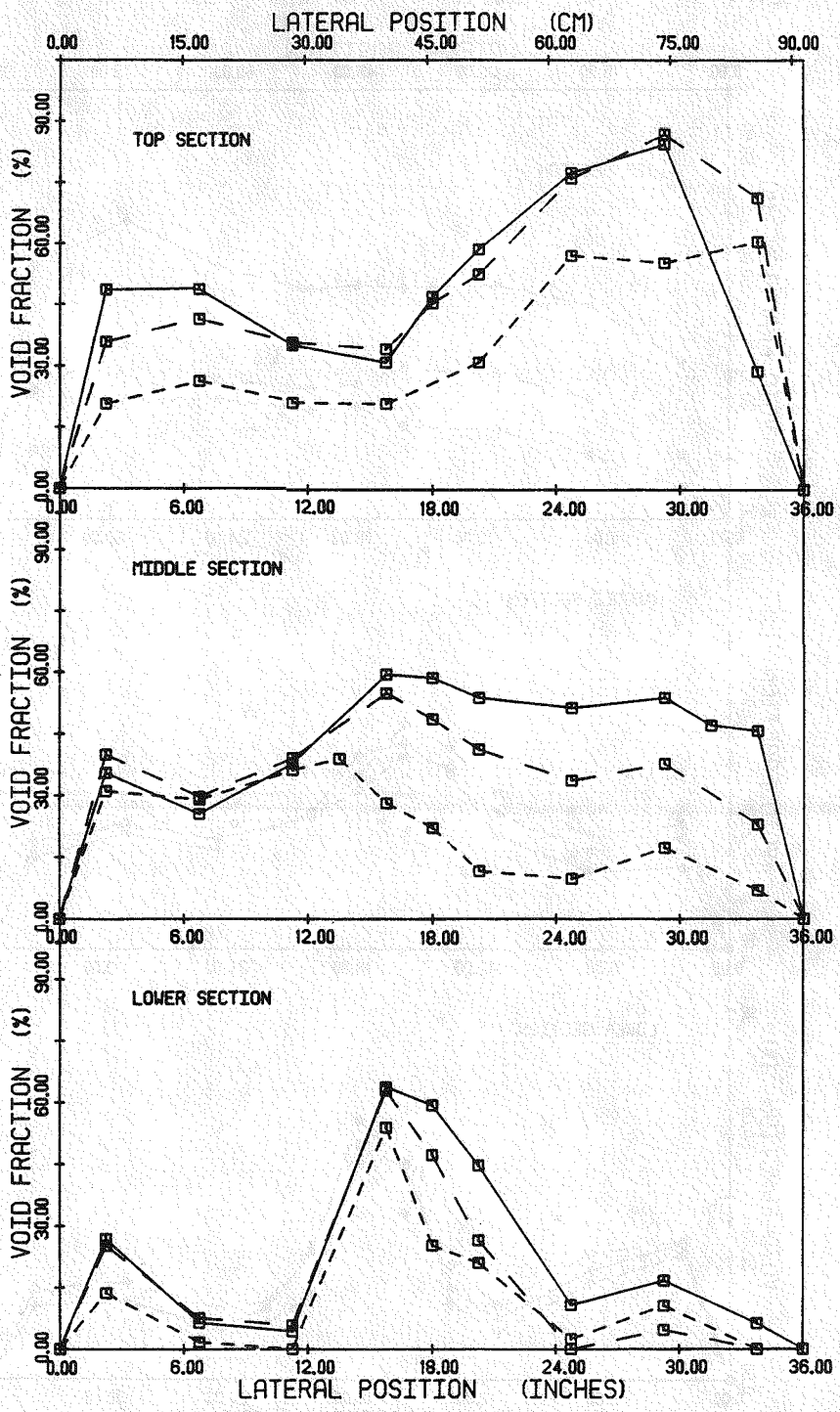


Figure 5.5 Void fraction for cases 4AN4, 5AN4 and 6AN4

| CASE | SYMBOL | LIQUID MASS FLUX KG/HR.M$^2$ | FLOW SPLIT IN#4 : IN#1 | QUALITY | RODS IN | PRESSURE KPA |
|---|---|---|---|---|---|---|
| 4BN4 | | 1.125 E6 | 62.5% : 37.5% | 0.3% | NO | 62.7 |
| 5BN4 | | 1.125 E6 | 62.5% : 37.5% | 0.6% | NO | 67.2 |
| 6BN4 | | 1.125 E6 | 62.5% : 37.5% | 0.9% | NO | 68.9 |

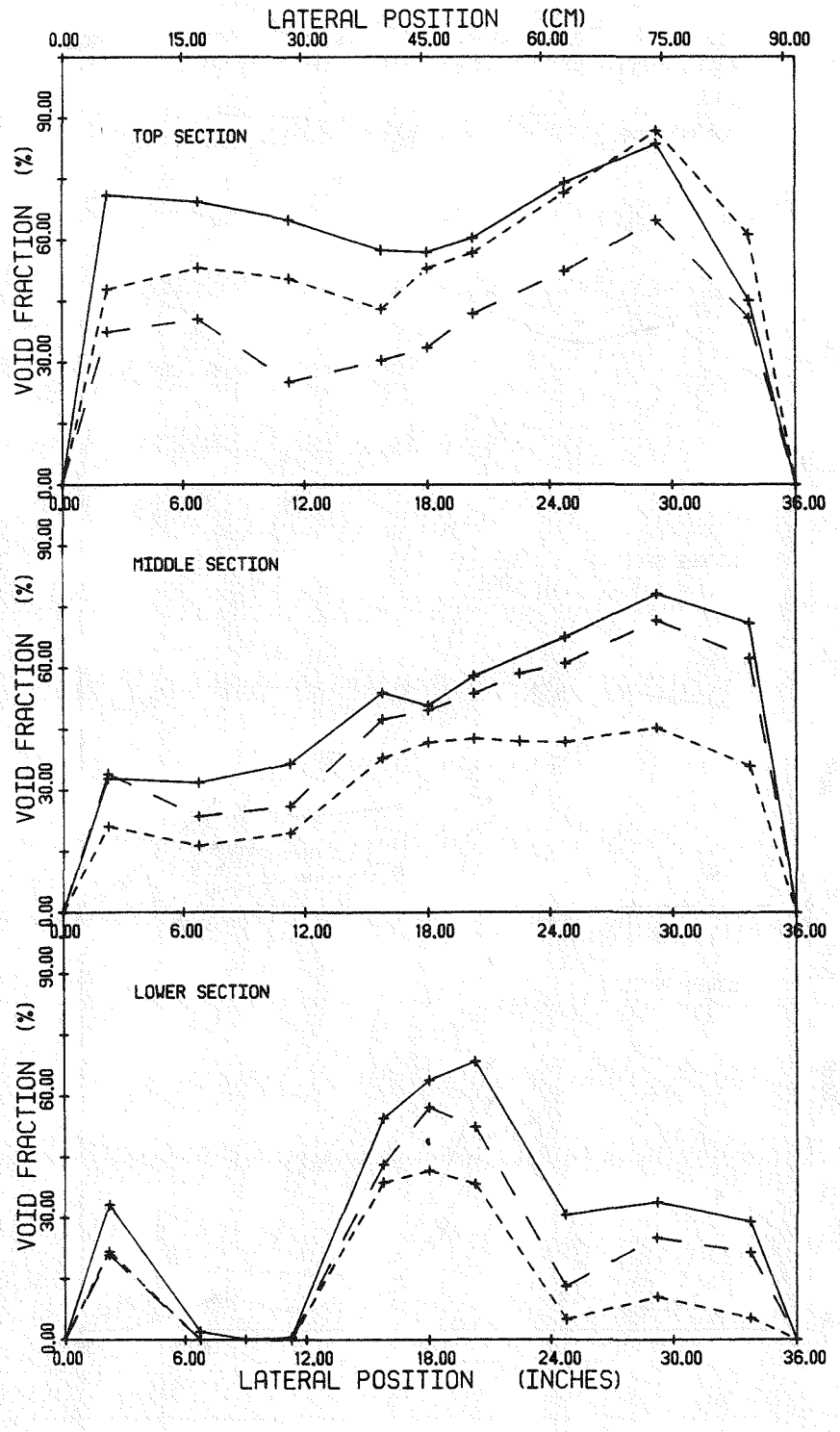


Figure 5.6 Void fraction for cases 4BN4, 5BN4 and 6BN4

| CASE | SYMBOL | LIQUID MASS FLUX KG/HR.M² | FLOW SPLIT IN#4 : IN#1 | QUALITY | RODS IN | PRESSURE KPA |
|---|---|---|---|---|---|---|
| 4CN4 | | 1.125 E6 | 37.5% : 62.5% | 0.3% | NO | 59.5 |
| 5CN4 | | 1.125 E6 | 37.5% : 62.5% | 0.6% | NO | 61.4 |
| 6CN4 | | 1.125 E6 | 37.5% : 62.5% | 0.9% | NO | 62.9 |

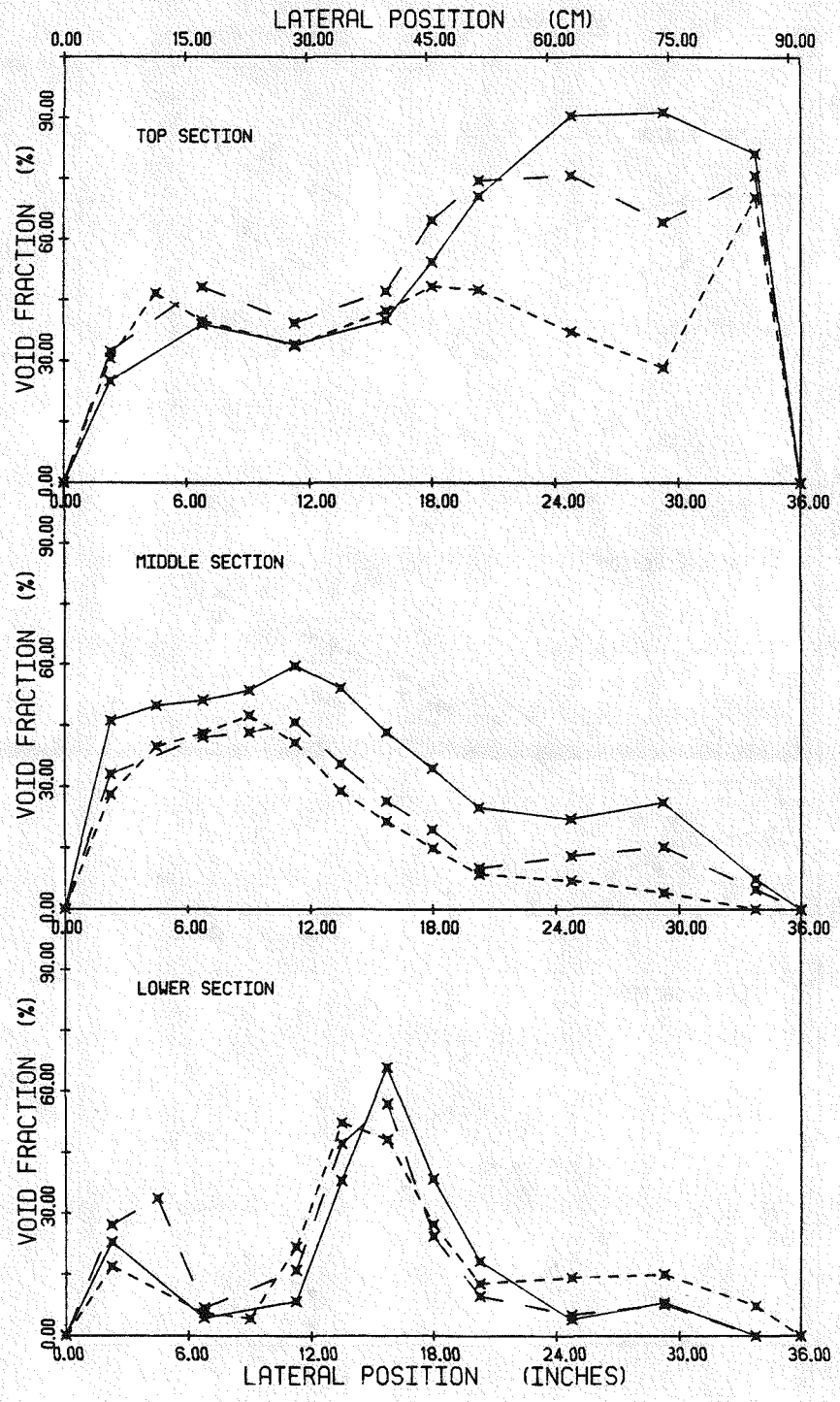


Figure 5.7 Void fraction for cases 4CN4, 5CN4 and 6CN4

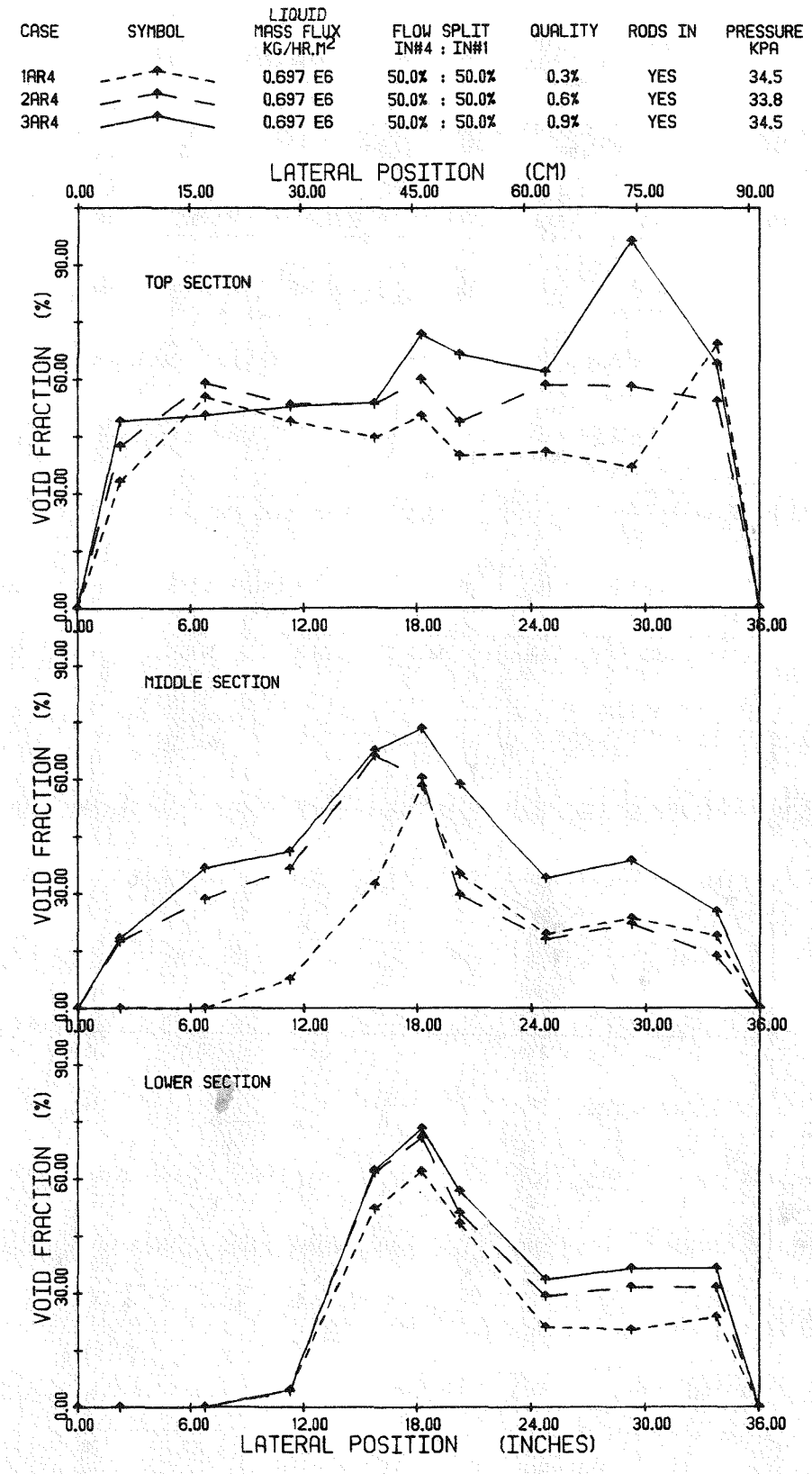


Figure 5.8 Void fraction for cases 1AR4, 2AR4 and 3AR4

| CASE | SYMBOL | LIQUID MASS FLUX KG/HR.M$^2$ | FLOW SPLIT IN#4 : IN#1 | QUALITY | RODS IN | PRESSURE KPA |
|---|---|---|---|---|---|---|
| 1BR4 | | 0.697 E6 | 62.5% : 37.5% | 0.3% | YES | 34.5 |
| 2BR4 | | 0.697 E6 | 62.5% : 37.5% | 0.6% | YES | 34.5 |
| 3BR4 | | 0.697 E6 | 62.5% : 37.5% | 0.9% | YES | 34.5 |

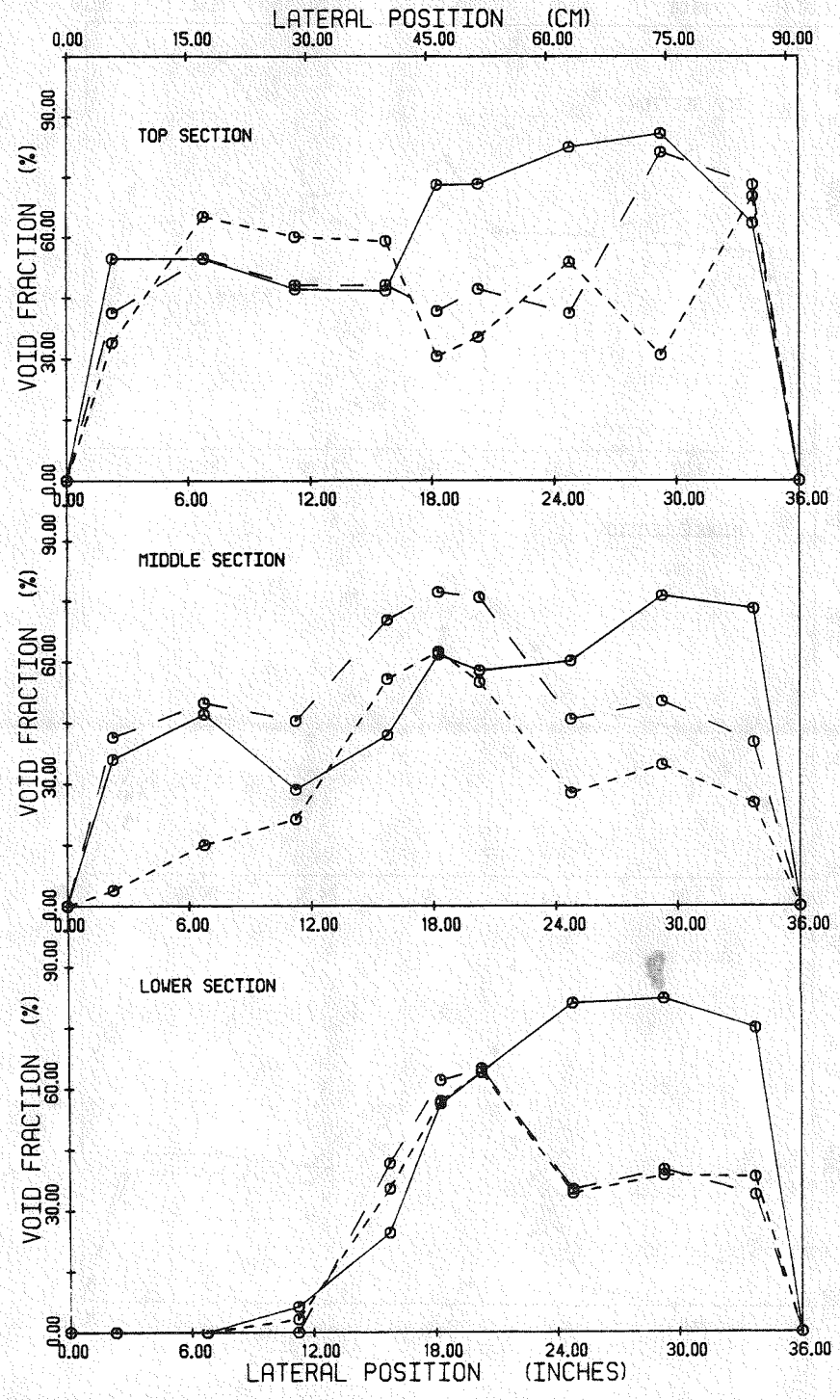


Figure 5.9 Void fraction for cases 1BR4, 2BR4 and 3BR4

| CASE | SYMBOL | LIQUID MASS FLUX KG/HR.M$^2$ | FLOW SPLIT IN#4 : IN#1 | QUALITY | RODS IN | PRESSURE KPA |
|---|---|---|---|---|---|---|
| 1CR4 | | 0.697 E6 | 37.5% : 62.5% | 0.3% | YES | 33.8 |
| 2CR4 | | 0.697 E6 | 37.5% : 62.5% | 0.6% | YES | 33.8 |
| 3CR4 | | 0.697 E6 | 37.5% : 62.5% | 0.9% | YES | 34.5 |

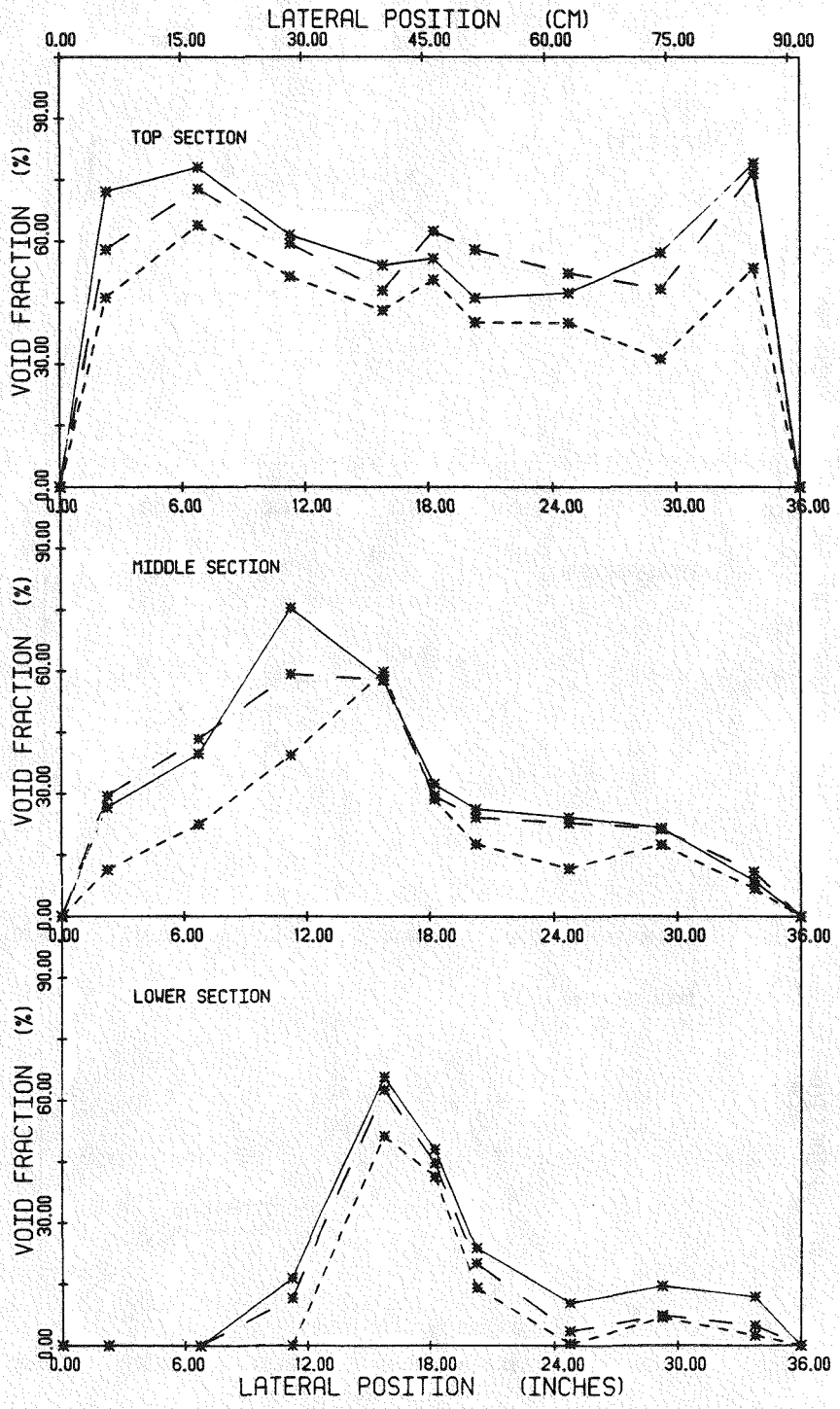


Figure 5.10 Void fraction for cases 1CR4, 2CR4 and 3CR4

| CASE | SYMBOL | LIQUID MASS FLUX KG/HR.M$^2$ | FLOW SPLIT IN#4 : IN#1 | QUALITY | RODS IN | PRESSURE KPA |
|---|---|---|---|---|---|---|
| 4AR4 | | 1.395 E6 | 50.0% : 50.0% | 0.3% | YES | 75.1 |
| 5AR4 | | 1.395 E6 | 50.0% : 50.0% | 0.6% | YES | 78.1 |
| 6AR4 | | 1.395 E6 | 50.0% : 50.0% | 0.9% | YES | 81.4 |

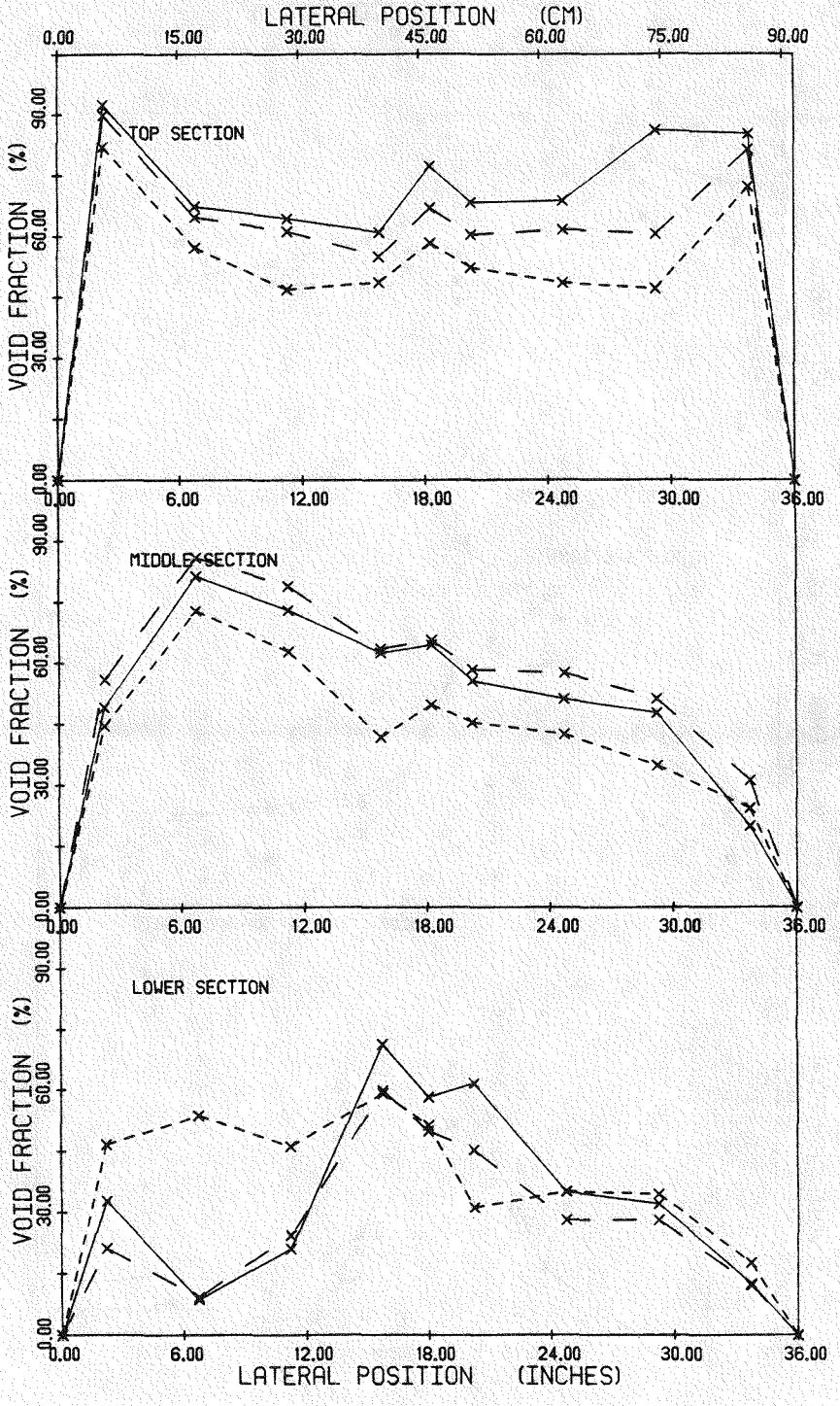


Figure 5.11 Void fraction for cases 4AR4, 5AR4 and 6AR4

| CASE | SYMBOL | LIQUID MASS FLUX KG/HR.M² | FLOW SPLIT IN#4 : IN#1 | QUALITY | RODS IN | PRESSURE KPA |
|---|---|---|---|---|---|---|
| 4BR4 | | 1.395 E6 | 62.5% : 37.5% | 0.3% | YES | 76.3 |
| 5BR4 | | 1.395 E6 | 62.5% : 37.5% | 0.6% | YES | 80.5 |
| 6BR4 | | 1.395 E6 | 62.5% : 37.5% | 0.9% | YES | 85.0 |

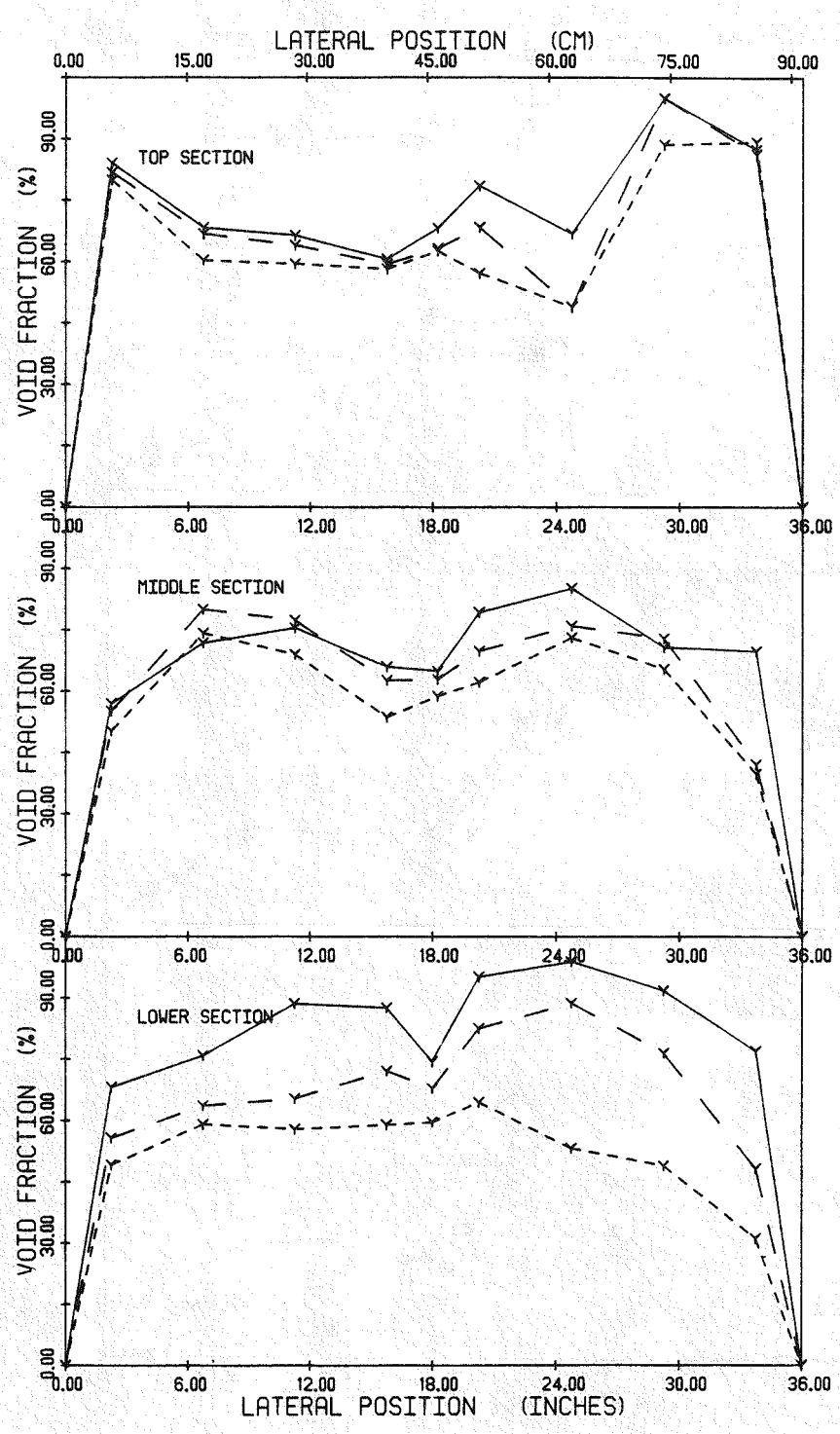


Figure 5.12 Void fraction for cases 4BR4, 5BR4 and 6BR4

| CASE | SYMBOL | LIQUID MASS FLUX KG/HR.M$^2$ | FLOW SPLIT IN#4 : IN#1 | QUALITY | RODS IN | PRESSURE KPA |
|---|---|---|---|---|---|---|
| 4CR4 | | 1.395 E6 | 37.5% : 62.5% | 0.3% | YES | 73.5 |
| 5CR4 | | 1.395 E6 | 37.5% : 62.5% | 0.6% | YES | 78.1 |
| 6CR4 | | 1.395 E6 | 37.5% : 62.5% | 0.9% | YES | 79.5 |

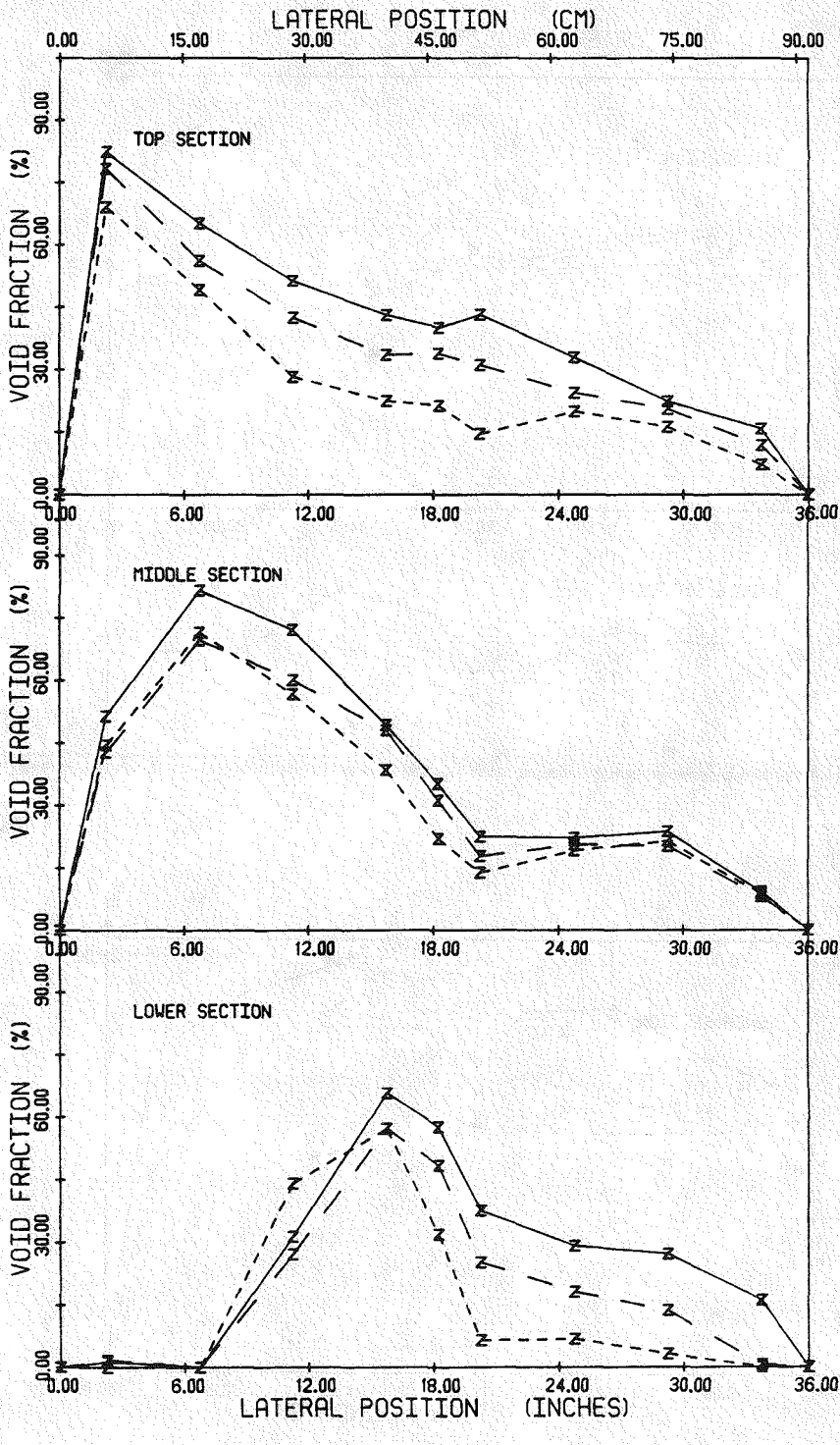


Figure 5.13 Void fraction for cases 4CR4, 5CR4 and 6CR4

| CASE | SYMBOL | LIQUID MASS FLUX KG/HR.M$^2$ | FLOW SPLIT IN#4 : IN#1 | QUALITY | RODS IN | PRESSURE KPA |
|---|---|---|---|---|---|---|
| 1AN4 | | 0.562 E6 | 50.0% : 50.0% | 0.3% | NO | 31.3 |
| 1BN4 | | 0.562 E6 | 62.5% : 37.5% | 0.3% | NO | 31.4 |
| 1CN4 | | 0.562 E6 | 37.5% : 62.5% | 0.3% | NO | 30.9 |

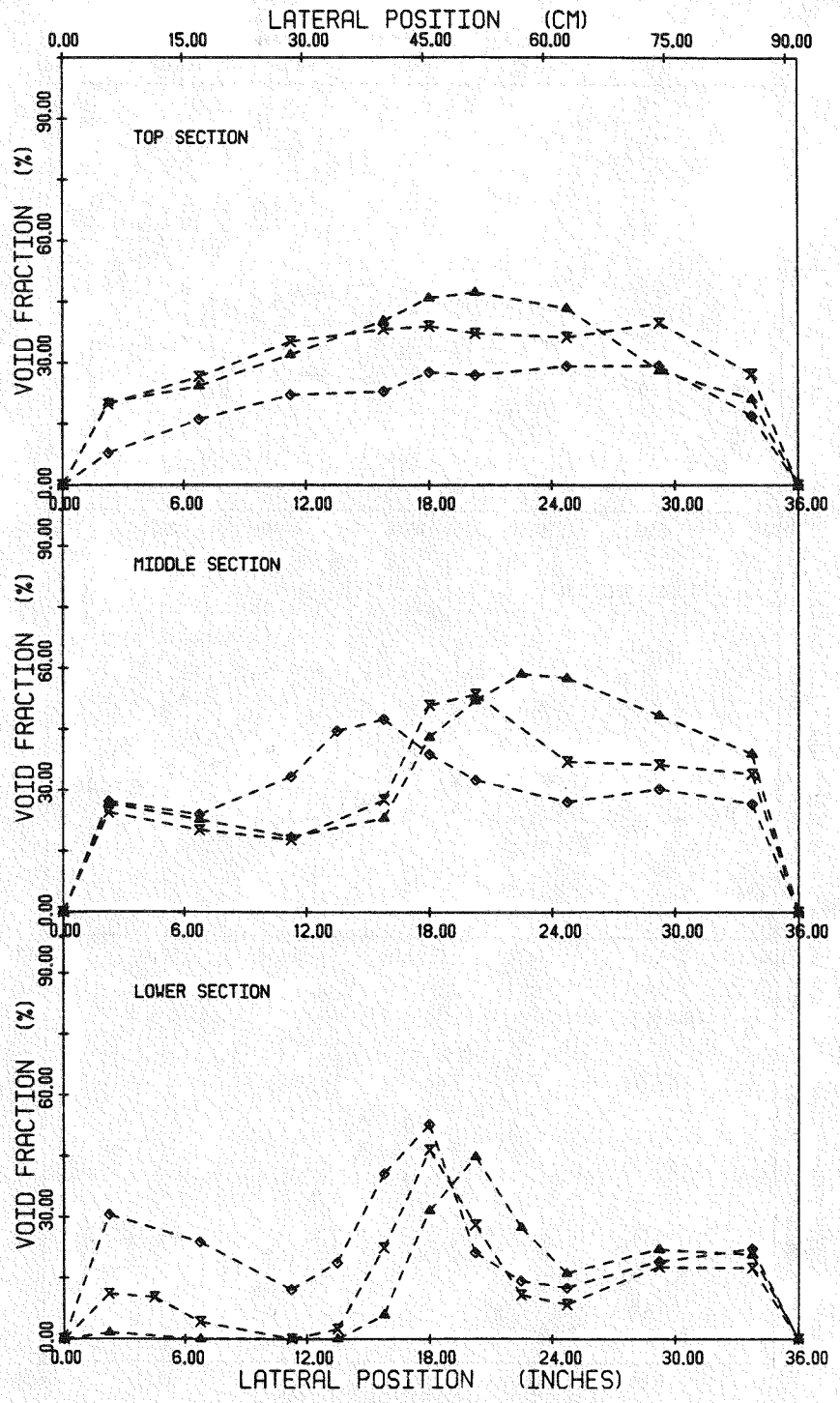


Figure 5.14 Void fraction for cases 1AN4, 1BN4 and 1CN4

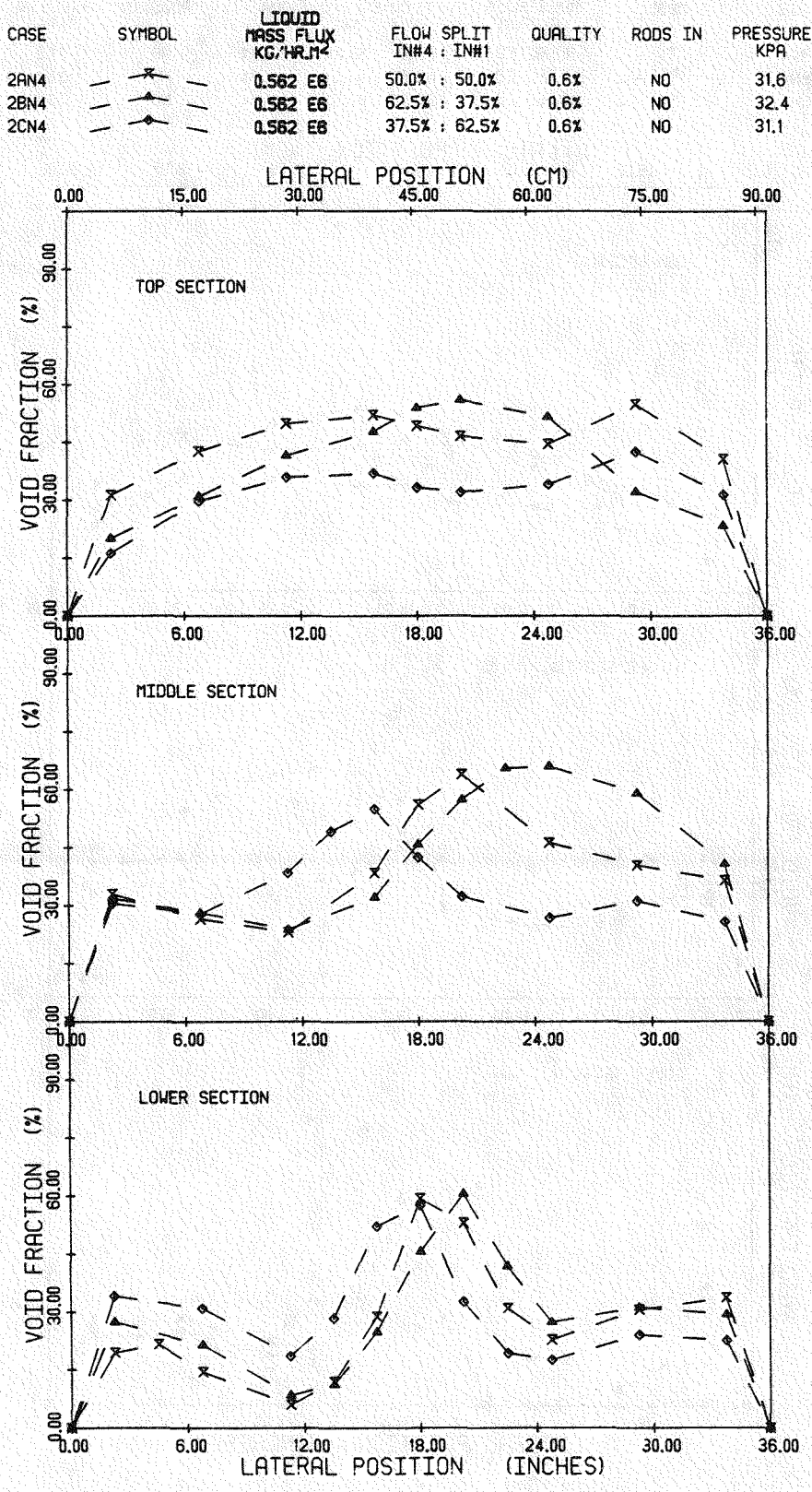


Figure 5.15 Void fraction for cases 2AN4, 2BN4 and 2CN4

| CASE | SYMBOL | LIQUID MASS FLUX KG/HR.M$^2$ | FLOW SPLIT IN#4 : IN#1 | QUALITY | RODS IN | PRESSURE KPA |
|---|---|---|---|---|---|---|
| 3AN4 | | 0.562 E6 | 50.0% : 50.0% | 0.9% | NO | 31.4 |
| 3BN4 | | 0.562 E6 | 62.5% : 37.5% | 0.9% | NO | 32.4 |
| 3CN4 | | 0.562 E6 | 37.5% : 62.5% | 0.9% | NO | 31.0 |

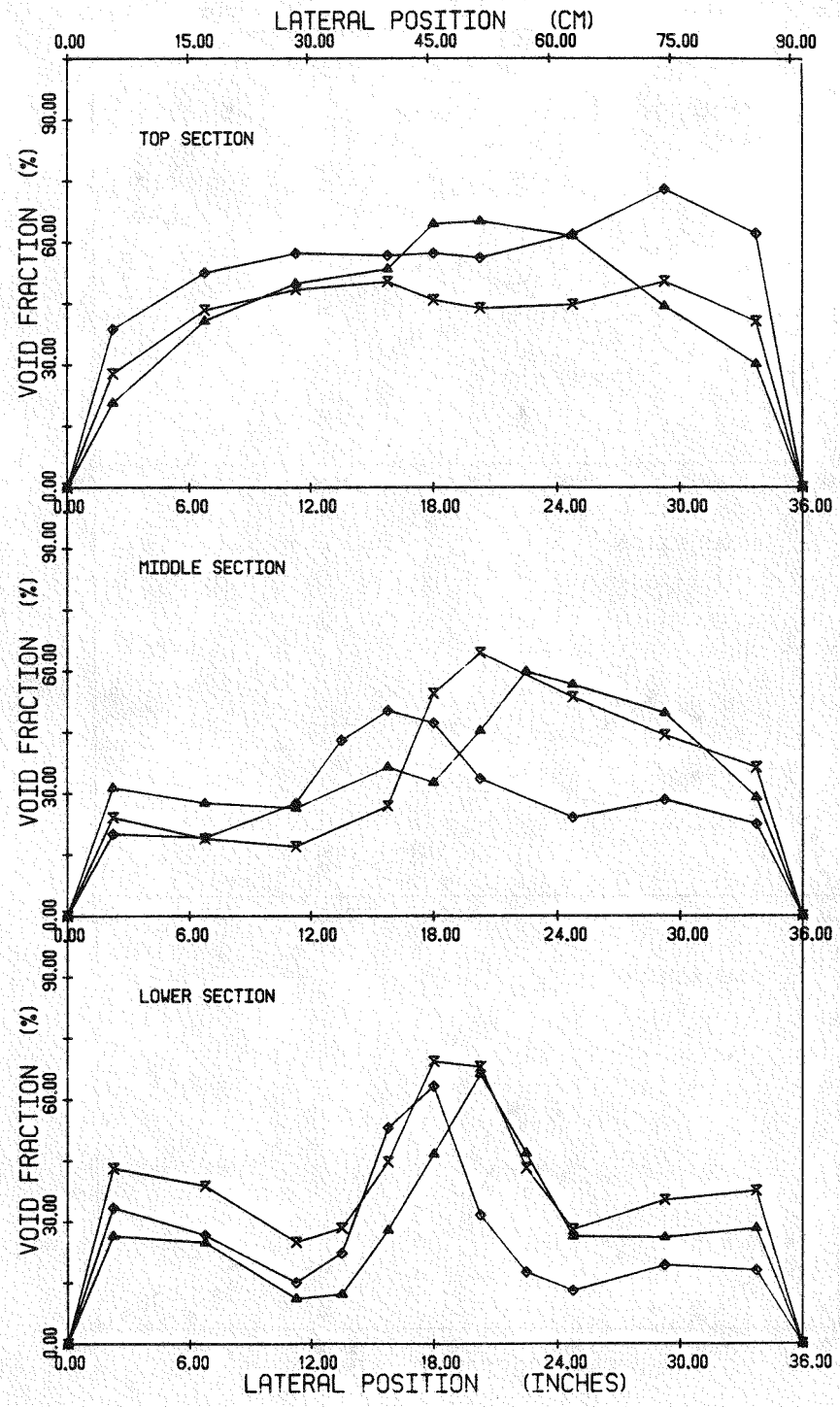


Figure 5.16 Void fraction for cases 3AN4, 3BN4 and 3CN4

| CASE | SYMBOL | LIQUID MASS FLUX KG/HR.M$^2$ | FLOW SPLIT IN#4 : IN#1 | QUALITY | RODS IN | PRESSURE KPA |
|---|---|---|---|---|---|---|
| 4AN4 | | 1.125 E6 | 50.0% : 50.0% | 0.3% | NO | 60.2 |
| 4BN4 | | 1.125 E6 | 62.5% : 37.5% | 0.3% | NO | 62.7 |
| 4CN4 | | 1.125 E6 | 37.5% : 62.5% | 0.3% | NO | 59.5 |

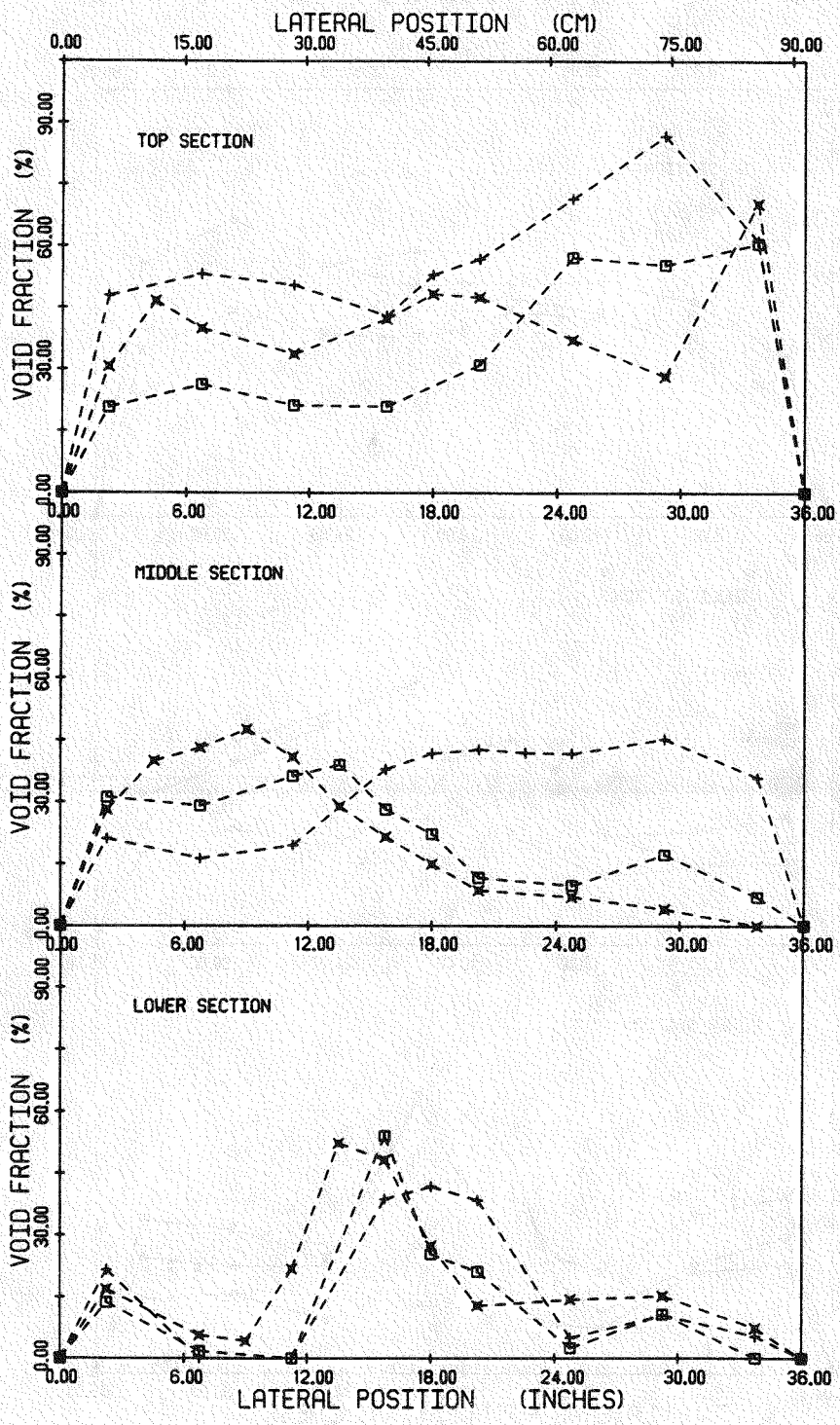


Figure 5.17 Void fraction for cases 4AN4, 4BN4 and 4CN4

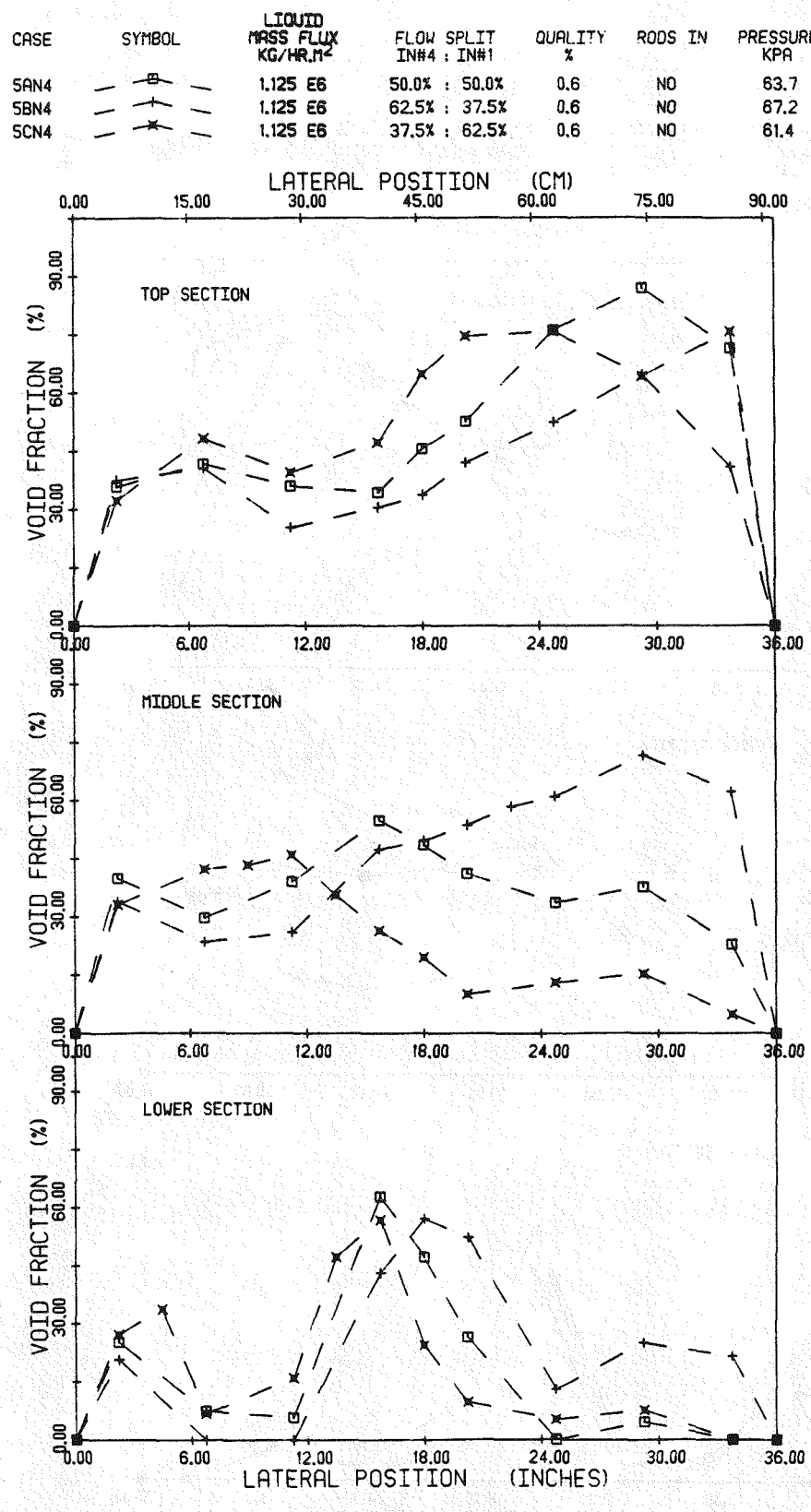


Figure 5.18 Void fraction for cases 5AN4, 5BN4 and 5CN4

| CASE | SYMBOL | LIQUID MASS FLUX KG/HR.M$^2$ | FLOW SPLIT IN#4 : IN#1 | QUALITY | RODS IN | PRESSURE KPA |
|---|---|---|---|---|---|---|
| 6AN4 | | 1.125 E6 | 50.0% : 50.0% | 0.9% | NO | 68.1 |
| 6BN4 | | 1.125 E6 | 62.5% : 37.5% | 0.9% | NO | 68.9 |
| 6CN4 | | 1.125 E6 | 37.5% : 62.5% | 0.9% | NO | 62.9 |

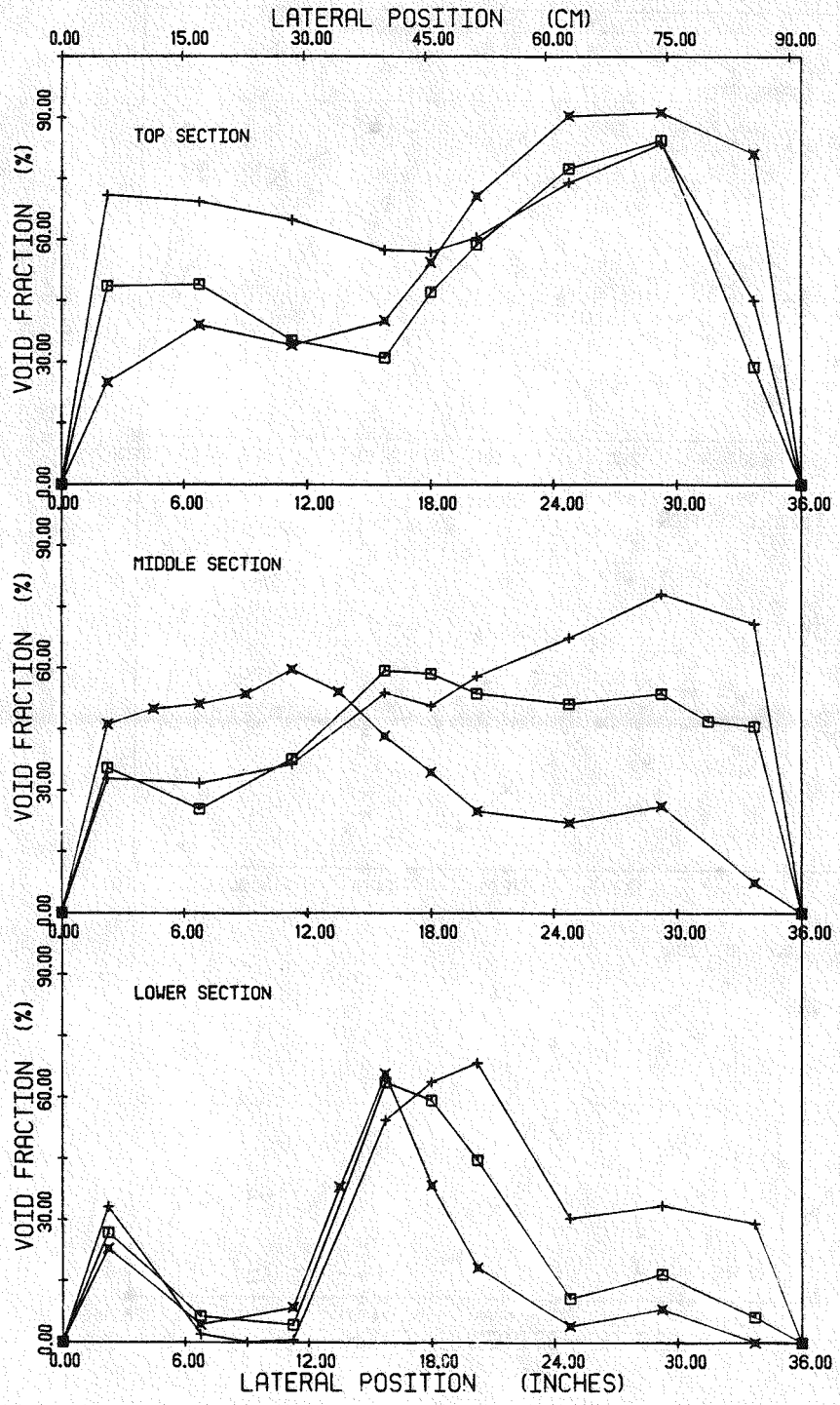


Figure 5.19 Void fraction for cases 6AN4, 6BN4 and 6CN4

| CASE | SYMBOL | LIQUID MASS FLUX KG/HR.M$^2$ | FLOW SPLIT IN#4 : IN#1 | QUALITY | RODS IN | PRESSURE KPA |
|---|---|---|---|---|---|---|
| 1AR4 | | 0.697 E6 | 50.0% : 50.0% | 0.3% | YES | 34.5 |
| 1BR4 | | 0.697 E6 | 62.5% : 37.5% | 0.3% | YES | 34.5 |
| 1CR4 | | 0.697 E6 | 37.5% : 62.5% | 0.3% | YES | 33.8 |

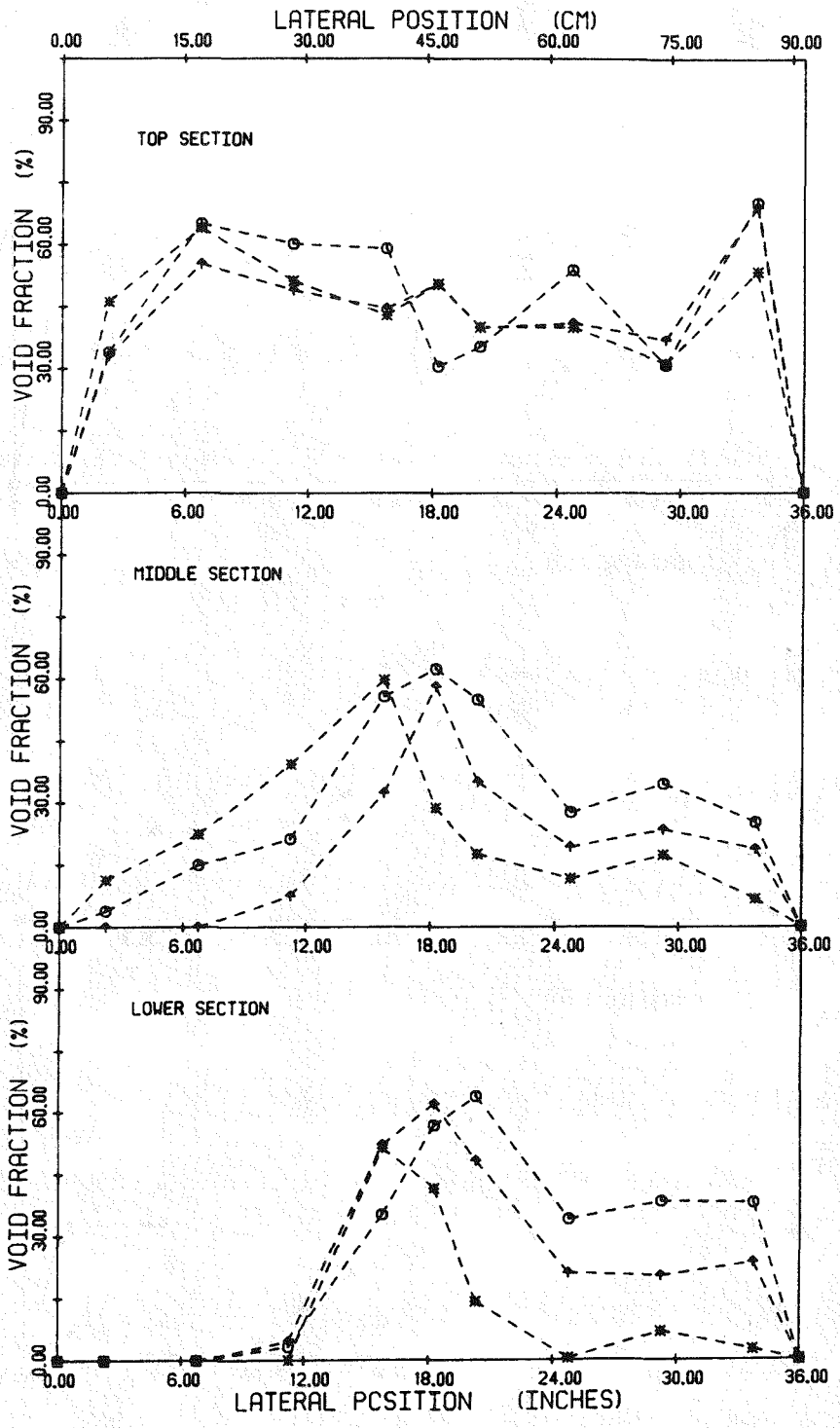


Figure 5.20 Void fraction for cases 1AR4, 1BR4 and 1CR4

| CASE | SYMBOL | LIQUID MASS FLUX KG/HRM² | FLOW SPLIT IN#4 : IN#1 | QUALITY | RODS IN | PRESSURE KPA |
|---|---|---|---|---|---|---|
| 2AR4 | | 0.697 E6 | 50.0% : 50.0% | 0.6% | YES | 33.8 |
| 2BR4 | | 0.697 E6 | 62.5% : 37.5% | 0.6% | YES | 34.5 |
| 2CR4 | | 0.697 E6 | 37.5% : 62.5% | 0.6% | YES | 33.8 |

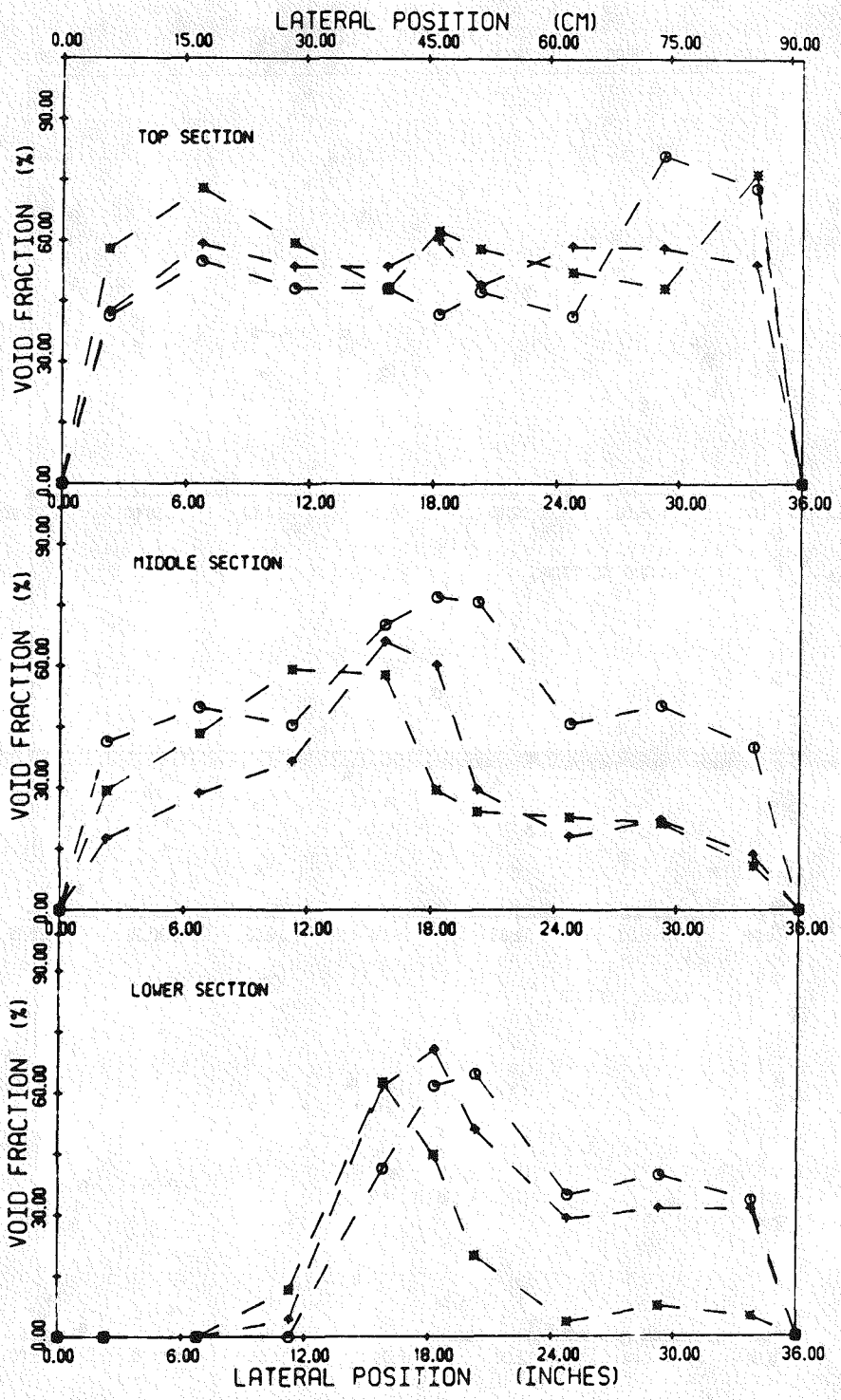


Figure 5.21 Void fraction for cases 2AR4, 2BR4 and 2CR4

| CASE | SYMBOL | LIQUID MASS FLUX KG/HR.M$^2$ | FLOW SPLIT IN#4 : IN#1 | QUALITY | RODS IN | PRESSURE KPA |
|---|---|---|---|---|---|---|
| 3AR4 | | 0.697 E6 | 50.0% : 50.0% | 0.9% | YES | 34.5 |
| 3BR4 | | 0.697 E6 | 62.5% : 37.5% | 0.9% | YES | 34.5 |
| 3CR4 | | 0.697 E6 | 37.5% : 62.5% | 0.9% | YES | 34.5 |

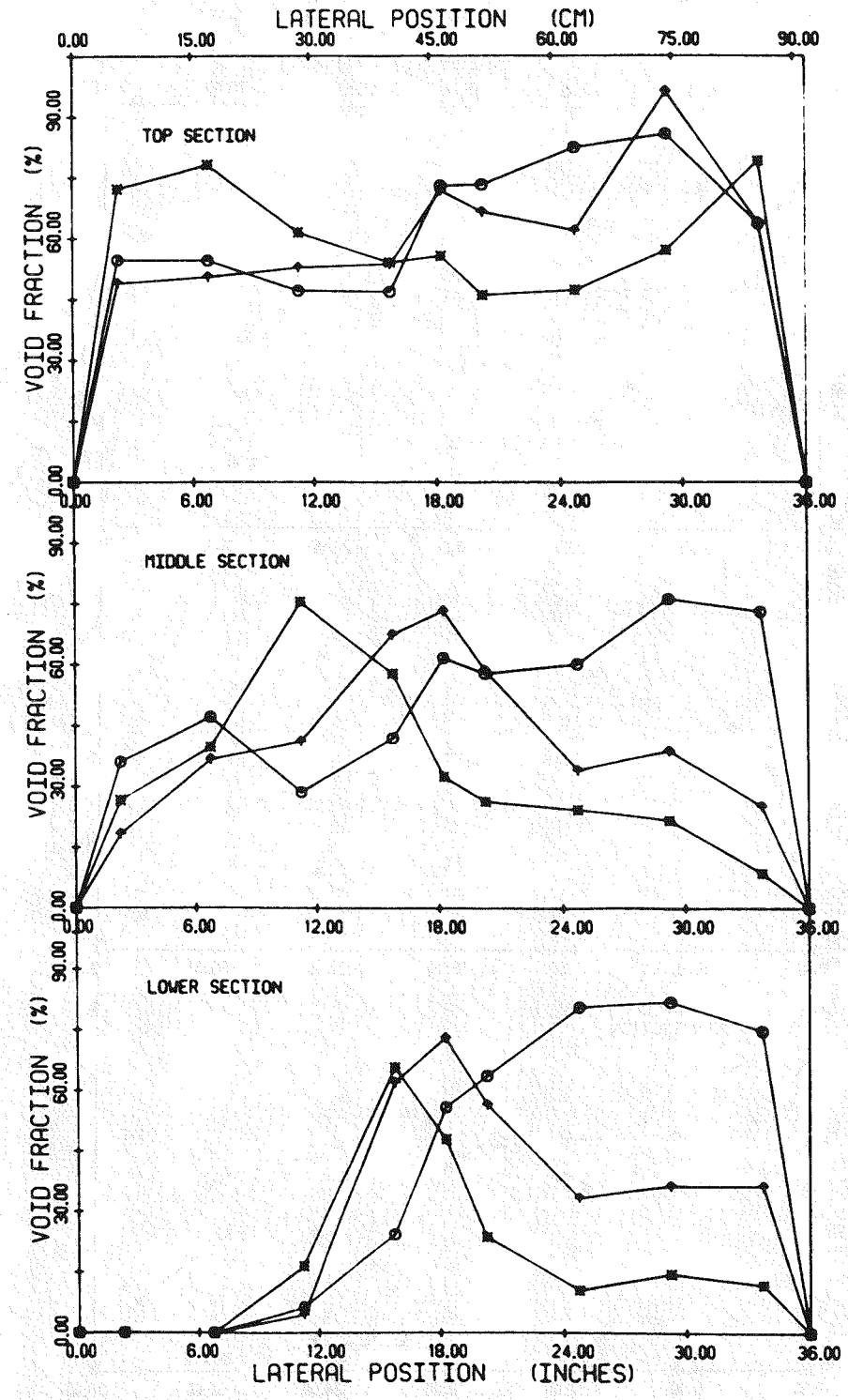


Figure 5.22 Void fraction for cases 3AR4, 3BR4 and 3CR4

| CASE | SYMBOL | LIQUID MASS FLUX KG/HR.M$^2$ | FLOW SPLIT IN#4 : IN#1 | QUALITY | RODS IN | PRESSURE KPA |
|---|---|---|---|---|---|---|
| 4AR4 | | 1.395 E6 | 50.0% : 50.0% | 0.3% | YES | 75.1 |
| 4BR4 | | 1.395 E6 | 62.5% : 37.5% | 0.3% | YES | 76.3 |
| 4CR4 | | 1.395 E6 | 37.5% : 62.5% | 0.3% | YES | 73.5 |

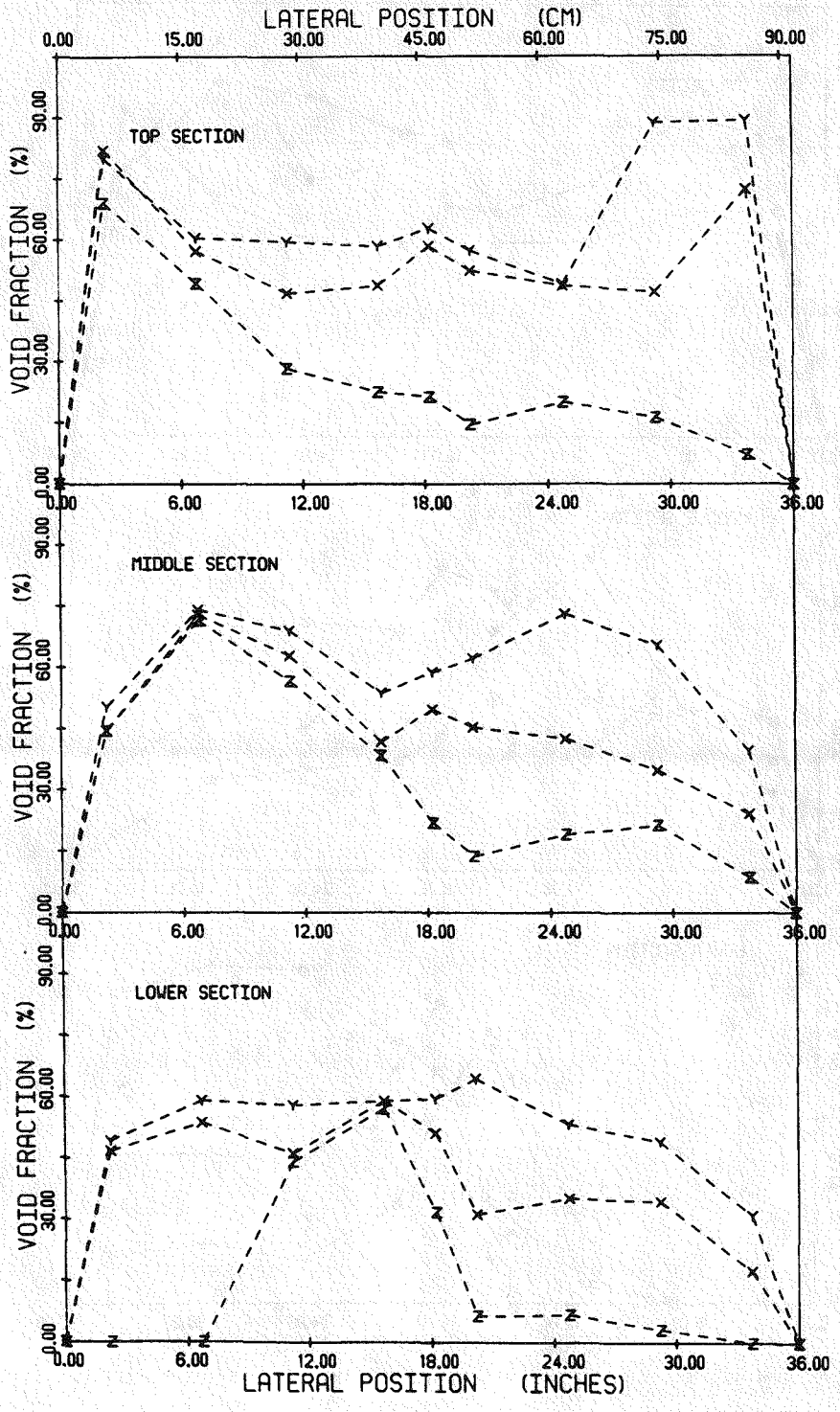


Figure 5.23 Void fraction for cases 4AR4, 4BR4 and 4CR4

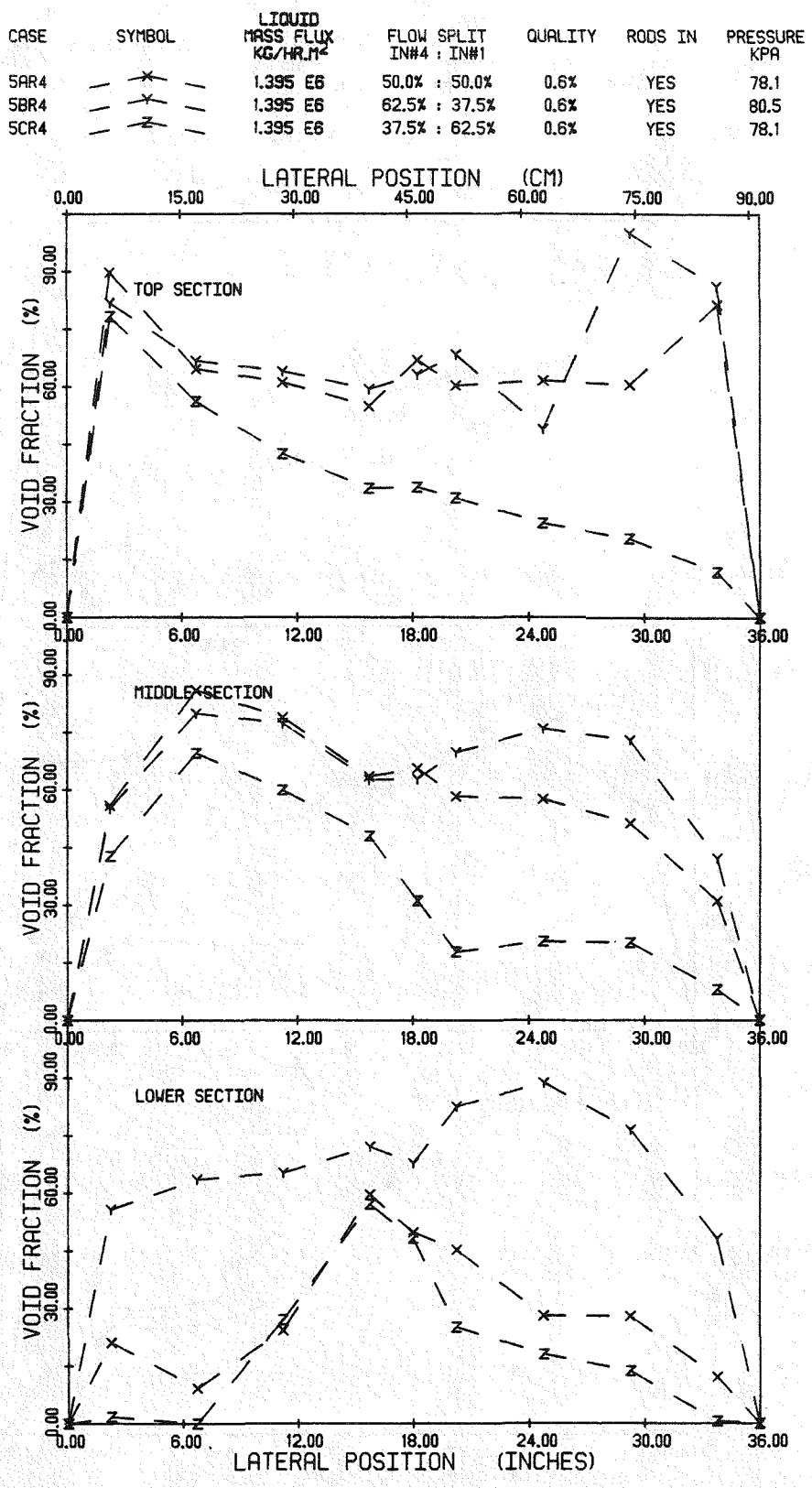


Figure 5.24 Void fraction for cases 5AR4, 5BR4 and 5CR4

| CASE | SYMBOL | LIQUID MASS FLUX KG/HR.M$^2$ | FLOW SPLIT IN#4 : IN#1 | QUALITY | RODS IN | PRESSURE KPA |
|---|---|---|---|---|---|---|
| 6AR4 | | 1.395 E6 | 50.0% : 50.0% | 0.9% | YES | 81.4 |
| 6BR4 | | 1.395 E6 | 62.5% : 37.5% | 0.9% | YES | 85.0 |
| 6CR4 | | 1.395 E6 | 37.5% : 62.5% | 0.9% | YES | 79.5 |

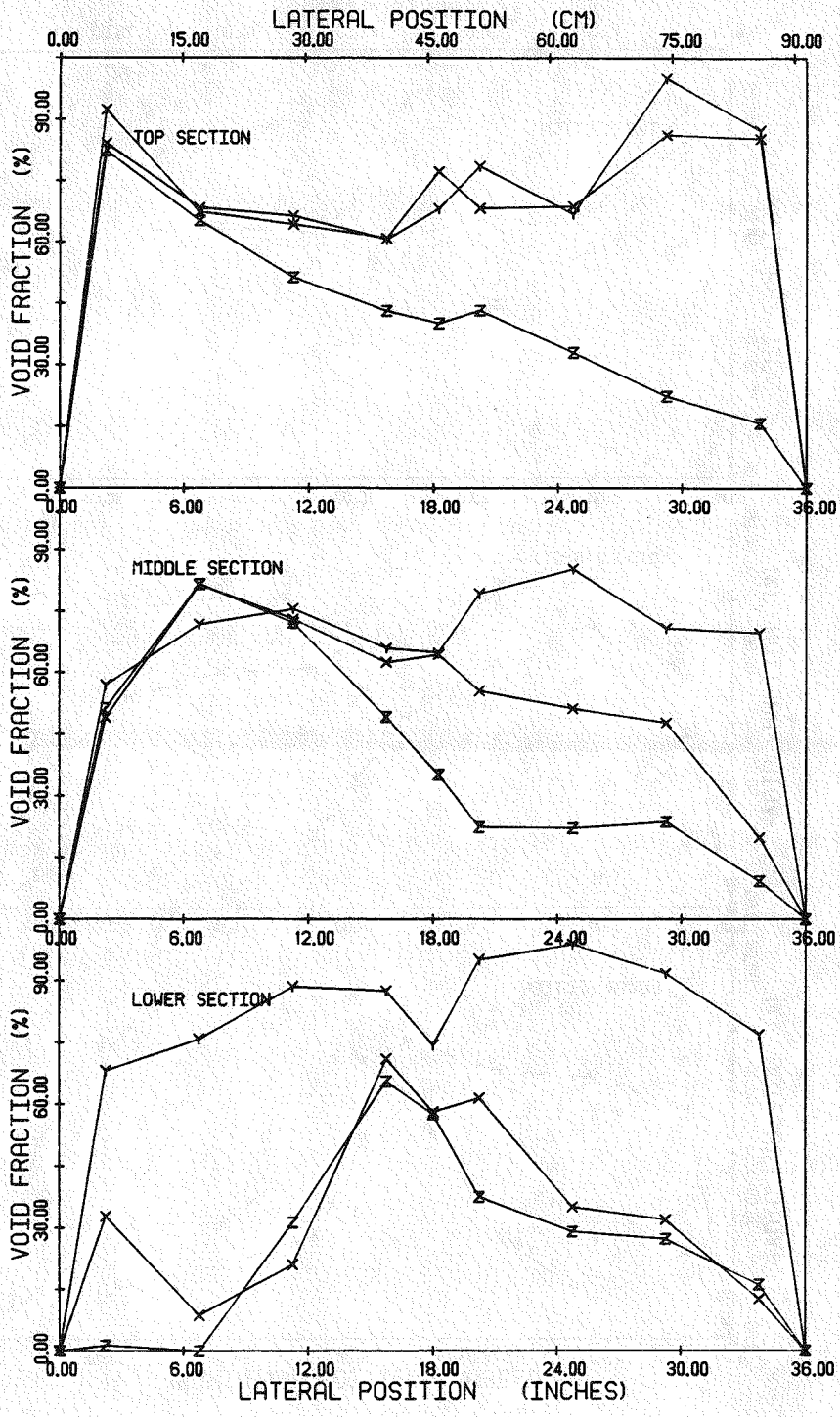


Figure 5.25 Void fraction for cases 6AR4, 6BR4 and 6CR4

| CASE | SYMBOL | LIQUID MASS FLUX KG/HR.M$^2$ | FLOW SPLIT IN#4 : IN#1 | QUALITY | RODS IN | PRESSURE KPA |
|---|---|---|---|---|---|---|
| 1AN4 | | 0.562 E6 | 50.0% : 50.0% | 0.3% | NO | 31.3 |
| 4AN4 | | 1.125 E6 | 50.0% : 50.0% | 0.3% | NO | 60.2 |

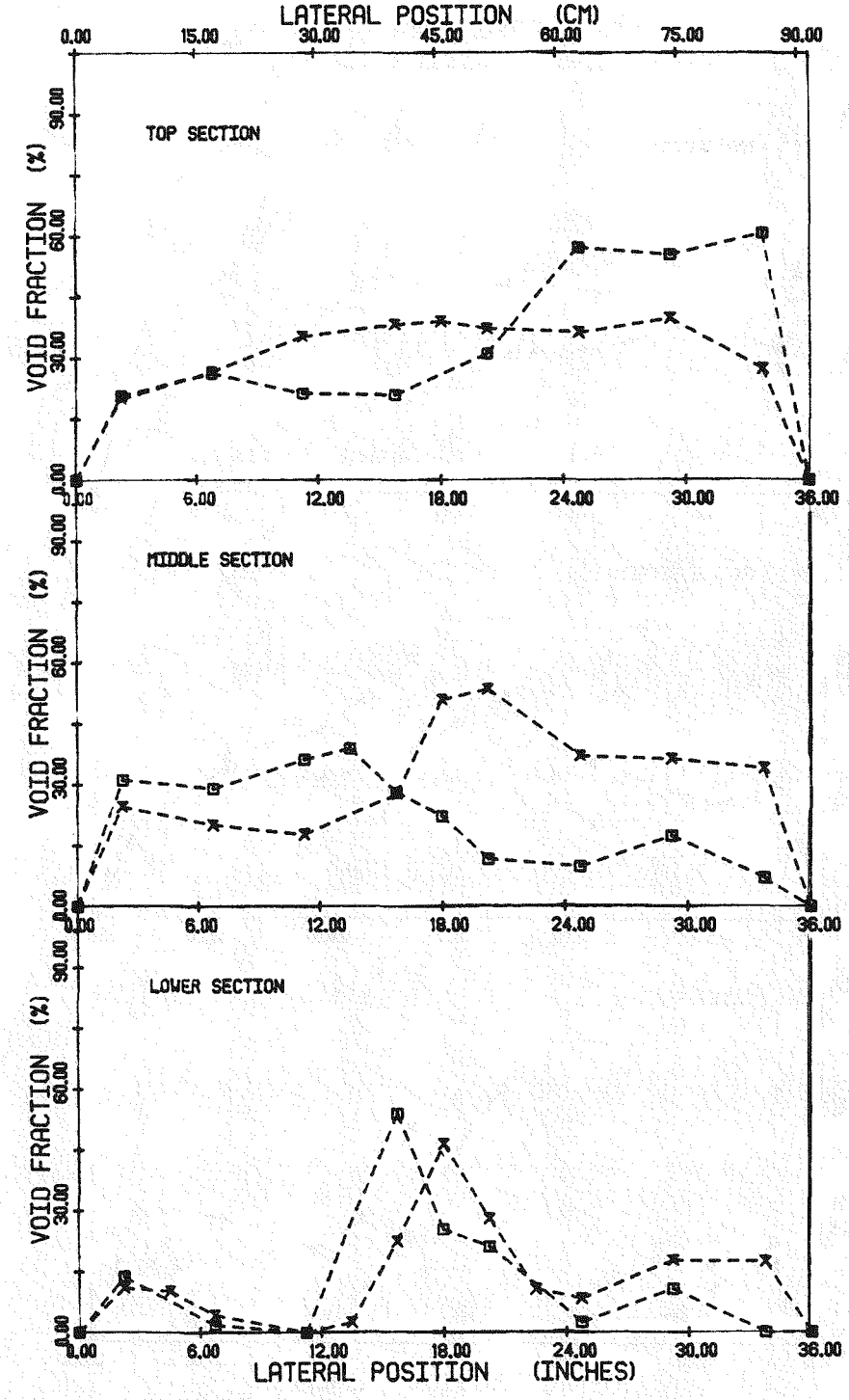


Figure 5.26 Void fraction for cases 1AN4 and 4AN4

| CASE | SYMBOL | LIQUID MASS FLUX KG/HR.M$^2$ | FLOW SPLIT IN#4 : IN#1 | QUALITY | RODS IN | PRESSURE KPA |
|---|---|---|---|---|---|---|
| 2AN4 | | 0.562 E6 | 50.0% : 50.0% | 0.6% | NO | 31.6 |
| 5AN4 | | 1.125 E6 | 50.0% : 50.0% | 0.6% | NO | 63.7 |

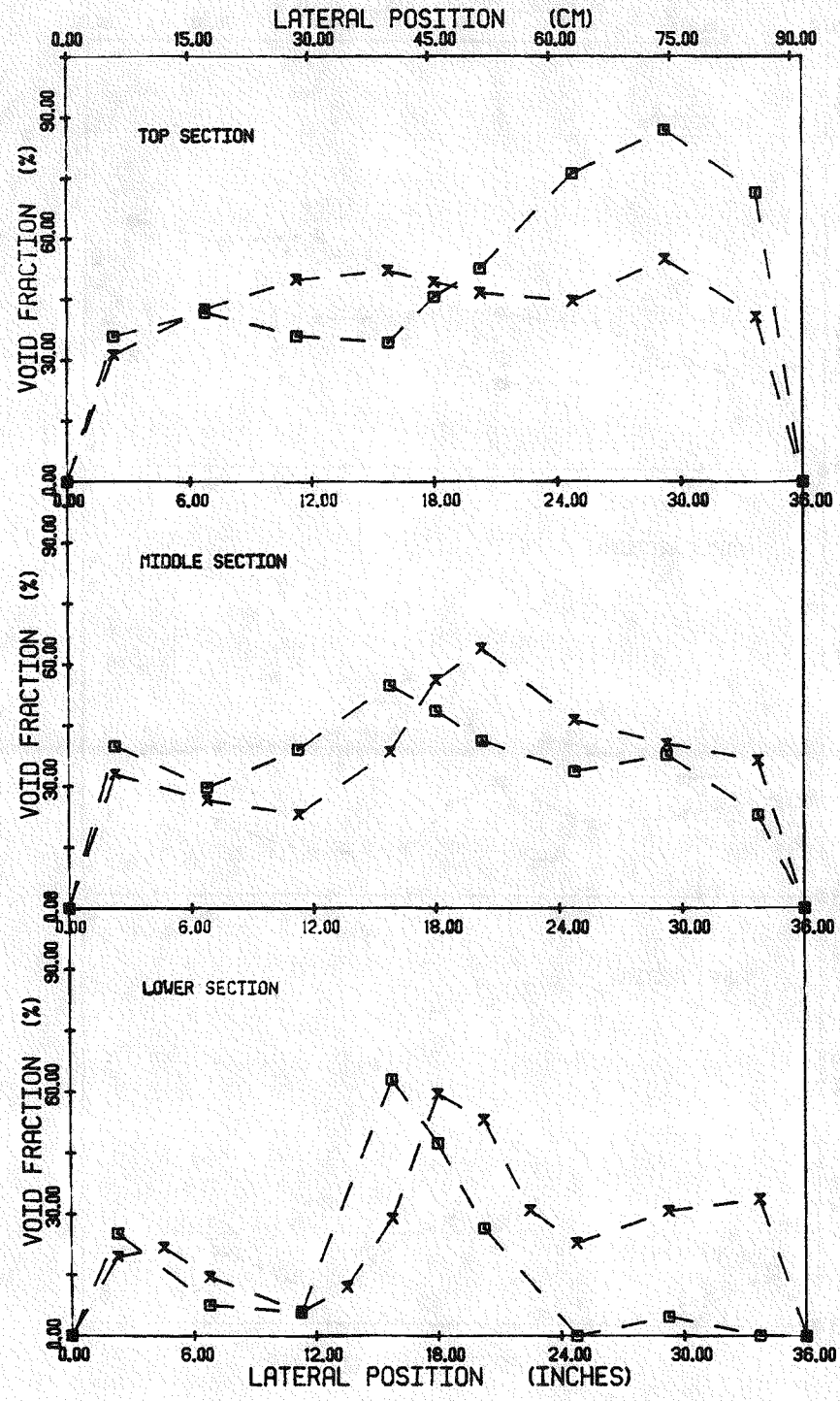


Figure 5.27 Void fraction for cases 2AN4 and 5AN4

| CASE | SYMBOL | LIQUID MASS FLUX KG/HR.M$^2$ | FLOW SPLIT IN#4 : IN#1 | QUALITY | RODS IN | PRESSURE KPA |
|---|---|---|---|---|---|---|
| 3AN4 | | 0.562 E6 | 50.0% : 50.0% | 0.9% | NO | 31.4 |
| 6AN4 | | 1.125 E6 | 50.0% : 50.0% | 0.9% | NO | 68.1 |

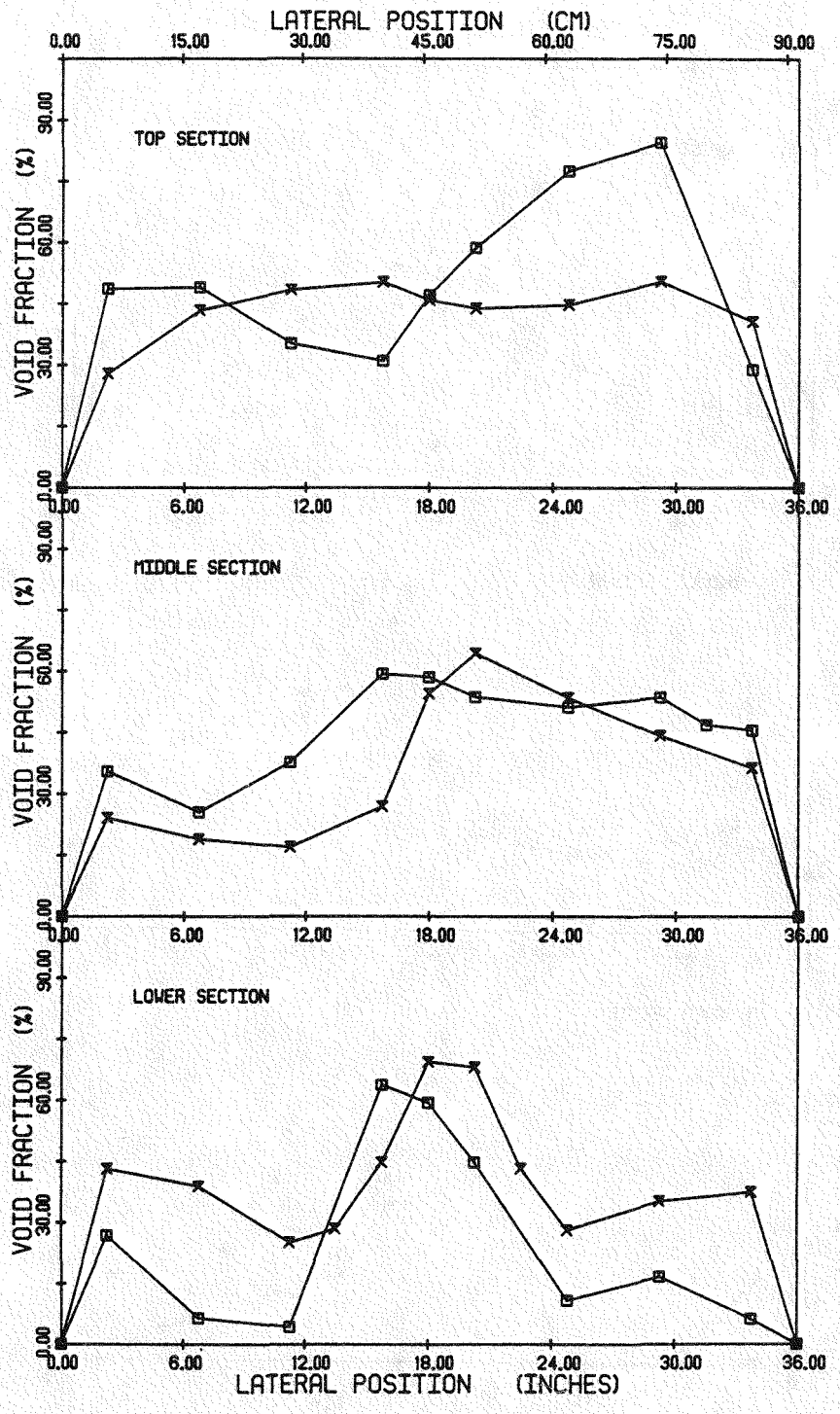


Figure 5.28 Void fraction for cases 3AN4 and 6AN4

| CASE | SYMBOL | LIQUID MASS FLUX KG/HR.M$^2$ | FLOW SPLIT IN#4 : IN#1 | QUALITY | RODS IN | PRESSURE KPA |
|---|---|---|---|---|---|---|
| 1BN4 | | 0.562 E6 | 62.5% : 37.5% | 0.3% | NO | 31.4 |
| 4BN4 | | 1.125 E6 | 62.5% : 37.5% | 0.3% | NO | 62.7 |

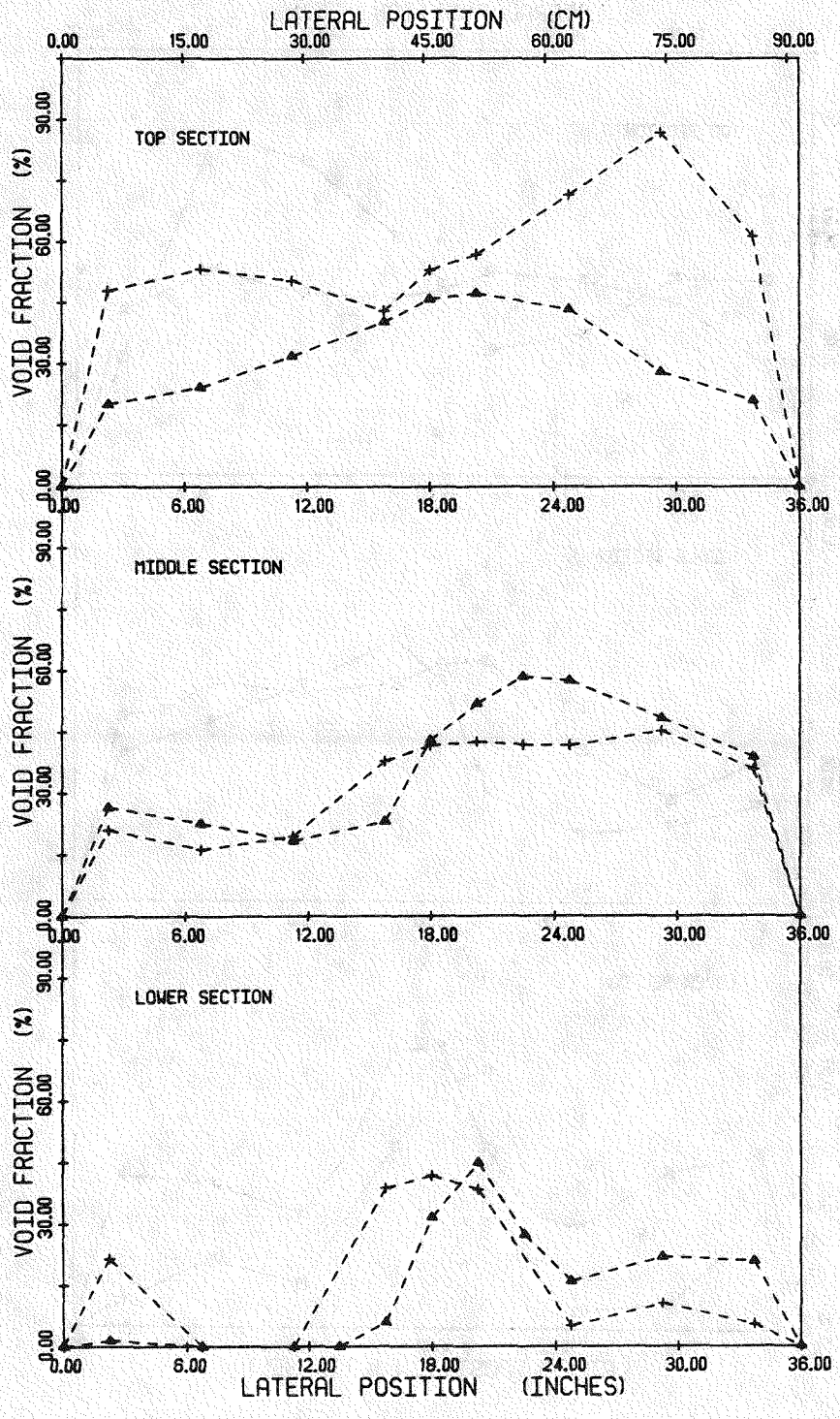


Figure 5.29 Void fraction for cases 1BN4 and 4BN4

| CASE | SYMBOL | LIQUID MASS FLUX KG/HR.M$^2$ | FLOW SPLIT IN#4 : IN#1 | QUALITY | RODS IN | PRESSURE KPA |
|---|---|---|---|---|---|---|
| 2BN4 | | 0.562 E6 | 62.5% : 37.5% | 0.6% | NO | 32.4 |
| 5BN4 | | 1.125 E6 | 62.5% : 37.5% | 0.6% | NO | 67.2 |

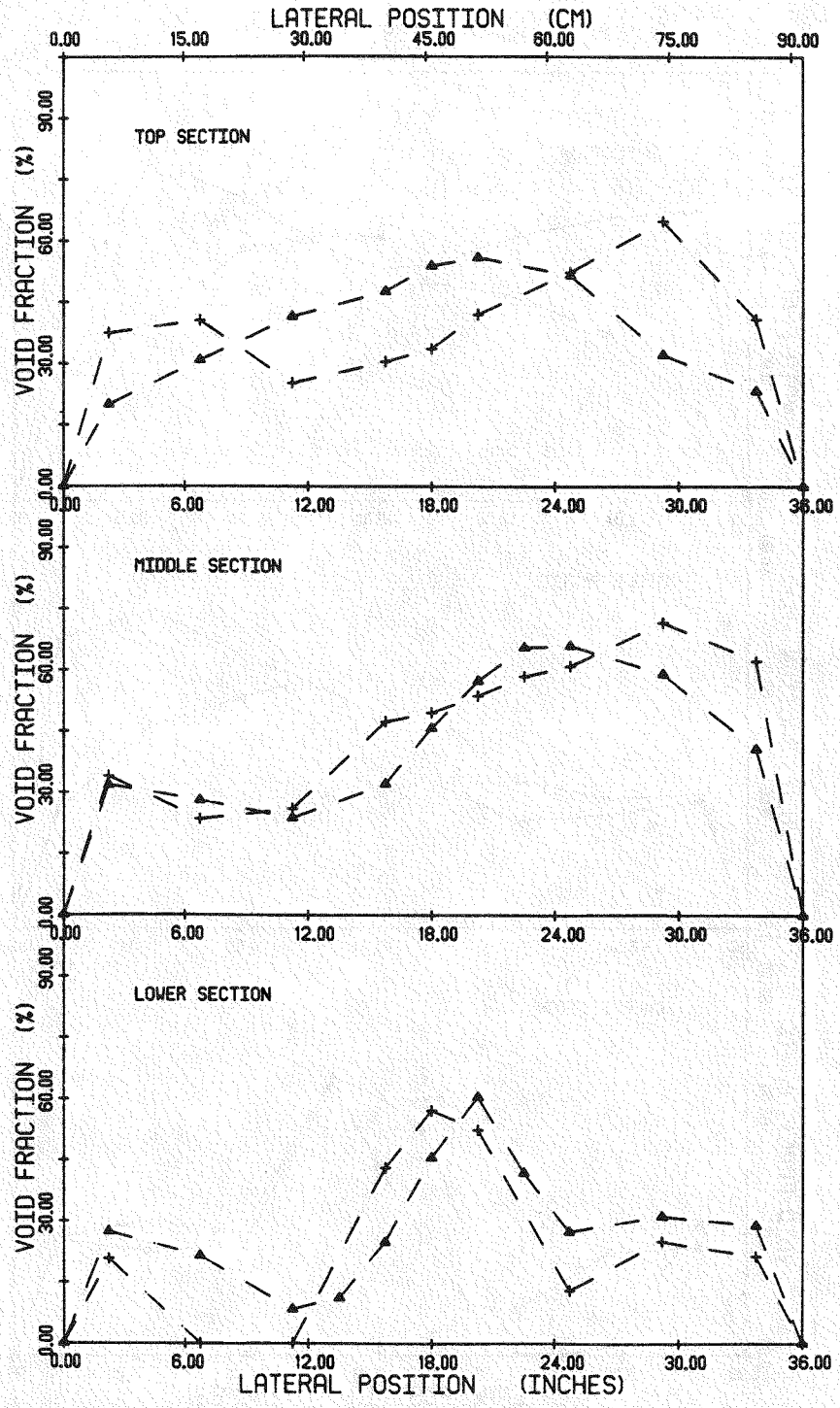


Figure 5.30 Void fraction for cases 2BN4 and 5BN4

| CASE | SYMBOL | LIQUID MASS FLUX KG/HR.M$^2$ | FLOW SPLIT IN#4 : IN#1 | QUALITY | RODS IN | PRESSURE KPA |
|---|---|---|---|---|---|---|
| 3BN4 | | 0.562 E6 | 62.5% : 37.5% | 0.9% | NO | 32.4 |
| 6BN4 | | 1.125 E6 | 62.5% : 37.5% | 0.9% | NO | 68.9 |

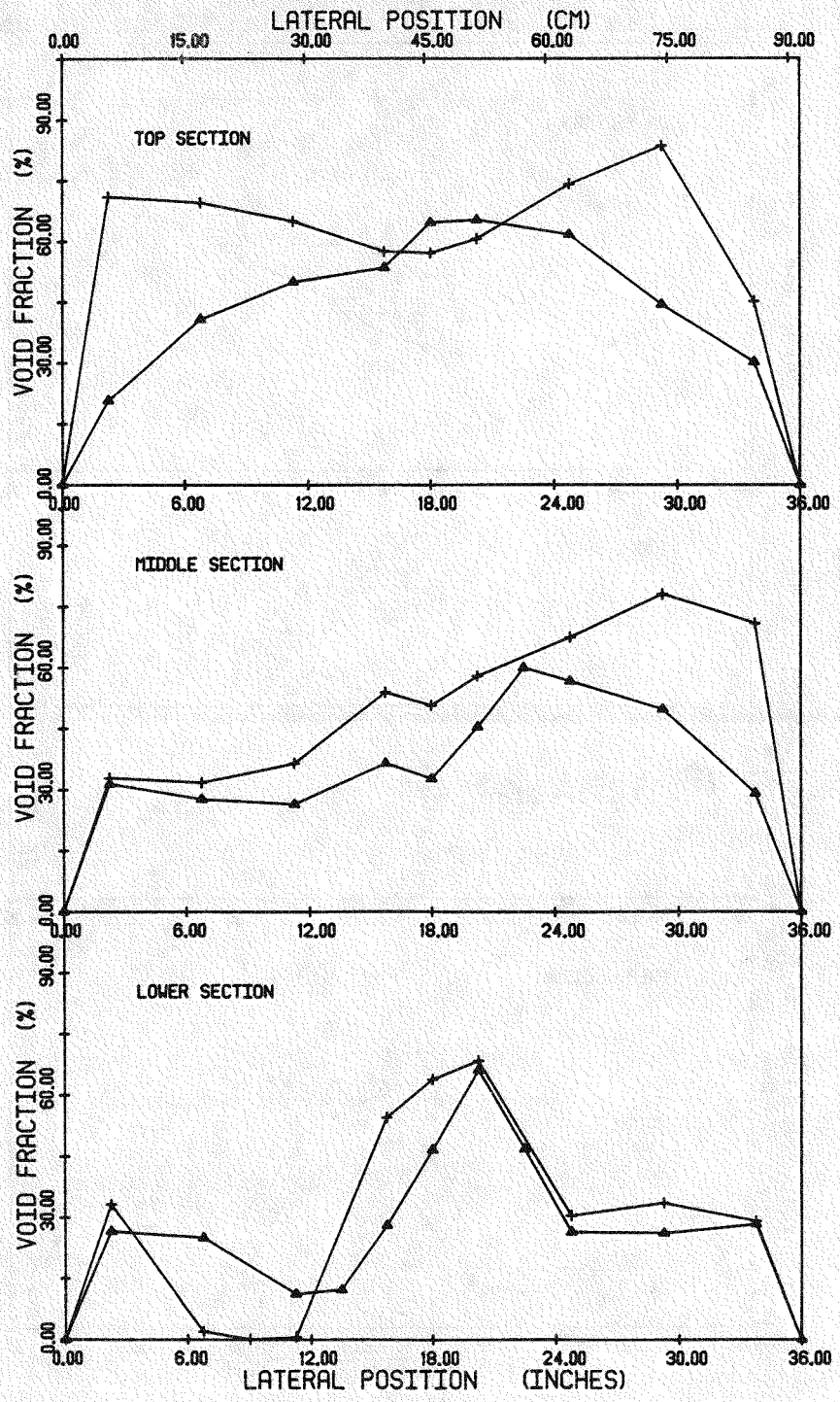


Figure 5.31 Void fraction for cases 3BN4 and 6BN4

| CASE | SYMBOL | LIQUID MASS FLUX KG/HR.M$^2$ | FLOW SPLIT IN#4 : IN#1 | QUALITY | RODS IN | PRESSURE KPA |
|---|---|---|---|---|---|---|
| 1CN4 | | 0.562 E6 | 37.5% : 62.5% | 0.3% | NO | 30.9 |
| 4CN4 | | 1.125 E6 | 37.5% : 62.5% | 0.3% | NO | 59.5 |

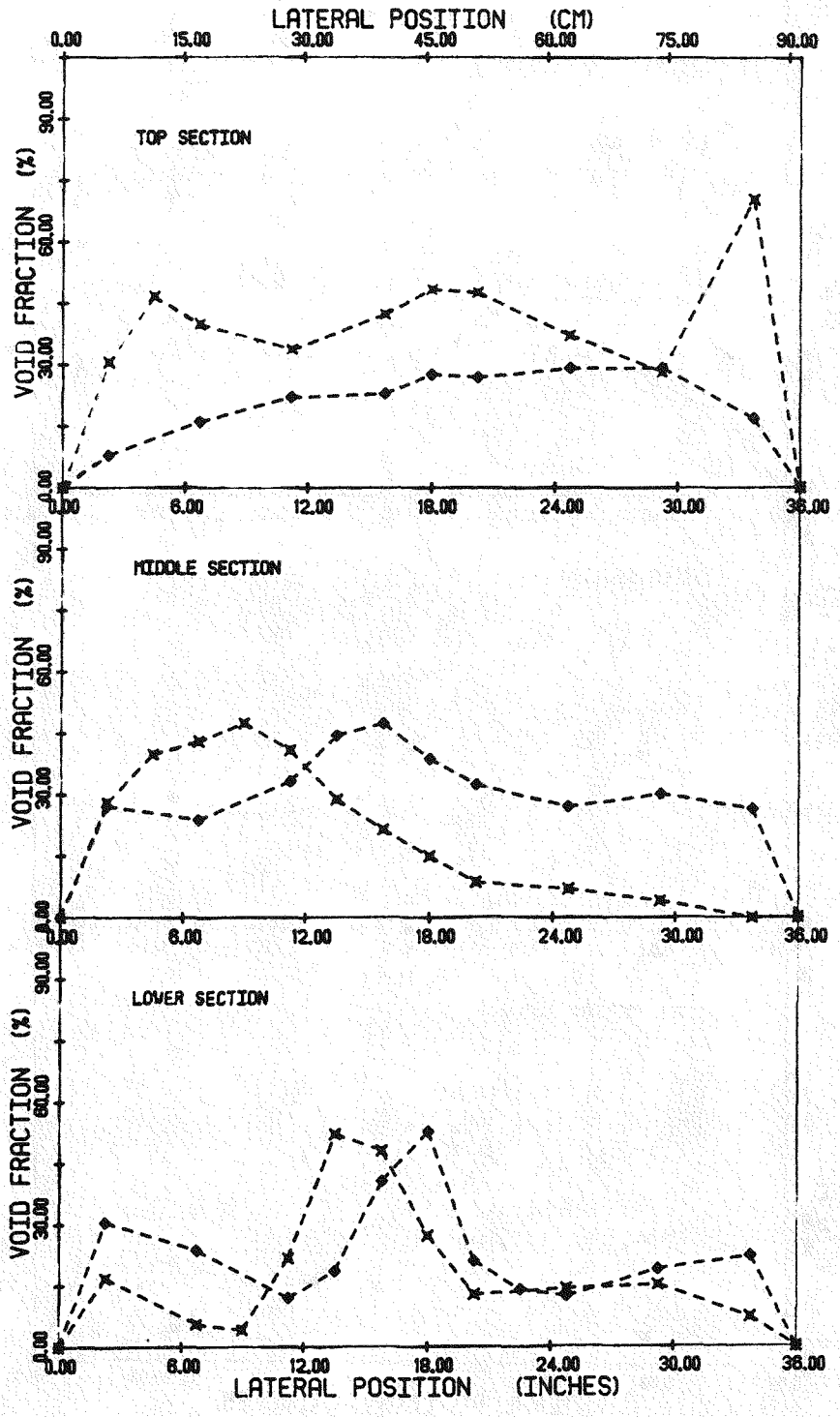


Figure 5.32 Void fraction for cases 1CN4 and 4CN4

| CASE | SYMBOL | LIQUID MASS FLUX KG/HR/M$^2$ | FLOW SPLIT IN#4 : IN#1 | QUALITY | RODS IN | PRESSURE KPA |
|---|---|---|---|---|---|---|
| 2CN4 | | 0.582 E6 | 37.5% : 62.5% | 0.6% | NO | 31.1 |
| 5CN4 | | 1.125 E6 | 37.5% : 62.5% | 0.6% | NO | 61.4 |

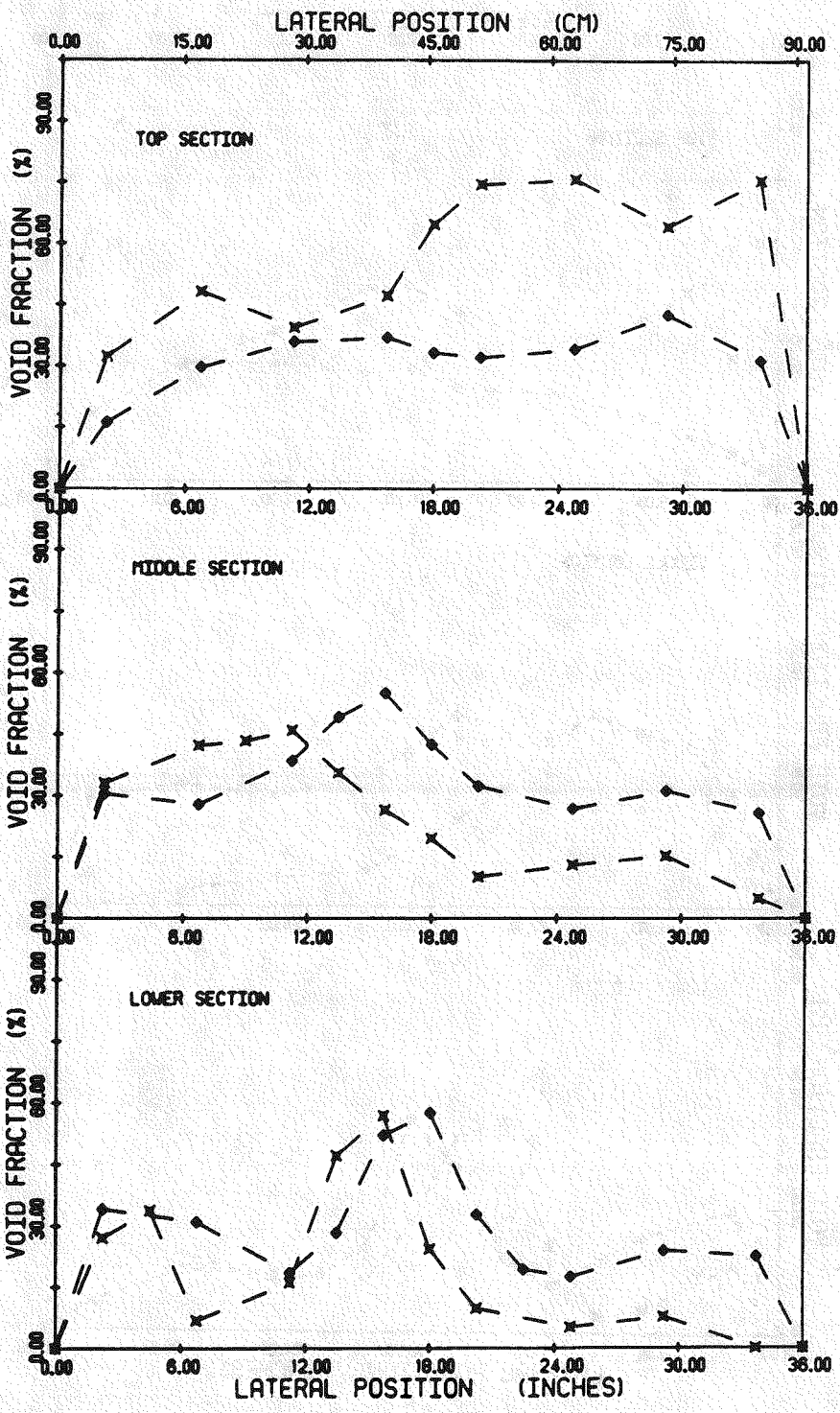


Figure 5.33 Void fraction for cases 2CN4 and 5CN4

| CASE | SYMBOL | LIQUID MASS FLUX KG/HR.M$^2$ | FLOW SPLIT IN#4 : IN#1 | QUALITY | RODS IN | PRESSURE KPA |
|---|---|---|---|---|---|---|
| 3CN4 | | 0.582 E6 | 37.5% : 62.5% | 0.9% | NO | 31.0 |
| 6CN4 | | 1.125 E6 | 37.5% : 62.5% | 0.9% | NO | 62.9 |

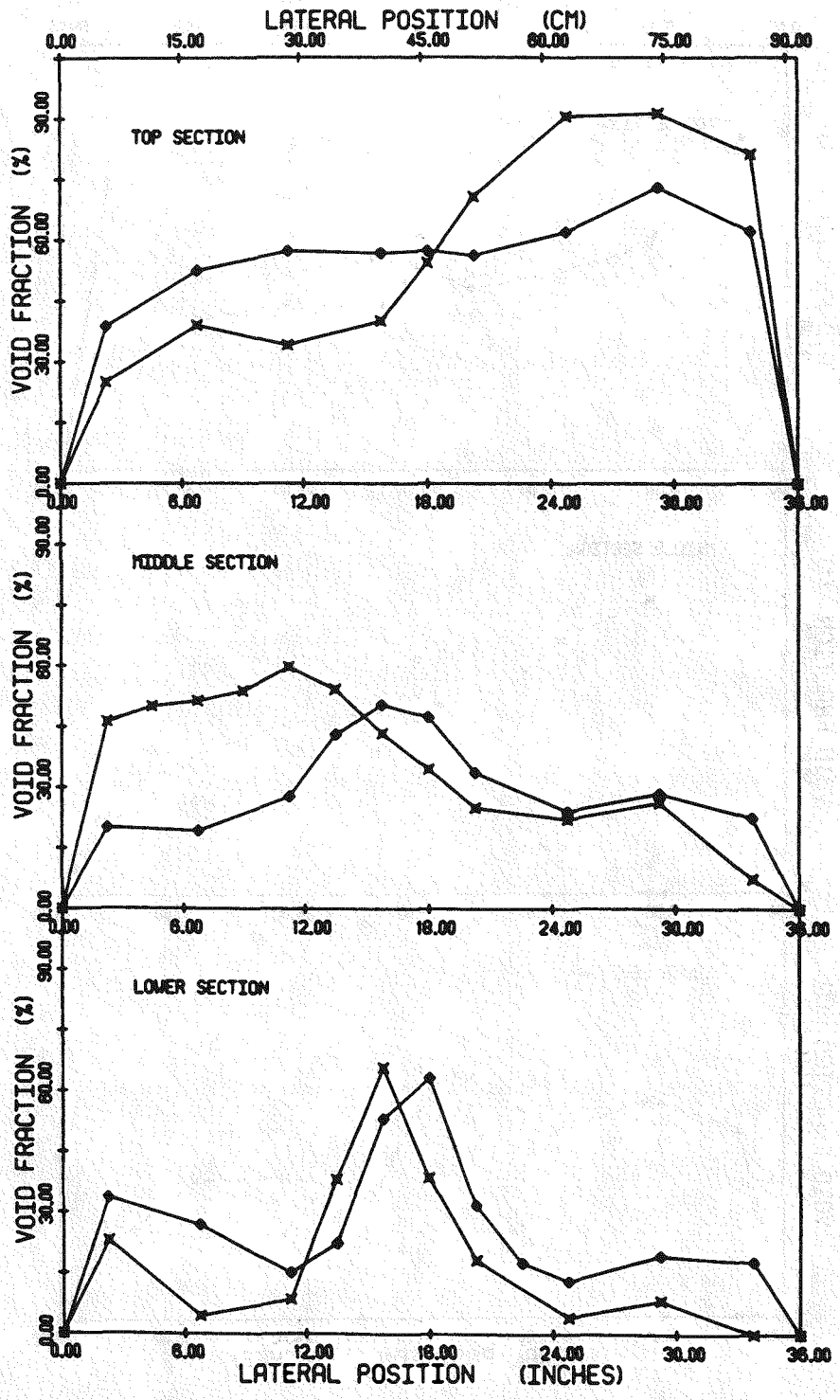


Figure 5.34 Void fraction for cases 3CN4 and 6CN4

| CASE | SYMBOL | LIQUID MASS FLUX KG/HR.M$^2$ | FLOW SPLIT IN#4 : IN#1 | QUALITY | RODS IN | PRESSURE KPA |
|---|---|---|---|---|---|---|
| 1AR4 | | 0.697 E6 | 50.0% : 50.0% | 0.3% | YES | 34.5 |
| 4AR4 | | 1.395 E6 | 50.0% : 50.0% | 0.3% | YES | 75.1 |

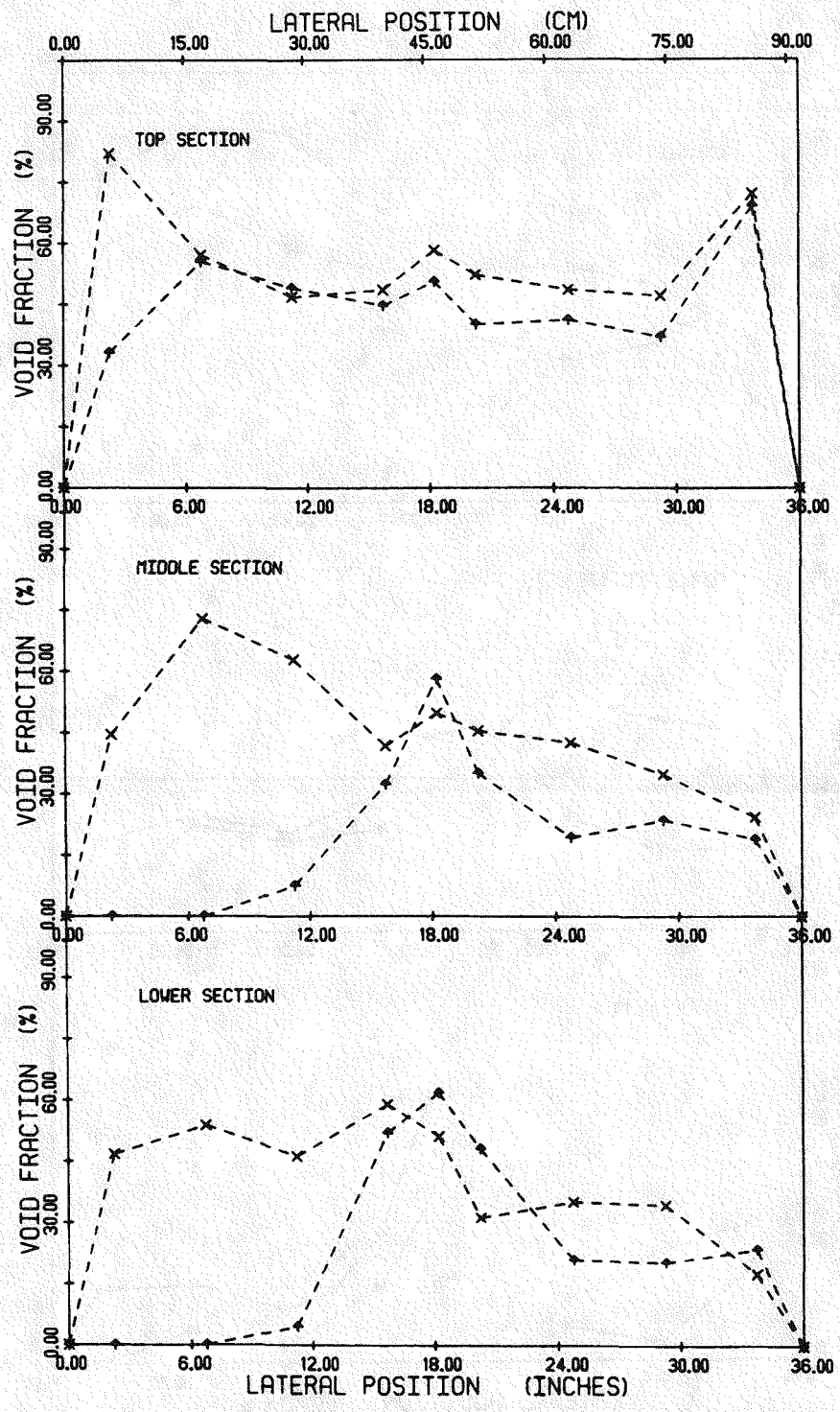


Figure 5.35 Void fraction for cases 1AR4 and 4AR4

| CASE | SYMBOL | LIQUID MASS FLUX KG/HR.M$^2$ | FLOW SPLIT IN#4 : IN#1 | QUALITY | RODS IN | PRESSURE KPA |
|---|---|---|---|---|---|---|
| 2AR4 | | 0.697 E6 | 50.0% : 50.0% | 0.6% | YES | 33.8 |
| 5AR4 | | 1.395 E6 | 50.0% : 50.0% | 0.6% | YES | 78.1 |

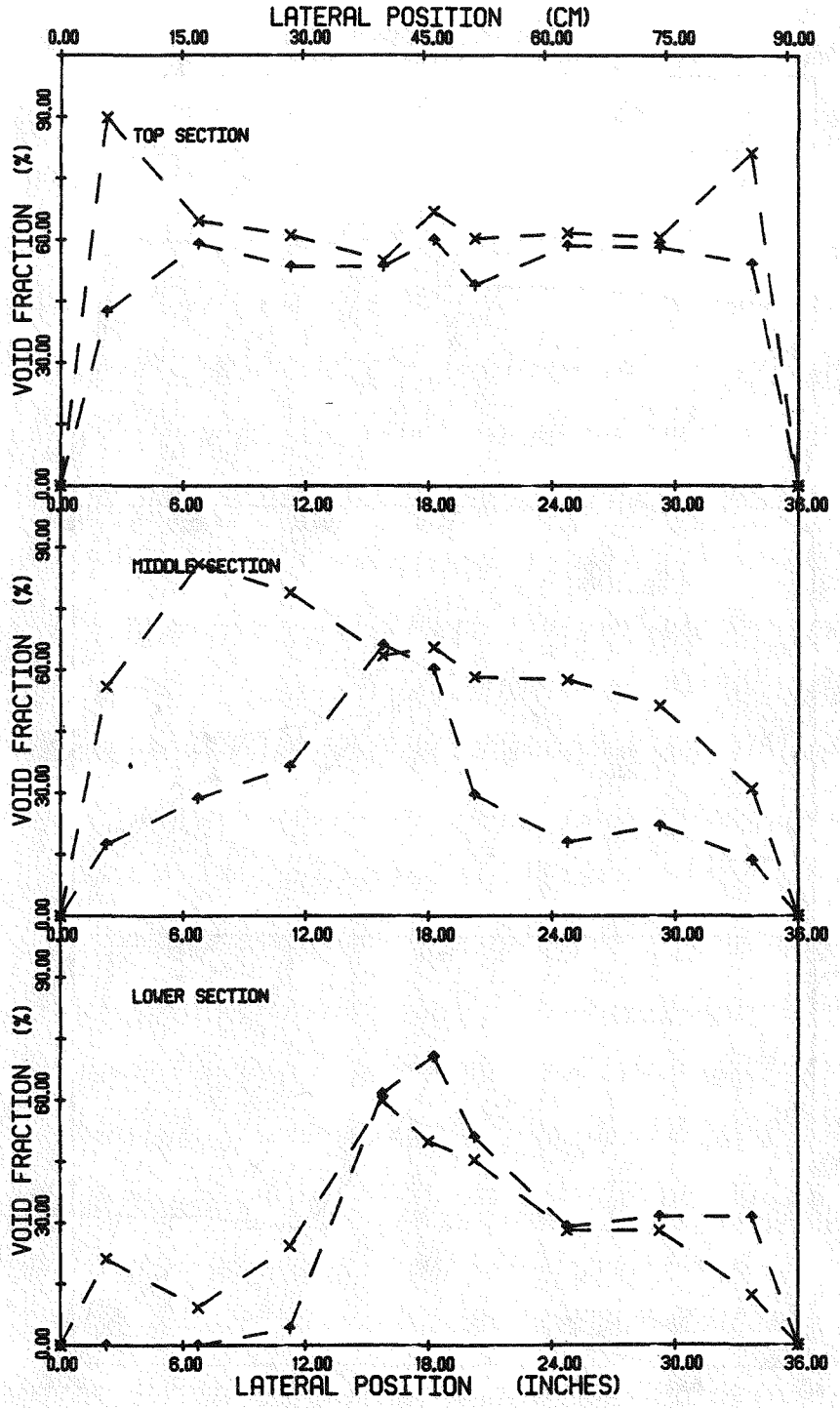


Figure 5.36 Void fraction for cases 2AR4 and 5AR4

| CASE | SYMBOL | LIQUID MASS FLUX KG/HR.M$^2$ | FLOW SPLIT IN#4 : IN#1 | QUALITY | RODS IN | PRESSURE KPA |
|---|---|---|---|---|---|---|
| 3AR4 | | 0.697 E6 | 50.0% : 50.0% | 0.9% | YES | 34.5 |
| 6AR4 | | 1.395 E6 | 50.0% : 50.0% | 0.9% | YES | 81.4 |

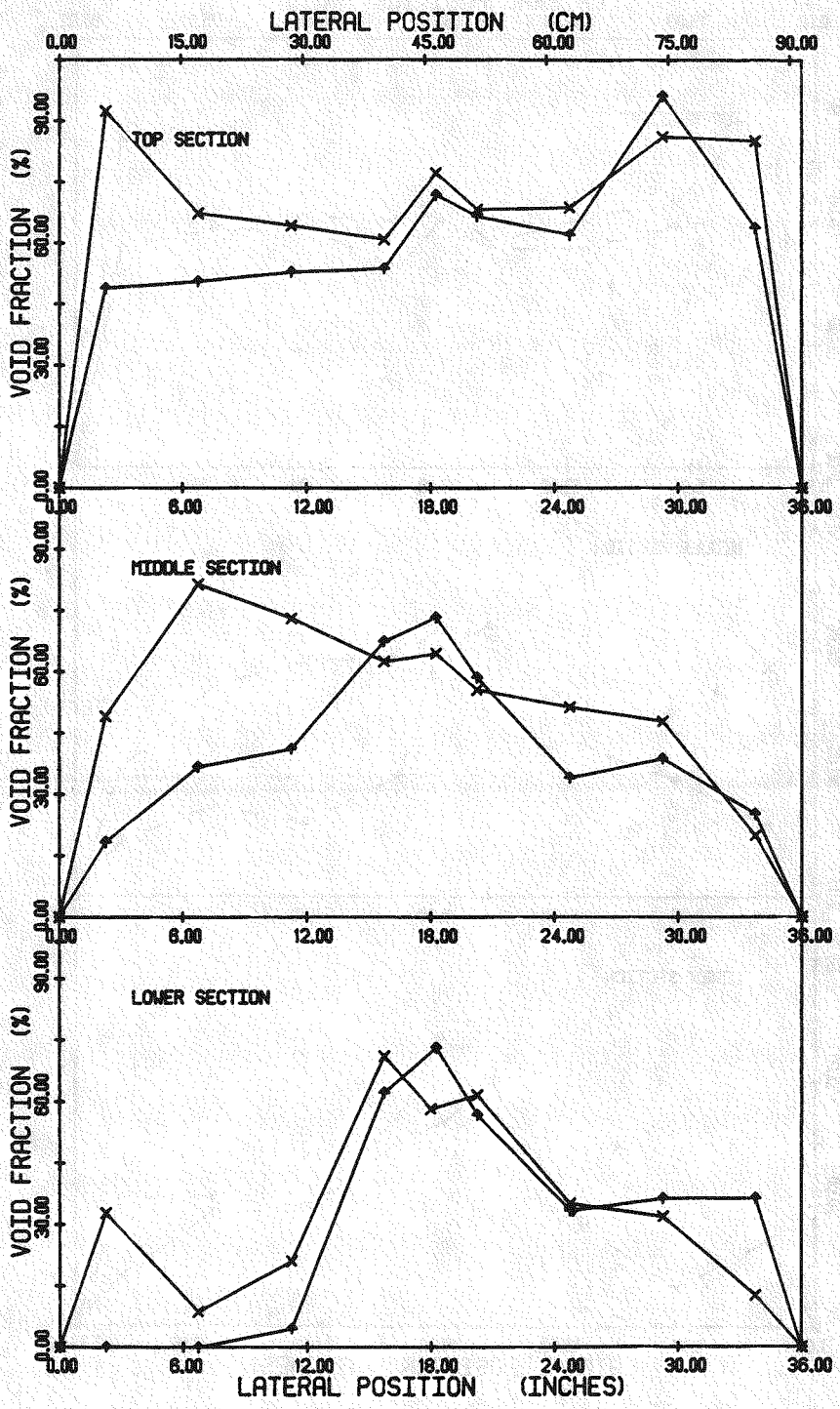


Figure 5.37 Void fraction for cases 3AR4 and 6AR4

| CASE | SYMBOL | LIQUID MASS FLUX KG/HR.M$^2$ | FLOW SPLIT IN#4 : IN#1 | QUALITY | RODS IN | PRESSURE KPA |
|---|---|---|---|---|---|---|
| 1BR4 | | 0.697 E6 | 62.5% : 37.5% | 0.3% | YES | 34.5 |
| 4BR4 | | 1.395 E6 | 62.5% : 37.5% | 0.3% | YES | 76.3 |

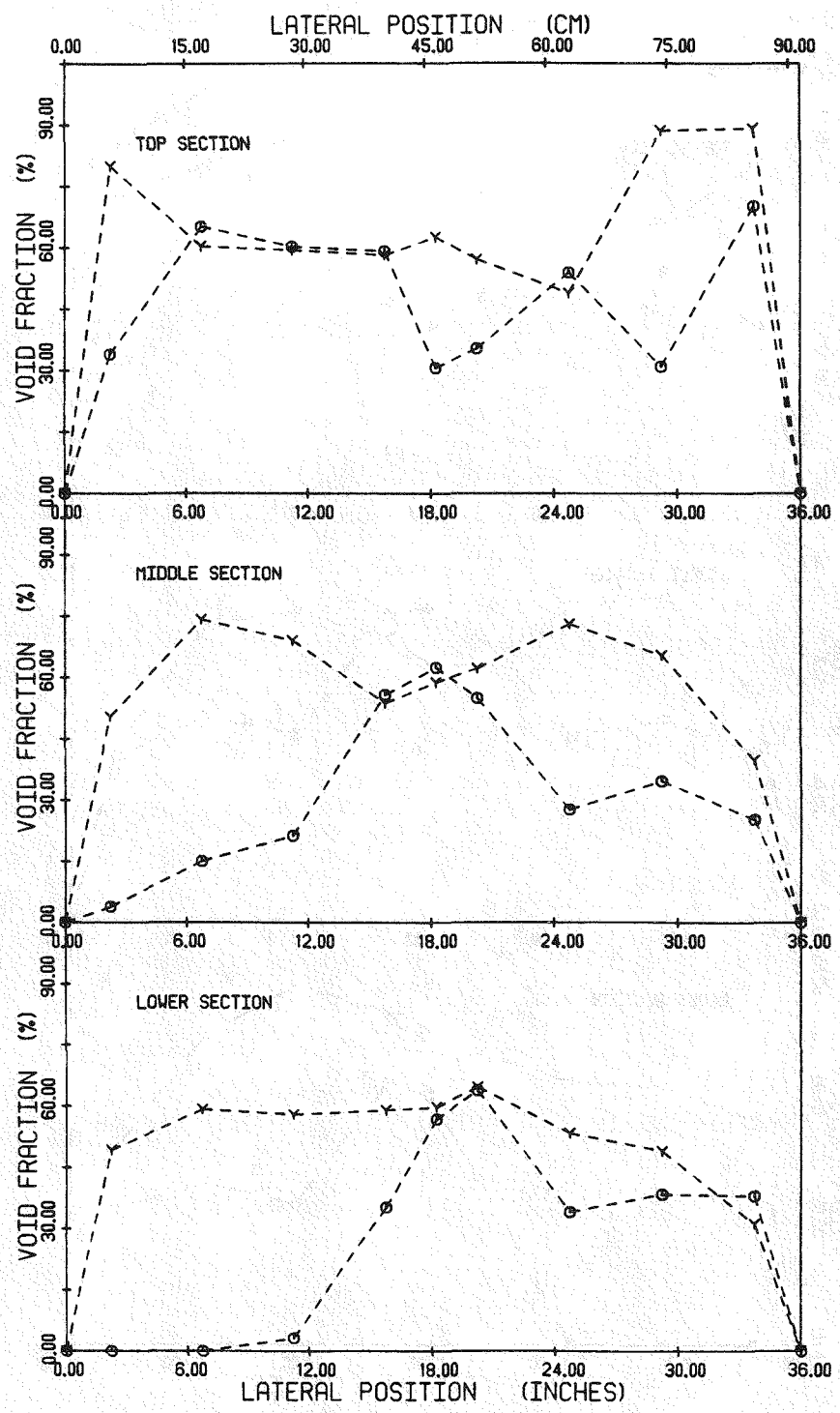


Figure 5.38 Void fraction for cases 1BR4 and 4BR4

| CASE | SYMBOL | LIQUID MASS FLUX KG/HR.M$^2$ | FLOW SPLIT IN#4 : IN#1 | QUALITY | RODS IN | PRESSURE KPA |
|---|---|---|---|---|---|---|
| 2BR4 | | 0.697 E6 | 62.5% : 37.5% | 0.6% | YES | 34.5 |
| 5BR4 | | 1.395 E6 | 62.5% : 37.5% | 0.6% | YES | 80.5 |

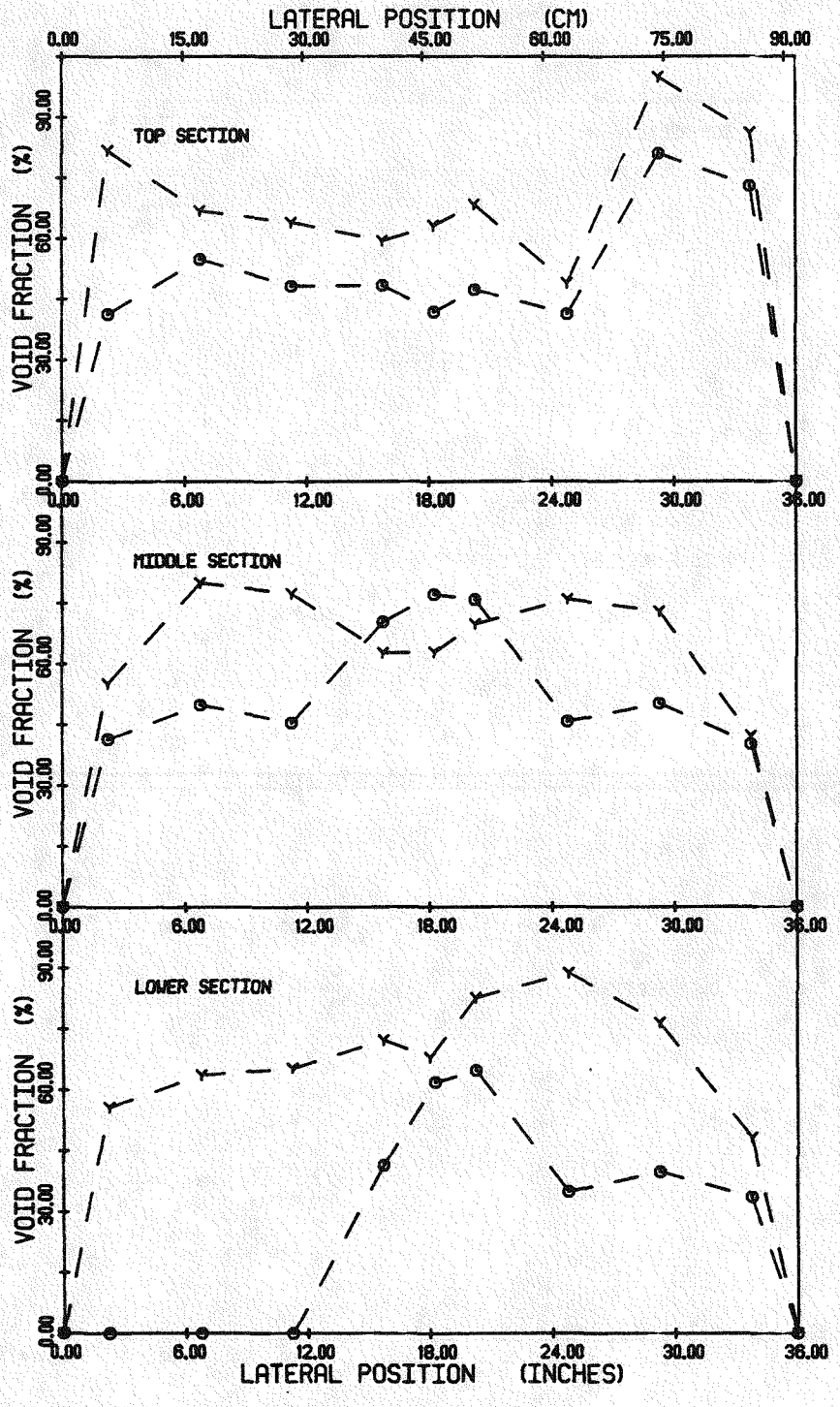


Figure 5.39 Void fraction for cases 2BR4 and 5BR4

| CASE | SYMBOL | LIQUID MASS FLUX KG/HR.M$^2$ | FLOW SPLIT IN#4 : IN#1 | QUALITY | RODS IN | PRESSURE KPA |
|---|---|---|---|---|---|---|
| 3BR4 | | 0.697 E6 | 62.5% : 37.5% | 0.9% | YES | 34.5 |
| 6BR4 | | 1.395 E6 | 62.5% : 37.5% | 0.9% | YES | 85.0 |

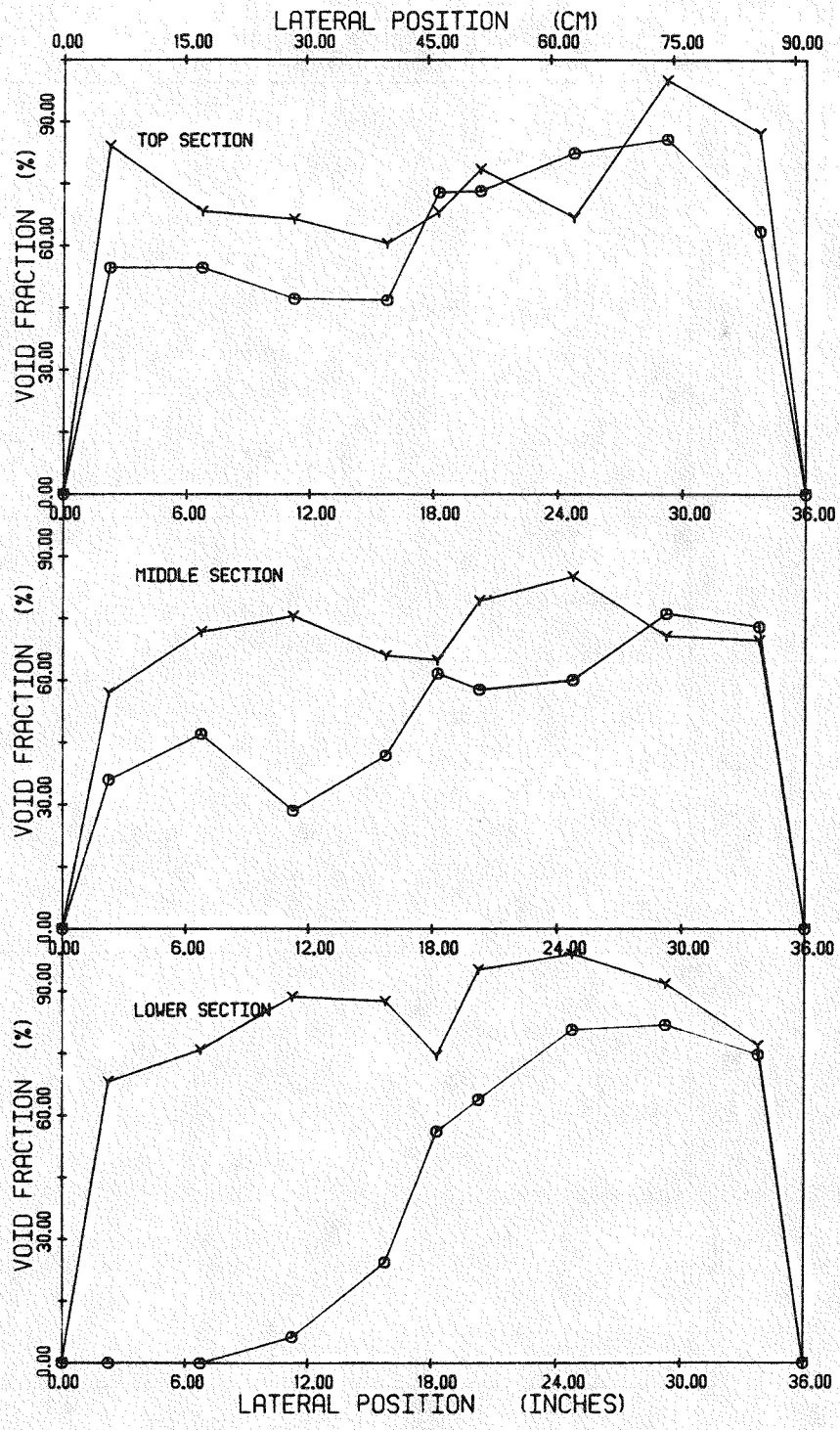


Figure 5.40 Void fraction for cases 3BR4 and 6BR4

| CASE | SYMBOL | LIQUID MASS FLUX KG/HR.M$^2$ | FLOW SPLIT IN#4 : IN#1 | QUALITY | RODS IN | PRESSURE KPA |
|---|---|---|---|---|---|---|
| 1CR4 | | 0.697 E6 | 37.5% : 62.5% | 0.3% | YES | 33.8 |
| 4CR4 | | 1.395 E6 | 37.5% : 62.5% | 0.3% | YES | 73.5 |

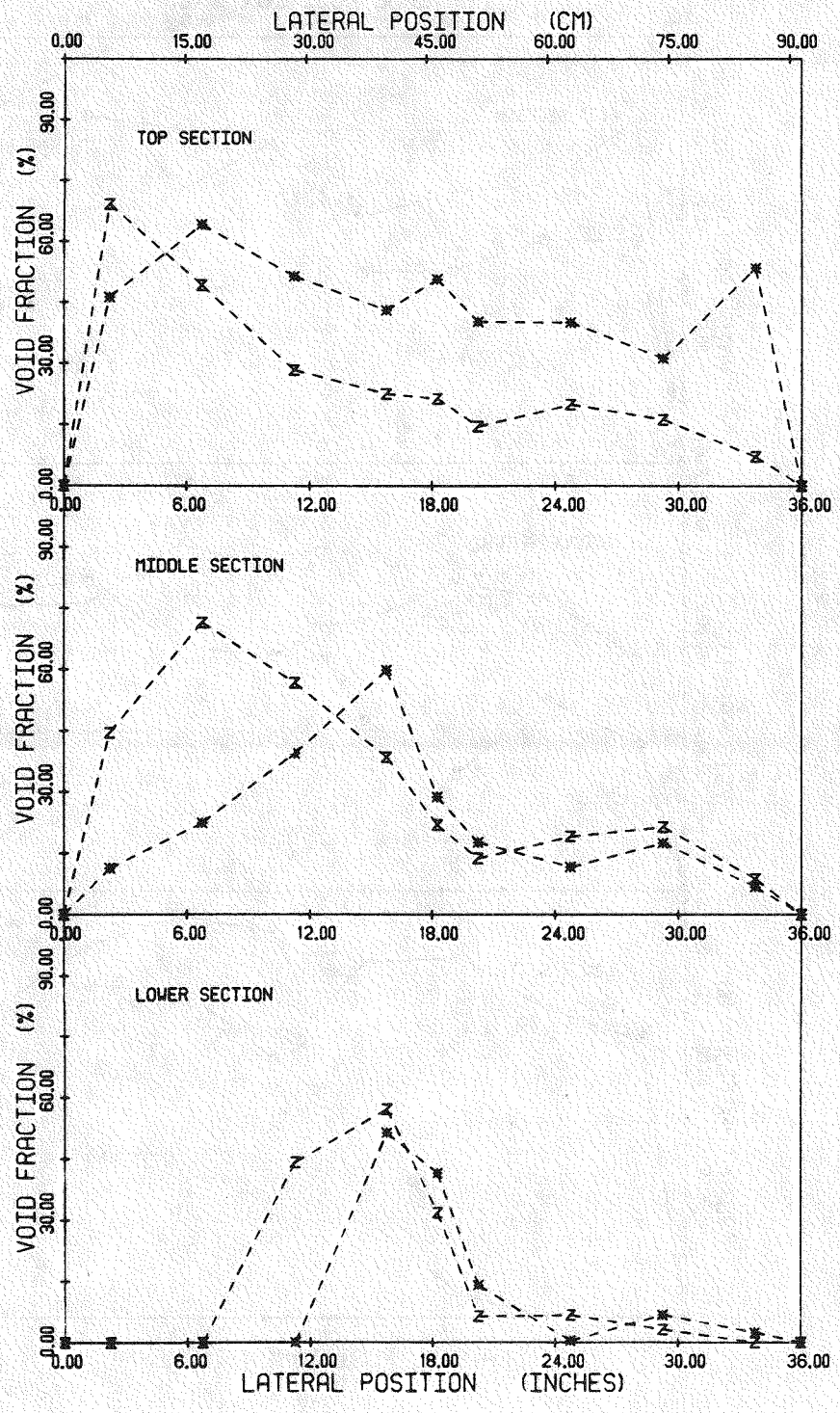


Figure 5.41 Void fraction for cases 1CR4 and 4CR4

| CASE | SYMBOL | LIQUID MASS FLUX KG/HR.M² | FLOW SPLIT IN#4 : IN#1 | QUALITY | RODS IN | PRESSURE KPA |
|---|---|---|---|---|---|---|
| 2CR4 | | 0.697 E6 | 37.5% : 62.5% | 0.6% | YES | 33.8 |
| 5CR4 | | 1.395 E6 | 37.5% : 62.5% | 0.6% | YES | 78.1 |

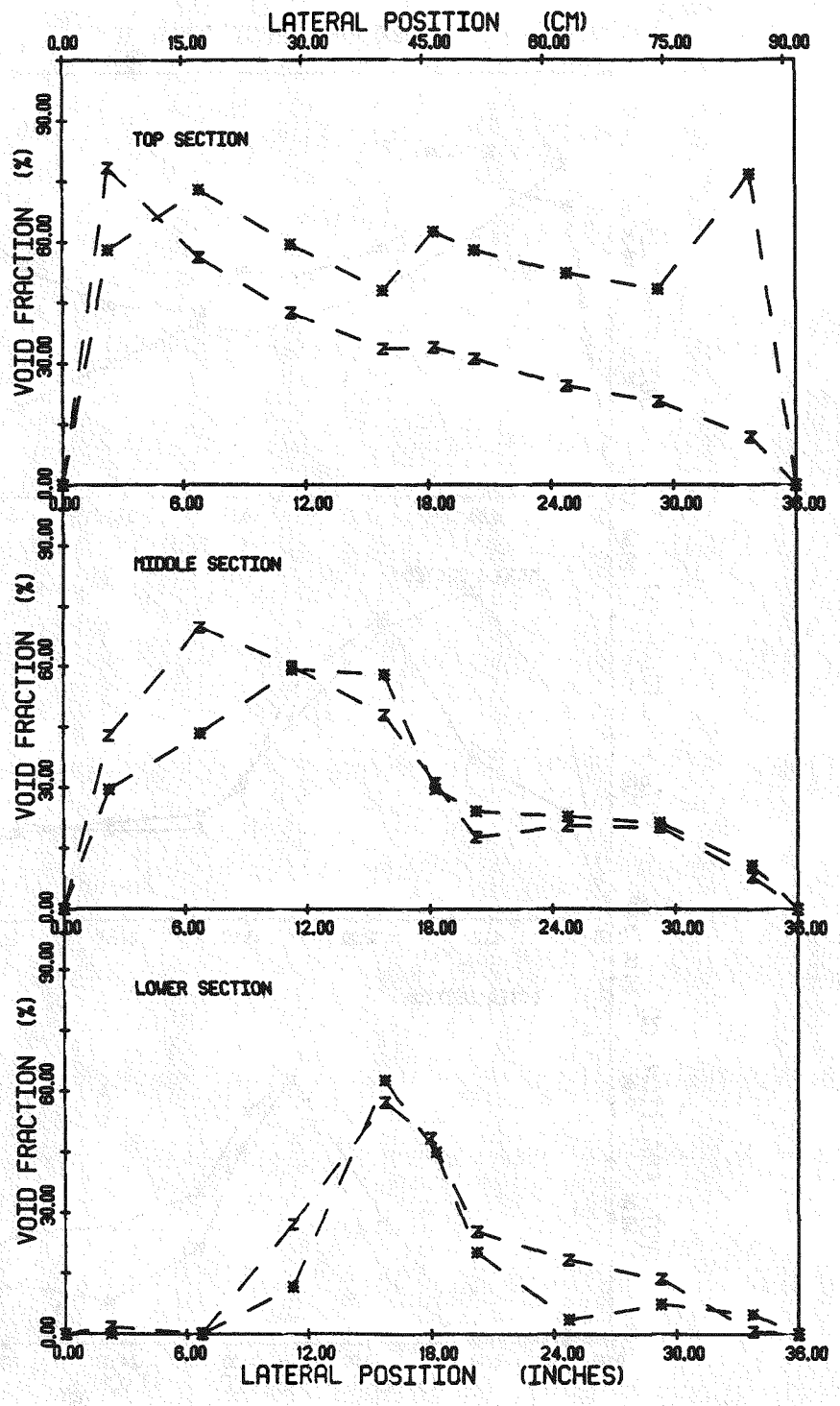


Figure 5.42 Void fraction for cases 2CR4 and 5CR4

| CASE | SYMBOL | LIQUID MASS FLUX KG/HR.M$^2$ | FLOW SPLIT IN#4 : IN#1 | QUALITY | RODS IN | PRESSURE KPA |
|---|---|---|---|---|---|---|
| 3CR4 | | 0.697 E6 | 37.5% : 62.5% | 0.9% | YES | 34.5 |
| 6CR4 | | 1.395 E6 | 37.5% : 62.5% | 0.9% | YES | 79.5 |

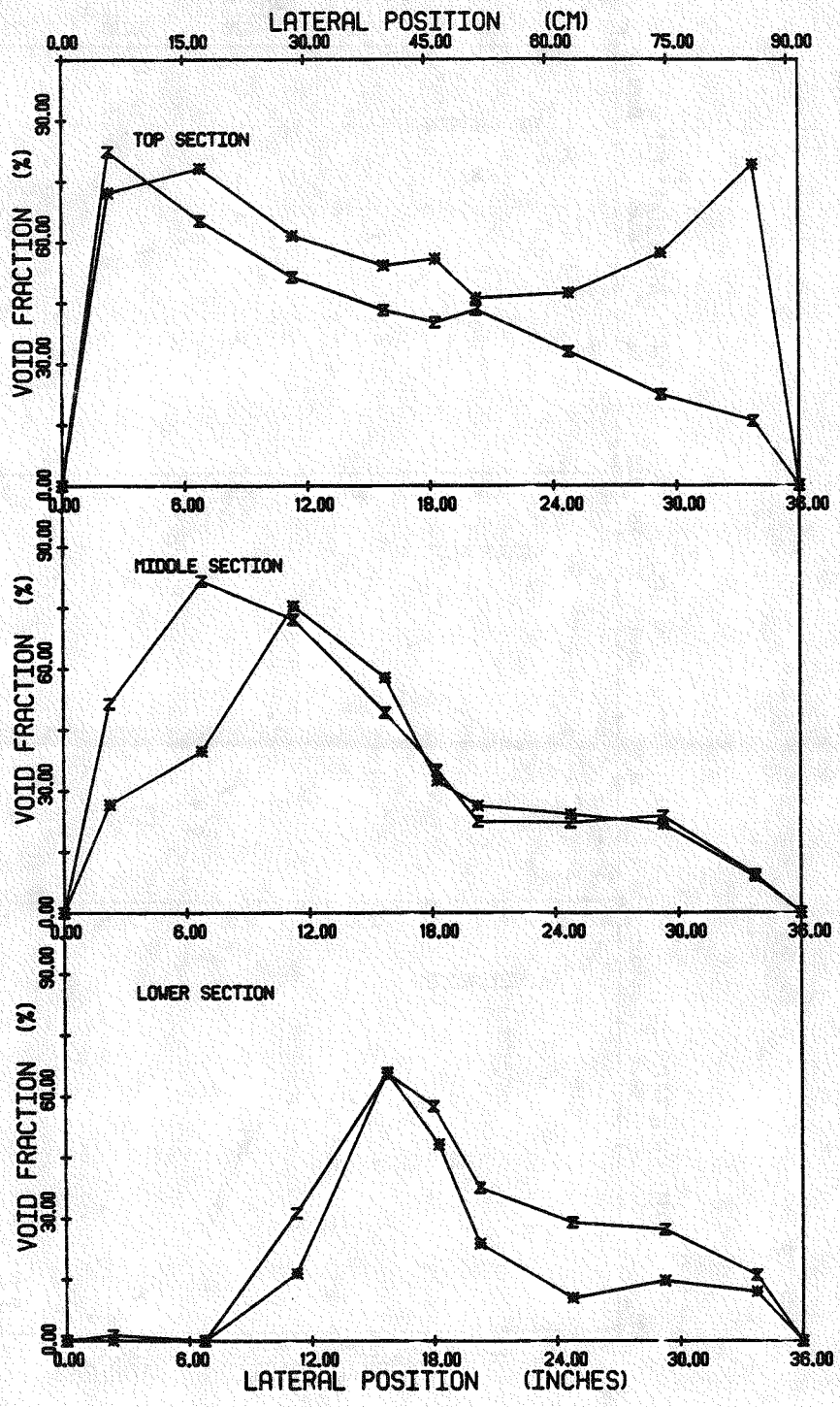


Figure 5.43 Void fraction for cases 3CR4 and 6CR4

| CASE | SYMBOL | LIQUID MASS FLUX KG/HR.M$^2$ | FLOW SPLIT IN#4 : IN#1 | QUALITY | RODS IN | PRESSURE KPA |
|---|---|---|---|---|---|---|
| 1AN4 | | 0.562 E6 | 50.0% : 50.0% | 0.3% | NO | 31.3 |
| 1AR4 | | 0.697 E6 | 50.0% : 50.0% | 0.3% | YES | 34.5 |

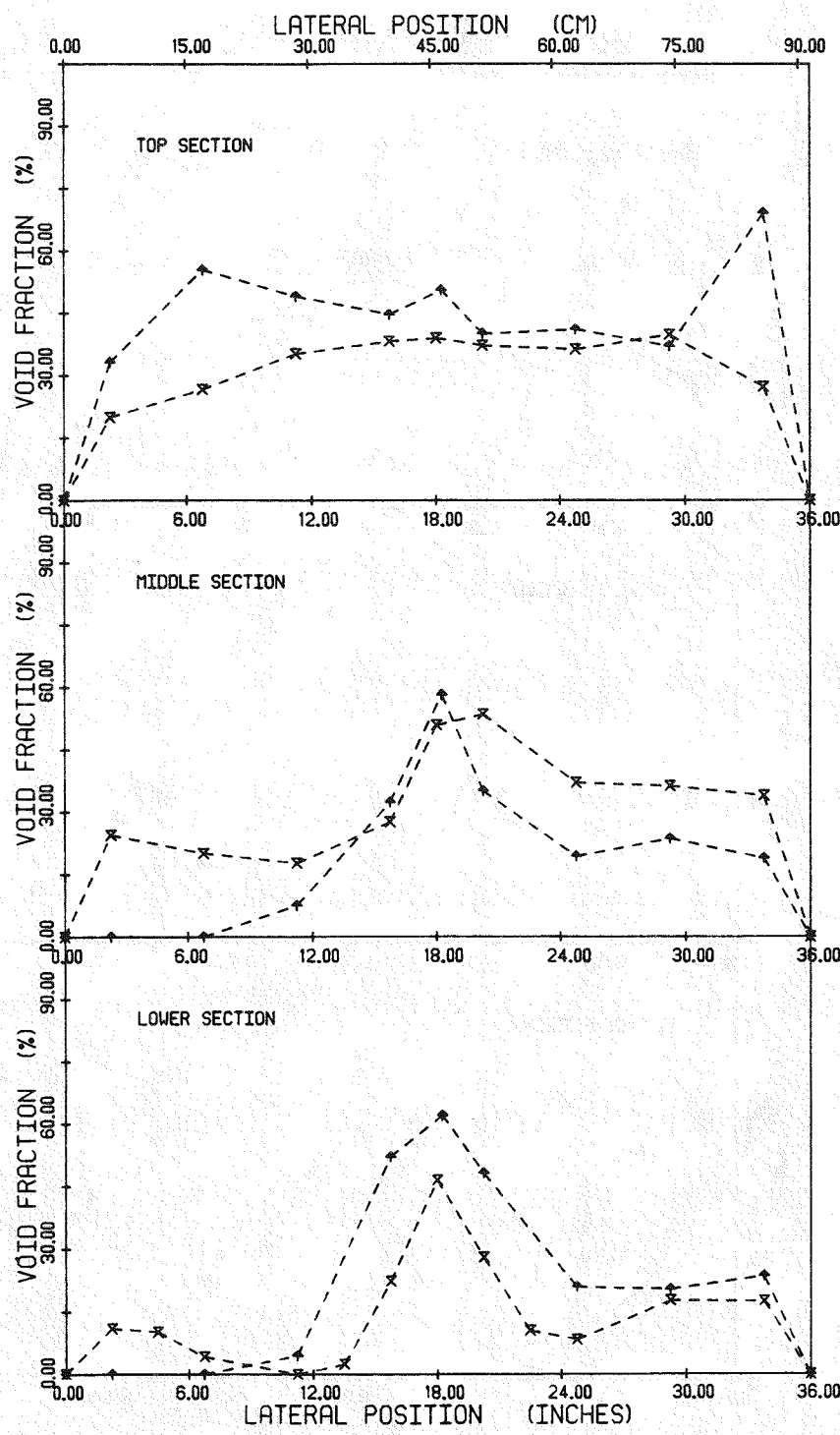


Figure 5.44 Void fraction for cases 1AN4 and 1AR4

| CASE | SYMBOL | LIQUID MASS FLUX KG/HR.M$^2$ | FLOW SPLIT IN#4 : IN#1 | QUALITY | RODS IN | PRESSURE KPA |
|---|---|---|---|---|---|---|
| 2AN4 | | 0.562 E6 | 50.0% : 50.0% | 0.6% | NO | 31.6 |
| 2AR4 | | 0.697 E6 | 50.0% : 50.0% | 0.6% | YES | 33.8 |

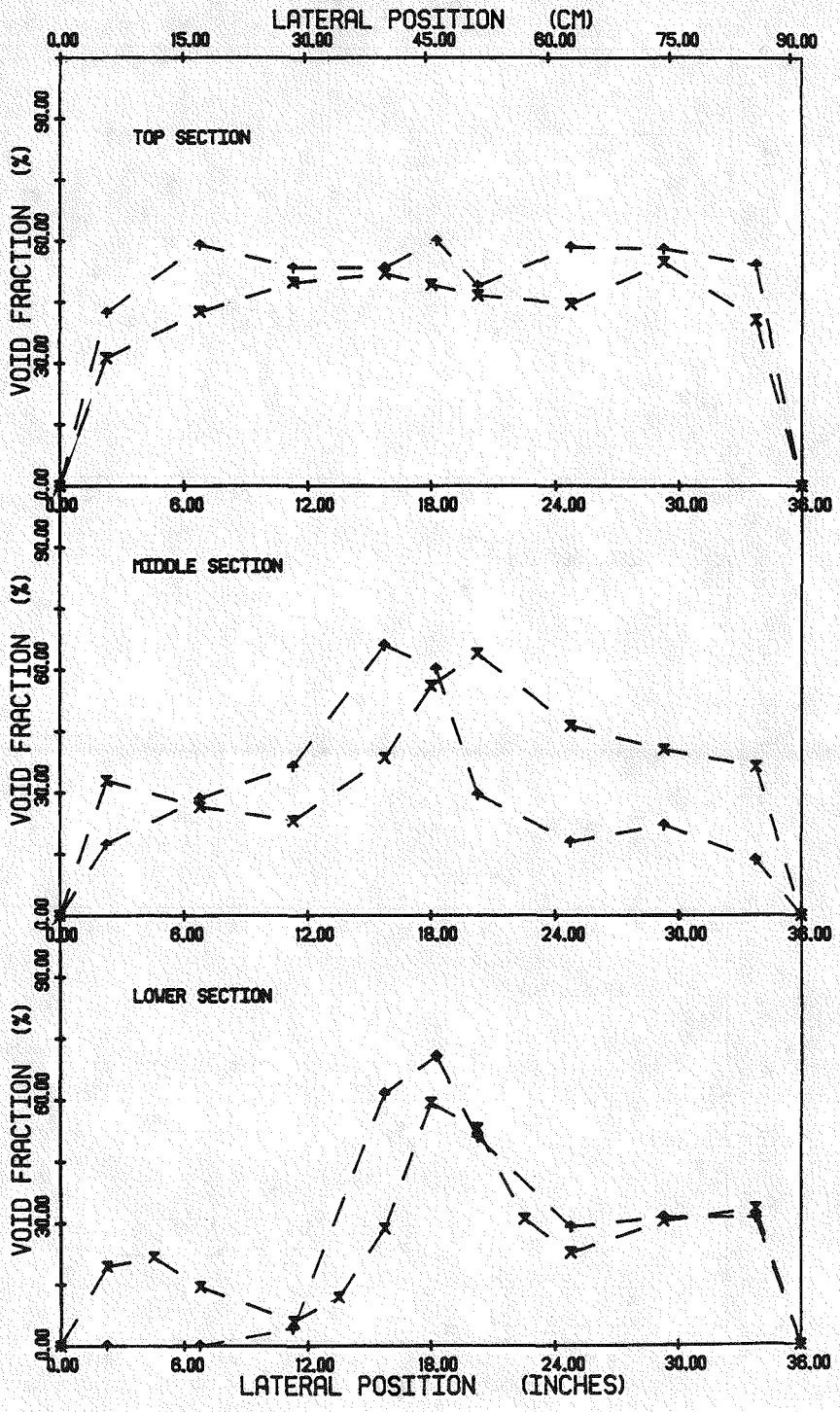


Figure 5.45 Void fraction for cases 2AN4 and 2AR4

| CASE | SYMBOL | LIQUID MASS FLUX KG/HR.M$^2$ | FLOW SPLIT IN#4 : IN#1 | QUALITY | RODS IN | PRESSURE KPA |
|---|---|---|---|---|---|---|
| 3AN4 | | 0.562 E6 | 50.0% : 50.0% | 0.9% | NO | 31.4 |
| 3AR4 | | 0.697 E6 | 50.0% : 50.0% | 0.9% | YES | 34.5 |

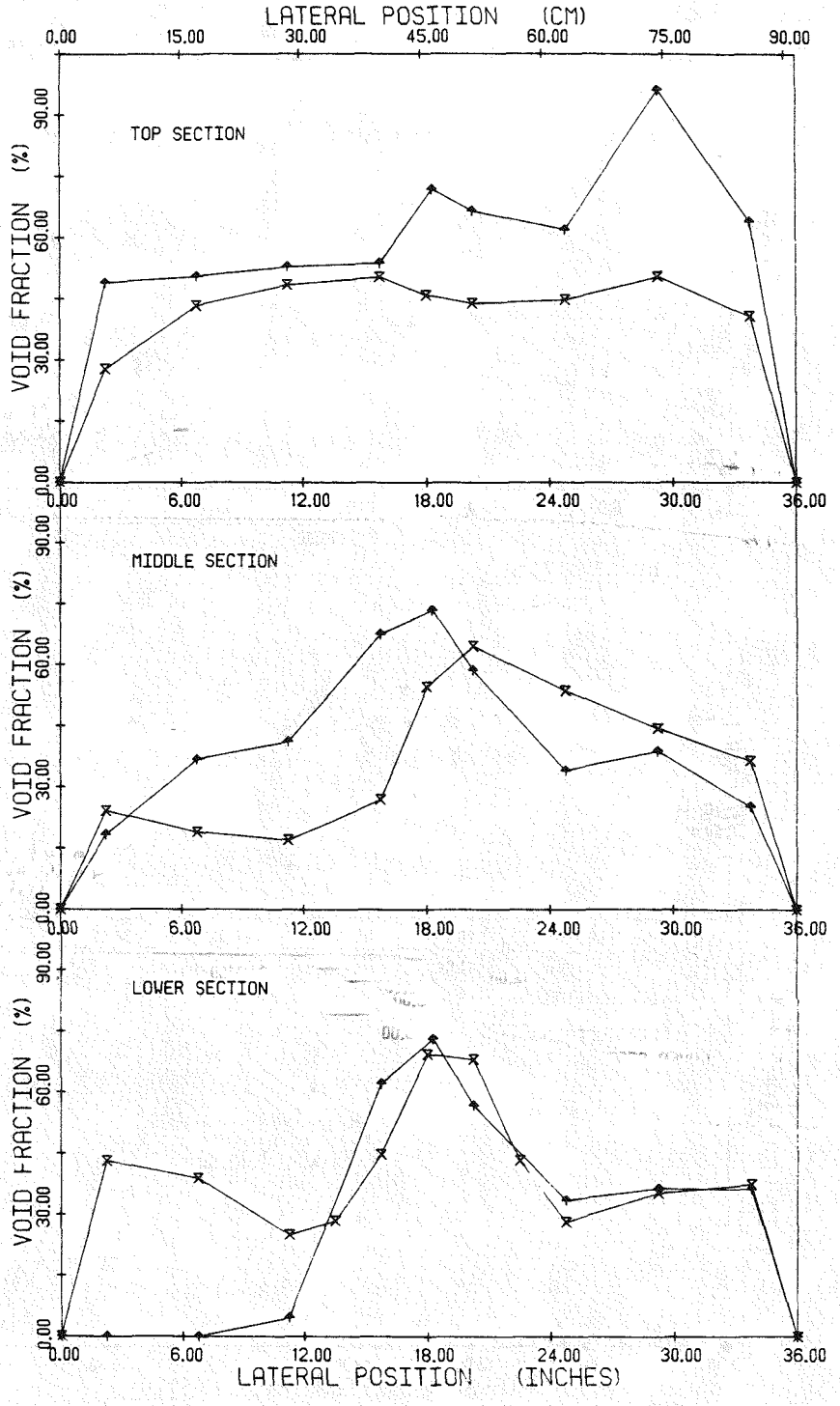


Figure 5.46 Void fraction for cases 3AN4 and 3AR4

| CASE | SYMBOL | LIQUID MASS FLUX KG/HR.M$^2$ | FLOW SPLIT IN#4 : IN#1 | QUALITY | RODS IN | PRESSURE KPA |
|---|---|---|---|---|---|---|
| 1BN4 | | 0.562 E6 | 62.5% : 37.5% | 0.3% | NO | 31.4 |
| 1BR4 | | 0.697 E6 | 62.5% : 37.5% | 0.3% | YES | 34.5 |

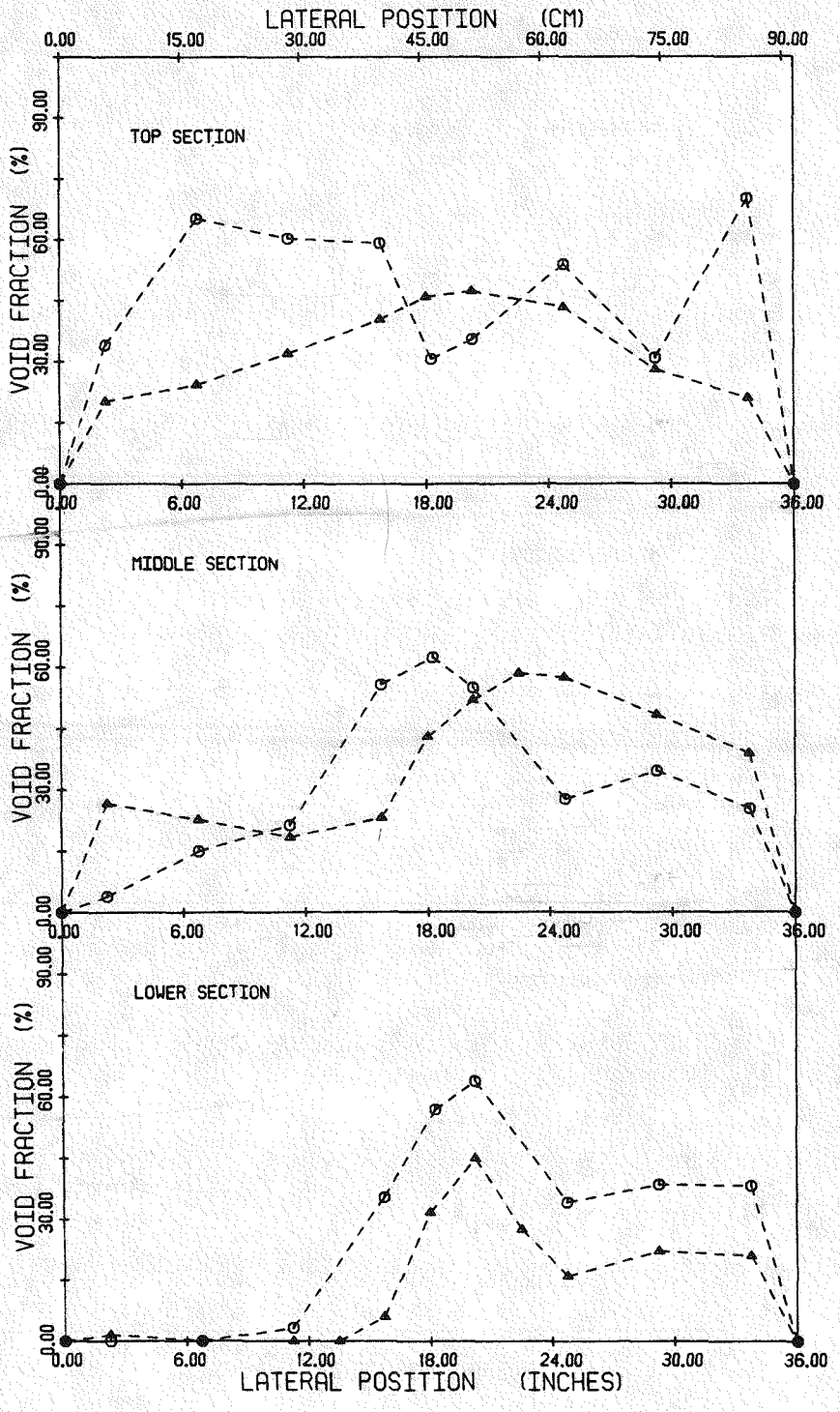


Figure 5.47 Void fraction for cases 1BN4 and 1BR4

| CASE | SYMBOL | LIQUID MASS FLUX KG/HR.M$^2$ | FLOW SPLIT IN#4 : IN#1 | QUALITY | RODS IN | PRESSURE KPA |
|---|---|---|---|---|---|---|
| 2BN4 | | 0.562 E6 | 62.5% : 37.5% | 0.6% | NO | 32.4 |
| 2BR4 | | 0.697 E6 | 62.5% : 37.5% | 0.6% | YES | 34.5 |

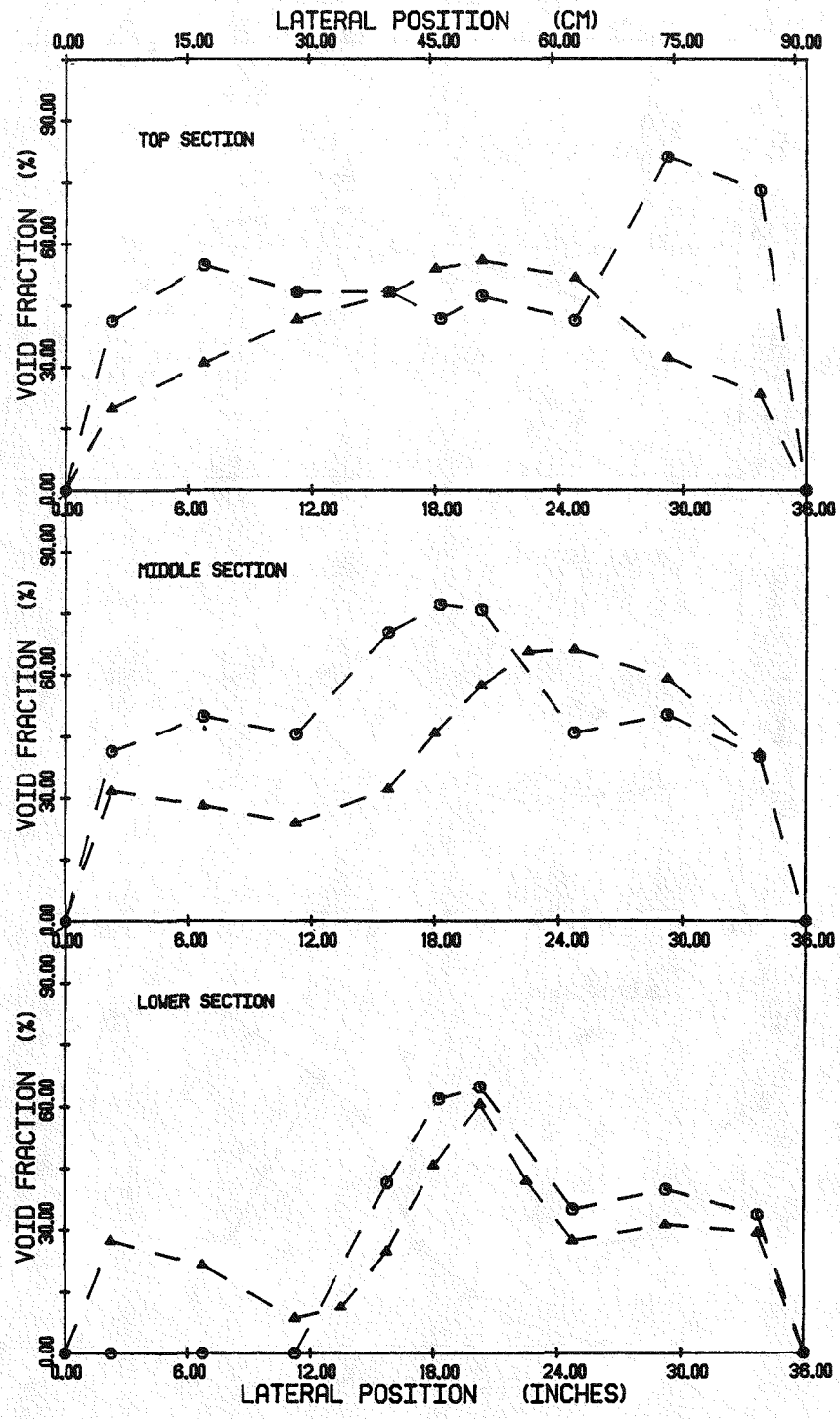


Figure 5.48 Void fraction for cases 2BN4 and 2BR4

| CASE | SYMBOL | LIQUID MASS FLUX KG/HR.M$^2$ | FLOW SPLIT IN#4 : IN#1 | QUALITY | RODS IN | PRESSURE KPA |
|---|---|---|---|---|---|---|
| 3BN4 | | 0.562 E6 | 62.5% : 37.5% | 0.9% | NO | 32.4 |
| 3BR4 | | 0.697 E6 | 62.5% : 37.5% | 0.9% | YES | 34.5 |

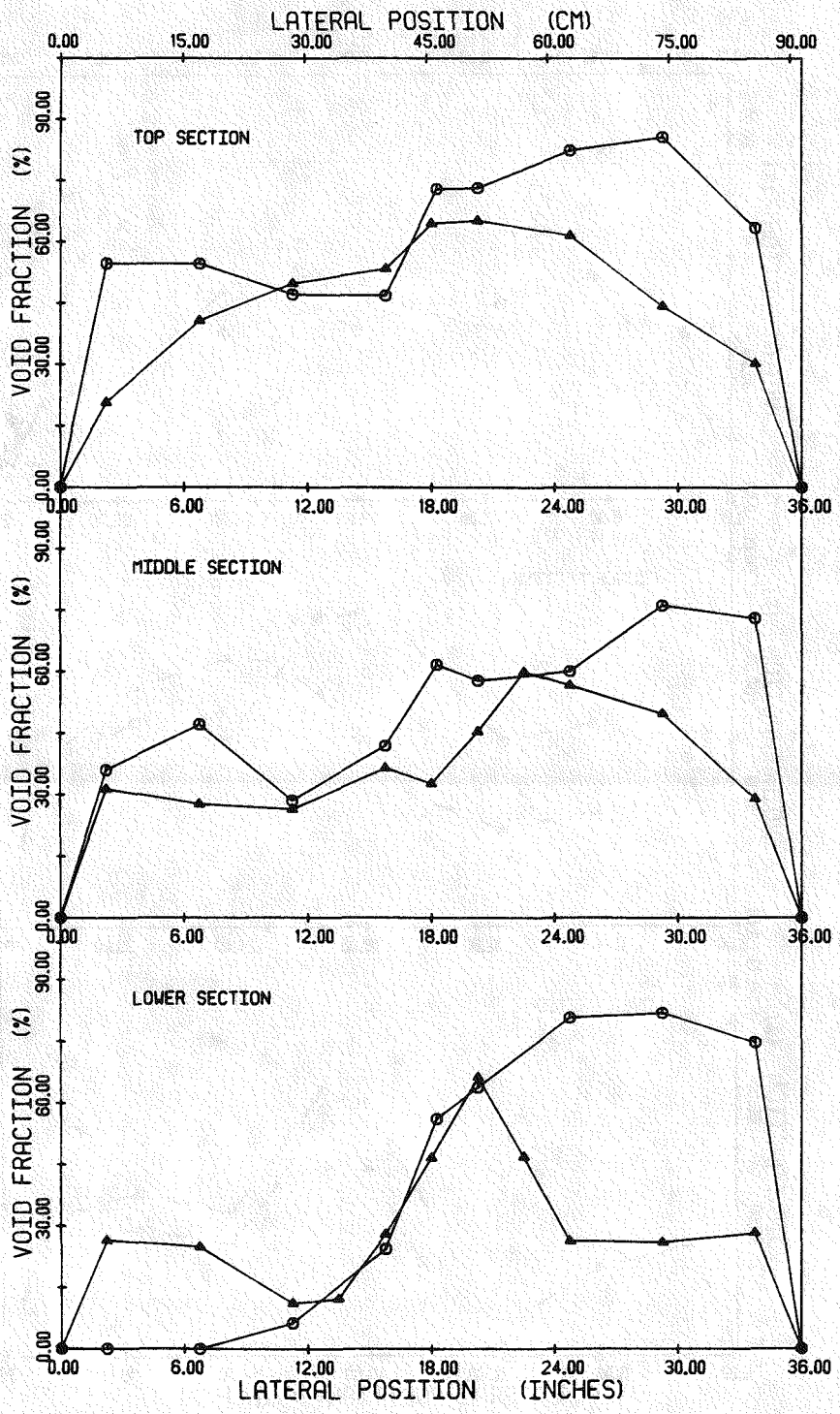


Figure 5.49 Void fraction for cases 3BN4 and 3BR4

| CASE | SYMBOL | LIQUID MASS FLUX KG/HR.M$^2$ | FLOW SPLIT IN#4 : IN#1 | QUALITY | RODS IN | PRESSURE KPA |
|---|---|---|---|---|---|---|
| 1CN4 | | 0.562 E6 | 37.5% : 62.5% | 0.3% | NO | 30.9 |
| 1CR4 | | 0.697 E6 | 37.5% : 62.5% | 0.3% | YES | 33.8 |

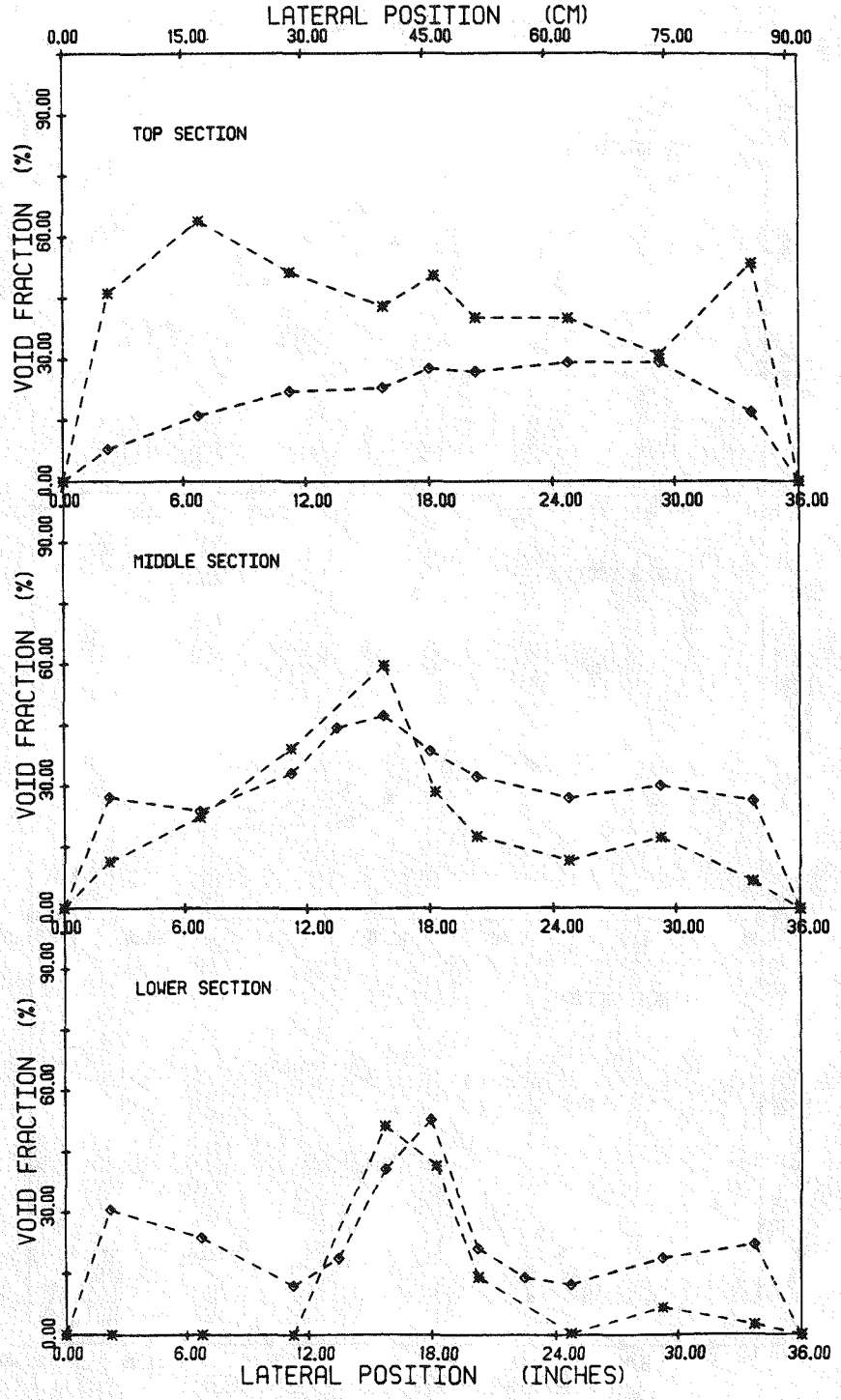


Figure 5.50 Void fraction for cases 1CN4 and 1CR4

| CASE | SYMBOL | LIQUID MASS FLUX KG/HR.M$^2$ | FLOW SPLIT IN#4 : IN#1 | QUALITY | RODS IN | PRESSURE KPA |
|---|---|---|---|---|---|---|
| 2CN4 | | 0.562 E6 | 37.5% : 62.5% | 0.6% | NO | 31.1 |
| 2CR4 | | 0.697 E6 | 37.5% : 62.5% | 0.6% | YES | 33.8 |

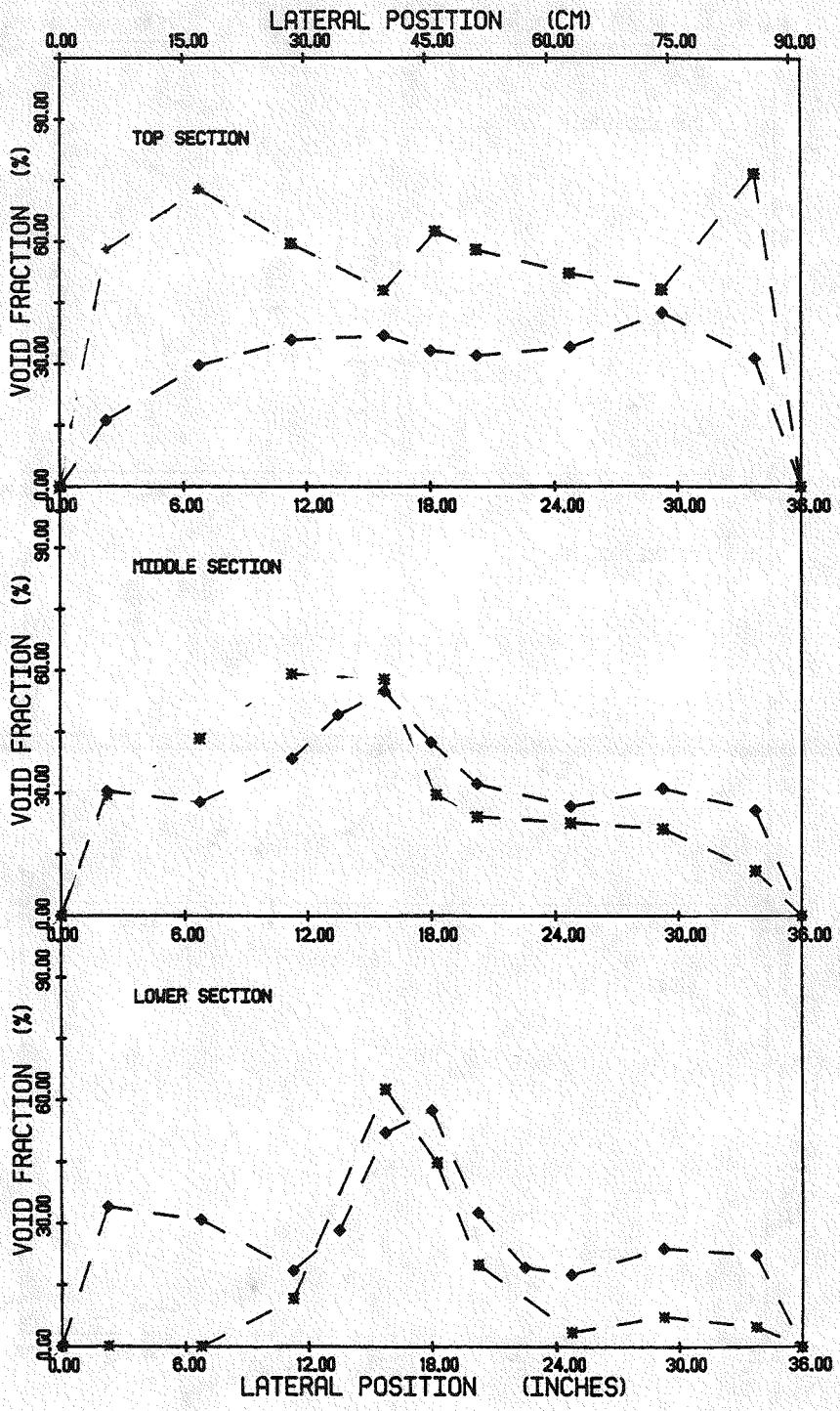


Figure 5.51 Void fraction for cases 2CN4 and 2CR4

| CASE | SYMBOL | LIQUID MASS FLUX KG/HR.M$^2$ | FLOW SPLIT IN#4 : IN#1 | QUALITY | RODS IN | PRESSURE KPA |
|---|---|---|---|---|---|---|
| 3CN4 | | 0.562 E6 | 37.5% : 62.5% | 0.9% | NO | 31.0 |
| 3CR4 | | 0.697 E6 | 37.5% : 62.5% | 0.9% | YES | 34.5 |

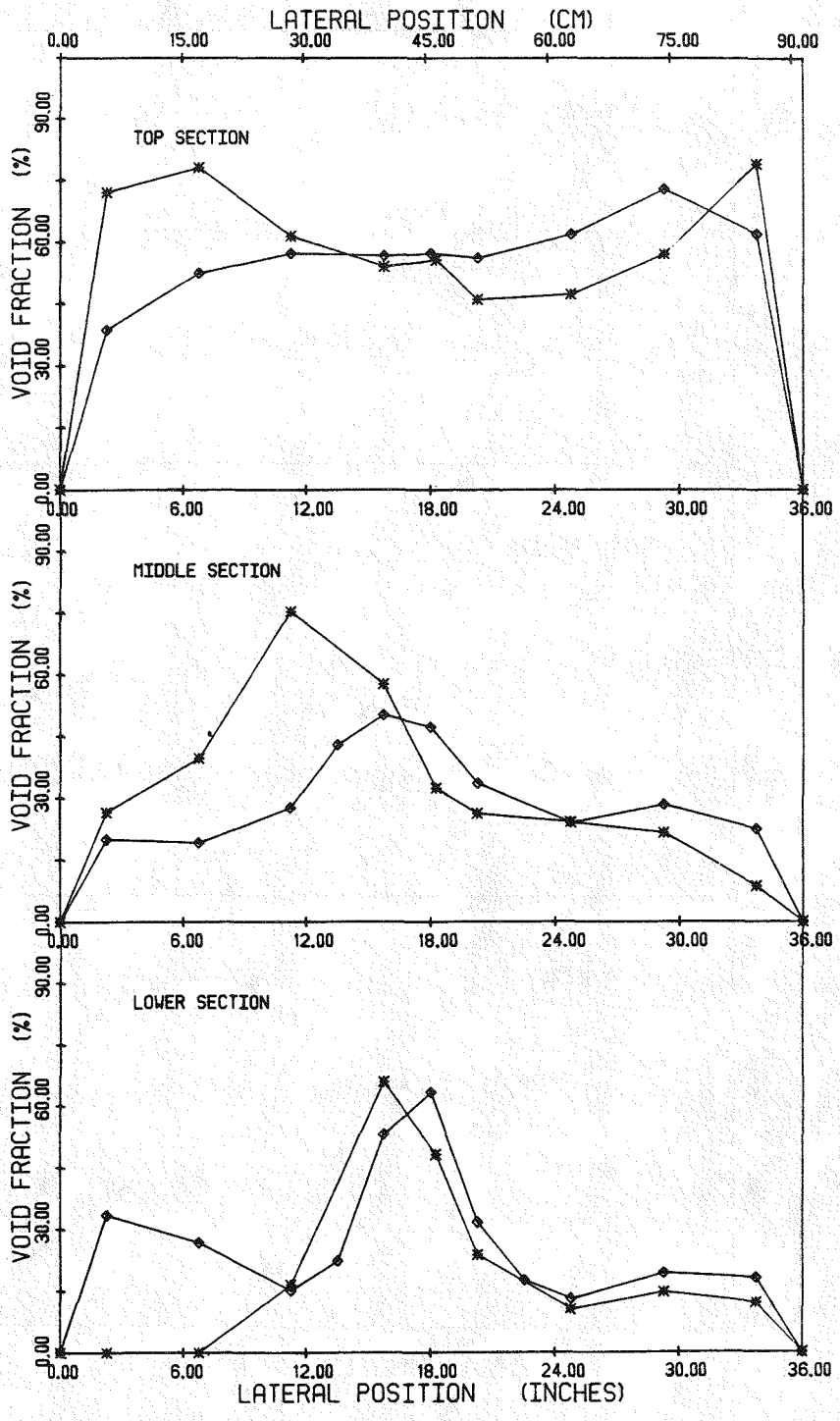


Figure 5.52 Void fraction for cases 3CN4 and 3CR4

| CASE | SYMBOL | LIQUID MASS FLUX KG/HR.M$^2$ | FLOW SPLIT IN#4 : IN#1 | QUALITY | RODS IN | PRESSURE KPA |
|---|---|---|---|---|---|---|
| 4AN4 | | 1.125 E6 | 50.0% : 50.0% | 0.3% | NO | 60.2 |
| 4AR4 | | 1.395 E6 | 50.0% : 50.0% | 0.3% | YES | 75.1 |

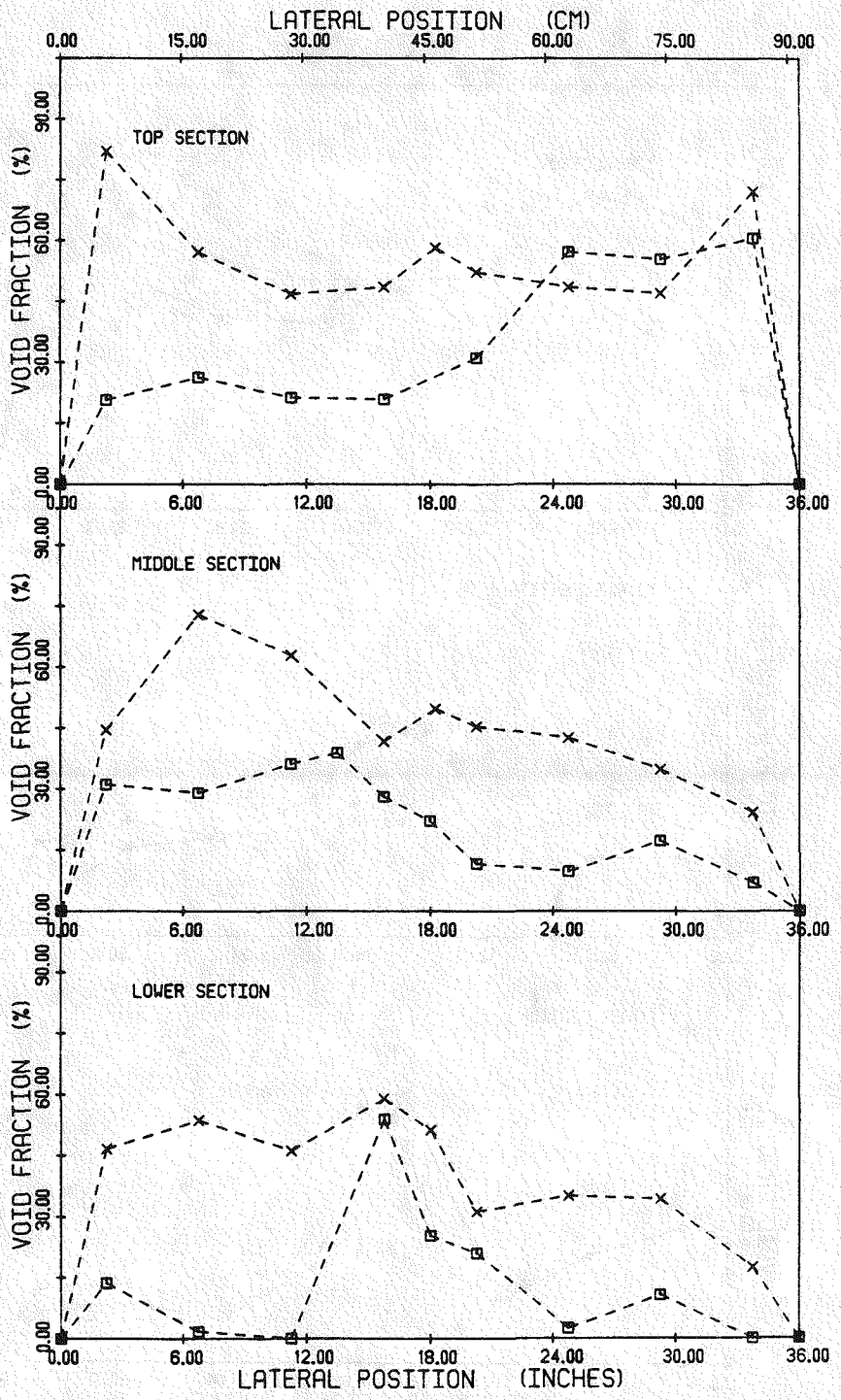


Figure 5.53 Void fraction for cases 4AN4 and 4AR4

| CASE | SYMBOL | LIQUID MASS FLUX KG/HR.M² | FLOW SPLIT IN#4 : IN#1 | QUALITY | RODS IN | PRESSURE KPA |
|---|---|---|---|---|---|---|
| 5AN4 | | 1.125 E6 | 50.0% : 50.0% | 0.6% | NO | 63.7 |
| 5AR4 | | 1.395 E6 | 50.0% : 50.0% | 0.6% | YES | 78.1 |

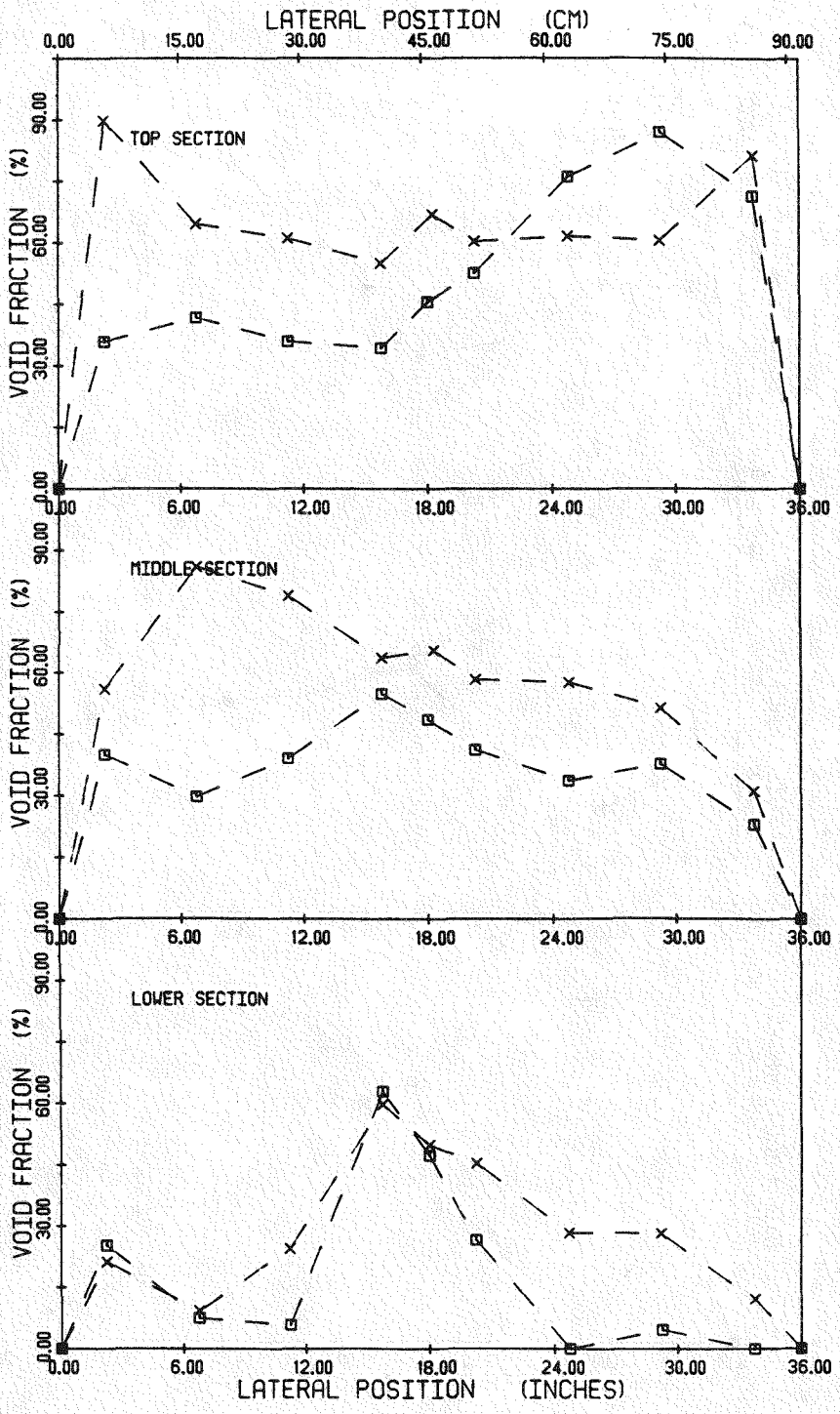


Figure 5.54 Void fraction for cases 5AN4 and 5AR4

| CASE | SYMBOL | LIQUID MASS FLUX KG/HR.M$^2$ | FLOW SPLIT IN#4 : IN#1 | QUALITY | RODS IN | PRESSURE KPA |
|---|---|---|---|---|---|---|
| 6AN4 | | 1.125 E6 | 50.0% : 50.0% | 0.9% | NO | 68.1 |
| 6AR4 | | 1.395 E6 | 50.0% : 50.0% | 0.9% | YES | 81.4 |

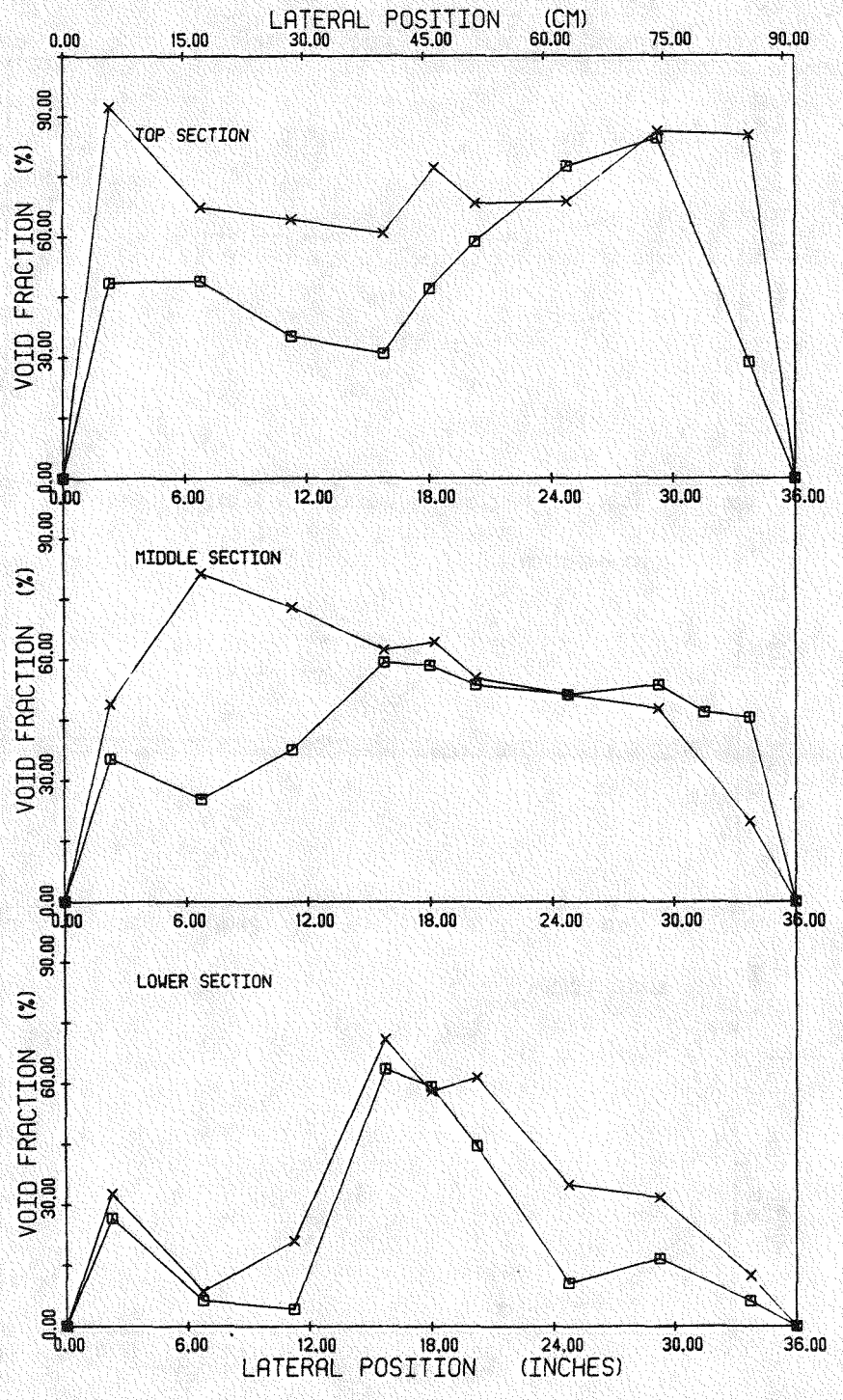


Figure 5.55 Void fraction for cases 6AN4 and 6AR4

| CASE | SYMBOL | LIQUID MASS FLUX KG/HR.M$^2$ | FLOW SPLIT IN#4 : IN#1 | QUALITY | RODS IN | PRESSURE KPA |
|---|---|---|---|---|---|---|
| 4BN4 | | 1.125 E6 | 62.5% : 37.5% | 0.3% | NO | 62.7 |
| 4BR4 | | 1.395 E6 | 62.5% : 37.5% | 0.3% | YES | 76.3 |

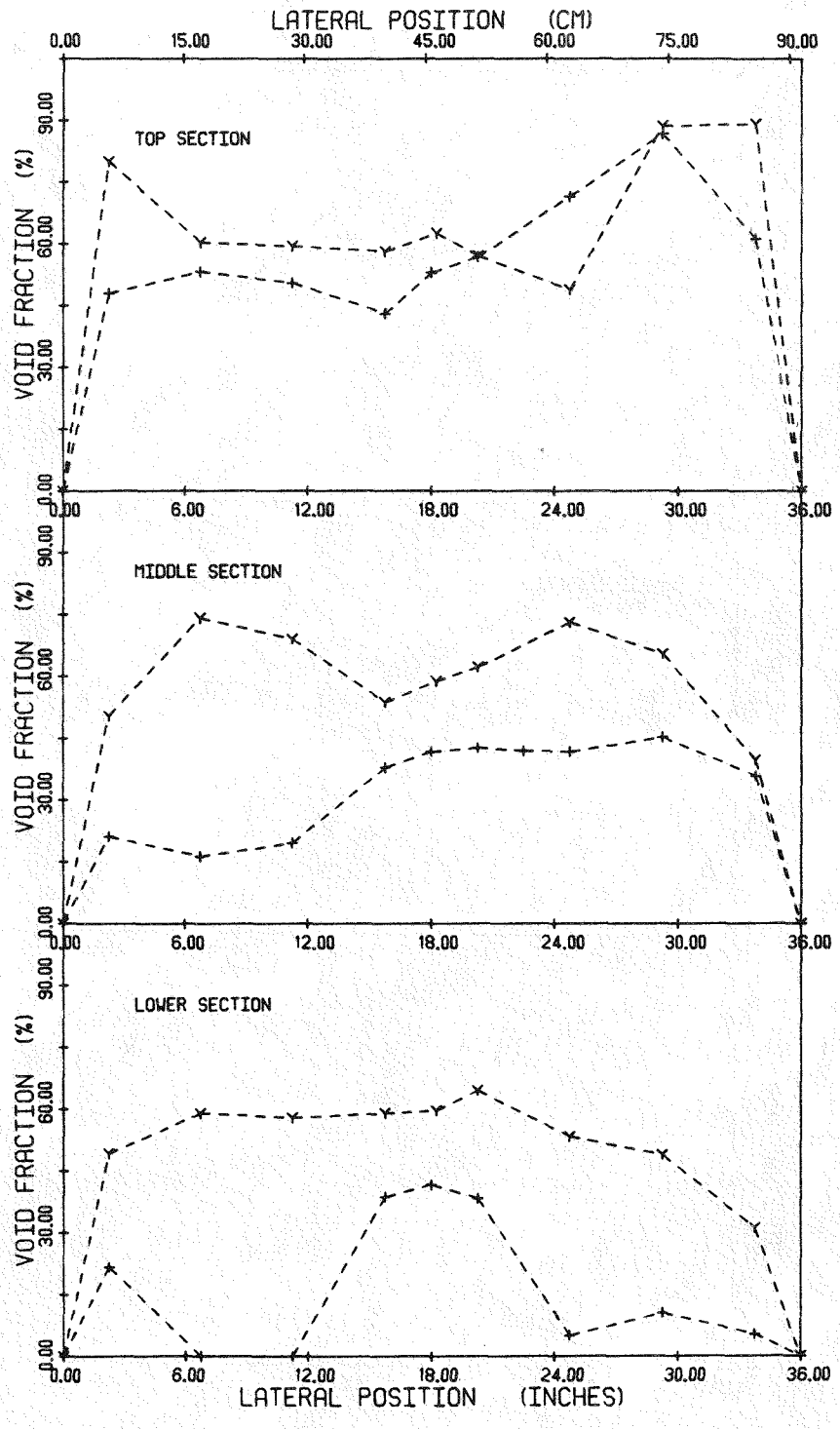


Figure 5.56 Void fraction for cases 4BN4 and 4BR4

| CASE | SYMBOL | LIQUID MASS FLUX KG/HR.M$^2$ | FLOW SPLIT IN#4 : IN#1 | QUALITY | RODS IN | PRESSURE KPA |
|---|---|---|---|---|---|---|
| 5BN4 | | 1.125 E6 | 62.5% : 37.5% | 0.6% | NO | 67.2 |
| 5BR4 | | 1.395 E6 | 62.5% : 37.5% | 0.6% | YES | 80.5 |

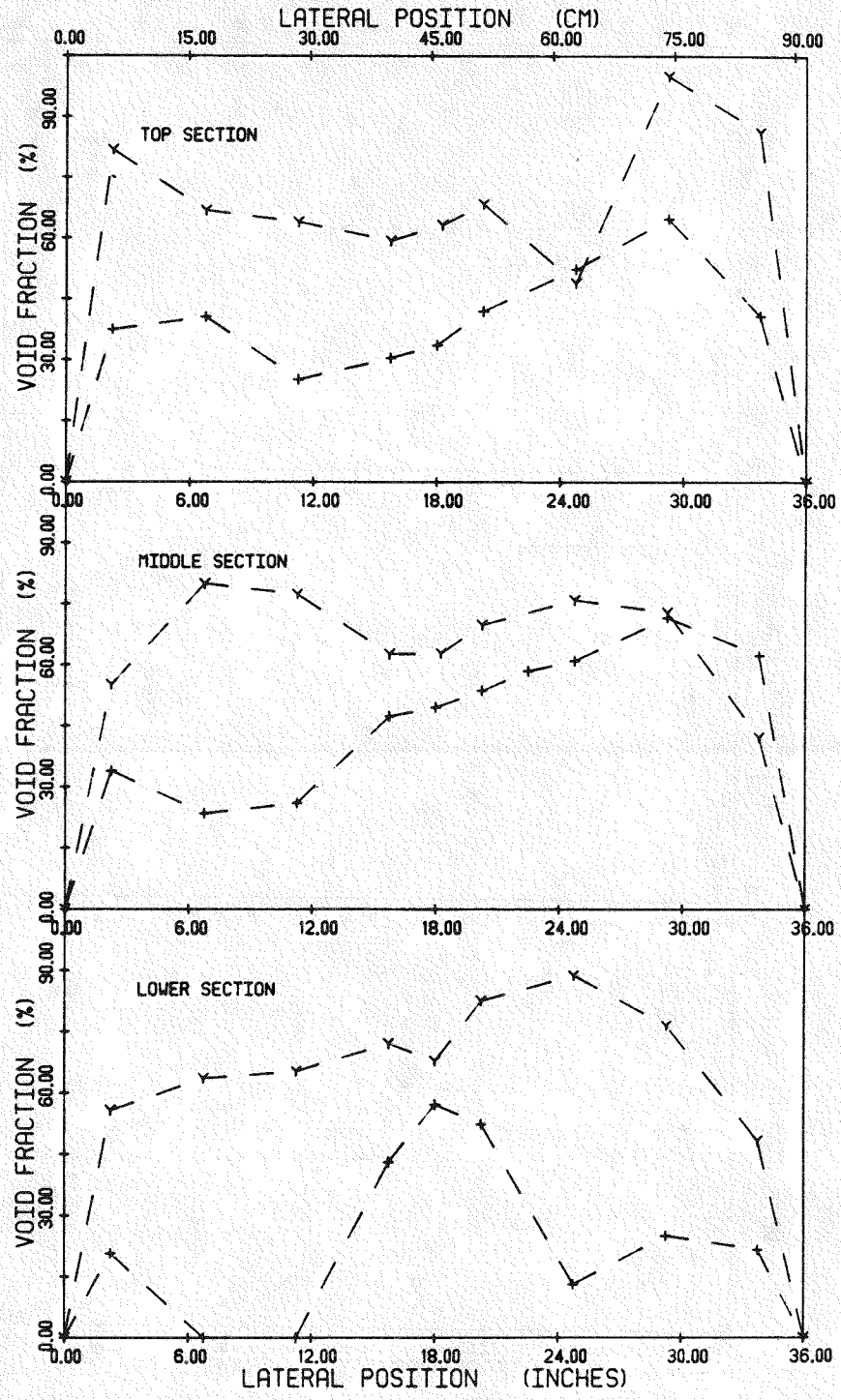


Figure 5.57 Void fraction for cases 5BN4 and 5BR4

| CASE | SYMBOL | LIQUID MASS FLUX KG/HR.M$^2$ | FLOW SPLIT IN#4 : IN#1 | QUALITY | RODS IN | PRESSURE KPA |
|---|---|---|---|---|---|---|
| 6BN4 | | 1.125 E6 | 62.5% : 37.5% | 0.9% | NO | 68.9 |
| 6BR4 | | 1.395 E6 | 62.5% : 37.5% | 0.9% | YES | 85.0 |

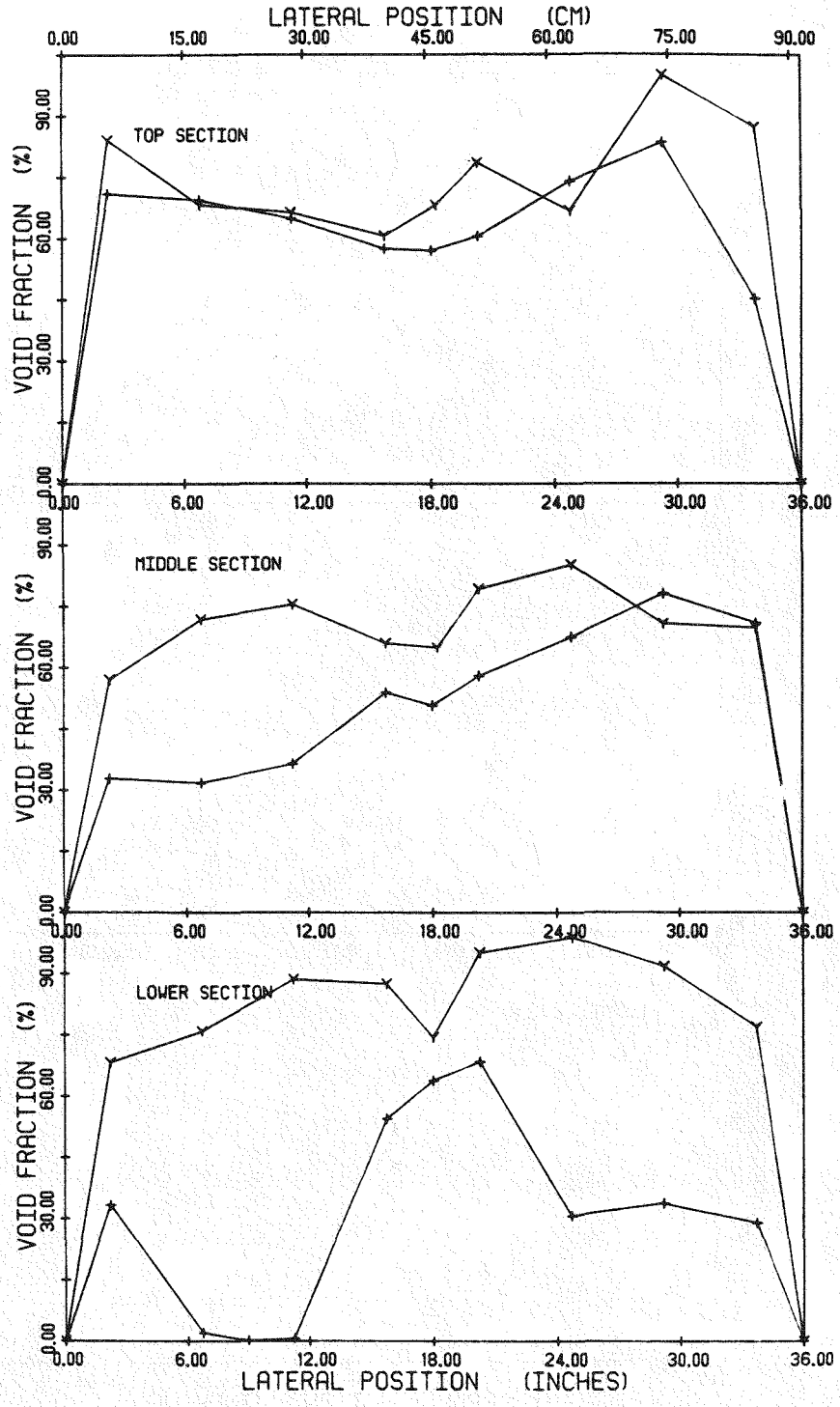


Figure 5.58 Void fraction for cases 6BN4 and 6BR4

| CASE | SYMBOL | LIQUID MASS FLUX KG/HR.M$^2$ | FLOW SPLIT IN#4 : IN#1 | QUALITY | RODS IN | PRESSURE KPA |
|---|---|---|---|---|---|---|
| 4CN4 | | 1.125 E6 | 37.5% : 62.5% | 0.3% | NO | 59.5 |
| 4CR4 | | 1.395 E6 | 37.5% : 62.5% | 0.3% | YES | 73.5 |

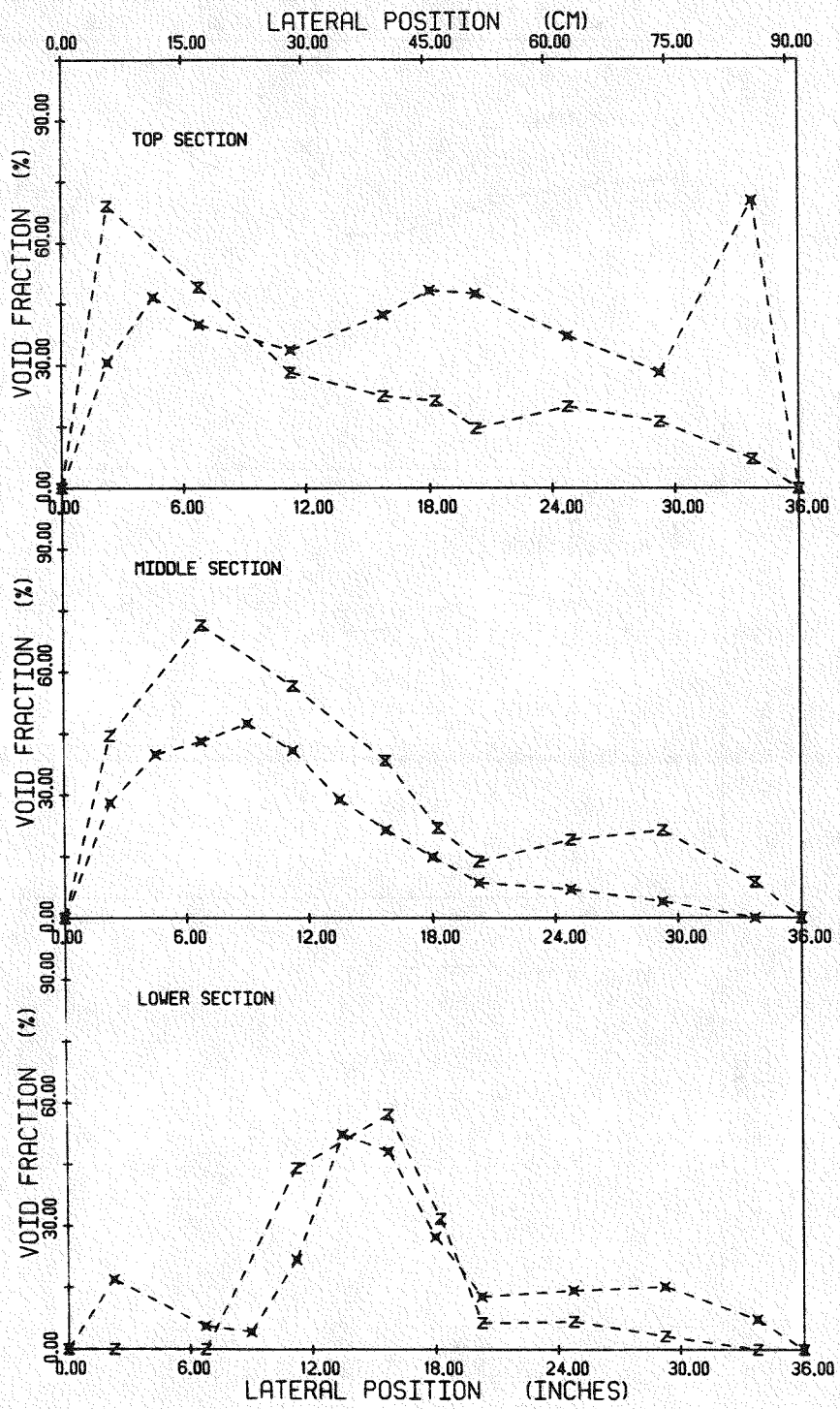


Figure 5.59 Void fraction for cases 4CN4 and 4CR4

| CASE | SYMBOL | LIQUID MASS FLUX KG/HR.M$^2$ | FLOW SPLIT IN#4 : IN#1 | QUALITY | RODS IN | PRESSURE KPA |
|---|---|---|---|---|---|---|
| 5CN4 | | 1.125 E6 | 37.5% : 62.5% | 0.6% | NO | 61.4 |
| 5CR4 | | 1.395 E6 | 37.5% : 62.5% | 0.6% | YES | 78.1 |

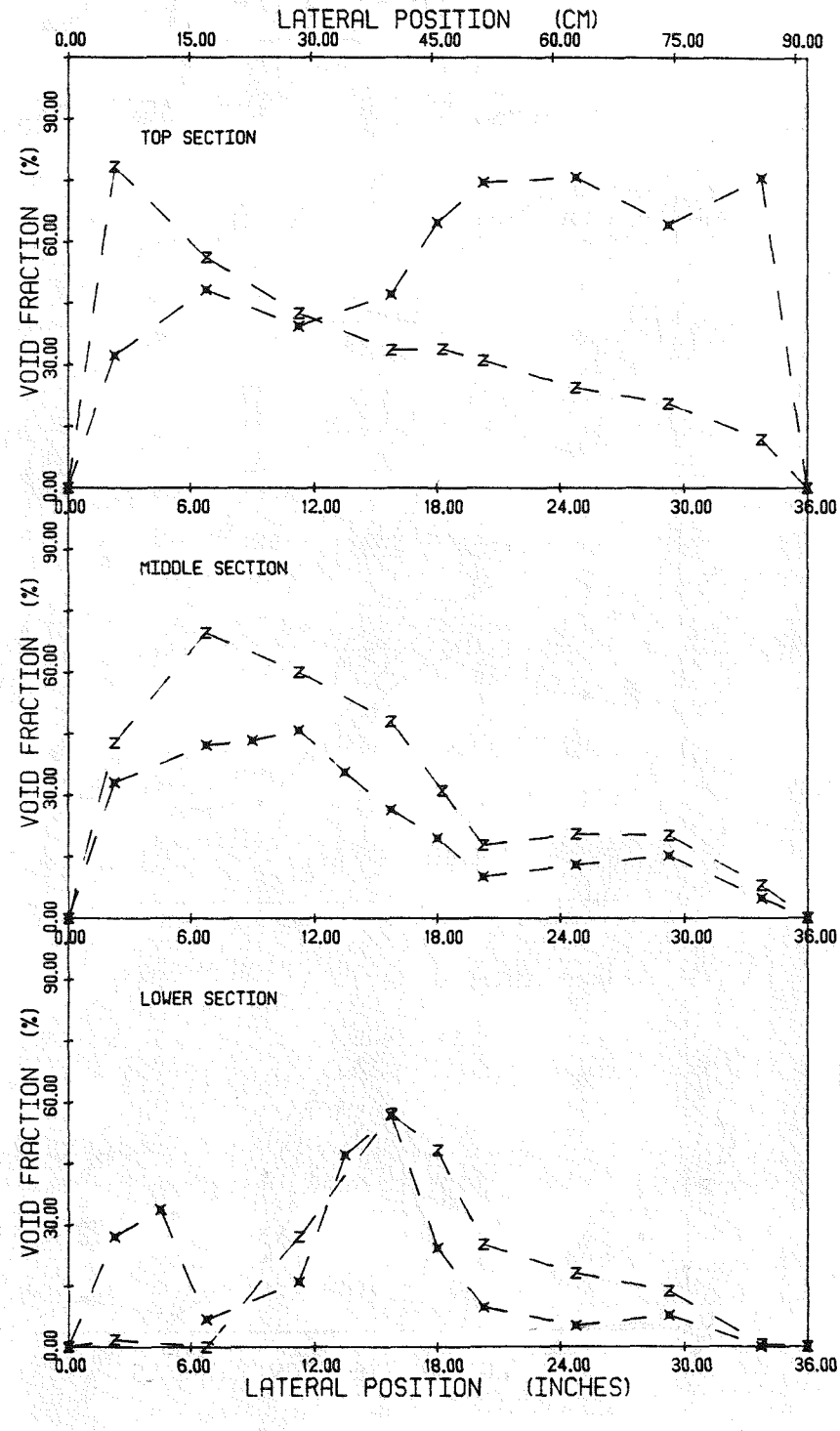


Figure 5.60 Void fraction for cases 5CN4 and 5CR4

| CASE | SYMBOL | LIQUID MASS FLUX KG/HR.M² | FLOW SPLIT IN#4 : IN#1 | QUALITY | RODS IN | PRESSURE KPA |
|---|---|---|---|---|---|---|
| 6CN4 | | 1.125 E6 | 37.5% : 62.5% | 0.9% | NO | 62.9 |
| 6CR4 | | 1.395 E6 | 37.5% : 62.5% | 0.9% | YES | 79.5 |

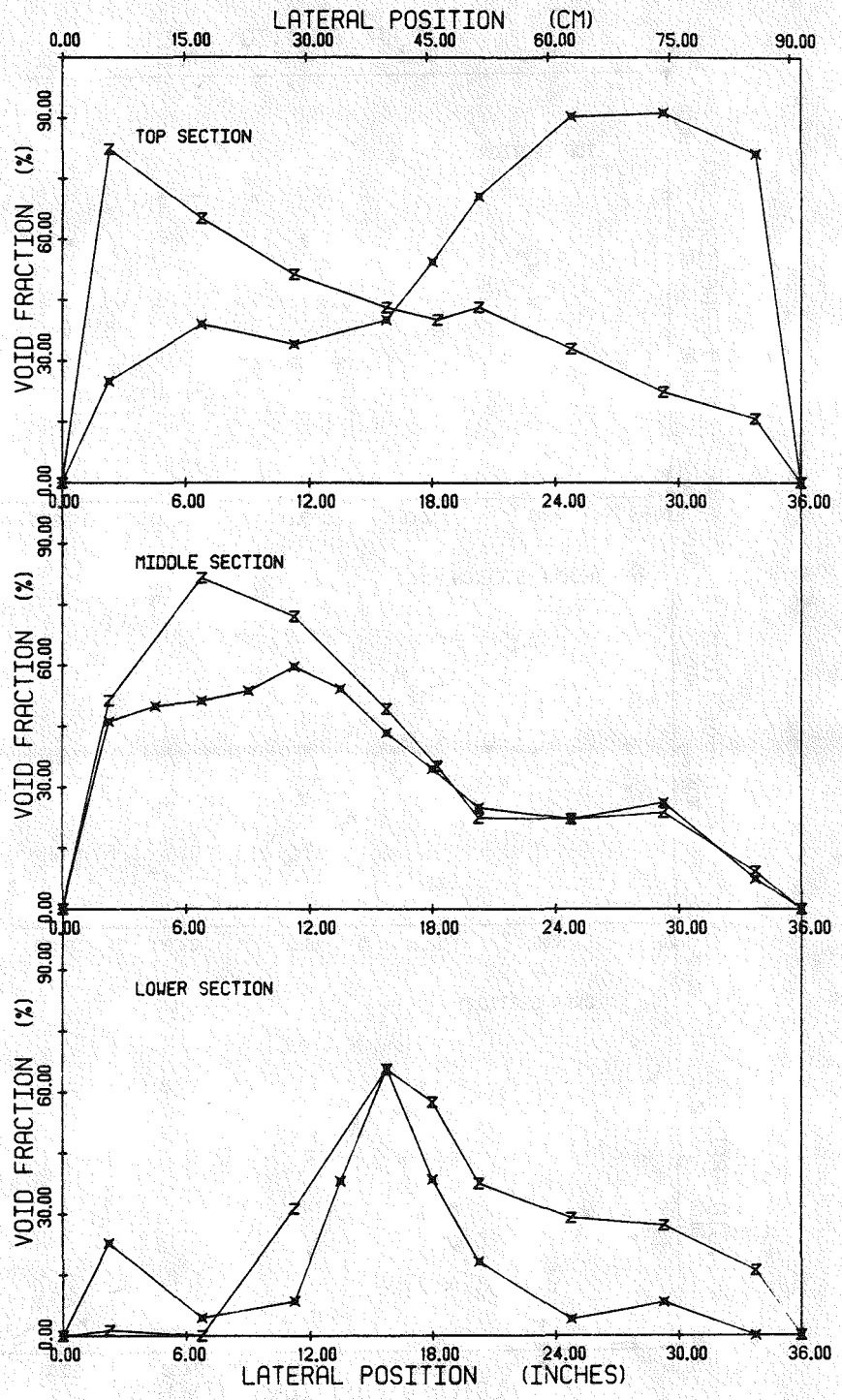


Figure 5.61 Void fraction for cases 6CN4 and 6CR4

For each of these plots, all of the other conditions are identical. A study of these plots and of the corresponding photographs of the flow conditions, Figs. 5.62 to 5.97, reveals the following:

(a) The flow was recirculating and turbulent: The general pattern of the directions of motion of the two-phase mixture is shown in Fig. 5.98. This figure was made on the basis of photographs (Figs. 5.62-5.97) and visual inspection of the test section during the experiments. As seen in Fig. 5.98, where the arrows represent the direction of flow, the two-phase mixture moved vertically upwards on entering the test section from port no. 4. On reaching a position near the top edge, most of the flow turned to the left and some of the flow exited out of port no. 2, while the rest turned and moved downward along the left edge of the test section. On reaching a position near the bottom of the test section (actual distance depends on the specific flow conditions), the flow turned to the right and joined the flow coming in from port no. 4. The rest of the flow from inlet no. 4 that reached the top edge turned to the right and then moved downwards. It mixed with the water coming in from port no. 1 and either went out of exit port no. 3, or turned and joined the two-phase mixture coming in from port no. 4. The two-phase mixture entering from port no. 4 also shedded two-phase vortices just after entering the test section. These were rotating counterclockwise on the left of the inlet and clockwise on the right. A generally similar pattern of flow is observed for the cases when rods are present, but the lateral velocities were smaller and there were fewer vortices. The air bubbles also did not reach as low on the left side of the test section as they did in the absence of rods.

(b) There was more than one flow regime in the test section: The large range of velocities and void fractions present simultaneously in the test section lead to the presence of several flow regimes. For most flow conditions, the phases were distributed in a certain manner in the test section. As can be seen in Fig. 5.98, the test section has been divided into eight (8) regions based on the visual appearance of the flow. In the test section, the boundaries between these regions are not as clear cut as they appear in this figure, and they are also constantly fluctuating. The size of the regions also depends strongly on the specific flow conditions maintained in the test section. As such, the regions and their boundaries shown in Fig. 5.98 should be treated as being very approximate.

Regions (B) and (D) did not contain any air bubbles and are therefore single-phase liquid regions. (H) is an air pocket with occasional entrained liquid droplets entering

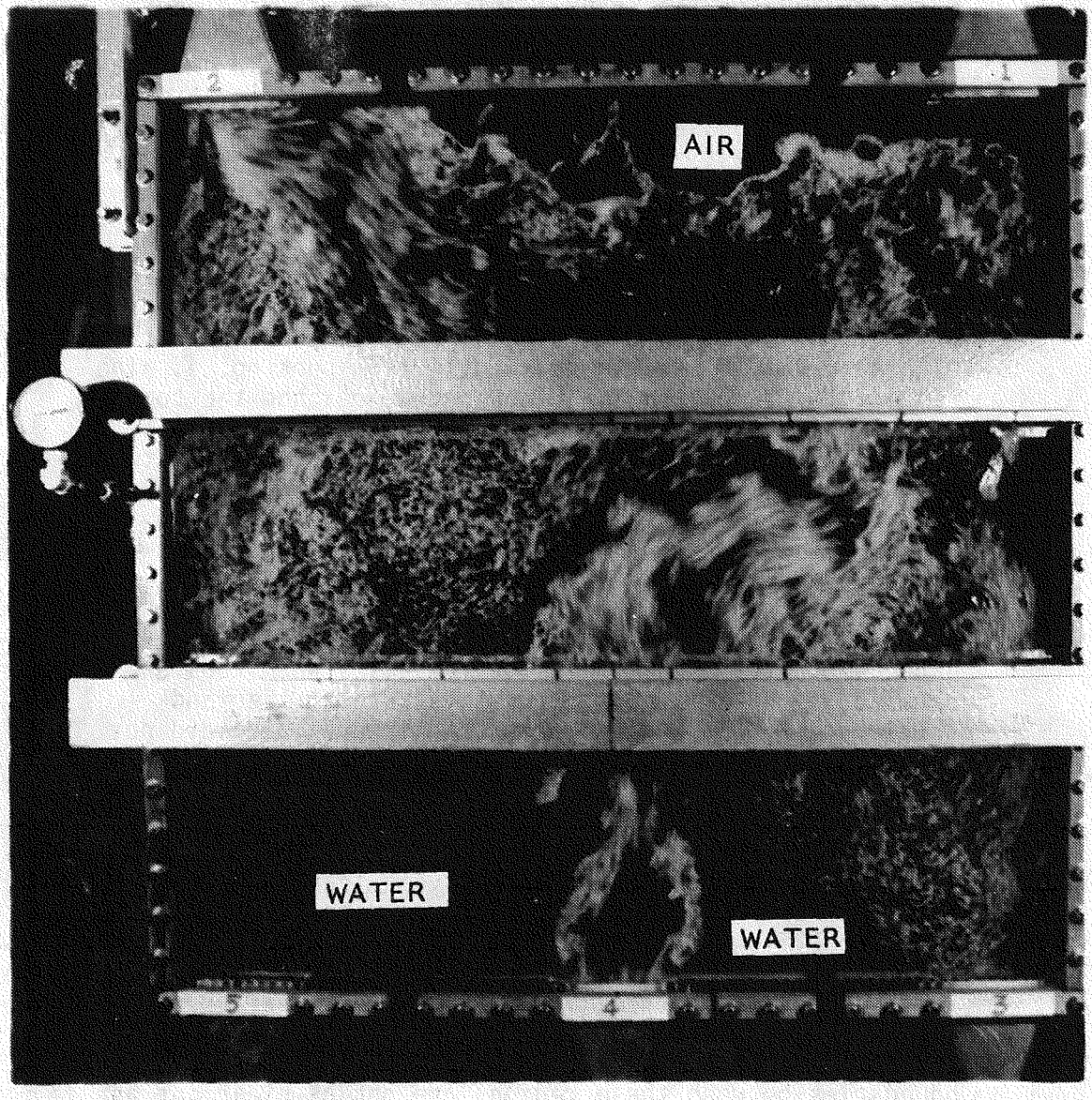


Figure 5.62 Picture of case 1AN4 (liquid mass flux = 0.562 X $10^6$ kg/hr-$m^2$; without rods; 50.0/50.0 flow split; and quality at inlet no. 4 = 0.3%)

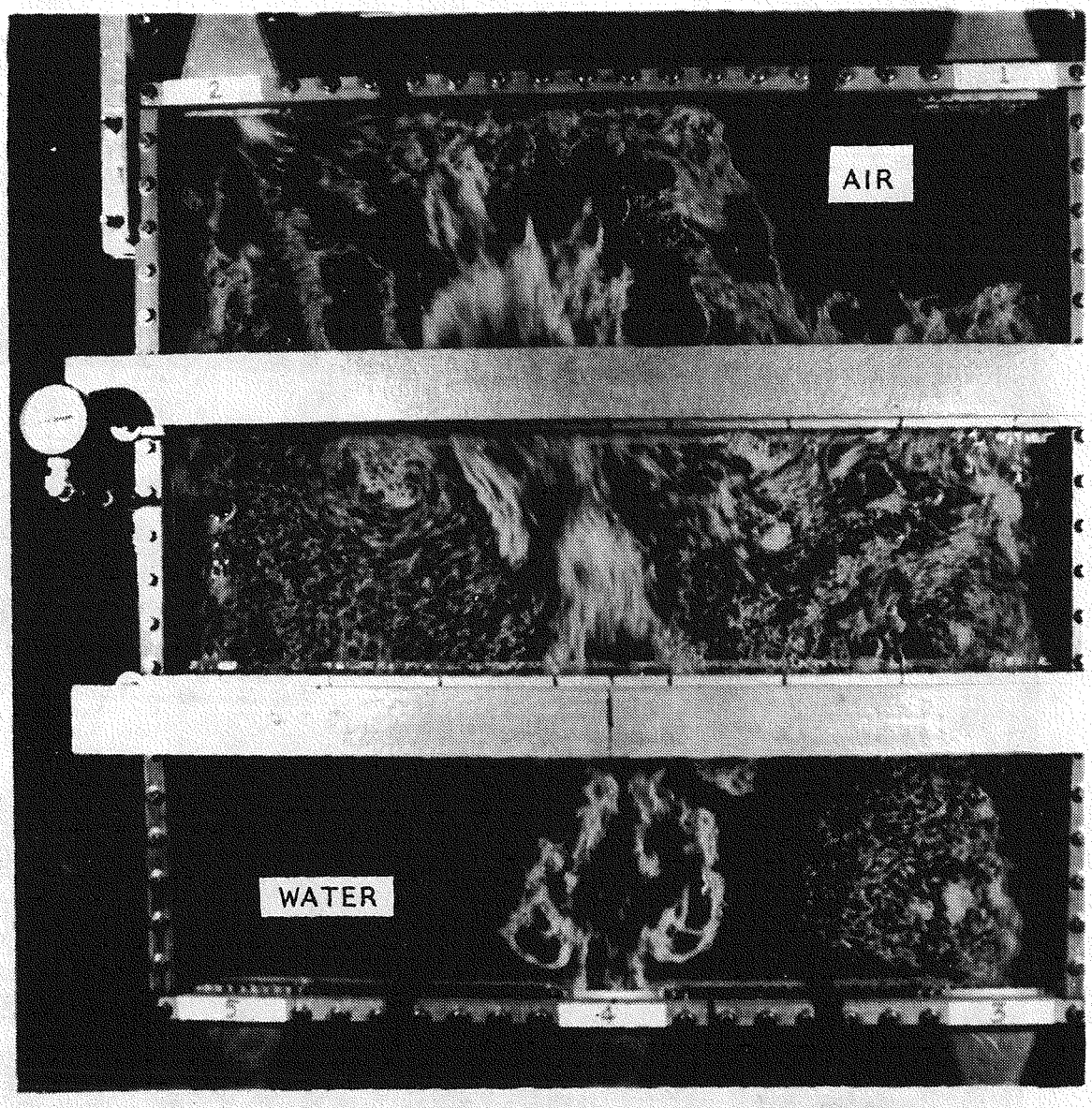


Figure 5.63 Picture of case 2AN4 (liquid mass flux = 0.562 X $10^6$ kg/hr-$m^2$; without rods; 50.0/50.0 flow split; and quality at inlet no. 4 = 0.6%)

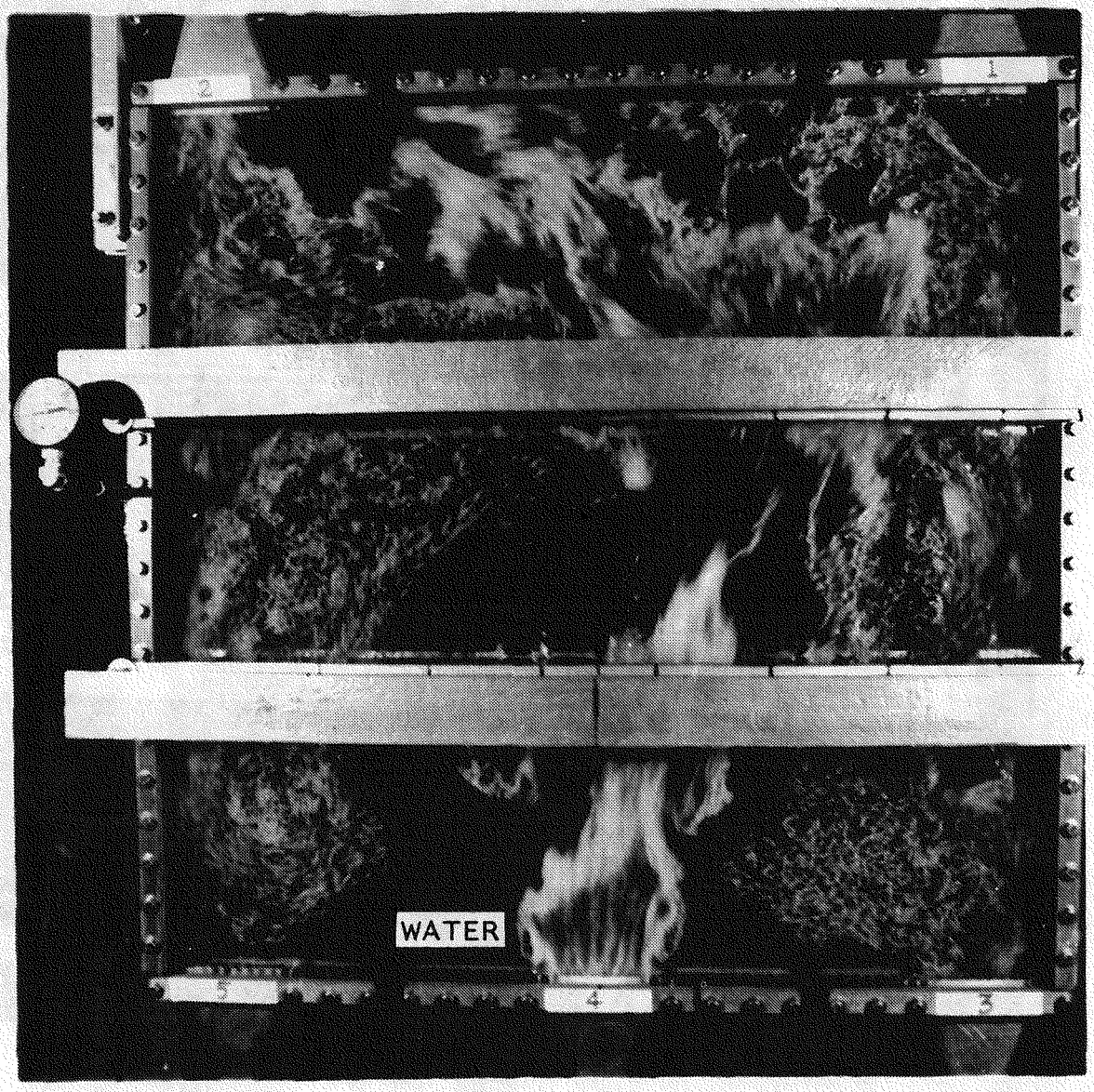


Figure 5.64 Picture of case 3AN4 (liquid mass flux = 0.562 X $10^6$ kg/hr-$m^2$; without rods; 50.0/50.0 flow split; and quality at inlet no. 4 = 0.9%)

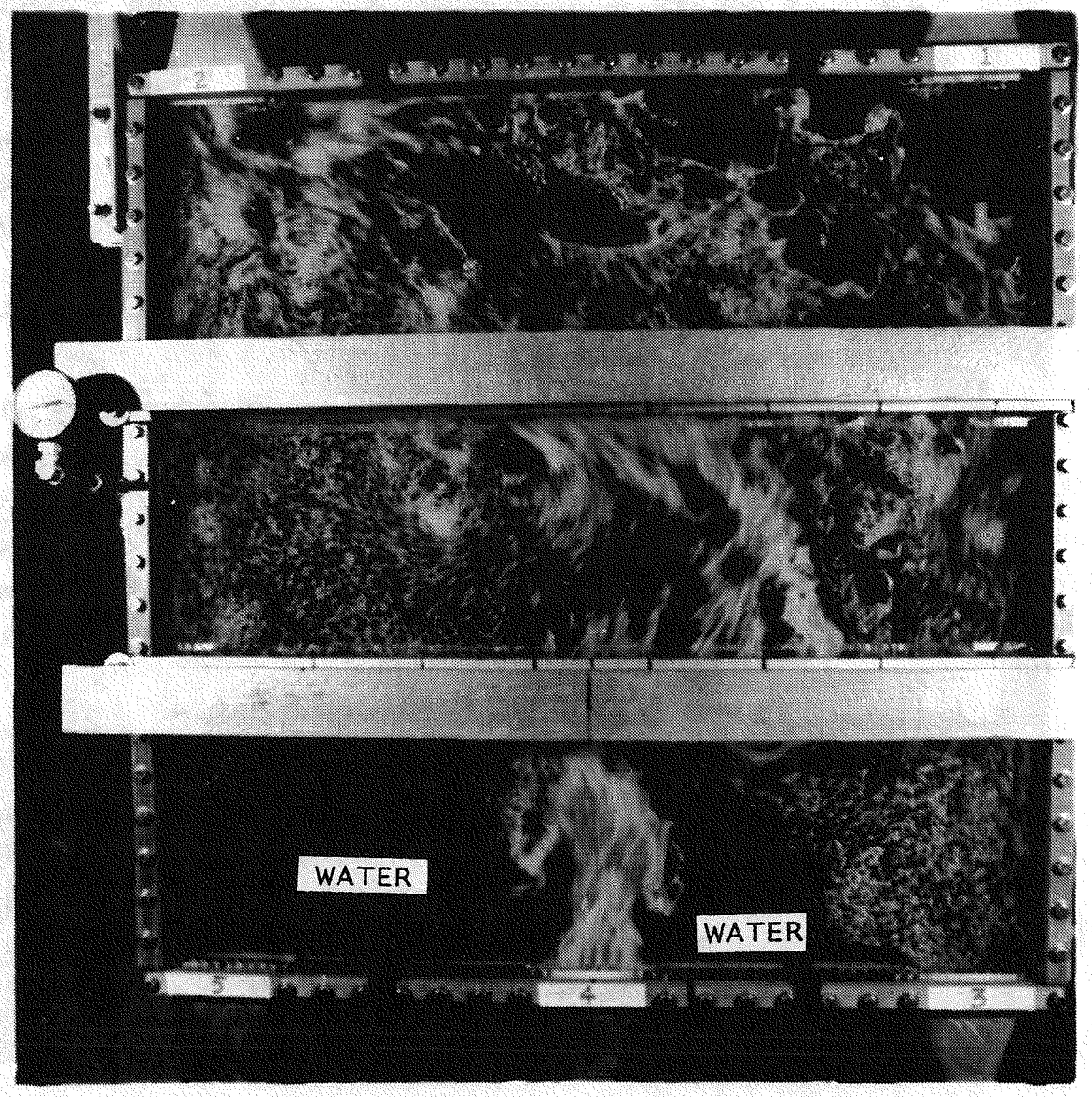


Figure 5.65 Picture of case 1BN4 (liquid mass flux = 0.562 X $10^6$ kg/hr-$m^2$; without rods; 62.5/37.5 flow split; and quality at inlet no. 4 = 0.3%)

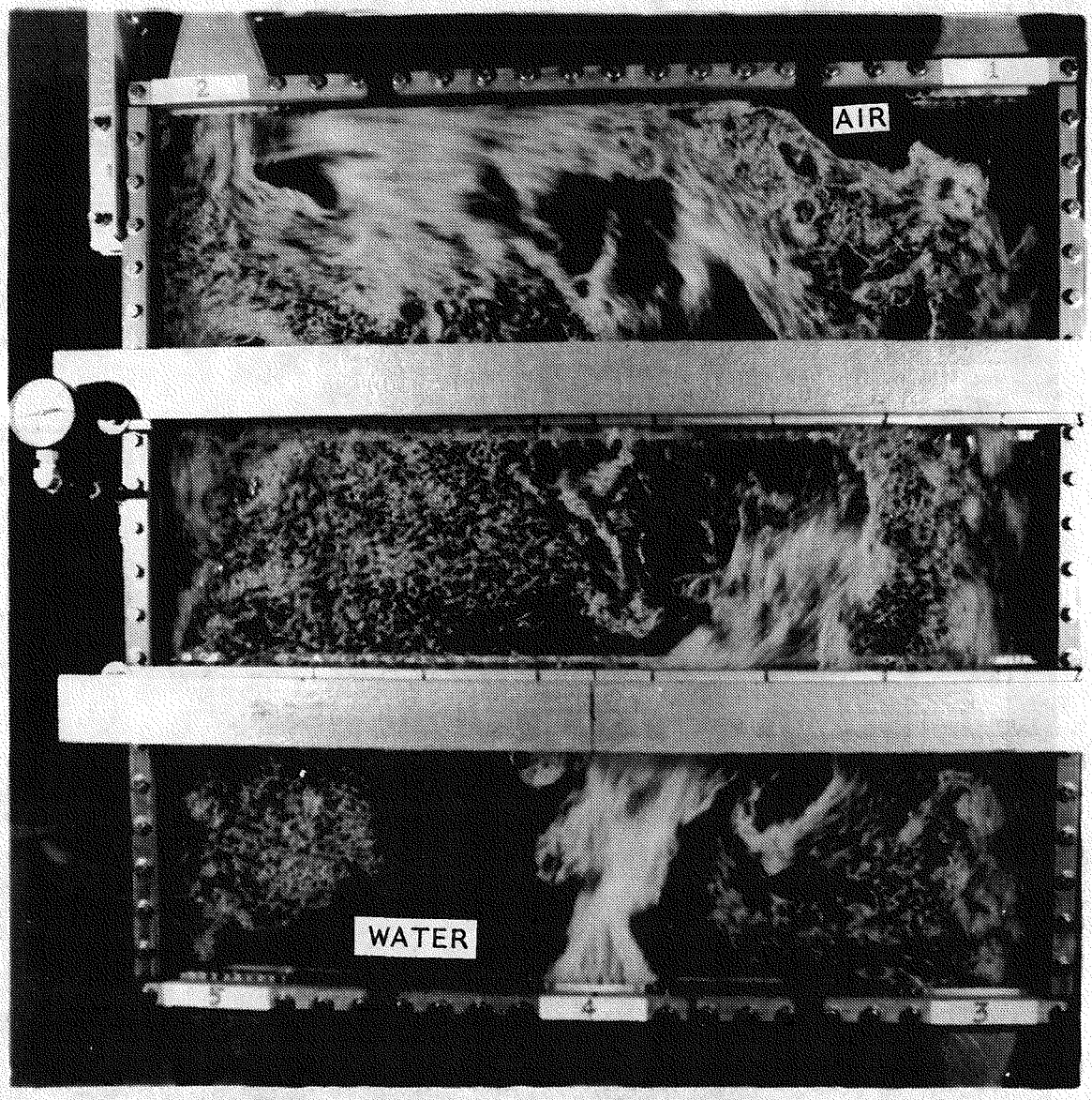


Figure 5.66 Picture of case 2BN4 (liquid mass flux = 0.562 X $10^6$ kg/hr-$m^2$; without rods; 62.5/37.5 flow split; and quality at inlet no. 4 = 0.6%)

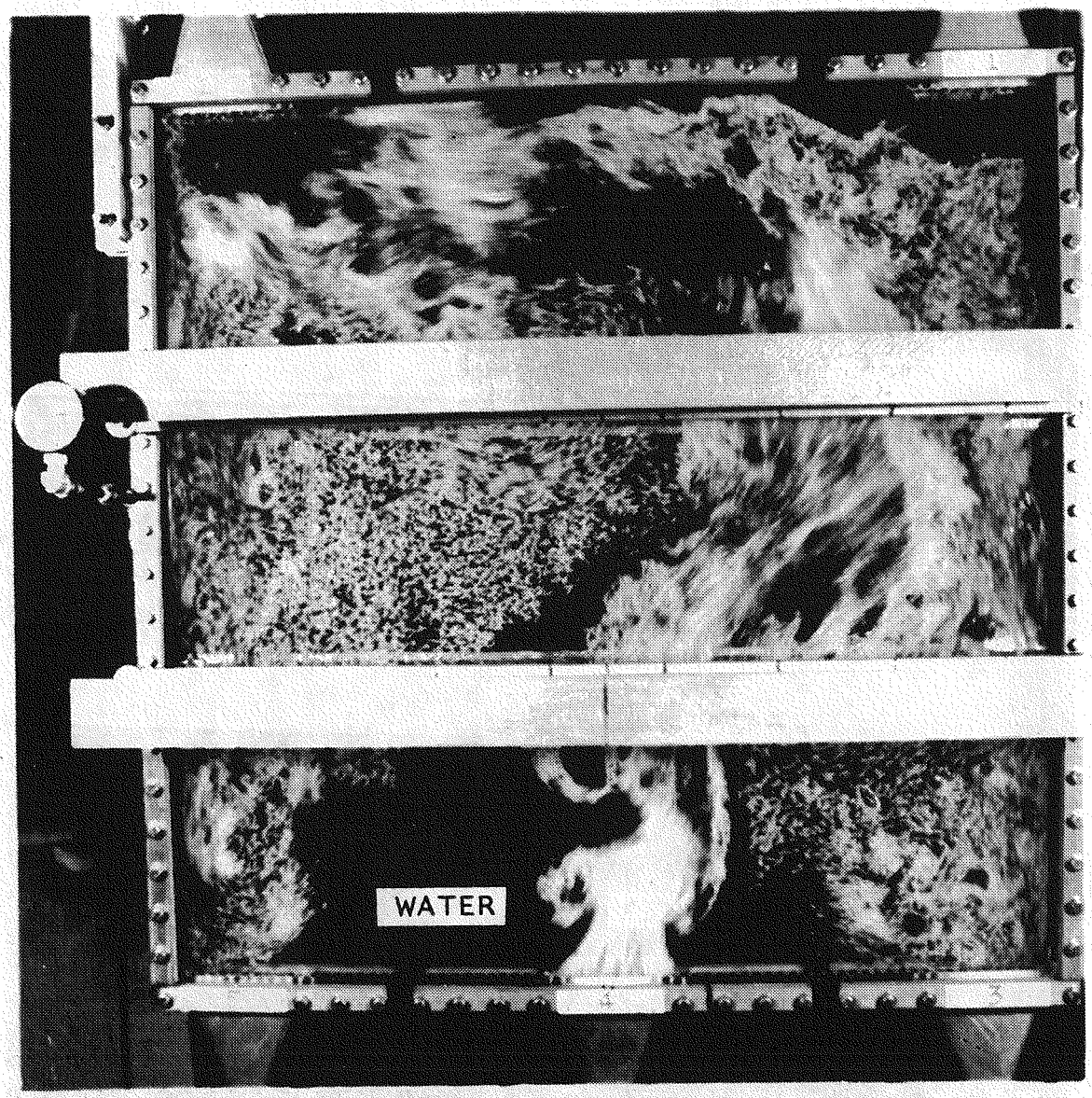


Figure 5.67 Picture of case 3BN4 (liquid mass flux = 0.562 X $10^6$ kg/hr-$m^2$; without rods; 62.5/37.5 flow split; and quality at inlet no. 4 = 0.9%)

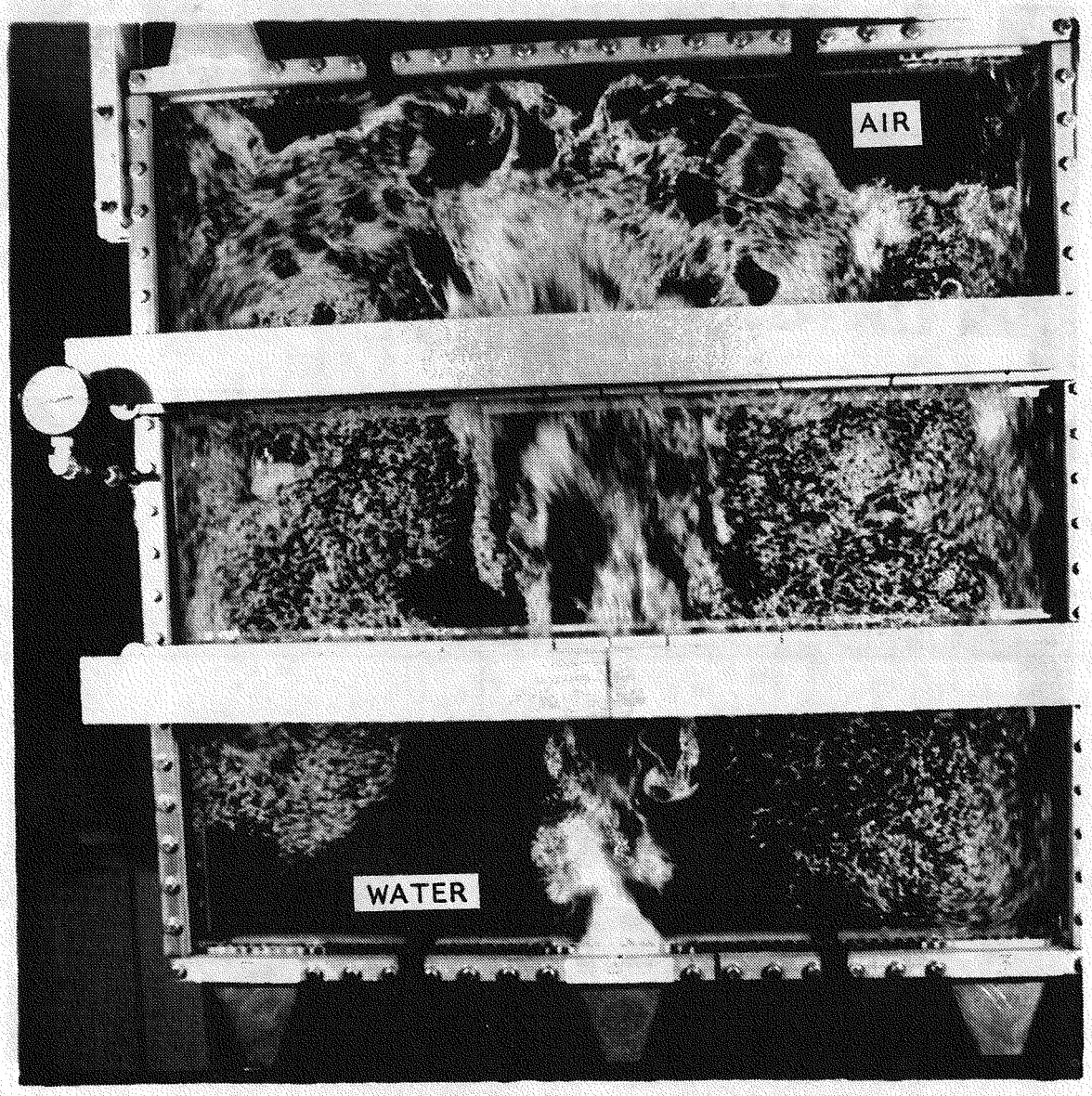


Figure 5.68 Picture of case 1CN4 (liquid mass flux = 0.562 X $10^6$ kg/hr-$m^2$; without rods; 37.5/62.5 flow split; and quality at inlet no. 4 = 0.3%)

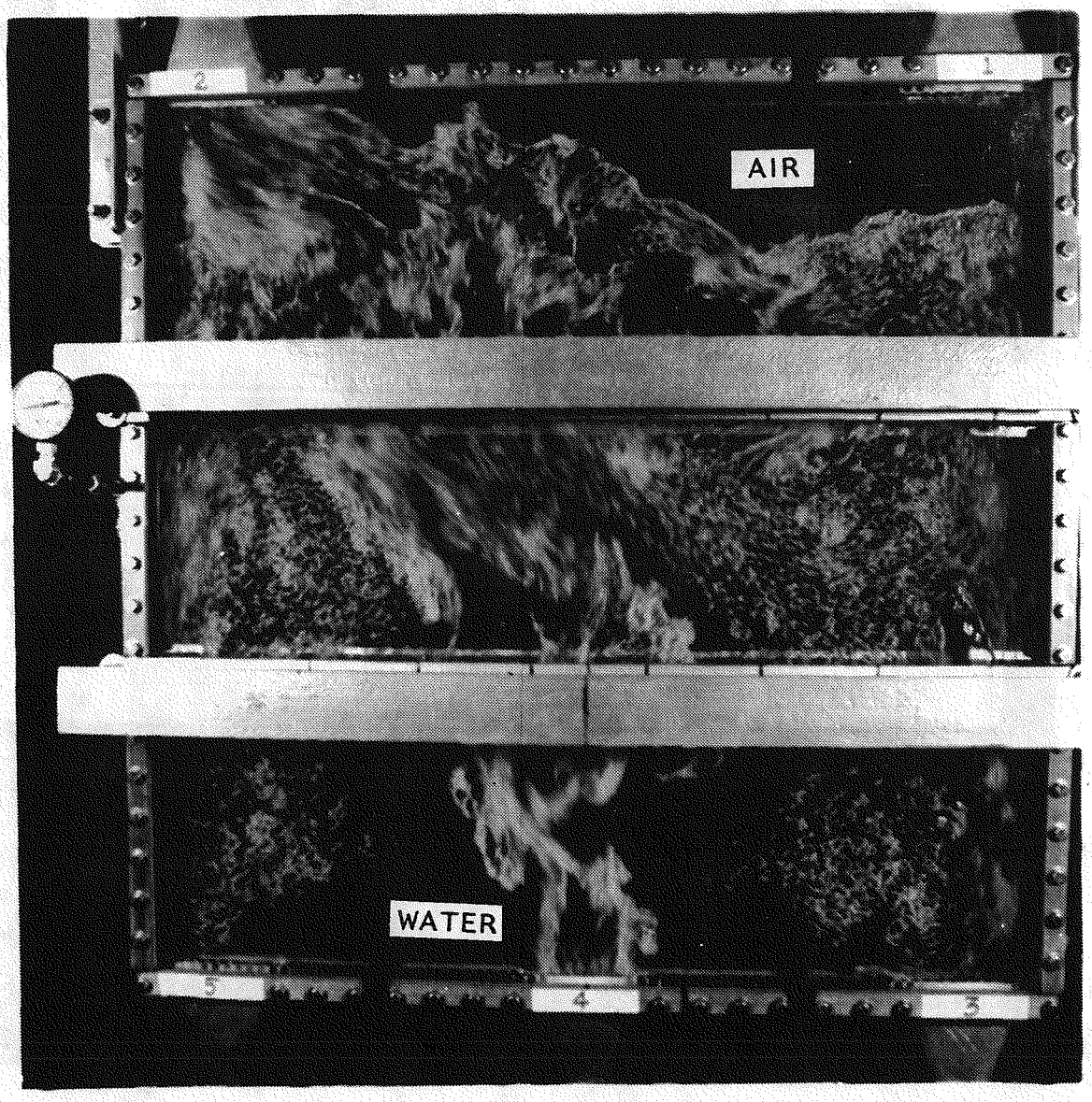


Figure 5.69 Picture of case 2CN4 (liquid mass flux = 0.562 X $10^6$ kg/hr-$m^2$; without rods; 37.5/62.5 flow split; and quality at inlet no. 4 = 0.6%)

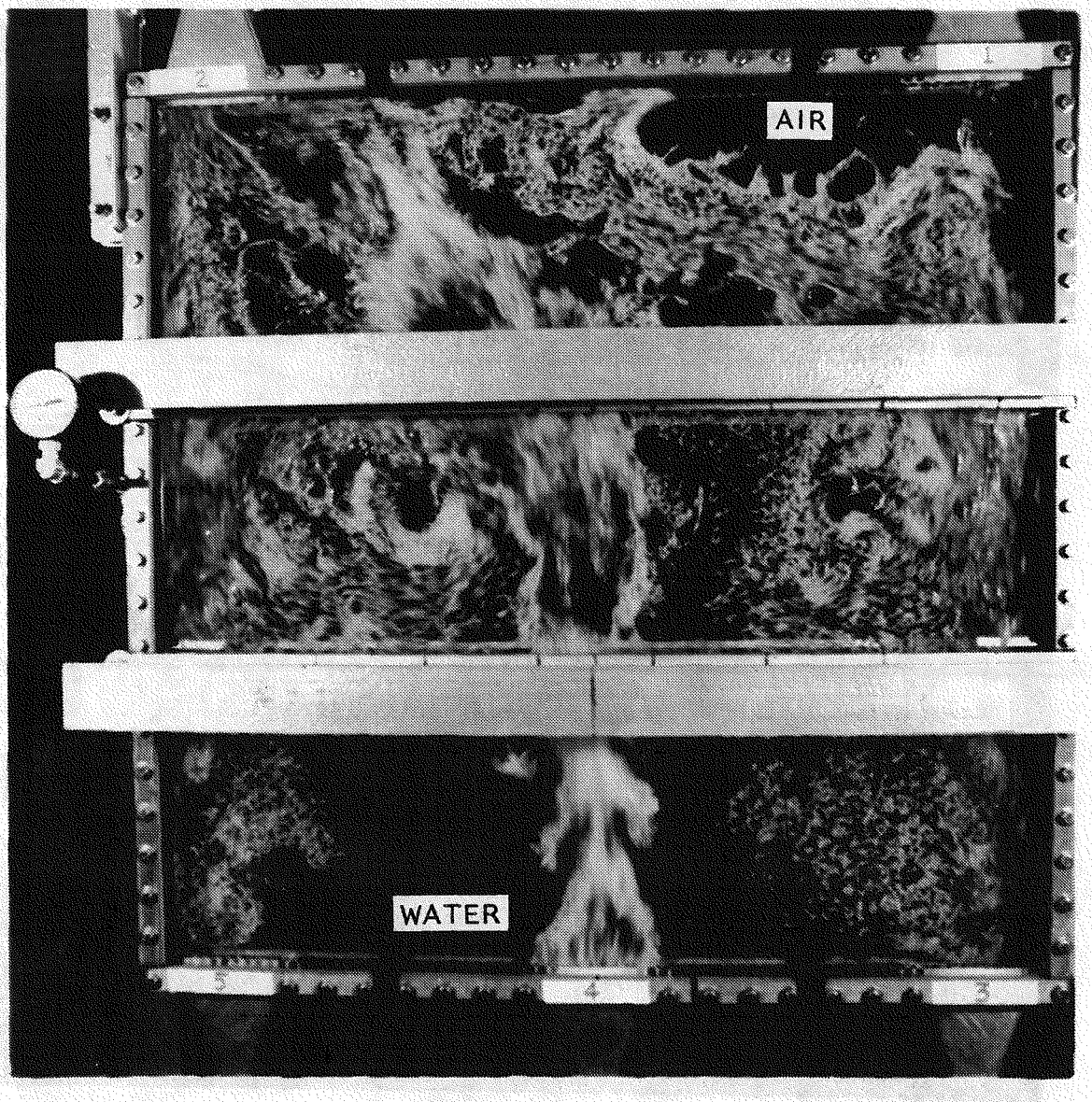


Figure 5.70 Picture of case 3CN4 (liquid mass flux = 0.562 X $10^6$ kg/hr-$m^2$; without rods; 37.5/62.5 flow split; and quality at inlet no. 4 = 0.9%)

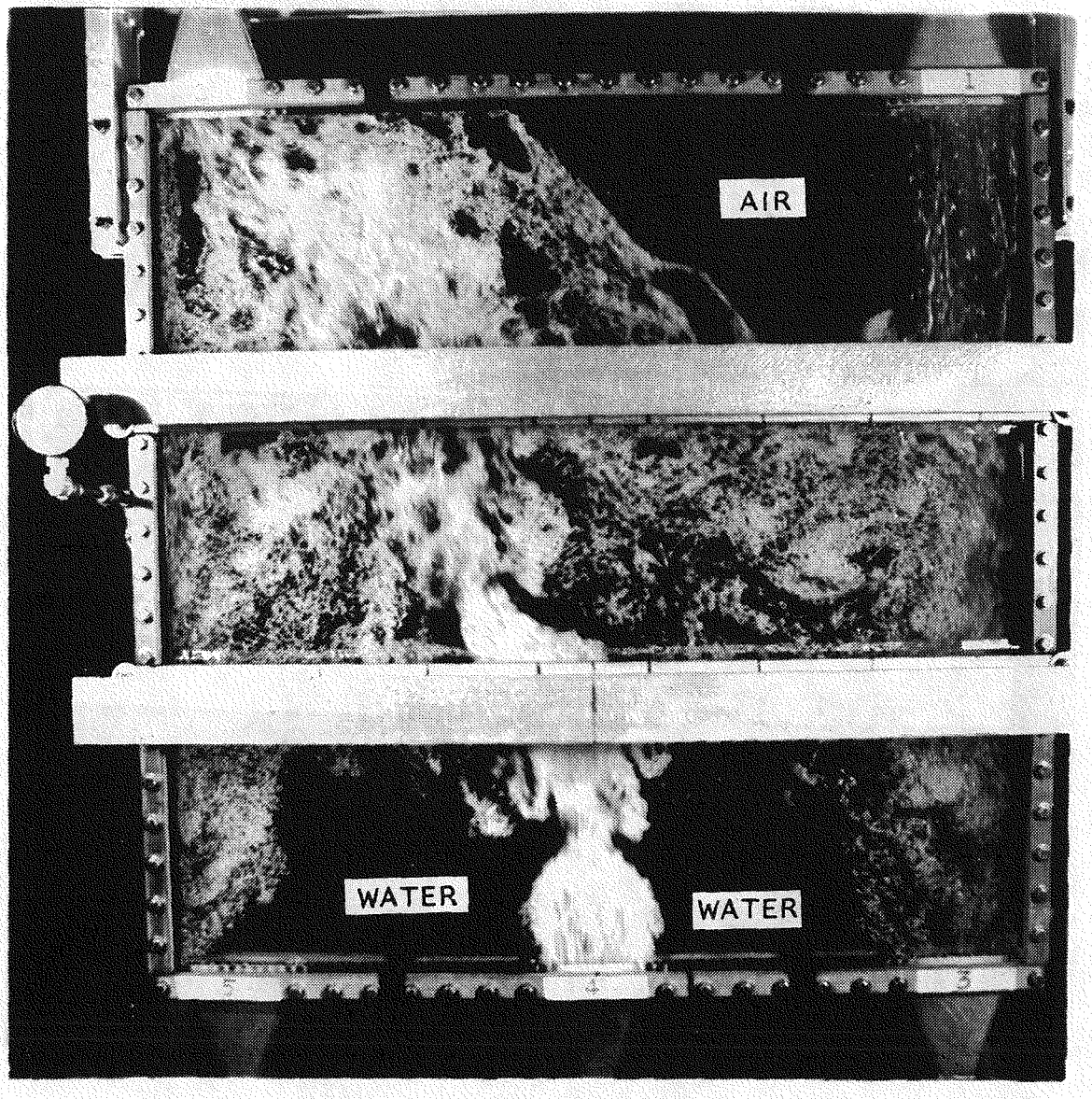


Figure 5.71 Picture of case 4AN4 (liquid mass flux = 1.125 X $10^6$ kg/hr-$m^2$; without rods; 50.0/50.0 flow split; and quality at inlet no. 4 = 0.3%)

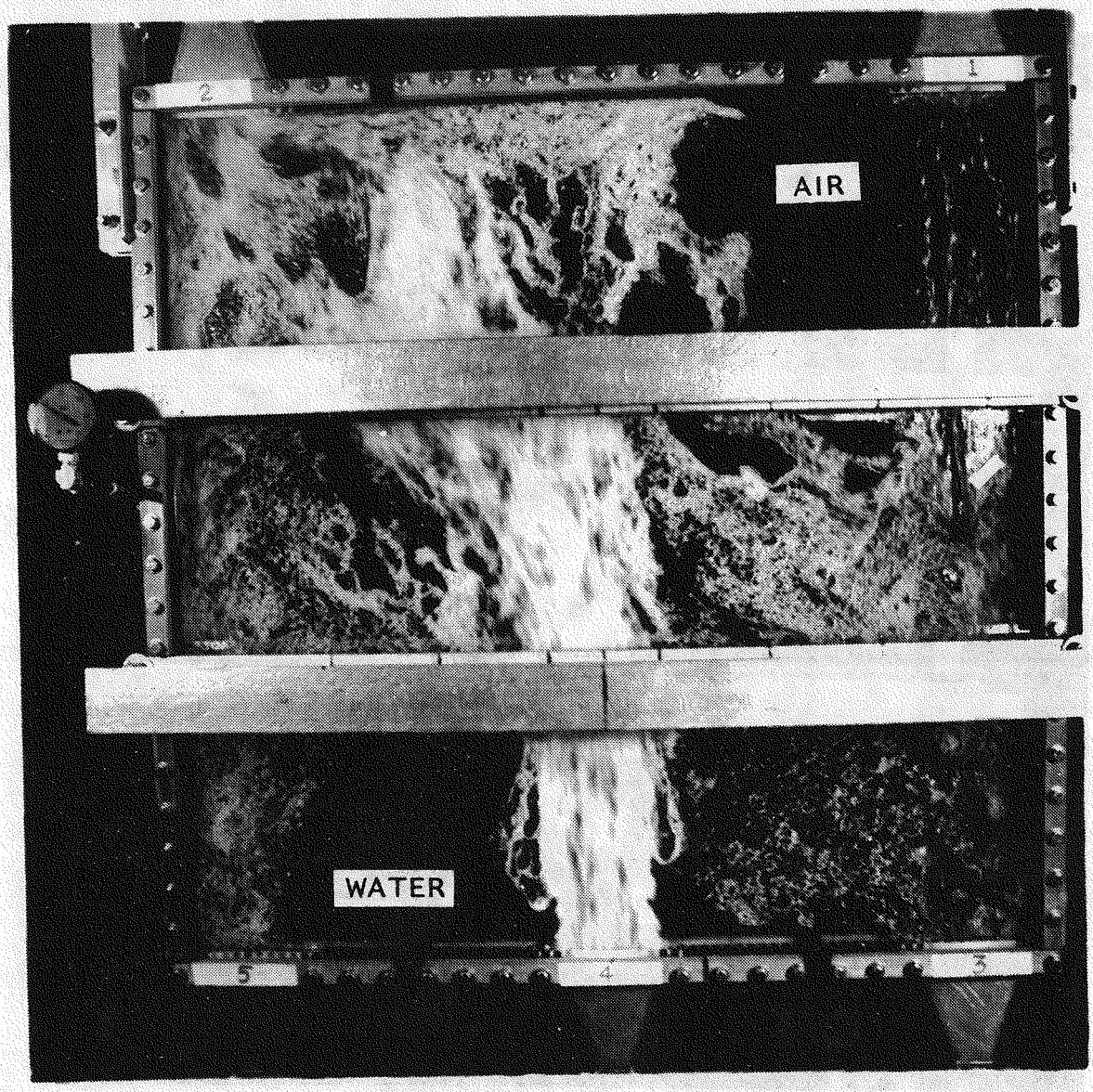


Figure 5.72 Picture of case 5AN4 (liquid mass flux = 1.125 X $10^6$ kg/hr-$m^2$; without rods; 50.0/50.0 flow split; and quality at inlet no. 4 = 0.6%)

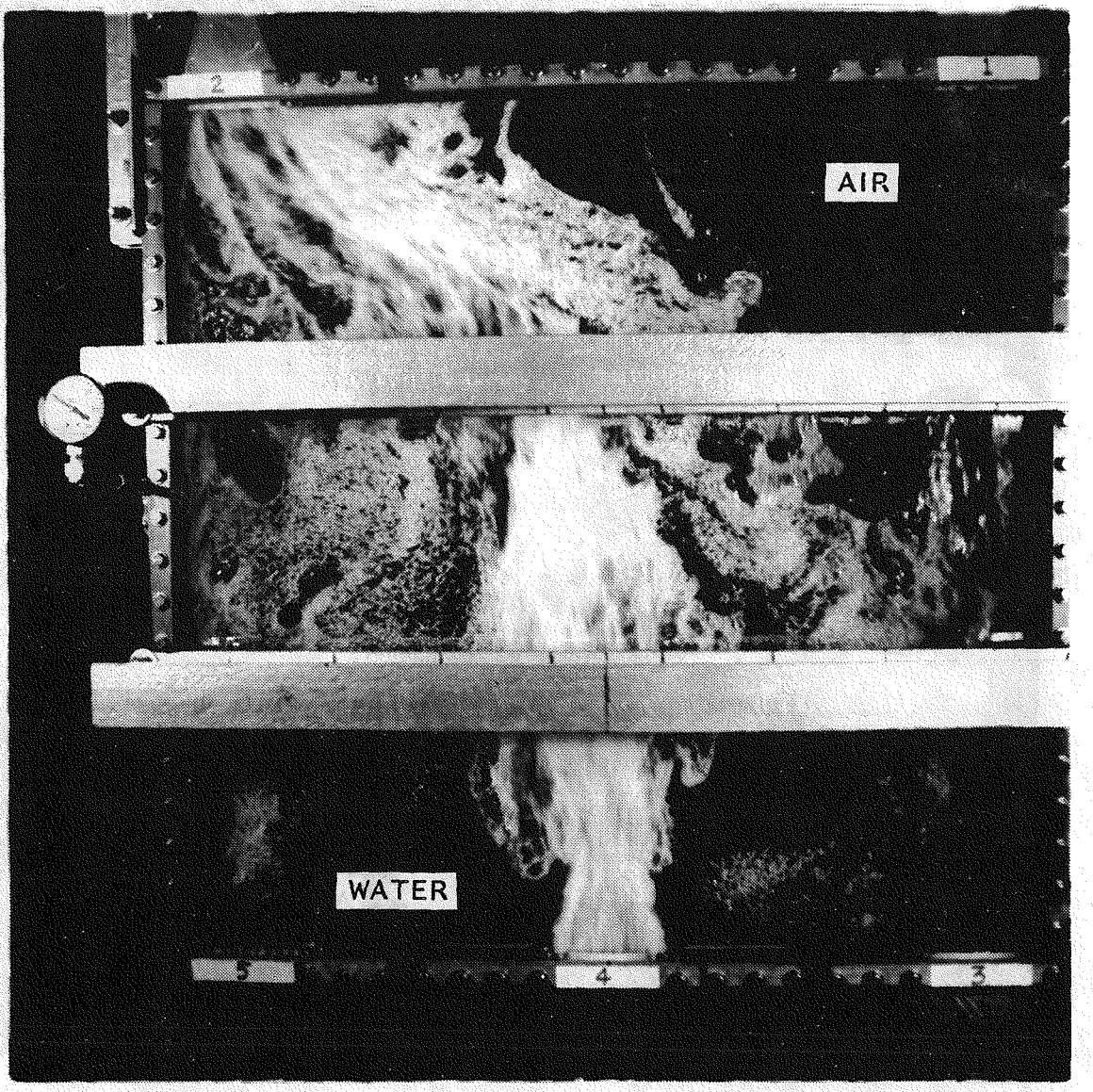


Figure 5.73 Picture of case 6AN4 (liquid mass flux = 1.125 X $10^6$ kg/hr-$m^2$; without rods; 50.0/50.0 flow split; and quality at inlet no. 4 = 0.9%)

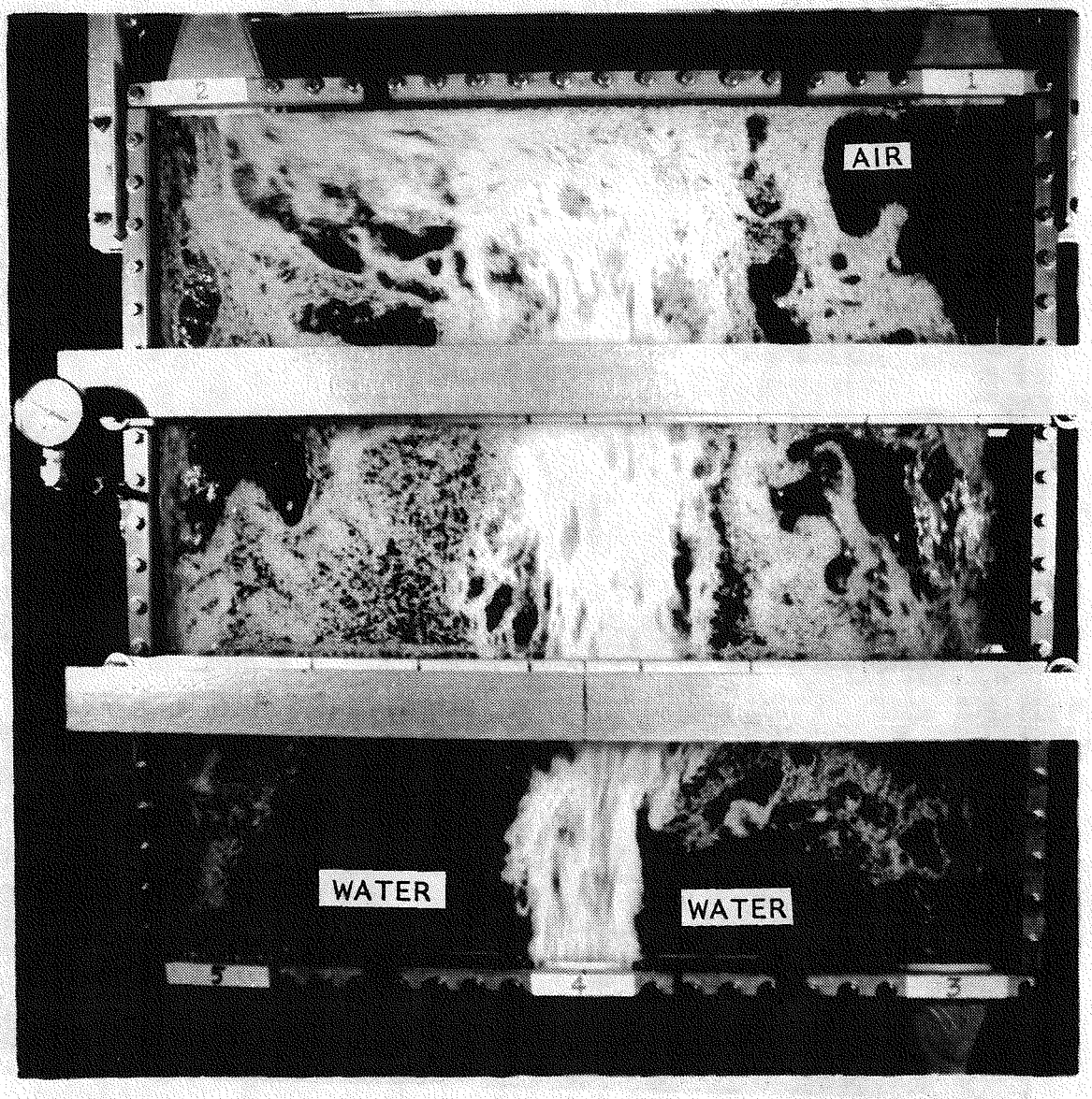


Figure 5.74 Picture of case 4BN4 (liquid mass flux = 1.125 X $10^6$ kg/hr-$m^2$; without rods; 62.5/37.5 flow split; and quality at inlet no. 4 = 0.3%)

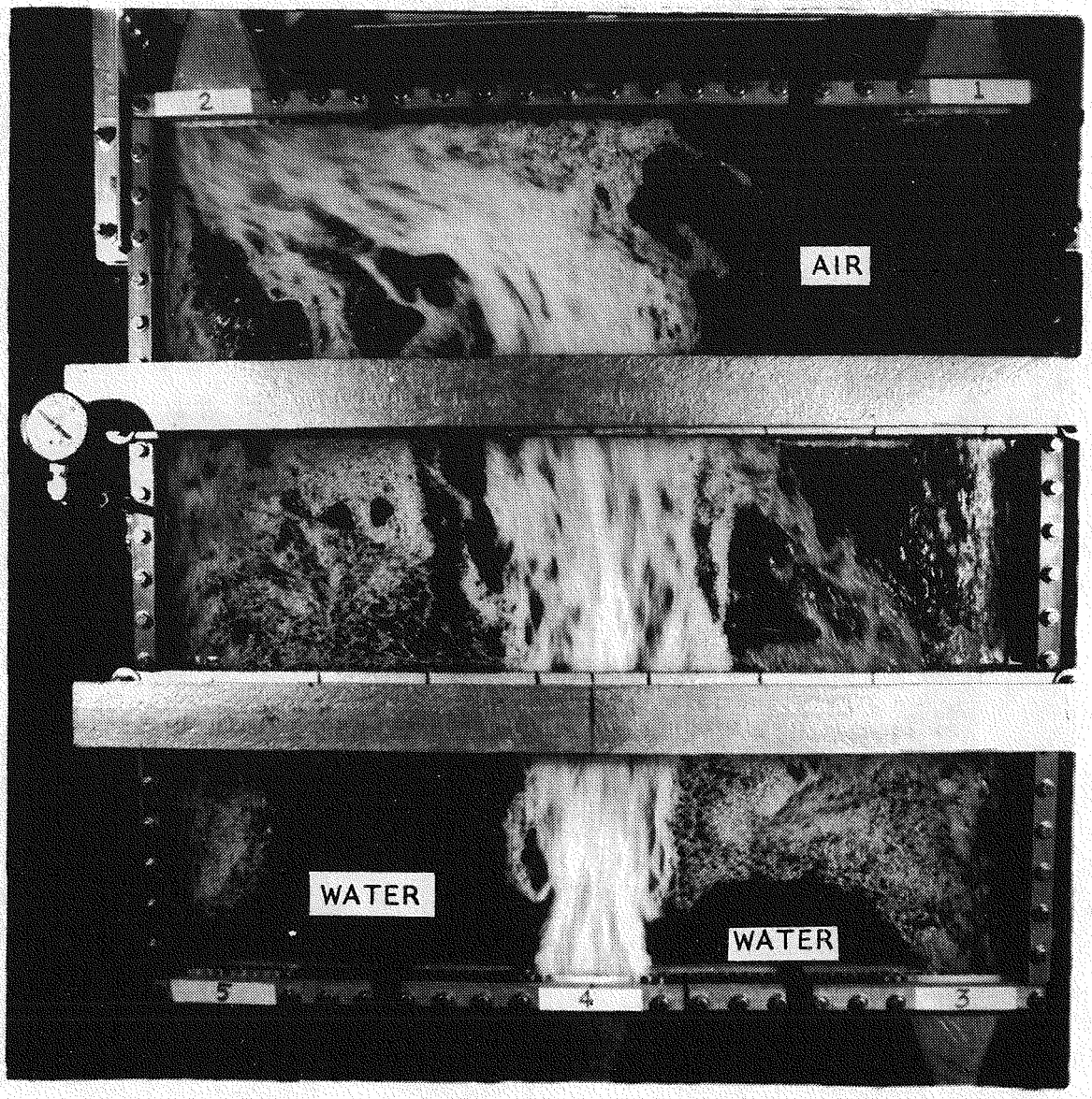


Figure 5.75 Picture of case 5BN4 (liquid mass flux = 1.125 X $10^6$ kg/hr-$m^2$; without rods; 62.5/37.5 flow split; and quality at inlet no. 4 = 0.6%)

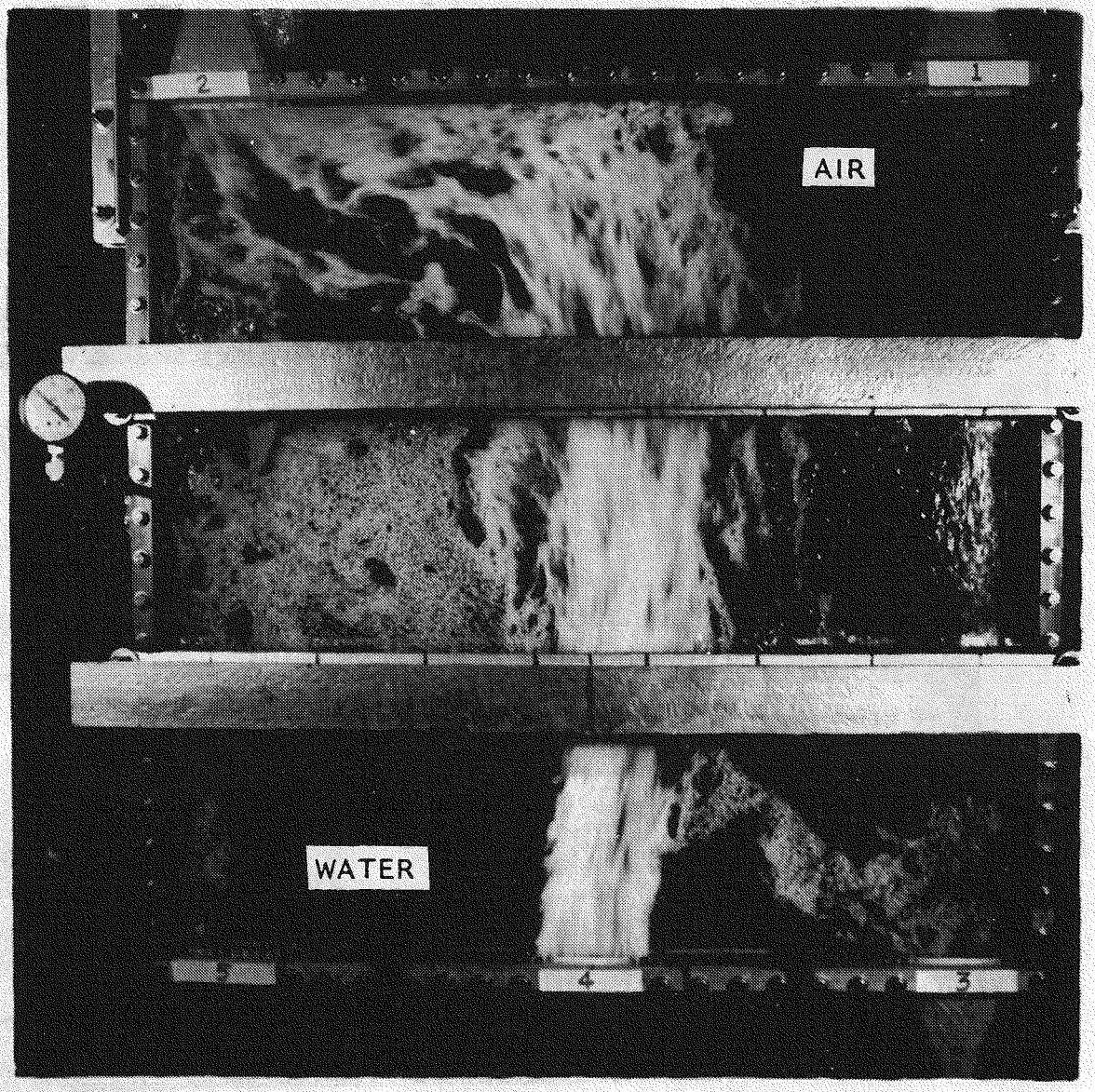


Figure 5.76 Picture of case 6BN4 (liquid mass flux = 1.125 X $10^6$ kg/hr-$m^2$; without rods; 62.5/37.5 flow split; and quality at inlet no. 4 = 0.9%)

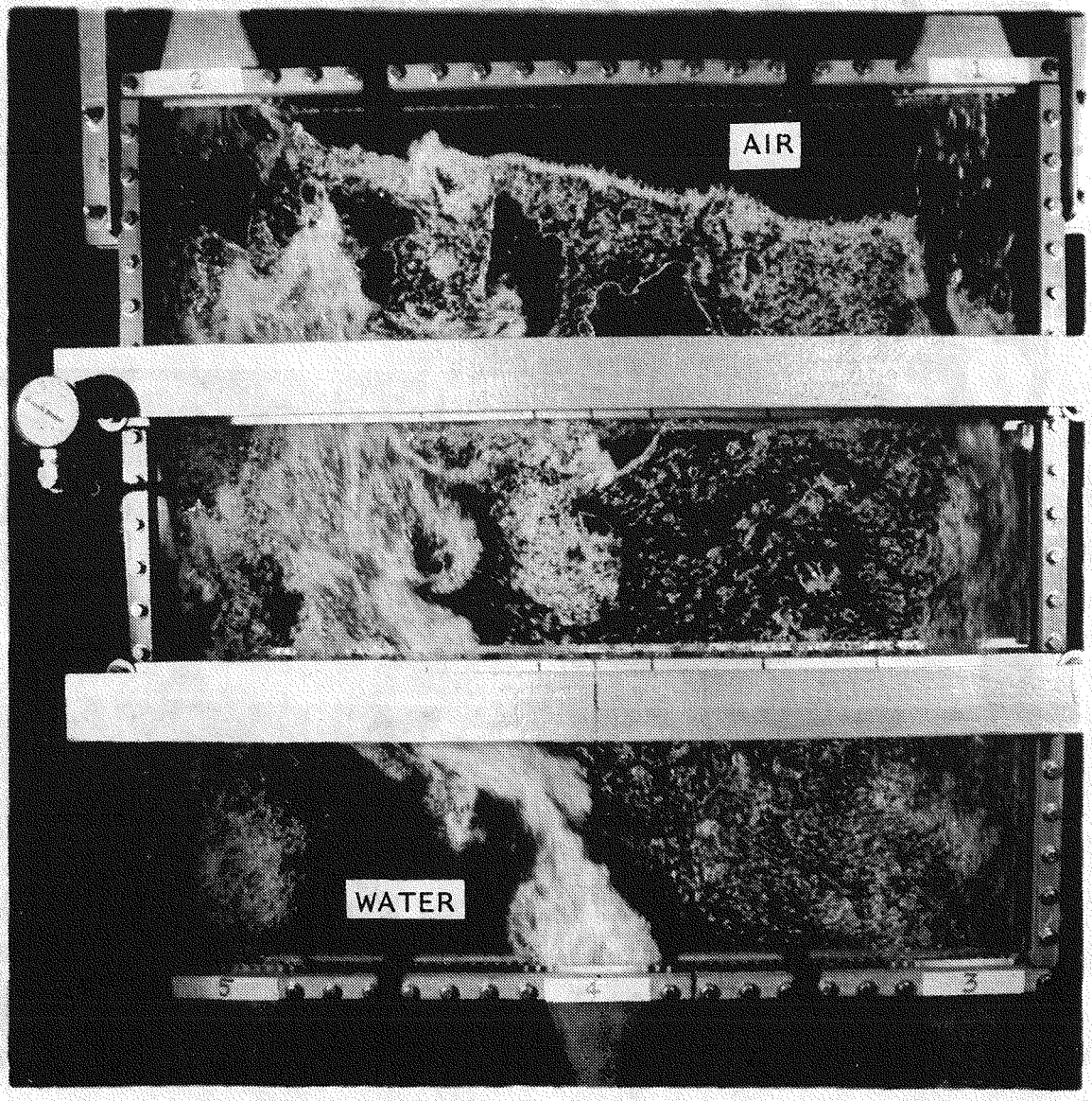


Figure 5.77 Picture of case 4CN4 (liquid mass flux = 1.125 X $10^6$ kg/hr-$m^2$; without rods; 37.5/62.5 flow split; and quality at inlet no. 4 = 0.3%)

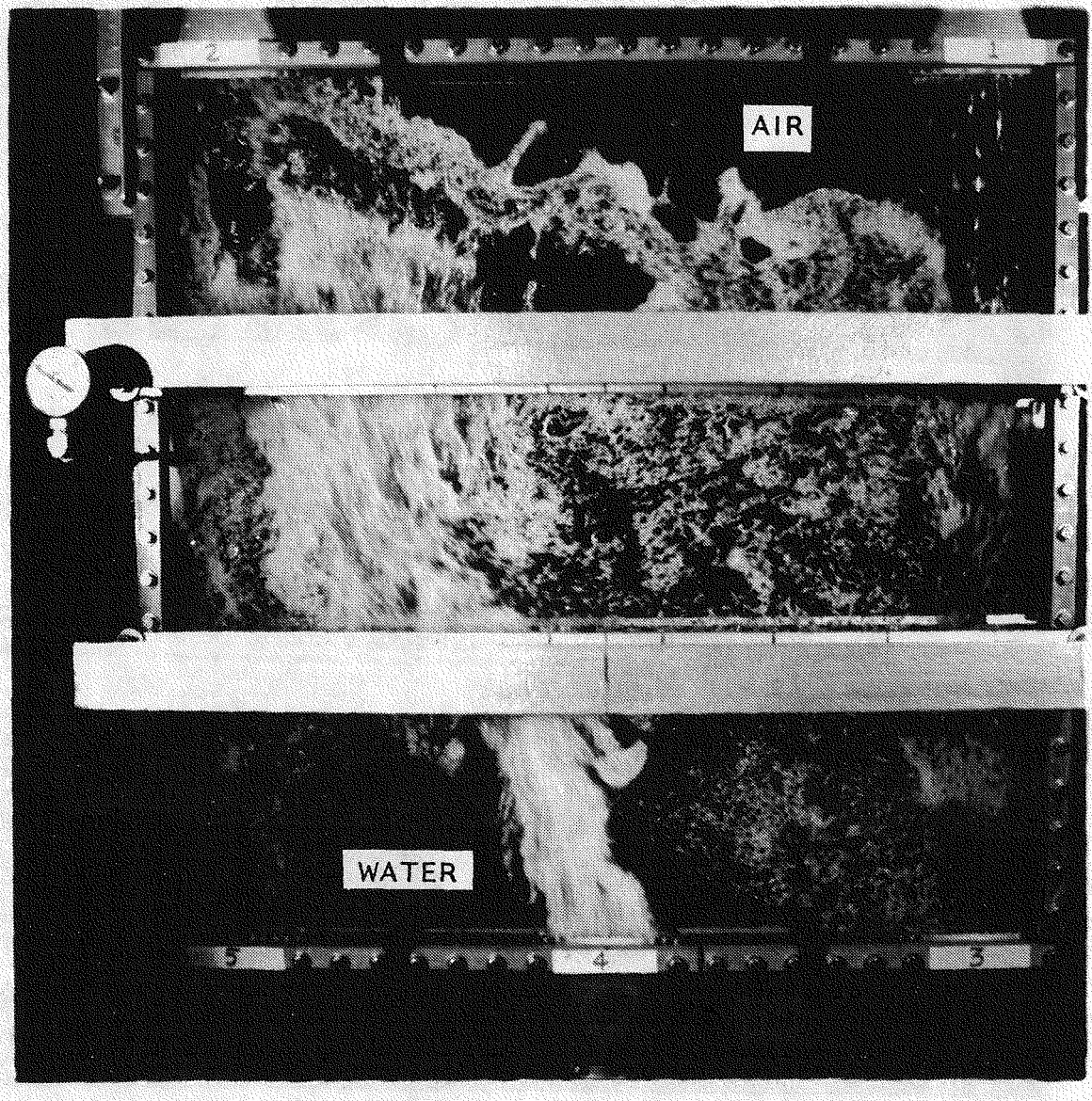


Figure 5.78 Picture of case 5CN4 (liquid mass flux = 1.125 X $10^6$ kg/hr-$m^2$; without rods; 37.5/62.5 flow split; and quality at inlet no. 4 = 0.6%)

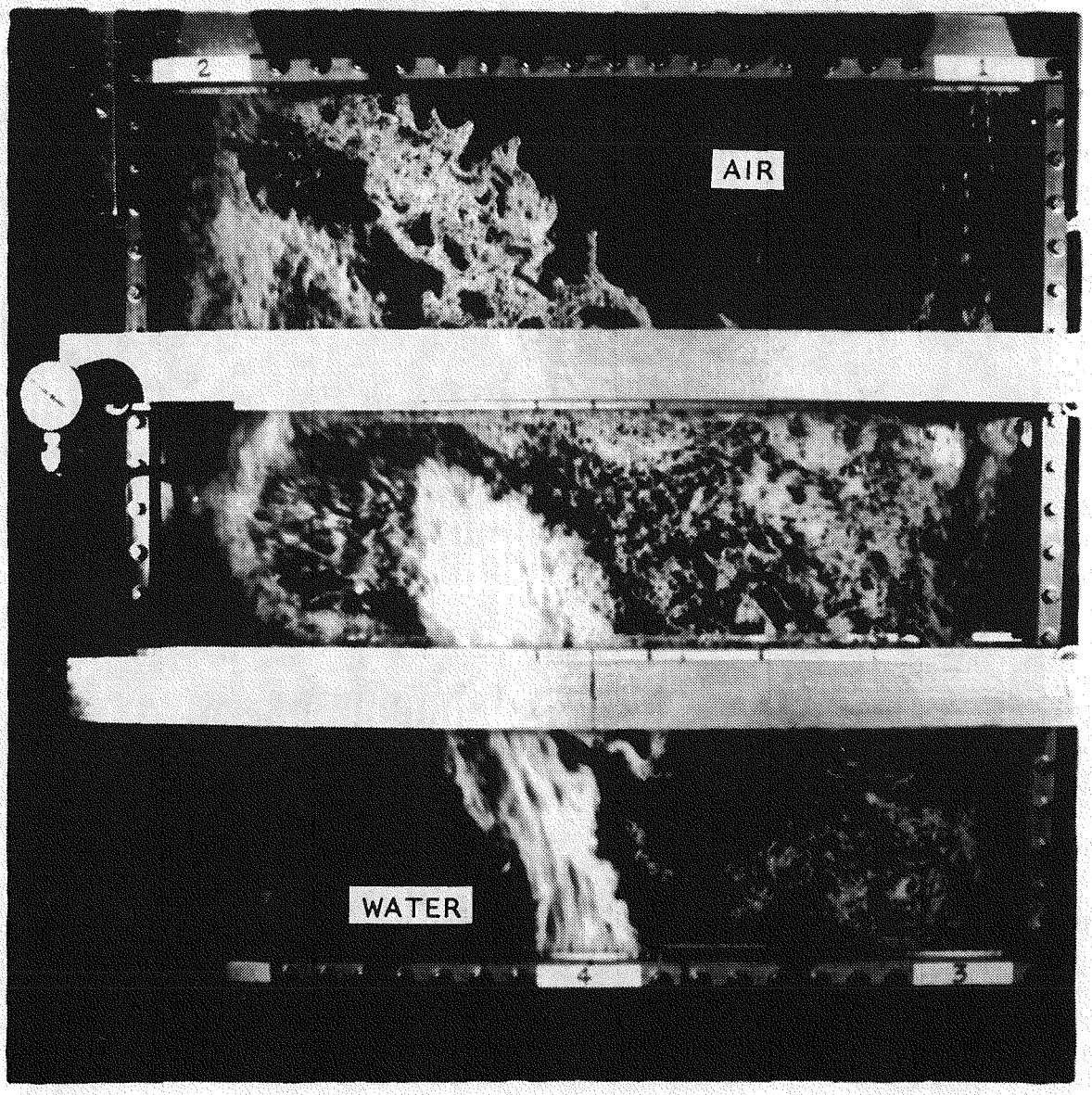


Figure 5.79 Picture of case 6CN4 (liquid mass flux = 1.125 X $10^6$ kg/hr-$m^2$; without rods; 37.5/62.5 flow split; and quality at inlet no. 4 = 0.9%)

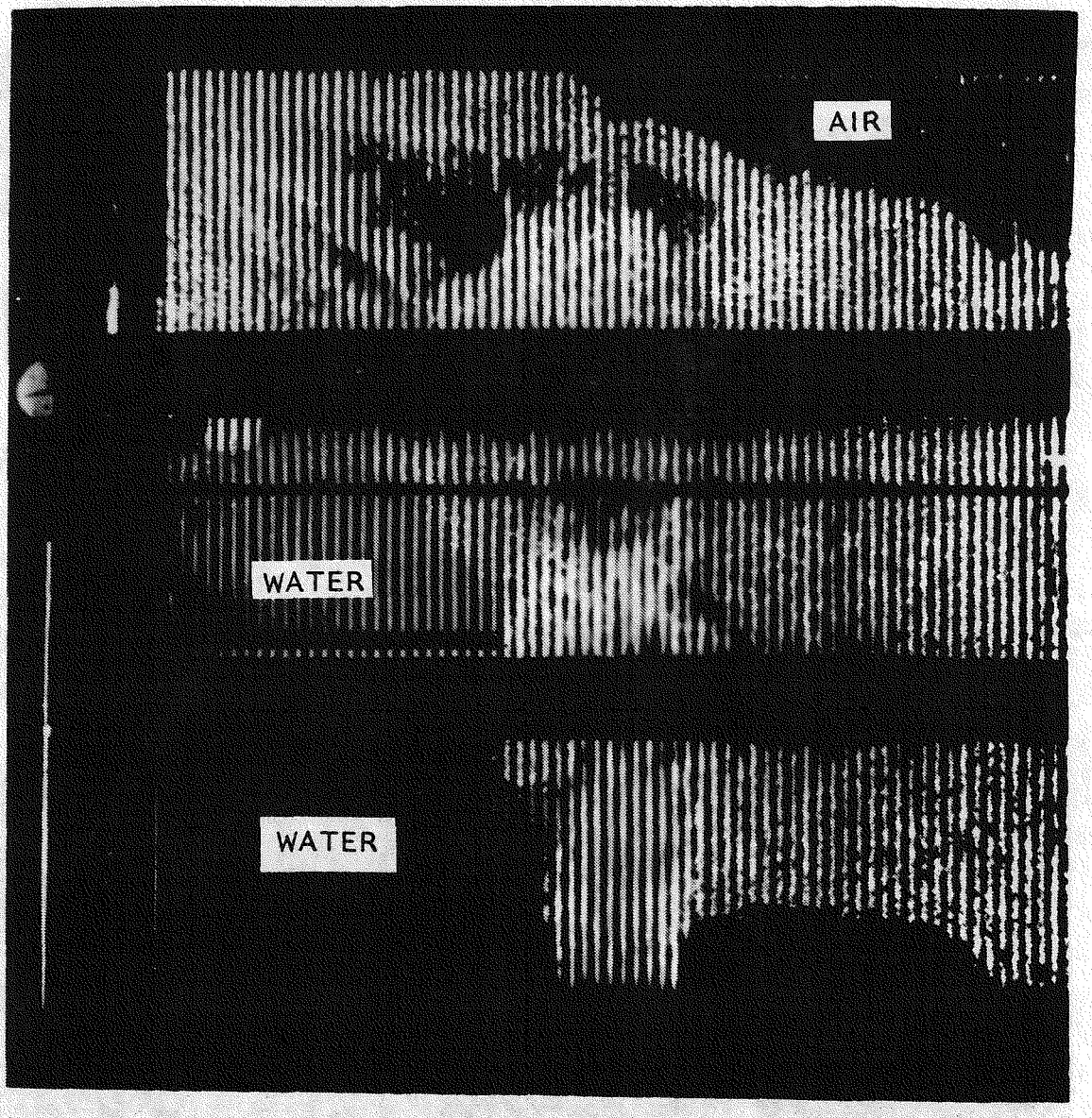


Figure 5.80 Picture of case 1AR4 (liquid mass flux = 0.697 X $10^6$ kg/hr-$m^2$; with rods; 50.0/50.0 flow split; and quality at inlet no. 4 = 0.3%)

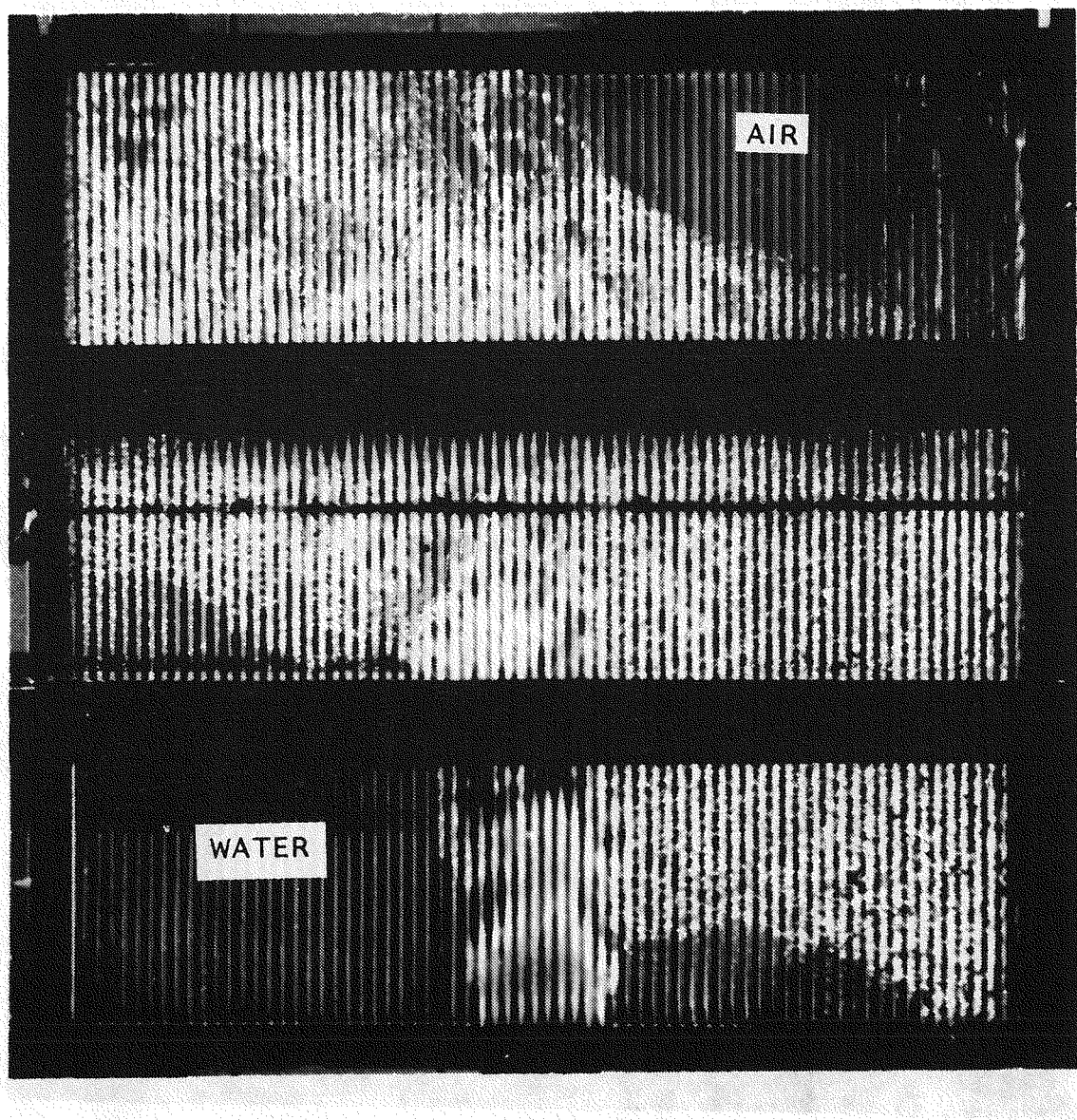


Figure 5.81 Picture of case 2AR4 (liquid mass flux = 0.697 X $10^6$ kg/hr-$m^2$; with rods; 50.0/50.0 flow split; and quality at inlet no. 4 = 0.6%)

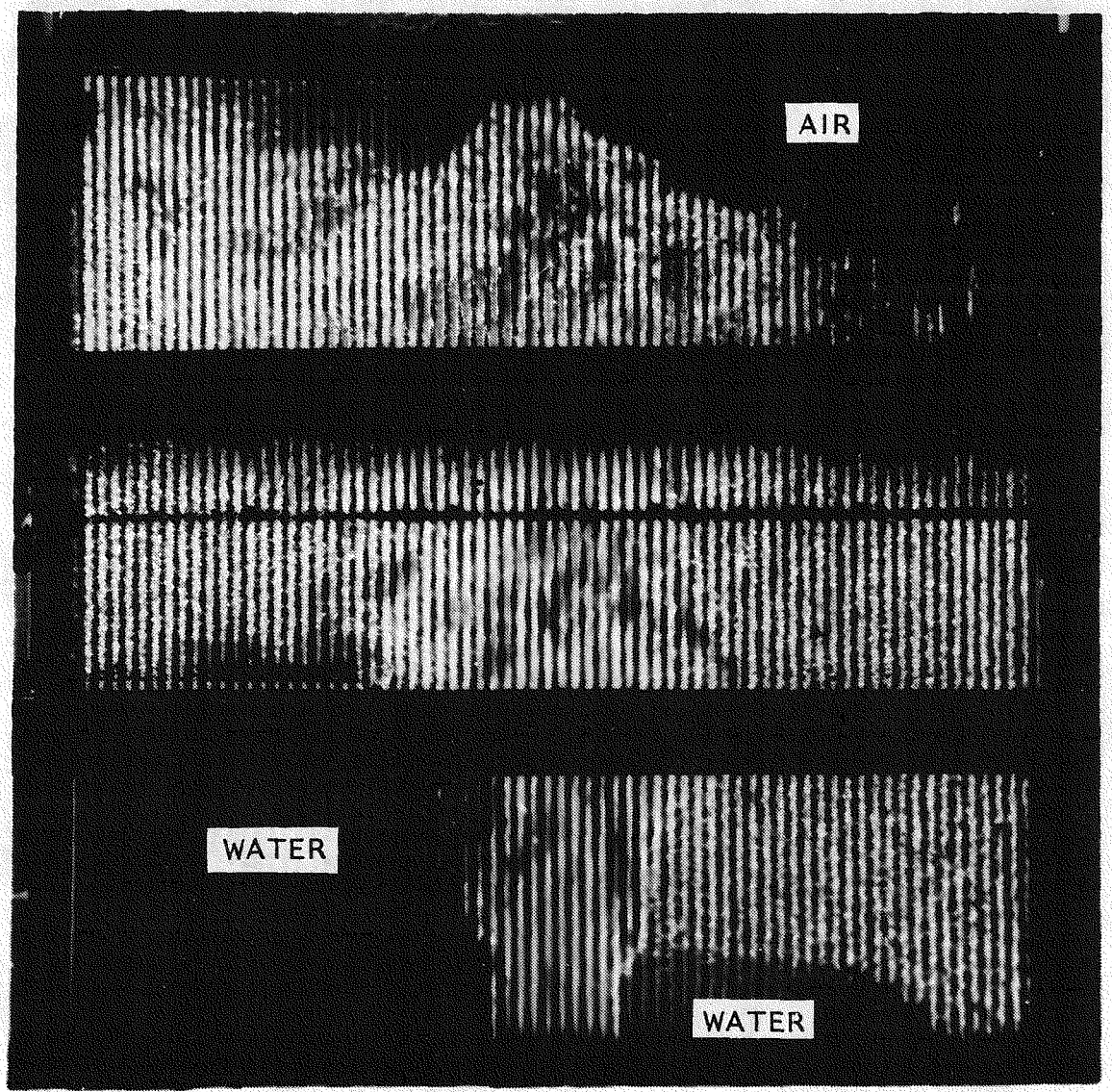


Figure 5.82 Picture of case 3AR4 (liquid mass flux = 0.697 X $10^6$ kg/hr-$m^2$; with rods; 50.0/50.0 flow split; and quality at inlet no. 4 = 0.9%)

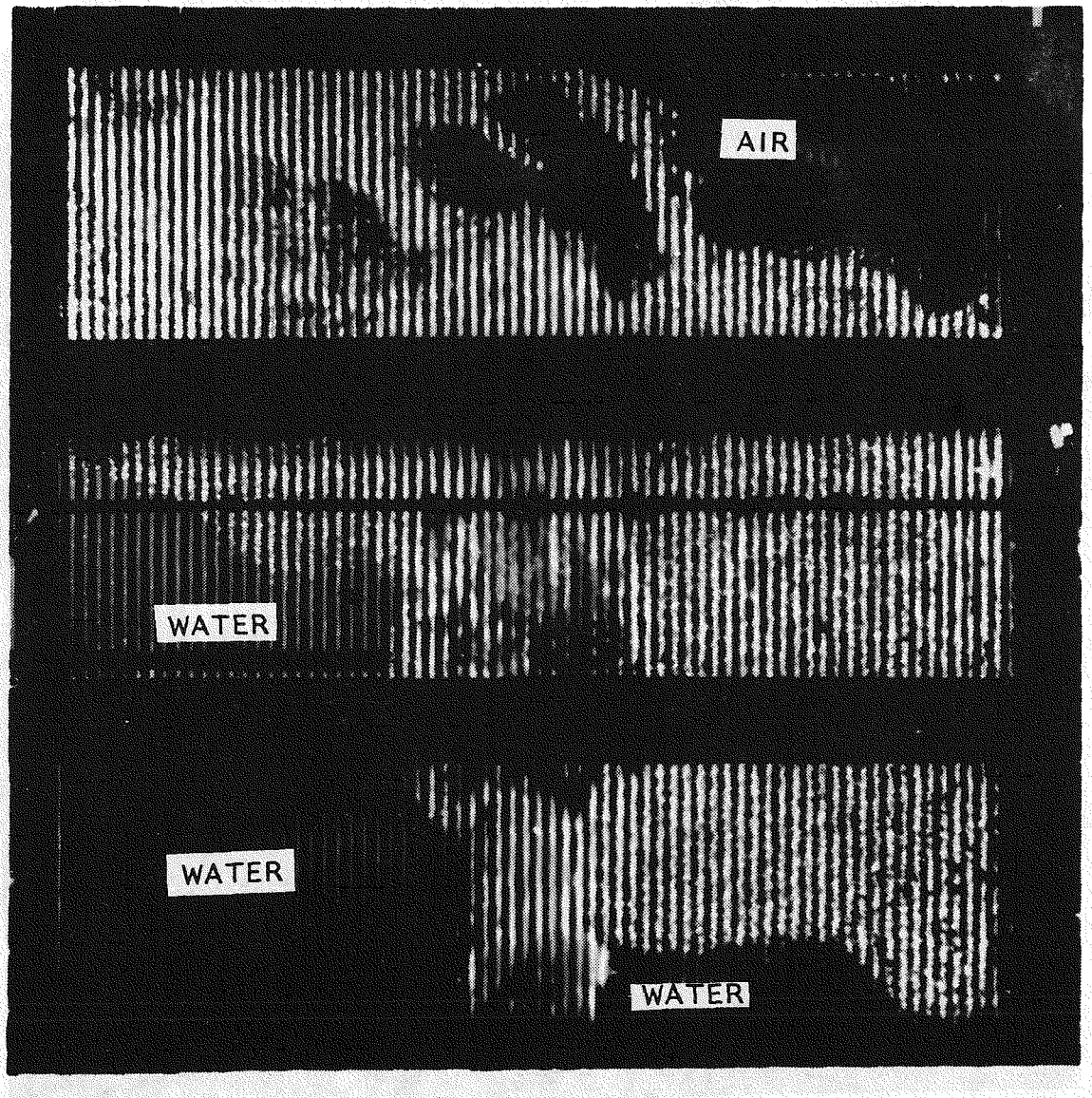


Figure 5.83 Picture of case 1BR4 (liquid mass flux = 0.697 X $10^6$ kg/hr-$m^2$; with rods; 62.5/37.5 flow split; and quality at inlet no. 4 = 0.3%)

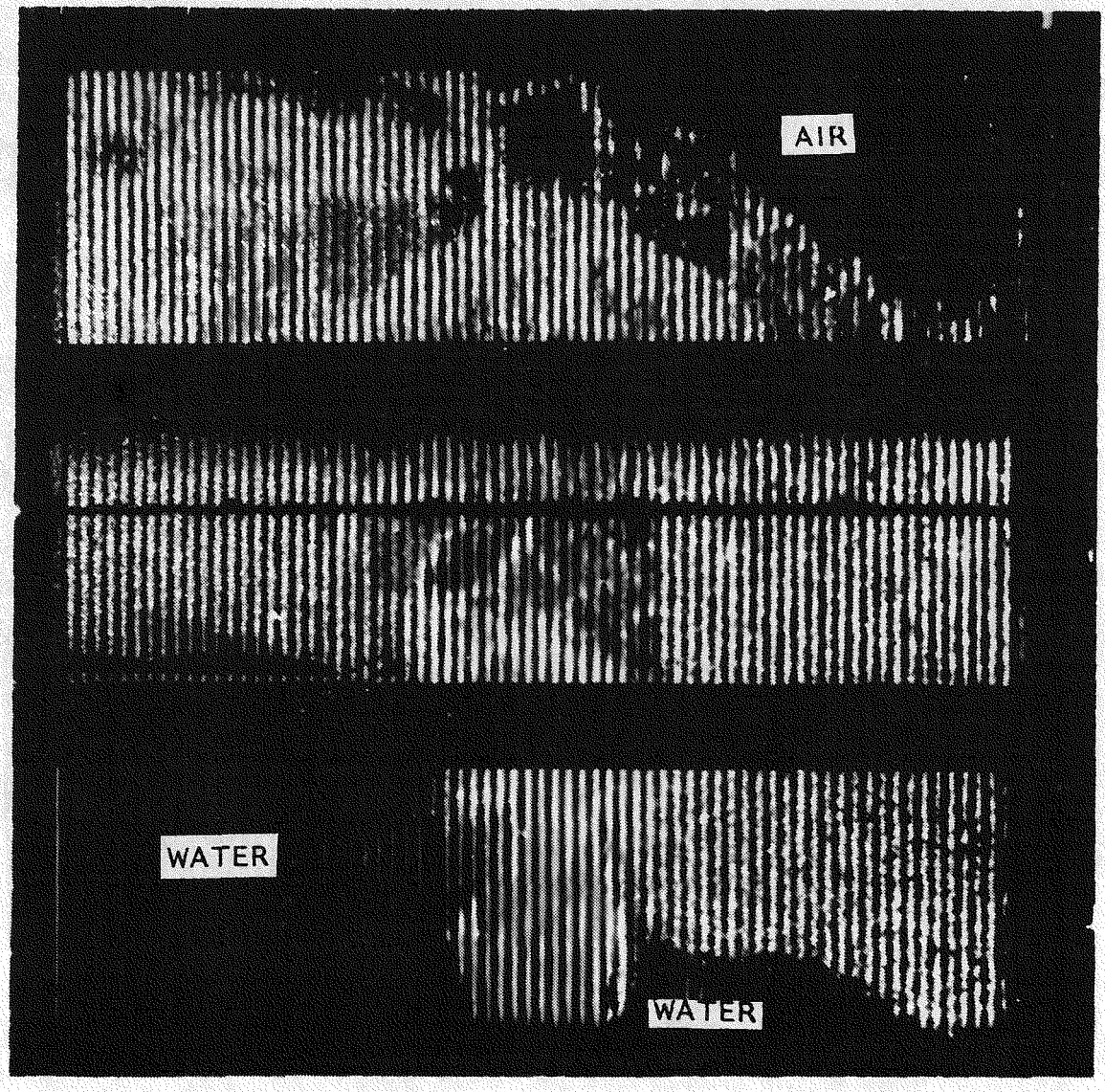


Figure 5.84 Picture of case 2BR4 (liquid mass flux = 0.697 X $10^6$ kg/hr-$m^2$; with rods; 62.5/37.5 flow split; and quality at inlet no. 4 = 0.6%)

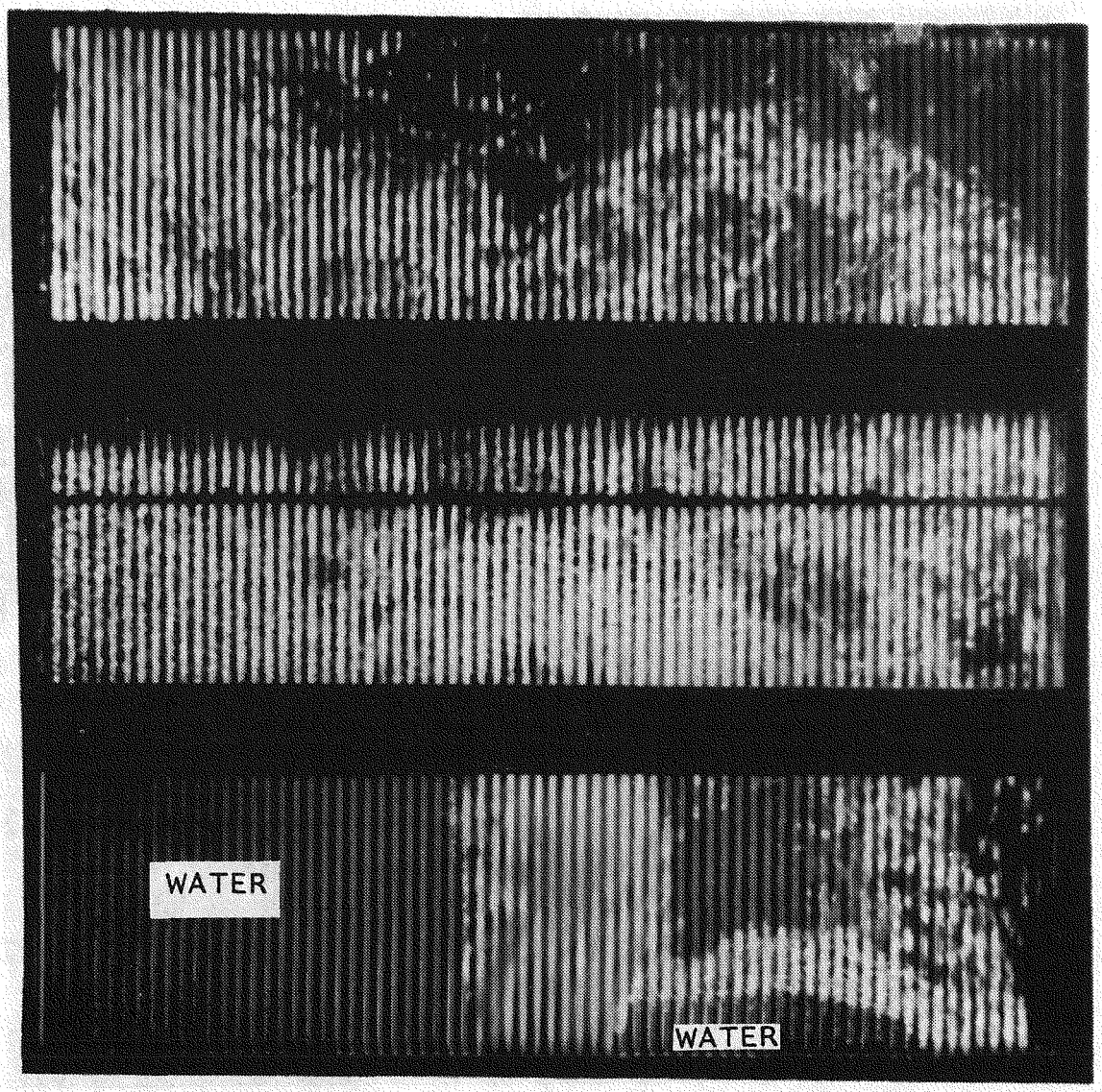


Figure 5.85 Picture of case 3BR4 (liquid mass flux = 0.697 X $10^6$ kg/hr-$m^2$; with rods; 62.5/37.5 flow split; and quality at inlet no. 4 = 0.9%)

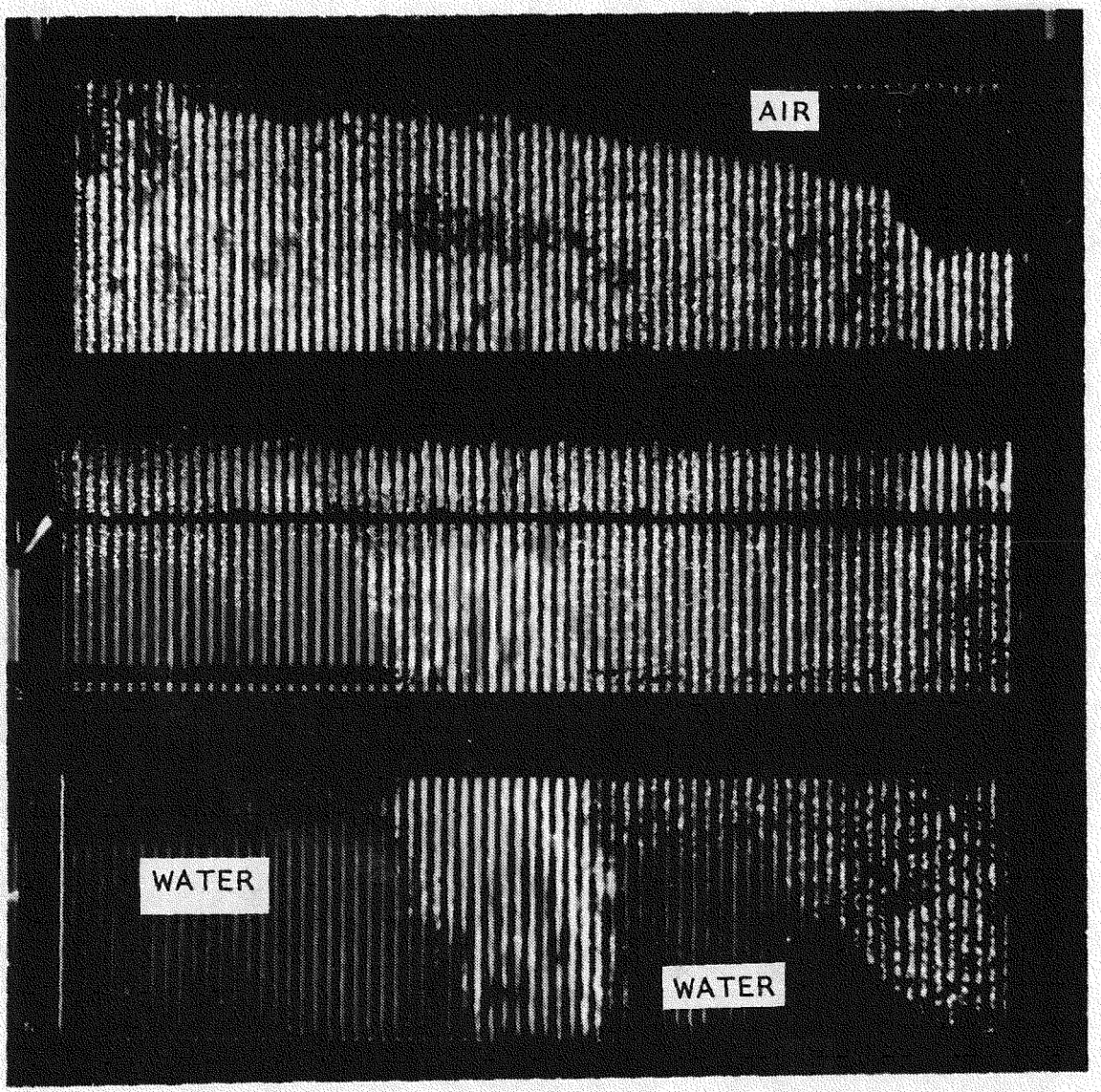


Figure 5.86 Picture of case 1CR4 (liquid mass flux = 0.697 X $10^6$ kg/hr-$m^2$; with rods; 37.5/62.5 flow split; and quality at inlet no. 4 = 0.3%)

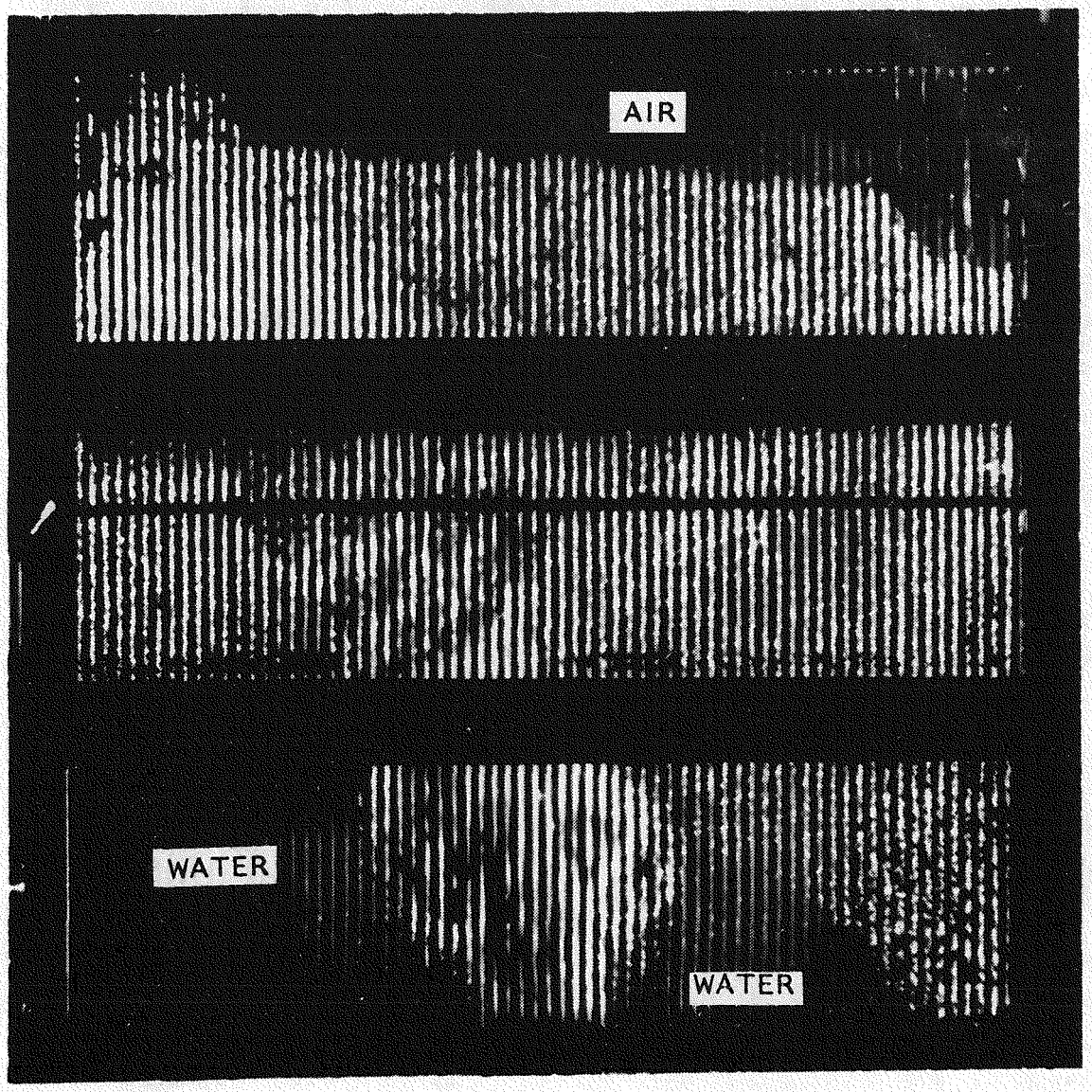


Figure 5.87 Picture of case 2CR4 (liquid mass flux = 0.697 X $10^6$ kg/hr-$m^2$; with rods; 37.5/62.5 flow split; and quality at inlet no. 4 = 0.6%)

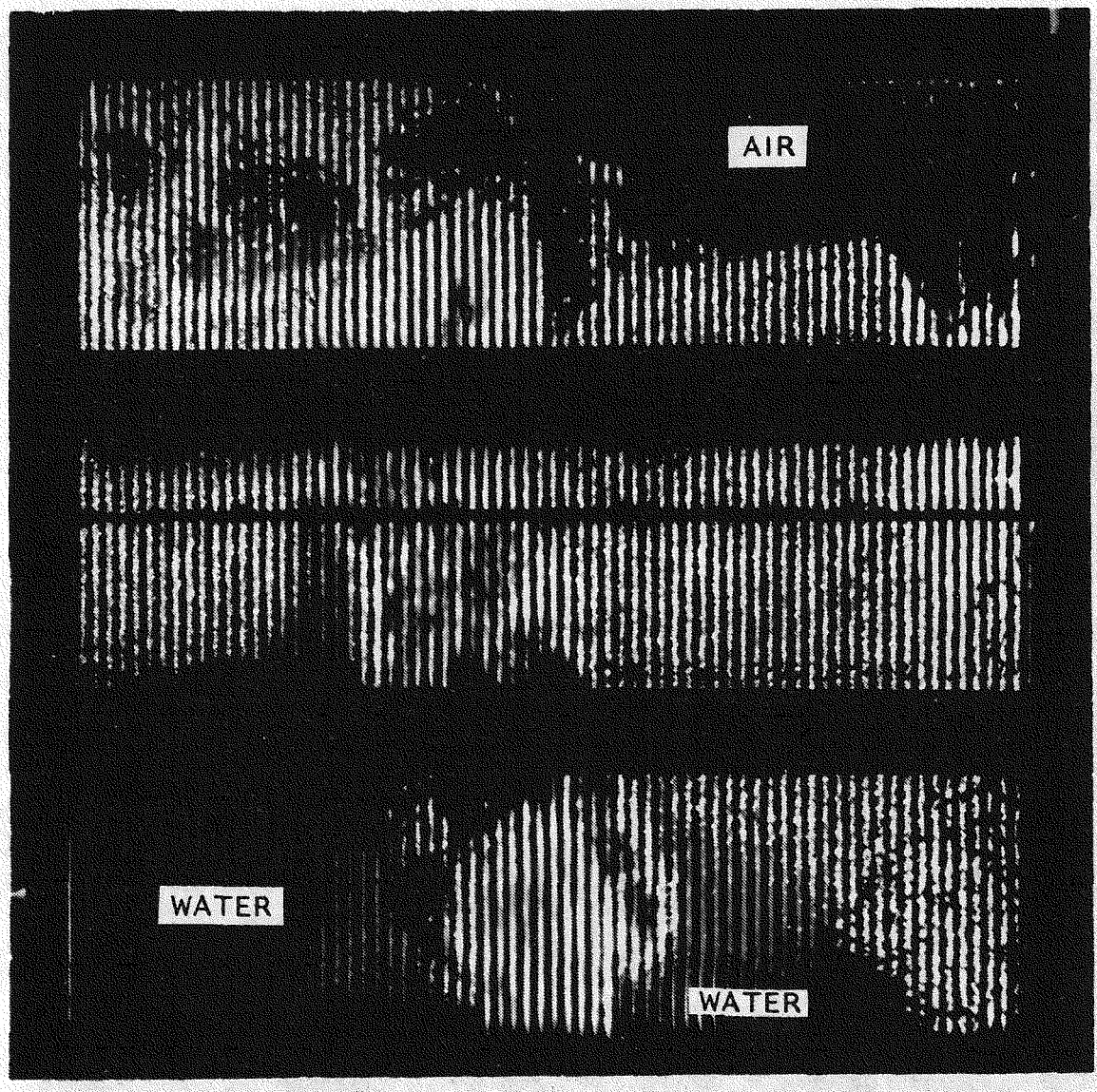


Figure 5.88 Picture of case 3CR4 (liquid mass flux = 0.697 X $10^6$ kg/hr-$m^2$; with rods; 37.5/62.5 flow split; and quality at inlet no. 4 = 0.9%)

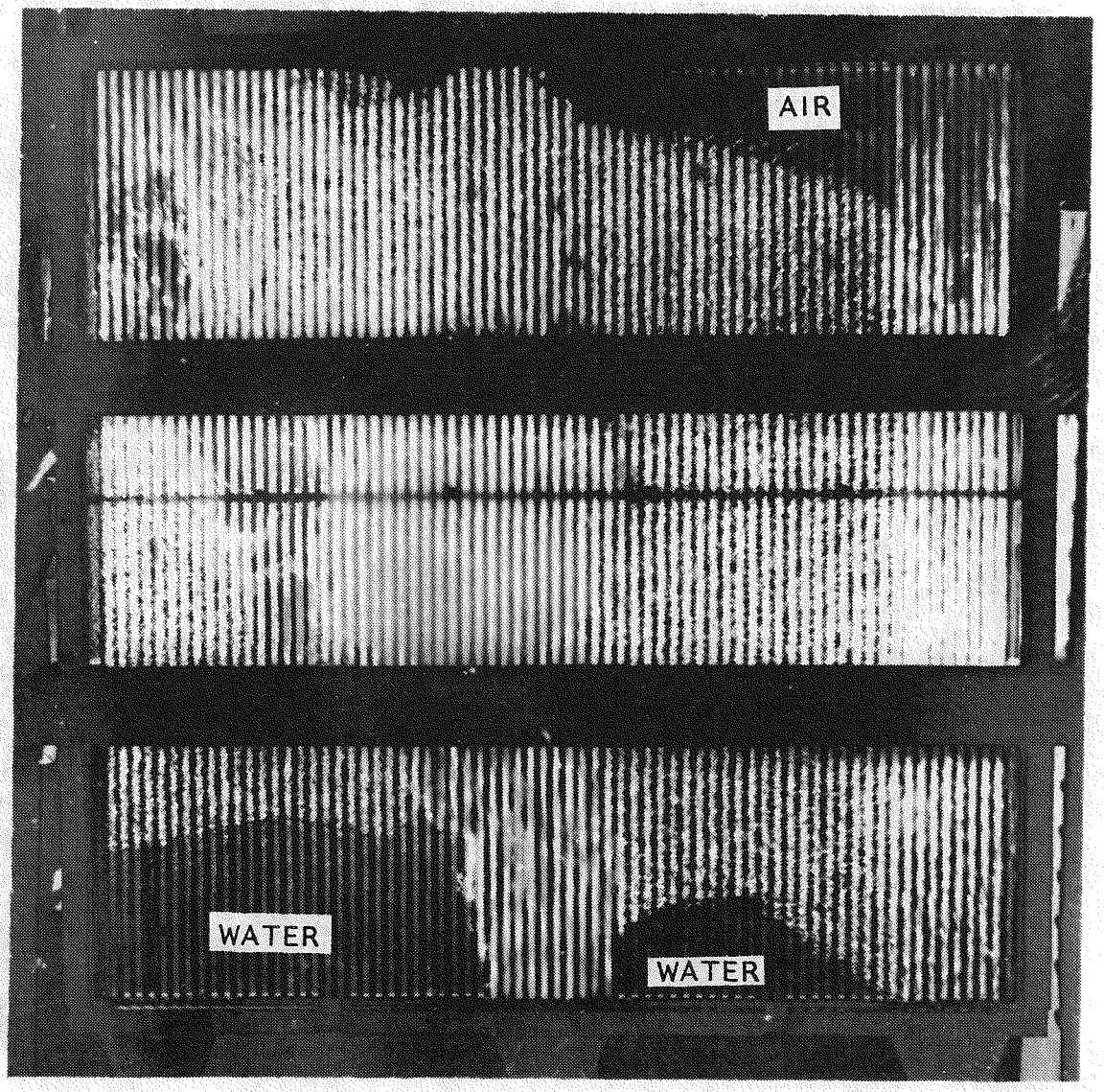


Figure 5.89 Picture of case 4AR4 (liquid mass flux = 1.395 X $10^6$ kg/hr-$m^2$; with rods; 50.0/50.0 flow split; and quality at inlet no. 4 = 0.3%)

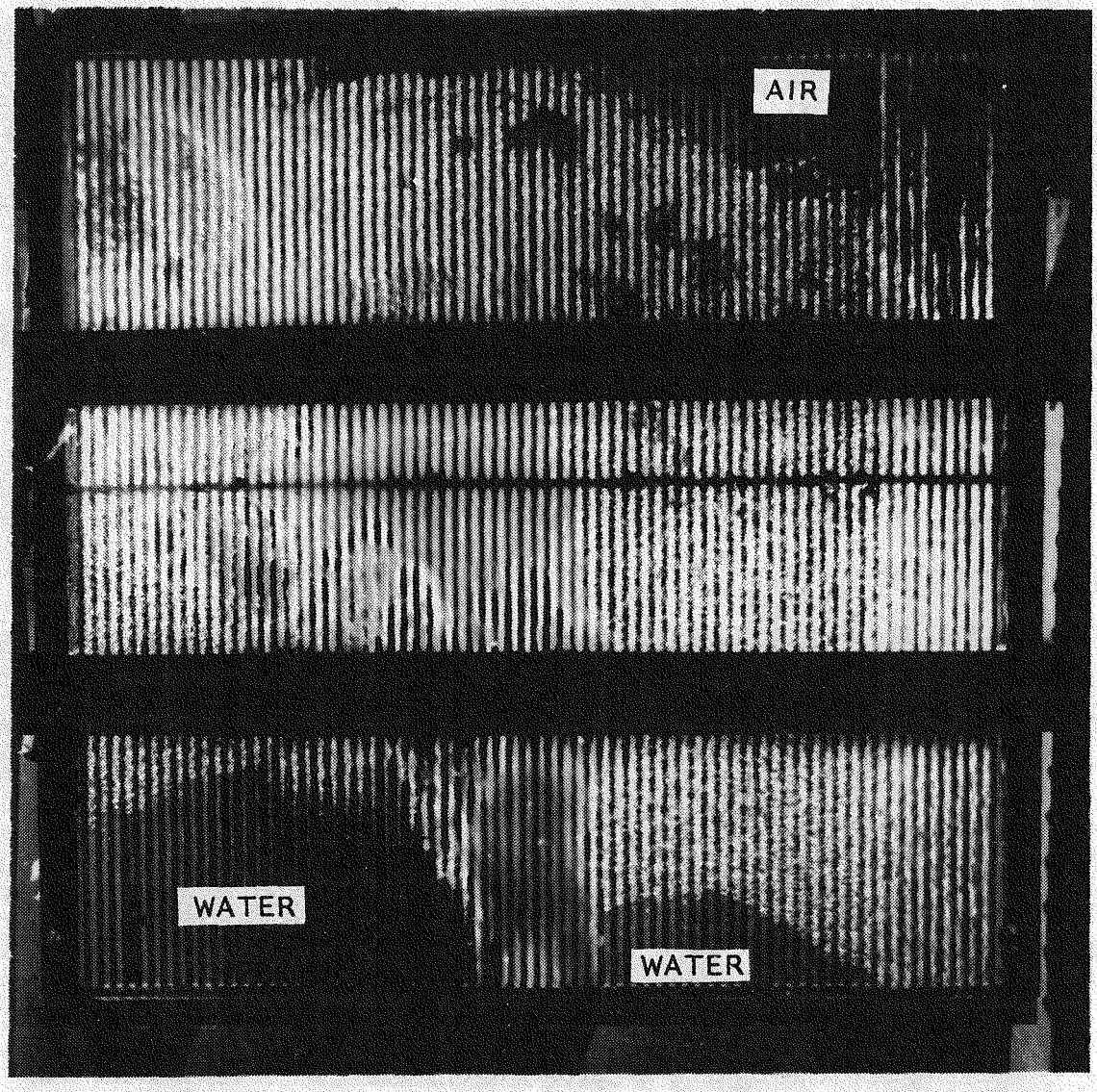


Figure 5.90 Picture of case 5AR4 (liquid mass flux = 1.395 X $10^6$ kg/hr-$m^2$; with rods; 50.0/50.0 flow split; and quality at inlet no. 4 = 0.6%)

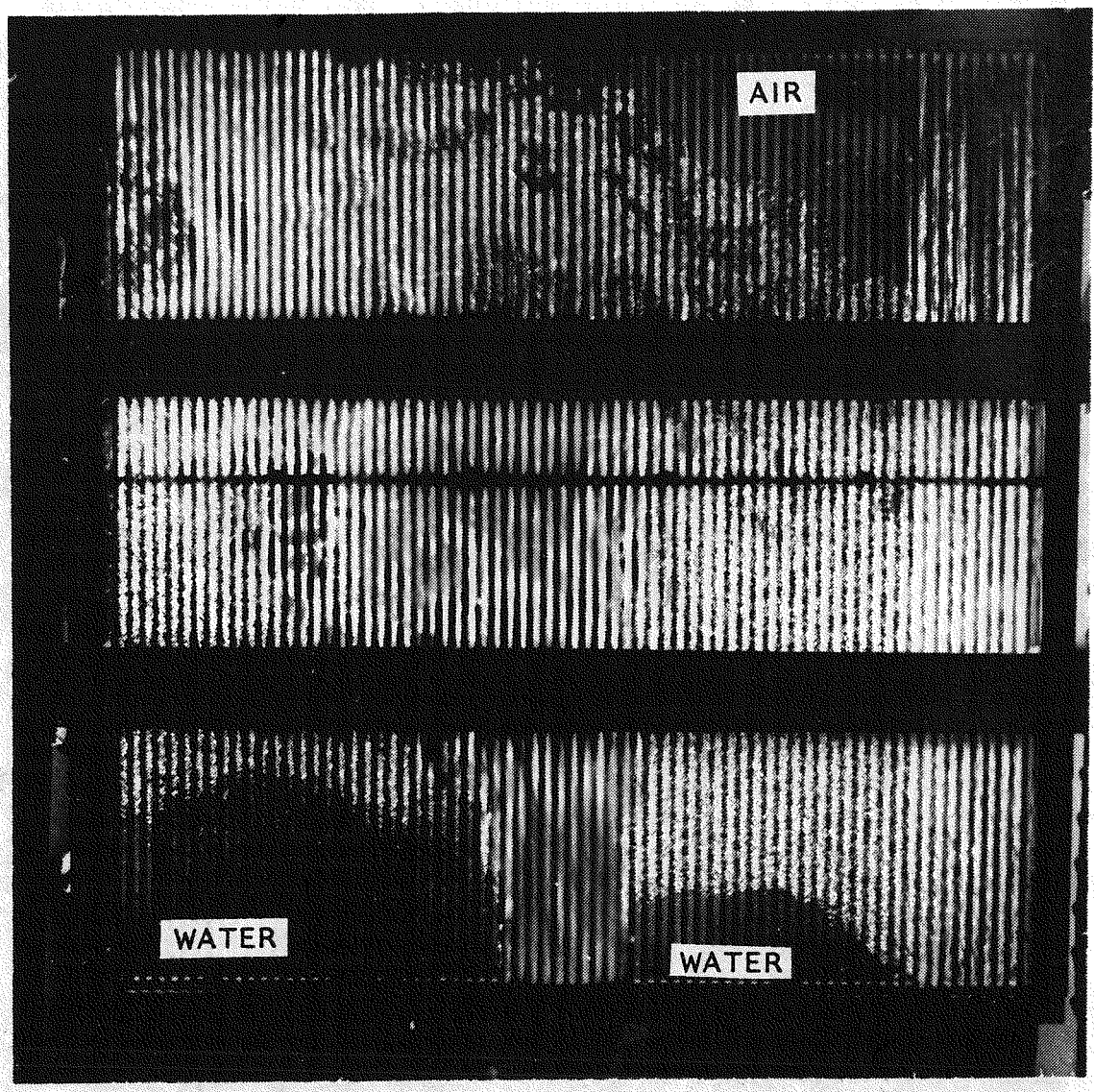


Figure 5.91 Picture of case 6AR4 (liquid mass flux = 1.395 X $10^6$ kg/hr-$m^2$; with rods; 50.0/50.0 flow split; and quality at inlet no. 4 = 0.9%)

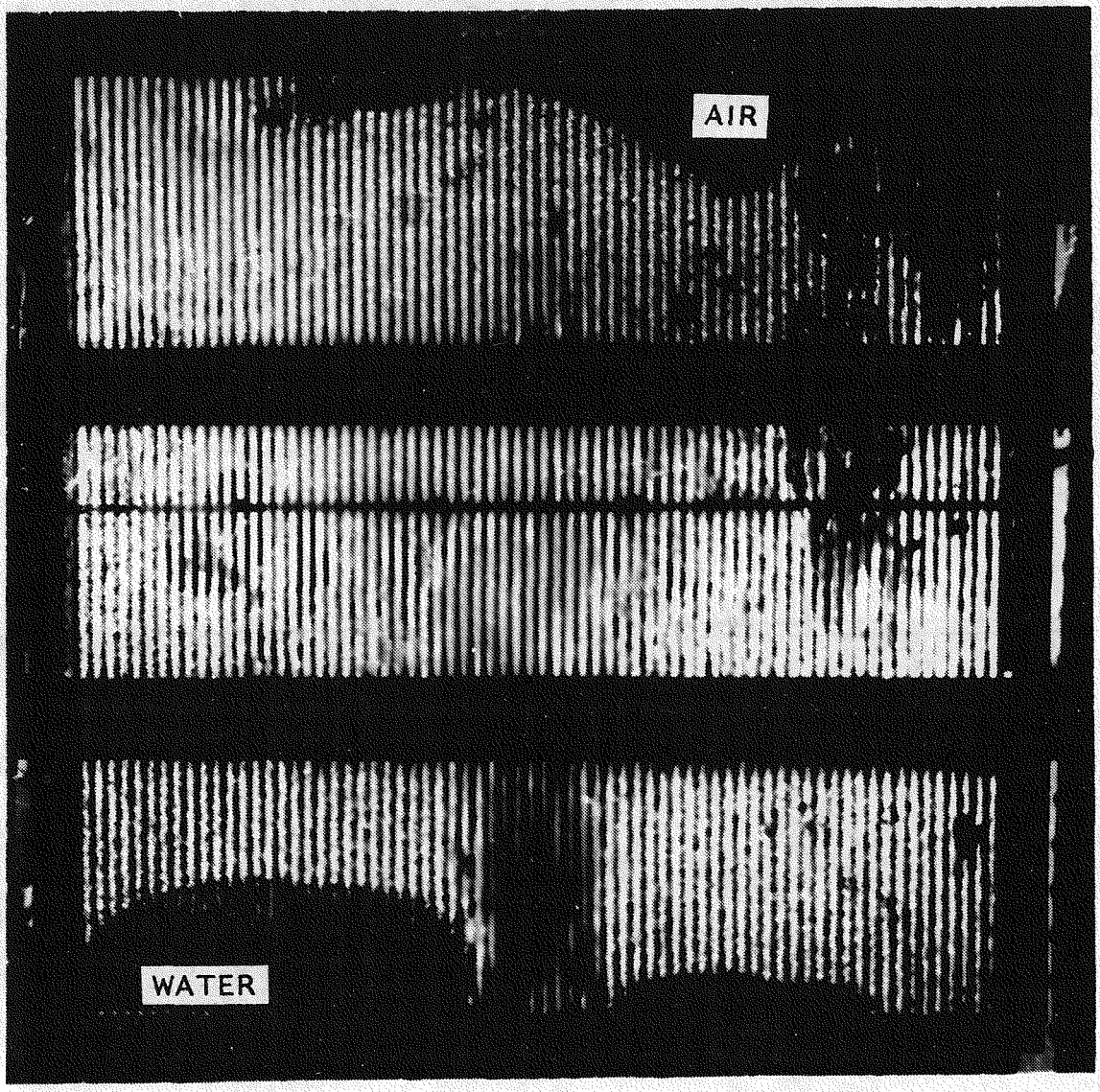


Figure 5.92 Picture of case 4BR4 (liquid mass flux = 1.395 X $10^6$ kg/hr-$m^2$; with rods; 62.5/37.5 flow split; and quality at inlet no. 4 = 0.3%)

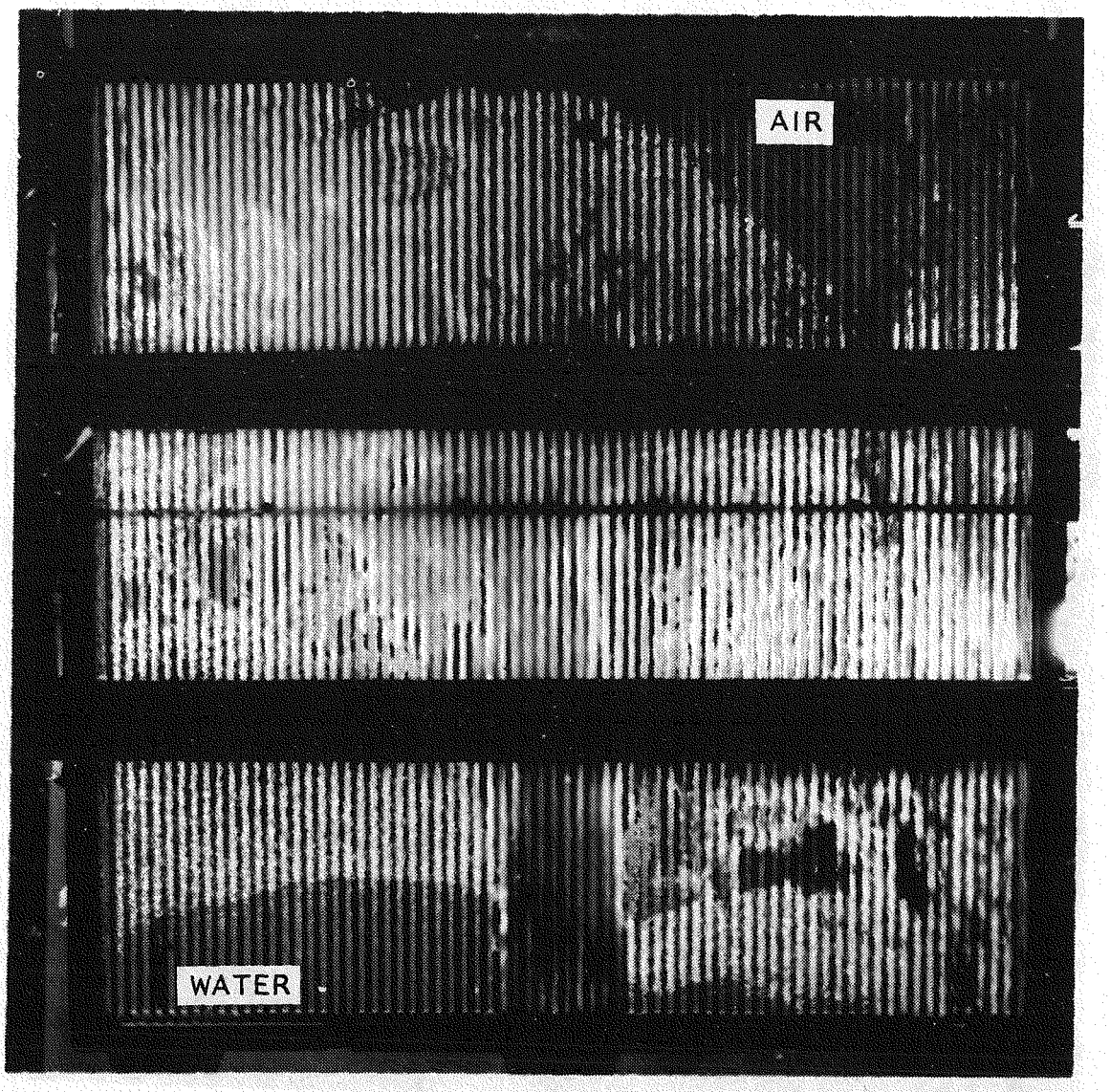


Figure 5.93 Picture of case 5BR4 (liquid mass flux = 1.395 X $10^6$ kg/hr-$m^2$; with rods; 62.5/37.5 flow split; and quality at inlet no. 4 = 0.6%)

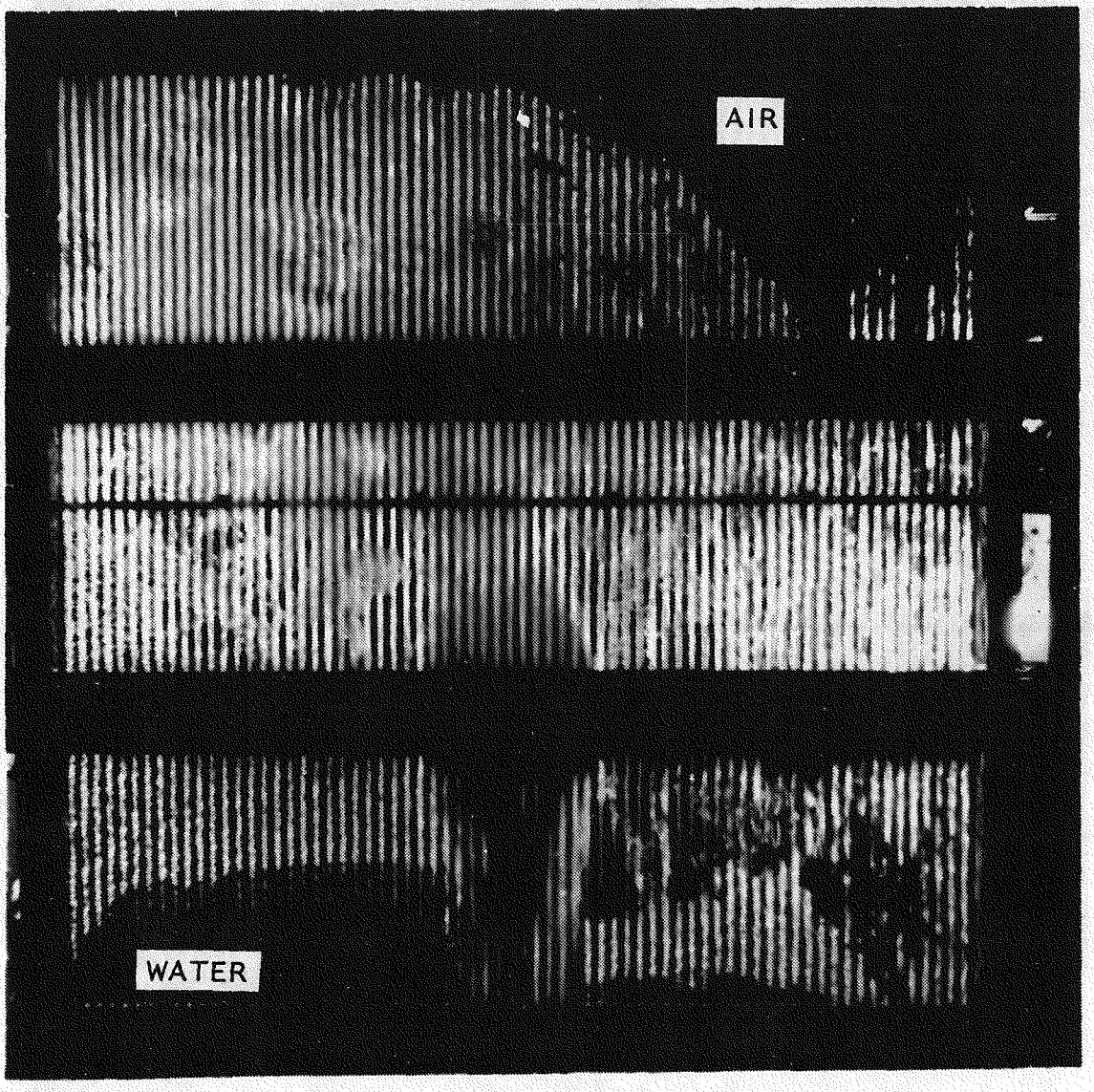


Figure 5.94 Picture of case 6BR4 (liquid mass flux = 1.395 X $10^6$ kg/hr-$m^2$; with rods; 62.5/37.5 flow split; and quality at inlet no. 4 = 0.9%)

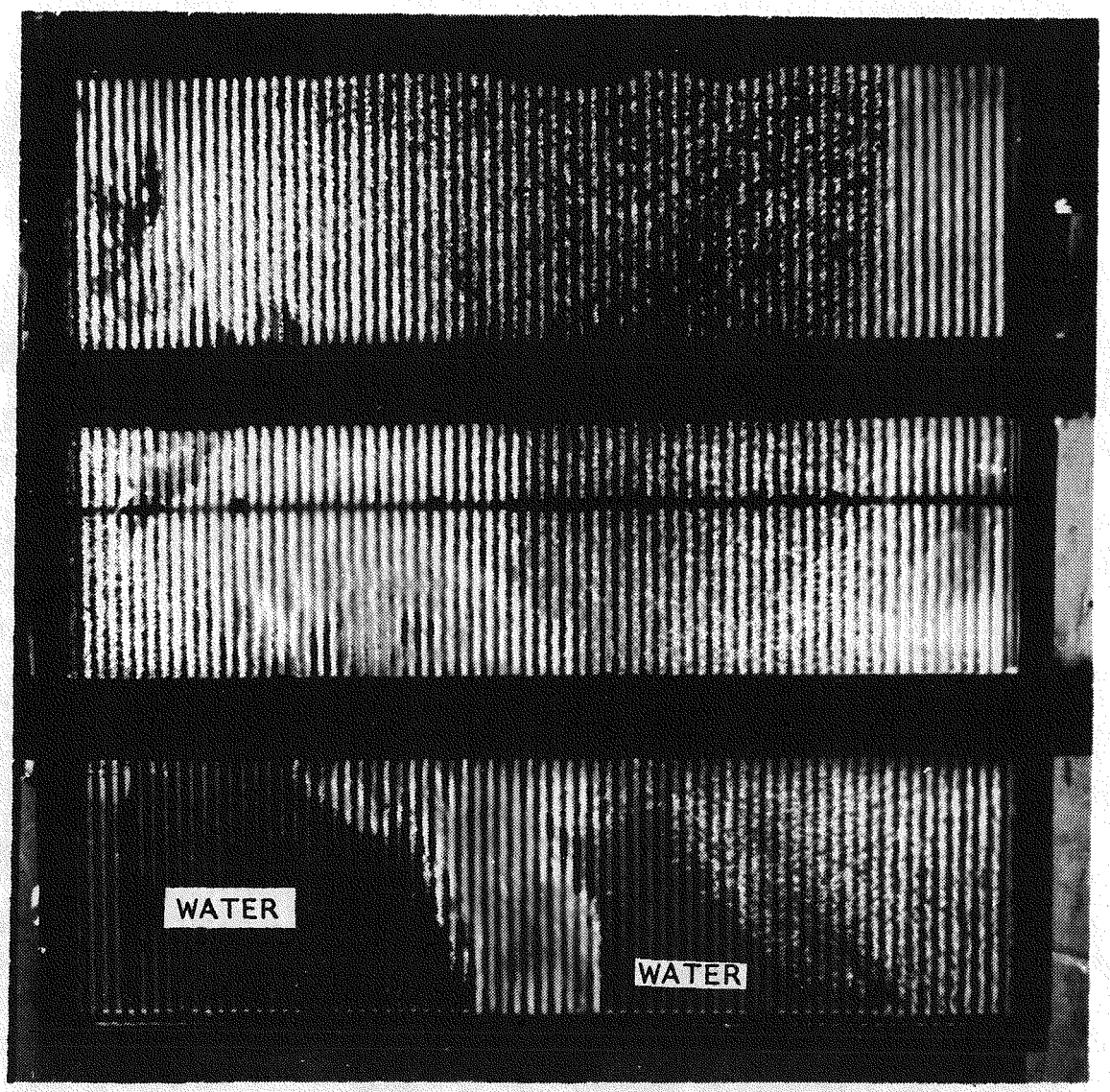


Figure 5.95 Picture of case 4CR4 (liquid mass flux = 1.395 X $10^6$ kg/hr-$m^2$; with rods; 37.5/62.5 flow split; and quality at inlet no. 4 = 0.3%)

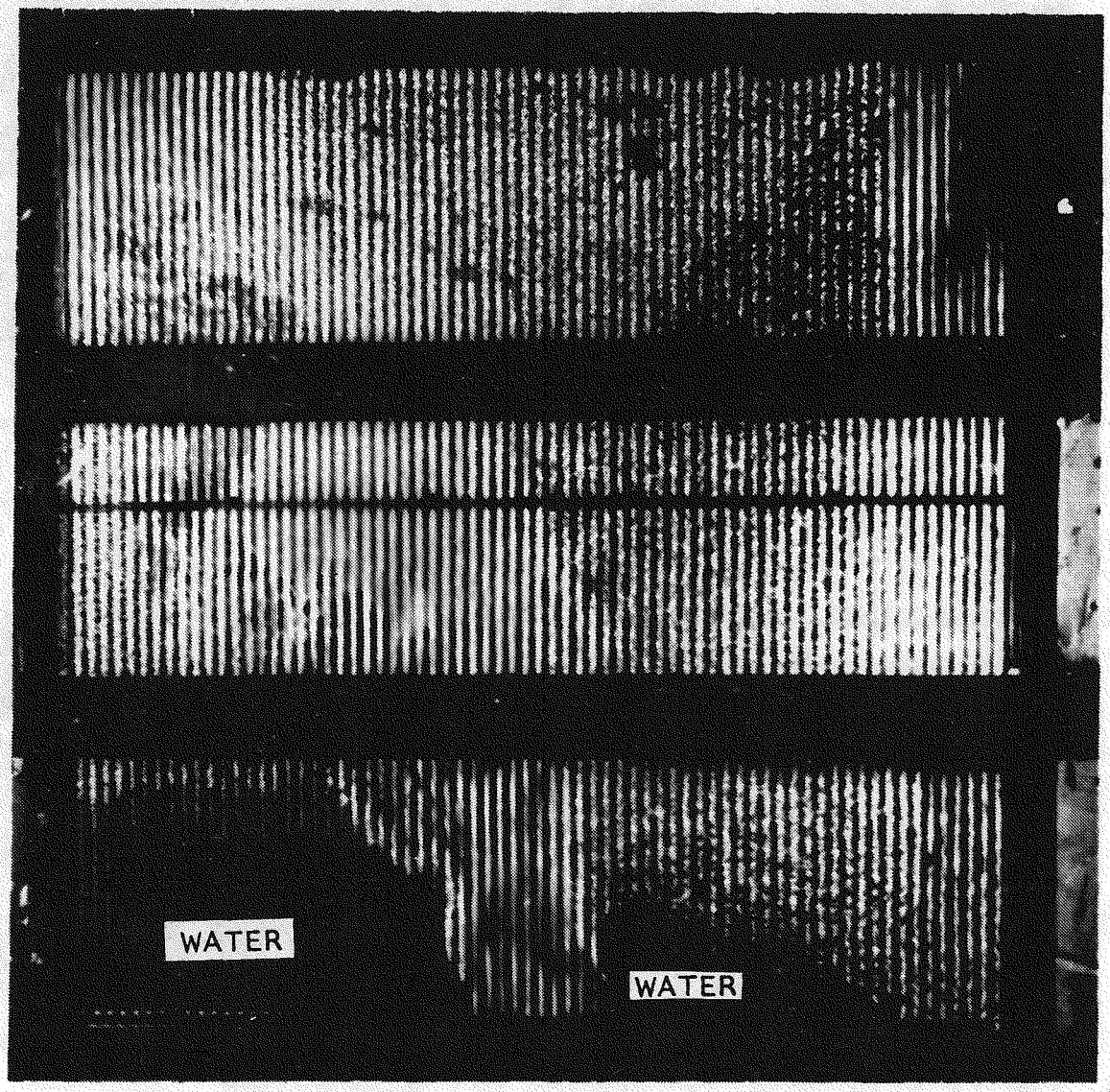


Figure 5.96 Picture of case 5CR4 (liquid mass flux = 1.395 X $10^6$ kg/hr-$m^2$; with rods; 37.5/62.5 flow split; and quality at inlet no. 4 = 0.6%)

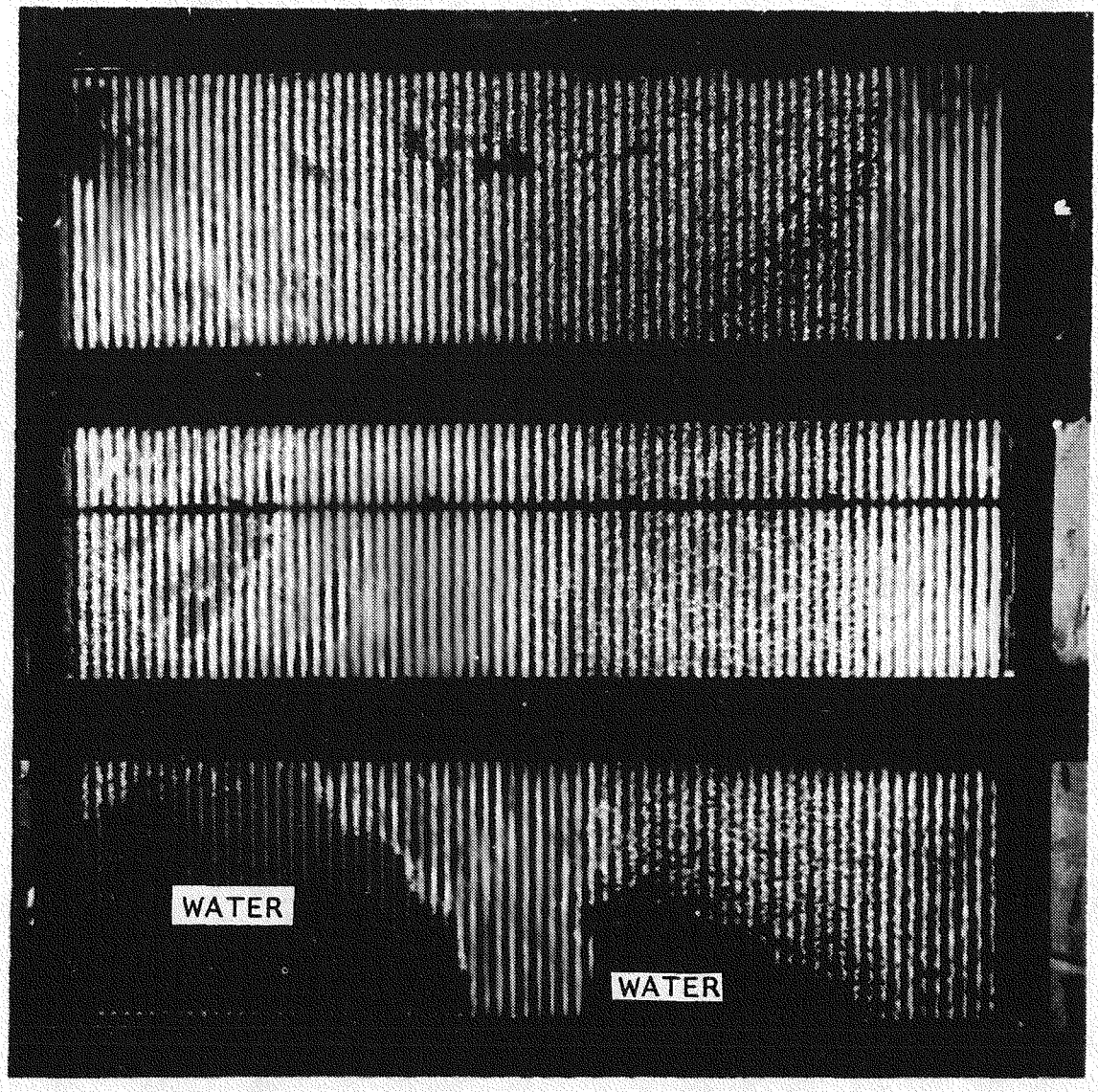


Figure 5.97 Picture of case 6CR4 (liquid mass flux = 1.395 X $10^6$ kg/hr-$m^2$; with rods; 37.5/62.5 flow split; and quality at inlet no. 4 = 0.9%)

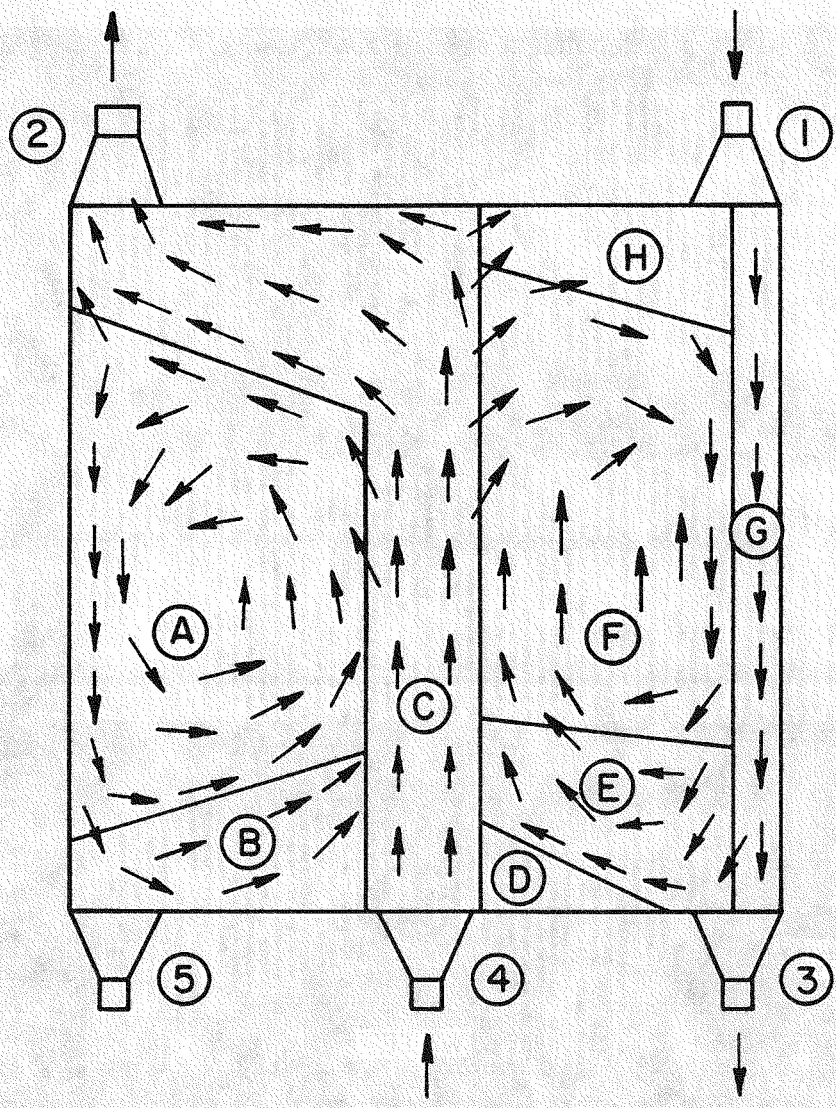


Figure 5.98 Division of the test section in eight regions based on visual observation of flow regimes (arrows indicate direction of flow)

it. Much of this region remained single-phase throughout the experiments. Region (A) was generally bubbly flow with the bubble size being approximately 0.25 inch (0.635 cm) in diameter. Slugs were observed in the upper areas of (A). The flow velocity was too high to observe the flow structure in region (C) near the inlet, but higher up in region (C), the flow was seen to be slug or churn-turbulent flow. Region (E) was generally bubbly flow. Region (F) depended strongly on the flow conditions. For most flow conditions, it was bubbly flow with occasional slugs, especially in its upper region. In cases when the flow split between inlets 4 and 1 was 62.5/37.5 (ie: a smaller flow entering from port no. 1), region (H) extended farther down. As the inlet quality increased, region (F) disappeared and there was a large air space extending down to (E). Liquid droplets entered this air space from region (C) and fell onto the horizontal air/water interface which was present at several inches from the lower edge of the test section. (eg: see Figs. 5.74-5.76, 5.85, 5.92-5.94). A liquid film flowed down both plexiglass walls. Region (G) consisted of water entering from port no. 1. It is mostly pure liquid with a few small entrained air bubbles. Its width depended on the quantity of water entering from port no. 1. These flow regimes generally appeared to be the same for the cases when rods were present, as well as when they were absent. With rods, region (B) is generally larger than without rods.

(c) Variation of void fractions with flow conditions: Since data was taken at three axial locations, 7.5" (19.1 cm), 17" (43.2 cm) and 28.5" (72.4 cm), above the bottom edge of the test section, most of the present discussion will be limited to these cross sections of the test section. For other locations, one can get an indea of the void fraction by comparing the data available with the pictures of the flows. It should be remembered that the photographs show the flow configuration as it existed at the instant the photograph was taken, whereas the plots were made from data taken for six (6) minutes. Since the flow configuration was constantly changing, the photographs only give a representative picture of the flow for a given case.

The effect of flow quality: As can be seen in Figs. 5.2 to 5.13, an increase in inlet quality generally causes the void fraction to be higher throughout the test section. (In these as well as in the rest of the void fraction plots, the small dashed lines represent 0.3% inlet flow quality, the large dashed lines represent 0.6% inlet flow quality, and the solid lines represent 0.9% inlet flow quality.) In cases 1CN4, 2CN4 and 3CN4, Fig. 5.4, it can be seen that the void fractions are similar in the

lower and middle section, but are widely different in the top section. In the high flow, equal flow split cases (ie: 4AN4, 5AN4, and 6AN4), it can be seen in Fig. 5.5 that the void fraction on the right side of the middle section rises sharply as the flow quality increases. This can be seen in Figs. 5.71, 5.72 and 5.73 as an enlargement of the air space in the upper right hand side (ie: as region (H) of Fig. 5.98 increases in size). In Fig. 5.6 (ie: cases 4BN4, 5BN4, and 6BN4), this effect is seen in both the middle and lower sections. The air space in these cases comes down into the lower section, as can be seen in Figs. 5.74-5.76. For cases 4CN4, 5CN4, and 6CN4, shown in Fig. 5.7, this effect is limited to the top section. From these three figures (ie: Figs. 5.5-5.7), we see that the higher the liquid inflow from inlet port no. 1 (top right hand side), the smaller is the size of the air space. (Liquid inflow from port no. 1 increases as we go from B to A to C flow splits.) Alternatively, we can say that the higher the total quantity of air through inlet port no. 4, the larger is the air space in the upper right hand side. Using Figs. 5.8 to 5.12 and the corresponding pictures of the flows in Figs. 5.80 to 5.94, a similar trend is seen for the cases when rods are present. Such a trend is not seen in Fig. 5.13, 5.95-5.97 for cases 4CR4, 5CR4, and 6CR4. In these cases, the liquid downflow from port no. 1 is high and we do not have a substantial air space. For the cases with rods and low flow rates, shown in Figs. 5.8-5.10 and Figs. 5.80-5.88, there is a progressive reduction in the size of the single-phase liquid region on the left of inlet no. 4 (ie: region B in Fig. 5.98) with increases in flow quality. For the high flow cases with rods, this liquid region is almost constant in size (Figs. 5.89-5.97).

The effect of flow split: These cases are plotted in Figs. 5.14 through 5.25. For the case of unequal flow splits between the two inlets, the void fraction is decidely higher on one side of the test section. Thus, for all cases with higher inlet flow through port no. 4 than through no. 1 (ie: the 62.5/37.5 flow split [all cases with B as the second digit]), the void fraction is higher in the right hand side of the test section as compared to the left hand side. In cases 4BR4, 5BR4, and 6BR4, the void fraction is high in both sides. This is seen to be the pattern in all three sections. In cases with the 37.5/62.5 flow split (ie: all cases with C as the second digit) the void fraction is higher in the left half of the test section as compared to the right half. These distinctions are more evident in the results for the lower and middle sections. In the top section, the pattern is sometimes reversed: the cases with flow split 37.5/62.5 have higher void fraction to the left in cases with

rods especially for high flow rates, and slightly to the right in cases without rods, again especially at the higher flow rates. Cases with A as the second digit, that is, cases having equal flow split (50/50) between inlet ports no. 4 and no. 1, do not show such behavior. In the top section, for all such cases, the void fraction is slightly higher in the right side of the test section than in the left side. In the middle section, it is generally higher to the left than the right except for cases 1AN4, 2AN4, and 3AN4 (ie: low flow, no rods). In the lower section, it is higher to the right. As seen from Figs. 5.14 to 5.25, the location where the void fraction is maximum across a section for cases of equal flow splits is generally between the locations where the void fraction peaks for corresponding cases of the other two flow splits (ie: cases involving B and C).

The effect of flow rate: The effect of flow rate is shown in Figs. 5.26 to 5.43. For cases without rods having 62.5/37.5 flow split, there is no striking difference between the void fraction profiles when the flow rate goes from low to high flow (eg: see Figs. 5.29-5.31). For cases having a 50/50 flow split, Figs. 5.26-5.28, the low flow cases have higher void fraction to the right of the test section, while high flow rate caused the void fraction to be higher in the left side of the test section in the lower and middle sections. In the top section, it is the other way around. A similar effect is seen in Figs. 5.32-5.34 for a 37.5/62.5 flow split. For all cases involving rods, the void fraction is higher in the test section when the flow rate is higher, especially on the left side of the two-phase inlet in the lower and middle sections.

The effect of rods: The effect of rods is shown in Figs. 5.44 through 5.61. In most of these comparisons, we see that the void fraction is higher in the presence of rods than without the rods. This could be because of homogenization of the flow by the rods which causes the void fraction to be higher. In Figs. 5.59-5.61, in the top section in the right hand side, the void fraction is higher without rods than with rods. This is due to the absence of the air space in cases 4CR4, 5CR4, and 6CR4, as can be seen in the pictures of the flow in Figs. 5.95-5.97.

## 5.7 Pictures of the Flows

To help visualize the flow patterns, photographs were taken of the test section for all the flow conditions for which void fraction data was taken. These are attached as Figs. 5.62 to 5.97.

Figures 5.62-5.70 are for the low flow rate, no rods cases (ie: for cases 1AN4, 2AN4, 3AN4, 1BN4, 2BN4, 3BN4, 1CN4, 2CN4 and 3CN4). These were taken with a shutter speed of 125 (ie: 1/125 sec exposure).

Figures 5.71-5.79 are for high flow rate, no rods cases (ie: for case 4AN4, 5AN4, 6AN4, 4BN4, 5BN4, 6BN4, 4CN4, 5CN4, and 6CN4). These were taken with a shutter speed of 400 (ie: 1/400 sec exposure).

Figures 5.80-5.88 are for low flow, with the rods installed (ie: for cases 1AR4, 2AR4, 3AR4, 1BR4, 2BR4, 3BR4, 1CR4, 2CR4 and 3CR4). These were taken with a shutter speed of 125 (ie: an exposure time = 1/125 sec).

Figures 5.89-5.97 are for high flow, with the rods installed (ie: for cases 4AR4, 5AR4, 6AR4, 4BR4, 5BR4, 6BR4, 4CR4, 5CR4 and 6CR4). These were taken with a shutter speed of 250 (ie: 1/250 sec exposure time).

It can be seen in these photographs and the void fraction data that the effect of the rods is to suppress internal recirculation, and thus to induce more or less uniaxial flows.

## 5.8 Test Section Bowing Measurements

The amount by which the plexiglass walls of the test section bowed out was measured at several locations for different system pressures. This is important to know since bowing increases the channel depth in which the fluid is flowing and can change the characteristics of the flow. The amount of bowing taking place was measured by placing two micrometers on the lead shield-detector support system, one on each side of the test section. A reading was taken when the micrometers touched the test section glass surface. Water was then filled into the test section and all inlets and outlets were closed. The air compressor was turned on and high pressure air was allowed to enter the test section at a very slow rate. Since the outlets were closed, pressure started building up inside the test section. When it reached a desired value, the air inlet valve was closed. The two micrometers were again adjusted to touch the test section and readings were taken on each of them. The difference in the readings when the test section was empty and when it is under a certain pressure gives the amount of bowing due to the pressure. Table 5.8 gives these data. It is seen that, as expected, the bowing is higher in the middle section than in the other two. Bowing also increases as we move away from the sides and towards the center. The bowing in the lower section is seen to be consistently higher than that in the top section. This is due, at least in part, to the hydrostatic head between the lower and the top sections (ie: the lower section is at a slightly higher pressure than the top section). The pressure listed in Table 5.8 is measured at 18" (45.7 cm) above the inside bottom of the test section.

## 5.9 Other Parameters Measured

Several other parameters were measured during the experiments. These include the water and air flow rates at the two outlets, the test section

Table 5.8 Amount by which the test section channel depth increases due to increase in pressure

| Measurement Station | Pressure psig (kpa) | Channel depth increase, mils (cm) at position from left edge of test section, inches (cm) | | | | |
|---|---|---|---|---|---|---|
| | | 18.25 (46.4) | 20.25 (51.4) | 24.75 (62.9) | 29.25 (74.3) | 33.75 (85.7) |
| Top | 15 (103.4) | 78 (0.1981) | 77 (0.1956) | 71 (0.1803) | 58 (0.1473) | 25 (0.0635) |
| | 10 (68.9) | 52 (0.1321) | 51 (0.1295) | 45 (0.1143) | 39 (0.0991) | 17 (0.0432) |
| | 5 (34.5) | 24 (0.0610) | 24 (0.0610) | 23 (0.0584) | 18 (0.0457) | 9 (0.0229) |
| Middle | 15 (103.4) | 122 (0.310)* | 121 (0.3073) | 112 (0.2845) | 86 (0.2184) | 29 (0.0737) |
| | 10 (68.9) | 86 (0.2184)* | 85 (0.2159) | 80 (0.2032) | 61 (0.1549) | 20 (0.0508) |
| | 5 (34.5) | 50 (0.127)* | 49 (0.1245) | 47 (0.1194) | 38 (0.0965) | 12 (0.0305) |
| Lower | 15 (103.4) | 86 (0.2184)* | 85 (0.2159) | 77 (0.1956) | 63 (0.1600) | 22 (0.0559) |
| | 10 (68.9) | 60 (0.1524)* | 59 (0.1499) | 54 (0.1372) | 43 (0.1092) | 15 (0.0381) |
| | 5 (34.5) | 35 (0.0889)* | 35 (0.0889) | 31 (0.0787) | 26 (0.0660) | 9 (0.0229) |

*Interpolated values by assuming symmetric bowing across test section.

pressure and the pressures at the two air/water seperators. These quantities were measured for each case every time it was being run for void fraction measurements, and again when the flows were repeated for taking the photographs. Their average values have been calculated and are tabulated in Table 5.9.1 in British units and in Table 5.9.2 in S.I. units. The pressures were measured by pressure gauges located in the test section at 18" (45.7 cm) above the inside bottom edge, and in the air vent pipes just above the air/water separators. The air outflow from separator no. 3 was small and measured by two rotameters in parallel, one having a range of zero to 200 SCFH (standard cubic feet per hour) and the other a range of zero to 100 SCFH. Air outflow rate from air/water sepration tank no. 2 was measured by an orifice meter with a water filled U-tube manometer. The sum of measured values of the air outflow rates from the two separator tanks matches to within 5% of measured values of the air inflow for most cases. For all cases it was within 10%. The water outflows were measured by two orifice meters with mercury filled manometers. The sizes of the orifice plates on the two liquid lines were such that one gave a much larger pressure difference than the other, and was therefore more accurate. This manometer was considered correct and the flow through the other line was calculated as the difference between the total flow and flow through this line.

Table 5.9.1 Measured values of pressures at the test section and at the air/water separators and air and water flow rates at the separators (British units)

| Case | Pressure (psig) | | | Air outflow rate (lbm/min) | | Liquid outflow rate (lbm/min) | |
|---|---|---|---|---|---|---|---|
| | Test Section | Sep #3 | Sep #2 | Sep #3 | Sep #2 | Sep #3 | Sep #2 |
| 1AN4 | 4.54 | 2.37 | 2.90 | 0.0171 | 0.31 | 101 | 139 |
| 2AN4 | 4.58 | 1.96 | 2.89 | 0.016 | 0.68 | 101 | 139 |
| 3AN4 | 4.55 | 2.20 | 2.87 | 0.0184 | 1.02 | 104 | 136 |
| 1BN4 | 4.56 | 2.04 | 3.85 | 0.0214 | 0.45 | 100 | 140 |
| 2BN4 | 4.70 | 2.33 | 2.87 | 0.0228 | 0.85 | 104 | 136 |
| 3BN4 | 4.70 | 2.3 | 2.87 | 0.0245 | 1.33 | 105 | 135 |
| 1CN4 | 4.48 | 1.87 | 2.64 | 0.0114 | 0.28 | 97 | 143 |
| 2CN4 | 4.51 | 2.13 | 2.91 | 0.0137 | 0.48 | 99 | 141 |
| 3CN4 | 4.50 | 2.07 | 2.89 | 0.0140 | 0.77 | 101 | 139 |
| 1AR4 | 5.0 | 2.6 | 3.0 | 0.0167 | 0.31 | 110 | 130 |
| 2AR4 | 4.9 | 2.0 | 2.93 | 0.0233 | 0.66 | 110 | 130 |
| 3AR4 | 5.0 | 2.23 | 2.97 | 0.0279 | 0.97 | 109 | 131 |
| 1BR4 | 5.0 | 2.7 | 3.13 | 0.0296 | 0.42 | 106 | 134 |
| 2BR4 | 5.0 | 2.43 | 3.08 | 0.0402 | 0.86 | 109 | 131 |
| 3BR4 | 5.0 | 2.33 | 3.05 | 0.342 | 1.00 | 115 | 125 |
| 1CR4 | 4.9 | 2.6 | 2.93 | 0.0126 | 0.26 | 106 | 134 |
| 2CR4 | 4.9 | 1.85 | 2.95 | 0.0152 | 0.45 | 110 | 130 |
| 3CR4 | 5.0 | 2.13 | 2.97 | 0.0167 | 0.75 | 110 | 130 |

Table 5.9.1 (Continued)

| Case | Pressure (psig) | | | Air outflow rate (lbm/min) | | Liquid outflow rate (lbm/min) | |
|---|---|---|---|---|---|---|---|
| | Test Section | Sep #3 | Sep #2 | Sep #3 | Sep #2 | Sep #3 | Sep #2 |
| 4AN4 | 8.74 | 5.97 | 4.96 | 0.053 | 0.65 | 222 | 258 |
| 5AN4 | 9.23 | 6.57 | 4.87 | 0.0637 | 1.40 | 227 | 253 |
| 6AN4 | 9.87 | 7.12 | 4.70 | 0.0708 | 2.08 | 233 | 247 |
| 4BN4 | 9.1 | 6.53 | 4.93 | 0.0687 | 0.82 | 224 | 256 |
| 5BN4 | 9.75 | 6.63 | 4.90 | 0.0746 | 1.70 | 231 | 249 |
| 6BN4 | 10.0 | 7.10 | 4.55 | 0.0779 | 2.65 | 238 | 242 |
| 4CN4 | 8.63 | 6.19 | 5.08 | 0.0402 | 0.5 | 222 | 258 |
| 5CN4 | 8.9 | 6.26 | 5.15 | 0.0474 | 1.02 | 227 | 253 |
| 6CN4 | 9.13 | 6.55 | 4.79 | 0.0534 | 1.52 | 230 | 250 |
| 4AR4 | 10.9 | 7.53 | 4.93 | 0.0968 | 0.6 | 234 | 246 |
| 5AR4 | 11.33 | 7.80 | 4.77 | 0.123 | 1.35 | 241 | 239 |
| 6AR4 | 11.8 | 7.83 | 4.5 | 0.153 | 1.95 | 246 | 234 |
| 4BR4 | 11.07 | 7.47 | 4.90 | 0.186 | 0.70 | 237 | 243 |
| 5BR4 | 11.68 | 7.73 | 4.87 | 0.224 | 1.58 | 243 | 237 |
| 6BR4 | 12.33 | 8.15 | 4.80 | 0.574 | 2.08 | 241 | 239 |
| 4CR4 | 10.67 | 7.50 | 4.93 | 0.020 | 0.50 | 238 | 242 |
| 5CR4 | 11.32 | 7.83 | 4.68 | 0.033 | 1.00 | 246 | 234 |
| 6CR4 | 11.53 | 8.37 | 4.67 | 0.075 | 1.53 | 248 | 232 |

Table 5.9.2 Measured values of pressures at the test section and at the air/water separators and air and water flow rates at the separators (S.I. units)

| Case | Pressure (kpa) | | | Air outflow rate (kg/hr) | | Liquid outflow rate (kg/hr) | |
|---|---|---|---|---|---|---|---|
| | Test Section | Sep #3 | Sep #2 | Sep #3 | Sep #2 | Sep #3 | Sep #2 |
| 1AN4 | 31.3 | 16.3 | 20.0 | 0.467 | 8.44 | 2749 | 3783 |
| 2AN4 | 31.6 | 13.5 | 19.9 | 0.437 | 18.50 | 2749 | 3783 |
| 3AN4 | 31.4 | 15.2 | 19.8 | 0.501 | 27.76 | 2830 | 3701 |
| 1BN4 | 31.4 | 14.1 | 26.5 | 0.582 | 12.25 | 2722 | 3810 |
| 2BN4 | 32.4 | 16.1 | 19.8 | 0.621 | 23.13 | 2830 | 3701 |
| 3BN4 | 32.4 | 15.9 | 19.8 | 0.668 | 36.20 | 2858 | 3674 |
| 1CN4 | 30.9 | 12.9 | 18.2 | 0.312 | 7.62 | 2640 | 3892 |
| 2CN4 | 31.1 | 14.7 | 20.1 | 0.374 | 13.06 | 2694 | 3837 |
| 3CN4 | 31.0 | 14.3 | 19.9 | 0.382 | 20.96 | 2748 | 3783 |
| 1AR4 | 34.5 | 17.9 | 20.7 | 0.453 | 8.44 | 3002 | 3530 |
| 2AR4 | 33.8 | 13.8 | 20.2 | 0.634 | 17.96 | 3002 | 3530 |
| 3AR4 | 34.5 | 15.4 | 20.5 | 0.759 | 26.40 | 2967 | 3565 |
| 1BR4 | 34.5 | 18.6 | 21.6 | 0.805 | 11.43 | 2885 | 3647 |
| 2BR4 | 34.5 | 16.8 | 21.2 | 1.093 | 23.40 | 2967 | 3565 |
| 3BR4 | 34.5 | 16.1 | 21.0 | 9.314 | 27.22 | 3130 | 3402 |
| 1CR4 | 33.8 | 17.9 | 20.2 | 0.342 | 7.08 | 2885 | 3647 |
| 2CR4 | 33.8 | 12.8 | 20.3 | 0.415 | 12.25 | 3002 | 3530 |
| 3CR4 | 34.5 | 14.7 | 20.5 | 0.454 | 20.41 | 3002 | 3530 |

Table 5.9.2 (Continued)

| Case | Pressure (kpa) | | | Air outflow rate (kg/hr) | | Liquid outflow rate (kg/hr) | |
|---|---|---|---|---|---|---|---|
| | Test Section | Sep #3 | Sep #2 | Sep #3 | Sep #2 | Sep #3 | Sep #2 |
| 4AN4 | 60.2 | 41.2 | 34.2 | 1.437 | 17.70 | 6042 | 7022 |
| 5AN4 | 63.7 | 45.3 | 33.6 | 1.733 | 38.10 | 6178 | 8666 |
| 6AN4 | 68.1 | 49.1 | 32.4 | 1.927 | 56.61 | 6341 | 8274 |
| 4BN4 | 62.7 | 45.0 | 34.0 | 1.871 | 22.32 | 6096 | 6967 |
| 5BN4 | 67.2 | 45.7 | 33.8 | 2.029 | 46.27 | 6287 | 6777 |
| 6BN4 | 68.9 | 48.9 | 31.4 | 2.120 | 72.12 | 6477 | 6586 |
| 4CN4 | 59.5 | 42.7 | 35.0 | 1.095 | 13.61 | 6042 | 7022 |
| 5CN4 | 61.4 | 43.2 | 35.5 | 1.289 | 27.76 | 6178 | 6886 |
| 6CN4 | 62.9 | 45.2 | 33.0 | 1.453 | 41.37 | 6260 | 6804 |
| 4AR4 | 75.1 | 51.9 | 34.0 | 2.634 | 16.33 | 6369 | 6695 |
| 5AR4 | 78.1 | 53.8 | 32.9 | 3.348 | 36.74 | 6559 | 6504 |
| 6AR4 | 81.4 | 54.0 | 31.0 | 4.159 | 53.07 | 6695 | 6368 |
| 4BR4 | 76.3 | 51.5 | 33.8 | 5.067 | 19.05 | 6450 | 6613 |
| 5BR4 | 80.5 | 53.5 | 33.6 | 6.108 | 43.00 | 6613 | 6450 |
| 6BR4 | 85.0 | 56.2 | 33.1 | 15.62 | 56.61 | 6559 | 6504 |
| 4CR4 | 73.5 | 51.7 | 34.0 | 0.556 | 13.61 | 6477 | 6586 |
| 5CR4 | 78.1 | 54.0 | 32.3 | 0.898 | 27.22 | 6695 | 6368 |
| 6CR4 | 79.5 | 57.7 | 32.2 | 2.05 | 41.64 | 6750 | 6314 |

## REFERENCES


1. M. Barasch, and R. T. Lahey, Jr., "The Measurement of Two-Dimensional Phase Separation Phenomena." NUREG/CR-1936, 1981.

2. T. J. Honan and R. T. Lahey, Jr., "The Measurement of Phase Separation in Wyes and Tees." NUREG/CR-0557, 1978.

3. R. D. Evans, "The Atomic Nucleus." McGraw Hill Book Co., N.Y., 1955.

4. Theodore Baumeister, Eugene A. Avallone and Theodore Baumeister III, eds., "Marks Standard Handbook for Mechanical Engineers." Eighth edition, McGraw Hill Book Co., N.Y., 1978.

5. G. F. Knoll, "Radiation Detection and Measurement." John Wiley & Sons, 1979.

APPENDIX-A

## TEST SECTION BOWING CALCULATIONS

In order to limit the amount of bowing in the plexiglass walls so that we can maintain the geometry of the flow channel and prevent flow bypass on the sides, we determined the amount of bowing as a function of pressure. We also determined the number of braces that were needed and the maximum pressure that the test section could be subjected to without creating excessive stresses in the plexiglass.

The well-known formulae(4) for a rectangular plate, for the maximum deflection, $y_p$, and maximum stress, $S_p$, are:

$$y_p = K_1 \, w \, r^4/ET^3, \text{ in} \qquad (A.1)$$

and,

$$S_p = K \, w \, r^2/T^2, \text{ lb/in}^2 \qquad (A.2)$$

where,

$w$ = pressure exerted on plate ($\text{lbf/in}^2$),

$r$ = length of the short side of plate (in),

$T$ = thickness of plate (in),

$E$ = elastic modulus of plate (psi),

$K$, $K_1$ = constants depending on whether the plate is fixed or simply supported, and on R/r (given in Table A.1). R is length of long side of plate (in).

Some relevant parameters for plexiglass and the test section are:

Plexiglass elastic modulus (E) ~ $3X10^5$ psi
tensile yield strength ~ 5500 psi

Width and height of plexiglass
undergoing bowing (R) = 36"
thickness of plexiglass (T) = 1"

We substitute these values in Eq. (A.1) to get the maximum deflection. This is listed in Table A.2 for several values of test section pressure (w) and number of braces. Substitution in Eq. (A.2) gives us the corresponding values of the maximum stress. The safety factor in the stress is:

$$\text{safety factor} = \frac{\text{tensile yield strength}}{\text{maximum tensile stress}}$$

Table A.1 Values of the parameters K and $K_1$ (4)

| R/r | Fixed Plate | | Plate Simply Supported | |
|---|---|---|---|---|
| | K | $K_1$ | K | $K_1$ |
| 1 | 0.308 | 0.0138 | 0.287 | 0.0443 |
| 1.5 | 0.454 | 0.0240 | 0.487 | 0.0843 |
| 2.0 | 0.497 | 0.0277 | 0.610 | 0.1106 |
| 3.0 | 0.500 | 0.028 | 0.713 | 0.1336 |
| 4.0 | 0.500 | 0.028 | 0.741 | 0.1400 |

Table A.2 Maximum deflection in plexiglass for different pressures and number of braces

| No. of braces | R/r | r inches | Maximum deflection (in) for various system pressures in psig (kpa) | | | | | |
|---|---|---|---|---|---|---|---|---|
| | | | 5 (34.5) | 10 (68.9) | 15 (103.4) | 20 (137.9) | 30 (206.8) | 40 (275.8) |
| | | | if plate is simply supported | | | | | |
| 0 | 1 | 36 | 1.24 | 2.48 | 3.72 | 4.96 | 7.44 | 9.92 |
| 1 | 2 | 18 | 0.193 | 0.387 | 0.580 | 0.774 | 1.16 | 1.55 |
| 2 | 3 | 12 | 0.0462 | 0.0923 | 0.139 | 0.185 | 0.277 | 0.369 |
| 3 | 4 | 9 | 0.0153 | 0.0306 | 0.0459 | 0.0612 | 0.0918 | 0.123 |
| | | | if plate is fixed | | | | | |
| 0 | 1 | 36 | 0.386 | 0.773 | 1.16 | 1.55 | 2.32 | 3.09 |
| 1 | 2 | 18 | 0.0485 | 0.0969 | 0.145 | 0.194 | 0.291 | 0.388 |
| 2 | 3 | 12 | 0.00968 | 0.0194 | 0.029 | 0.0387 | 0.0581 | 0.0774 |
| 3 | 4 | 9 | 0.00306 | 0.00612 | 0.00918 | 0.0122 | 0.0184 | 0.0245 |

This is also calculated and listed in Table A.3 along with the maximum stresses.

The values of $y_p$ and $S_p$ tabulated in these tables were made on the assumption that the braces are rigid. Actually, the braces will also bend slightly and the total bowing in plexiglass will be higher than listed.

We decided to use steel I-beams of dimensions 4" X 2.5" for the braces. Using the following equations for maximum deflection of a beam:

Fixed Beam: $y_b = Wl^3/384\ EI$

Simply Supported: $y_b = 5\ Wl^3/384\ EI$

where,

E = modulus of elasticity of beam material,

W = uniform load (total),

I = moment of inertia,

$y_b$ = maximum deflection in the beam,

l = length of the beam.

For the beams we used we have:

$E = 29 \times 10^6$ lb/in$^2$

I = 5.3

l = 40" (ie: extends 1" beyond test section on both sides)

W = w (psi) X $36^2$/no. of braces

We then obtain the maximum deflection in the beams as listed in Table A.4.

The maximum deflection in the plexiglass should be the sum of the deflection in the plexiglass plus the deflection of the braces. Assuming that both the plate and the beams are simply supported, the total maximum deflection in the plexiglass is shown in Table A.5. For the other extreme, if both the brace and plexiglass are fixed, the values are given in Table A.6. Tables A.7 and A.8 give the values of total deflection if plates are fixed and beam is simply supported (A.7) and vice versa (A.8).

With two braces in place, the measured values of the increase in depth of the test section are given in Table 5.8. If we assume that both sides of the test section bow out equally, the amount of bowing in each plexiglass sheet will be half of the values listed in that table. Thus, the maximum amount of bowing will be as given in Table A.9. It is seen from this table that the deflections in the top and lower sections match very

Table A.3 Maximum stress and safety factors for plexiglass for several pressures and number of braces

| No. of braces | R/r | r inches (cm) | Maximum stress, psi/kpa and (safety factor) for pressure in psi (kpa) | | | | | |
|---|---|---|---|---|---|---|---|---|
| | | | if plate is simply supported | | | | | |
| | | | 5 (34.5) | 10 (68.9) | 15 (103.4) | 20 (137.9) | 30 (206.8) | 40 (275.8) |
| 0 | 1 | 36 (91.44) | 1860/12820 (2.96) | 3720/25650 (1.48) | 5580/38470 (0.98) | 7440/51290 (0.74) | 11200/77220 (0.49) | 14900/102700 (0.37) |
| 1 | 2 | 18 (45.72) | 988/6812 (5.57) | 1980/13650 (2.78) | 2970/20480 (1.86) | 3950/27230 (1.39) | 5930/40880 (0.93) | 7910/54540 (0.69) |
| 2 | 3 | 12 (30.48) | 513/3537 (10.7) | 1030/7101 (5.36) | 1540/10620 (3.57) | 2050/14130 (2.68) | 3080/21240 (1.78) | 4110/28340 (1.34) |
| 3 | 4 | 9 (22.86) | 300/2068 (18.3) | 600/4136 (9.16) | 900/6205 (6.11) | 1200/8274 (4.58) | 1800/12410 (3.05) | 2400/16550 (2.29) |
| | | | if plate is fixed | | | | | |
| 0 | 1 | 36 (91.44) | 2000/13770 (2.76) | 3990/27510 (1.38) | 5990/41300 (0.92) | 7980/55020 (0.69) | 12000/82740 (0.46) | 16000/110300 (0.34) |
| 1 | 2 | 18 (45.72) | 805/5550 (6.83) | 1610/11100 (3.42) | 2420/16690 (2.28) | 3220/22200 (1.71) | 4830/33300 (1.14) | 6440/44400 (0.85) |
| 2 | 3 | 12 (30.48) | 360/2482 (15.3) | 720/4964 (7.64) | 1080/7446 (5.09) | 1440/9928 (3.82) | 2160/14890 (2.55) | 2880/19860 (1.91) |
| 3 | 4 | 9 (22.86) | 202/1393 (27.2) | 405/2792 (13.6) | 607/4185 (9.05) | 810/5585 (6.79) | 1220/8412 (4.53) | 1620/11170 (3.39) |

Table A.4 Maximum Deflection of the braces

| No. of braces | Maximum deflection (in) for various system pressures (psig) | | | | | |
|---|---|---|---|---|---|---|
| | simply supported | | | | | |
| | 5 | 10 | 15 | 20 | 30 | 40 |
| 1 | 0.0351 | 0.0703 | 0.1054 | 0.1405 | 0.211 | 0.281 |
| 2 | 0.0176 | 0.0351 | 0.0527 | 0.0703 | 0.105 | 0.140 |
| 3 | 0.0117 | 0.0234 | 0.0351 | 0.0468 | 0.0702 | 0.0937 |
| | fixed | | | | | |
| | 5 | 10 | 15 | 20 | 30 | 40 |
| 1 | 0.007 | 0.014 | 0.0211 | 0.0281 | 0.0422 | 0.0562 |
| 2 | 0.00351 | 0.0070 | 0.0105 | 0.0140 | 0.0211 | 0.0281 |
| 3 | 0.00234 | 0.00468 | 0.00703 | 0.00937 | 0.0141 | 0.0187 |

Table A.5 Sum of maximum deflection in plexiglass and in braces, if both are simply supported

| No. of braces | Maximum deflection (in) for various system pressures (psig) | | | | | |
|---|---|---|---|---|---|---|
| | 5 | 10 | 15 | 20 | 30 | 40 |
| 0 | 1.24 | 2.48 | 3.72 | 4.96 | 7.44 | 9.92 |
| 1 | 0.228 | 0.457 | 0.685 | 0.914 | 1.372 | 1.829 |
| 2 | 0.0638 | 0.1274 | 0.1912 | 0.2553 | 0.3820 | 0.509 |
| 3 | 0.0270 | 0.0540 | 0.0810 | 0.1080 | 0.1620 | 0.2162 |

Table A.6 Sum of maximum deflection in plexiglass and in braces, if both are fixed

| No. of braces | Maximum deflection (in) for various system pressures (psig) | | | | | |
|---|---|---|---|---|---|---|
| | 5 | 10 | 15 | 20 | 30 | 40 |
| 0 | 0.386 | 0.773 | 1.16 | 1.55 | 2.32 | 3.090 |
| 1 | 0.0555 | 0.1109 | 0.1661 | 0.2221 | 0.3332 | 0.4442 |
| 2 | 0.01319 | 0.02635 | 0.0395 | 0.0527 | 0.0792 | 0.1055 |
| 3 | 0.00540 | 0.01080 | 0.01621 | 0.02157 | 0.0325 | 0.0432 |

Table A.7 Sum of maximum deflection in plexiglass and in braces, if braces are simply supported and plexiglass is fixed

| No. of braces | Maximum deflection (in) for various system pressures (psig) | | | | | |
|---|---|---|---|---|---|---|
| | 5 | 10 | 15 | 20 | 30 | 40 |
| 0 | 0.386 | 0.773 | 1.16 | 1.55 | 2.32 | 3.090 |
| 1 | 0.0836 | 0.1672 | 0.2504 | 0.3345 | 0.502 | 0.669 |
| 2 | 0.02728 | 0.0545 | 0.0817 | 0.1090 | 0.1631 | 0.2174 |
| 3 | 0.01476 | 0.02952 | 0.04428 | 0.0590 | 0.0886 | 0.1182 |

Table A.8 Sum of maximum deflection in plexiglass and in braces, if braces are fixed and plexiglass is simply supported

| No. of braces | Maximum deflection (in) for various system pressures (psig) | | | | | |
|---|---|---|---|---|---|---|
| | 5 | 10 | 15 | 20 | 30 | 40 |
| 0 | 1.24 | 2.48 | 3.72 | 4.96 | 7.44 | 9.92 |
| 1 | 0.200 | 0.401 | 0.6011 | 0.8021 | 1.2032 | 1.6042 |
| 2 | 0.04971 | 0.0993 | 0.1490 | 0.199 | 0.2981 | 0.3971 |
| 3 | 0.01764 | 0.03528 | 0.05293 | 0.07057 | 0.1059 | 0.1412 |

closely with the values given in Table A.6, ie: when braces and plexiglass are both fixed. The slightly higher measured values in the lower section have been discussed in section 5.8. The limiting deflection is in the middle section where the measured values are between those given in Tables A.6 and A.7 or about 75% of the values listed in Table A.7. Assuming this to remain the case for more than two braces and at higher pressures, then to limit the bowing to 0.05", ie: a channel depth increase of 0.1" or 20% of the original value of 0.5", we must have more than 3 braces to reach apressure of 40 psig. Such a large number of braces would reduce the visible area of the test section. We therefore decided to keep the number of braces at two and operate the loop at a lower pressure. From Table A.3 we than have a safety factor of about 3.6 for 15 psi and two braces, which was considered acceptable.

Table A.9 Maximum amount of test section bowing and matching values from Tables A.6 and A.7

| Pressure | Maximum amount of bowing (in.) in test section | | | Bowing from Table A.6 | Bowing from Table A.7 times 0.75 |
|---|---|---|---|---|---|
| | Top | Middle | Lower | | |
| 15 | 0.039 | 0.061 | 0.043 | 0.0395 | .0613 |
| 10 | 0.026 | 0.043 | 0.030 | 0.0263 | .0409 |
| 5 | 0.012 | 0.025 | 0.018 | 0.0132 | .0205 |

# APPENDIX-B

## AIR FLOW RATE CALCULATIONS

The air mass flow rates required for the various inlet qualities that were needed for the cases that were run are calculated here. If X is the flow quality desired, $w_\ell$ is the liquid mass flow rate, and $w_g$ is the air mass flow rate, then,

$$X = w_g/(w_\ell + w_g)$$

where $w_\ell + w_g$ becomes the total mass flow rate (water + air). This equation can be rewritten as:

$$w_g = w_\ell \, (X/(1-X)) \qquad (B.1)$$

Equation (B.1) is used to calculate the air mass flow rates required. The mass flow, $w_\ell$, is the liquid mass flow entering inlet no. 4. The quality X is then the flow quality of the two-phase mixture entering from inlet no. 4 and is not dependent on the total liquid inflow (which comes through inlets 1 and 4). Table B.1 lists the relevant flow rates for all the cases that were run.

Table B.1 Air mass flows required for the cases run

| Case | Total liquid mass flow rate (lb/min) | (kg/hr) | Liquid flow rate in inlet no. 4 (lb/min) | (kg/hr) | Flow quality (%) | Air mass flow rate required (lb/min) | (kg/hr) |
|---|---|---|---|---|---|---|---|
| 1AN4 and 1AR4 | 240 | 6531.7 | 120 | 3265.8 | 0.3 | 0.3611 | 9.827 |
| 2AN4 and 2AR4 | 240 | 6531.7 | 120 | 3265.8 | 0.6 | 0.7243 | 19.713 |
| 3AN4 and 3AR4 | 240 | 6531.7 | 120 | 3265.8 | 0.9 | 1.0898 | 29.659 |
| 4AN4 and 4AR4 | 480 | 13063.4 | 240 | 6531.7 | 0.3 | 0.7222 | 19.654 |
| 5AN4 and 5AR4 | 480 | 13063.4 | 240 | 6531.7 | 0.6 | 1.4487 | 39.427 |
| 6AN4 and 6AR4 | 480 | 13063.4 | 240 | 6531.7 | 0.9 | 2.1796 | 59.319 |
| 1BN4 and 1BR4 | 240 | 6531.7 | 150 | 4082.3 | 0.3 | 0.4512 | 12.284 |
| 2BN4 and 2BR4 | 240 | 6531.7 | 150 | 4082.3 | 0.6 | 0.9054 | 24.642 |
| 3BN4 and 3BR4 | 240 | 6531.7 | 150 | 4082.3 | 0.9 | 1.3623 | 37.075 |
| 4BN4 and 4BR4 | 480 | 13063.4 | 300 | 8164.6 | 0.3 | 0.9027 | 24.568 |
| 5BN4 and 5BR4 | 480 | 13063.4 | 300 | 8164.6 | 0.6 | 1.8109 | 49.283 |
| 6BN4 and 6BR4 | 480 | 13063.4 | 300 | 8164.6 | 0.9 | 2.7245 | 74.149 |
| 1CN4 and 1CR4 | 240 | 6531.7 | 90 | 2449.4 | 0.3 | 0.2708 | 7.370 |
| 2CN4 and 2CR4 | 240 | 6531.7 | 90 | 2449.4 | 0.6 | 0.5433 | 14.785 |
| 3CN4 and 3CR4 | 240 | 6531.7 | 90 | 2449.4 | 0.9 | 0.8174 | 22.245 |
| 4CN4 and 4CR4 | 480 | 13063.4 | 180 | 4898.8 | 0.3 | 0.5416 | 14.740 |
| 5CN4 and 5CR4 | 480 | 13063.4 | 180 | 4898.8 | 0.6 | 1.0865 | 29.570 |
| 6CN4 and 6CR4 | 480 | 13063.4 | 180 | 4898.8 | 0.9 | 1.6347 | 44.489 |

# APPENDIX-C

## ORIFICE ARRANGEMENT

The following orifices were used at the given location. This was based on the expected flow rates.

### Water Side

(a) Low Flow (ie: total water flow rate of 240 lbm/min or 6532 kg/hr)
- Main line: 0.767" (1.948 cm) diameter
- Inlet no. 1: 0.767" (1.948 cm) diameter
- Sep. no. 2: 0.767" (1.948 cm) diameter
- Sep. no. 3: 1.1885" (3.019 cm) diameter

(b) High Flow (ie: total water flow rate of 480 lbm/min or 13063 kg/hr)
- Main line: 1.1885" (3.019 cm) diameter
- Inlet no. 1: 0.767" (1.948 cm) diameter for flow splits A and B
  1.1885" (3.019 cm) diameter for flow split C
- Sep. no. 2: 1.1885" (3.019 cm) diameter
- Sep. no. 3: 0.767" (1.948 cm) diameter

### Air Side

(a) Low Flow (air flow rates range from 0.27 lbm/min to 1.36 lbm/min or 7.37 kg/hr to 37.07 kg/hr)
- Main line: 0.445" (1.130 cm) diameter
- Sep. no. 2: 0.445" (1.130 cm) diameter

(b) High Flow (air flow rates range from 0.542 lbm/min to 2.72 lbm/min or 14.74 kg/hr to 74.15 kg/hr)
- Main line: 0.654" (1.661 cm) diameter
- Sep. no. 2: 0.654" (1.661 cm) diameter